ADVANCED NEUROIMAGING METHODS FOR STUDYING AUTISM DISORDER

EDITED BY: Alessandro Grecucci, Roma Siugzdaite and Remo Job
PUBLISHED IN: Frontiers in Neuroscience

frontiers Research Topics

frontiers

ISSN 1664-8714
ISBN 978-2-88945-316-0
DOI 10.3389/978-2-88945-316-0

About Frontiers

Frontiers is more than just an open-access publisher of scholarly articles: it is a pioneering approach to the world of academia, radically improving the way scholarly research is managed. The grand vision of Frontiers is a world where all people have an equal opportunity to seek, share and generate knowledge. Frontiers provides immediate and permanent online open access to all its publications, but this alone is not enough to realize our grand goals.

Frontiers Journal Series

The Frontiers Journal Series is a multi-tier and interdisciplinary set of open-access, online journals, promising a paradigm shift from the current review, selection and dissemination processes in academic publishing. All Frontiers journals are driven by researchers for researchers; therefore, they constitute a service to the scholarly community. At the same time, the Frontiers Journal Series operates on a revolutionary invention, the tiered publishing system, initially addressing specific communities of scholars, and gradually climbing up to broader public understanding, thus serving the interests of the lay society, too.

Dedication to Quality

Each Frontiers article is a landmark of the highest quality, thanks to genuinely collaborative interactions between authors and review editors, who include some of the world's best academicians. Research must be certified by peers before entering a stream of knowledge that may eventually reach the public - and shape society; therefore, Frontiers only applies the most rigorous and unbiased reviews.

Frontiers revolutionizes research publishing by freely delivering the most outstanding research, evaluated with no bias from both the academic and social point of view.

By applying the most advanced information technologies, Frontiers is catapulting scholarly publishing into a new generation.

What are Frontiers Research Topics?

Frontiers Research Topics are very popular trademarks of the Frontiers Journals Series: they are collections of at least ten articles, all centered on a particular subject. With their unique mix of varied contributions from Original Research to Review Articles, Frontiers Research Topics unify the most influential researchers, the latest key findings and historical advances in a hot research area! Find out more on how to host your own Frontiers Research Topic or contribute to one as an author by contacting the Frontiers Editorial Office: **researchtopics@frontiersin.org**

ADVANCED NEUROIMAGING METHODS FOR STUDYING AUTISM DISORDER

Topic Editors:
Alessandro Grecucci, University of Trento, Italy
Roma Siugzdaite, Ghent University, Belgium
Remo Job, University of Trento, Italy

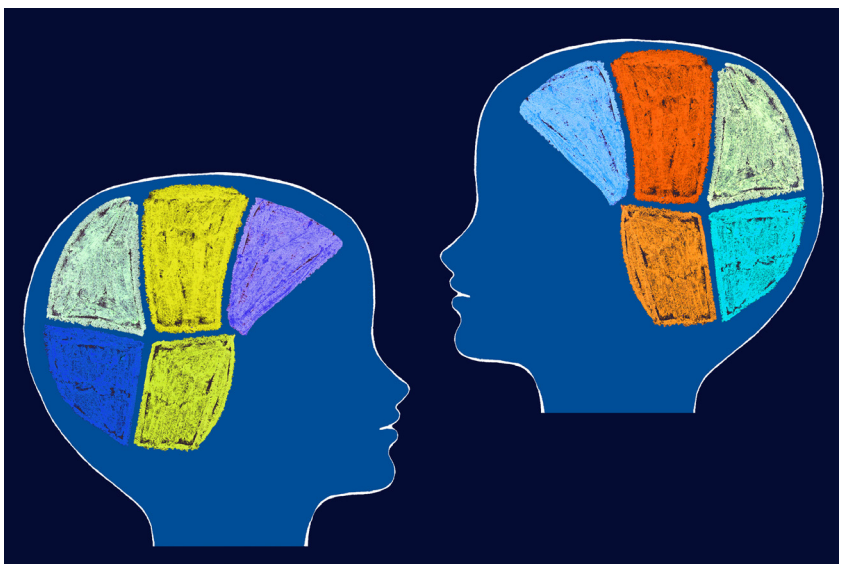

Image by Lorenza Caroli

In the last twenty years, many attempts have been made to provide neurobiological models of autism. Functional, structural and connectivity analyses have highlighted reduced responses in key social areas, such as amygdala, medial prefrontal cortex, cingulate cortex, and superior temporal sulcus. However, these studies present discrepant results and some of them have been questioned for methodological limitations. The aim of this research topic is to present advanced neuroimaging methods able to capture the complexity of the neural deficits displayed in autism. This special issue presents new studies using structural and functional MRI, as well as magnetoencephalography, and novel protocols to analyze data (Analysis of Cluster Variability, Noise Reduction Strategies, Source-based Morphometry, Functional Connectivity Density, Restriction Spectrum Imaging and the others). We believe it is time to integrate data provided by different techniques and methodologies in order to have a better understanding of autism.

Citation: Grecucci, A., Siugzdaite, R., Job, R., eds. (2017). Advanced Neuroimaging Methods for Studying Autism Disorder. Lausanne: Frontiers Media. doi: 10.3389/978-2-88945-316-0

Table of Contents

frontiers in Neuroscience

EDITORIAL
published: 26 September 2017
doi: 10.3389/fnins.2017.00533

Editorial: Advanced Neuroimaging Methods for Studying Autism Disorder

Alessandro Grecucci[1]*, *Roma Siugzdaite*[2] and *Remo Job*[1]

[1] Clinical and Affective Neuroscience Lab (CLIAN Lab), Department of Psychology and Cognitive Sciences, University of Trento, Trento, Italy, [2] Department of Experimental Psychology, Faculty of Psychology and Educational Sciences, Ghent University, Ghent, Belgium

Keywords: autism, neuroscience method, neuroimaging, fMRI, functional connectivity

Editorial on the Research Topic

Advanced Neuroimaging Methods for Studying Autism Disorder

Autism spectrum disorder (ASD) is a pervasive developmental disorder that affects 1 in 68 children (Christensen et al., 2016), and whose causes are still mostly unknown. Autistic symptomatology is characterized by impairments in social interaction, communication, and emotional abilities, while sparing basic cognitive skills. Many attempts have been made to provide neurobiological models of autism. Functional, structural, and connectivity analyses based on magnetic resonance imaging data have highlighted reduced responses in key social areas, such as amygdala, medial prefrontal cortex, cingulate cortex, and superior temporal sulcus. However, these studies present discrepant results and some of them have been questioned for methodological limitations. During the last few years, new neuroimaging methodologies have been developed providing more sophisticated techniques and more precise methods for investigating brain structure and function.

The aim of this research topic is to present advanced neuroimaging methods able to capture the complexity of the neural deficits displayed in autism. We present new studies using structural and functional MRI, as well as Magnetoencephalography, and novel protocols to analyze data (Analysis of Cluster Variability, Noise Reduction Strategies, Source-based Morphometry, Functional Connectivity Density, Restriction Spectrum Imaging and others). Understanding the main differences between patients and controls is of fundamental importance in at least four aspects. First, to help scholars develop more comprehensive models of autism. Second, to improve the diagnosis of autism based on objective neural markers rather than on subjective behavioral measures. Third, to facilitate early diagnosis of ASD, following clinical observations according to which the earlier the diagnosis, the better is the outcome of interventions. Fourth, a better knowledge of the neural mechanism of autism can refine and even create new treatment protocols to help these individuals. The theories and methods for studying autism presented in this state-of-the-art research topic are strongly grounded in affective neuroscience and bring together scientists describing new ways to understand the developmental pathology with innovative neuroimaging protocols and fresh ideas on the problems of diagnosis and intervention.

The issue starts with two methodological papers. Vidal et al. explore the possibility of using the Analysis of Cluster Variability to identify alterations in clustering structure of functional brain networks, and, through this method, they are able to show an atypical organization of domain-specific functional brain modules in ASD. Jann et al. evaluate the effectiveness of different noise strategies to improve perfusion-based connectivity analyses, suggesting that the removal of physiological noise and motion parameters is critical for detecting altered connectivity in neurodevelopmental disorders such as ASD.

OPEN ACCESS

Edited by:
Ahmet O. Caglayan,
Istanbul Bilim University, Turkey

Reviewed by:
Allison Jack,
George Washington University, United States
Lei Ding,
University of Oklahoma, United States

***Correspondence:**
Alessandro Grecucci
alessandro.grecucci@unitn.it

Specialty section:
This article was submitted to Child and Adolescent Psychiatry, a section of the journal Frontiers in Neuroscience

Received: *09 June 2017*
Accepted: *13 September 2017*
Published: *26 September 2017*

Citation:
Grecucci A, Siugzdaite R and Job R (2017) Editorial: Advanced Neuroimaging Methods for Studying Autism Disorder. Front. Neurosci. 11:533. doi: 10.3389/fnins.2017.00533

Two morphometric studies explore the possibility of structural differences in ASD individuals. Eilam-Stock et al. apply Voxel-based Morphometry to a large sample of ASD children, trying to overcome the limitations of previous studies that used smaller samples. Decreased gray matter volume in posterior brain regions, as well as increased gray matter volume in frontal brain regions, were found in individuals with ASD. Building on the limitations of univariate approaches to morphological analyses, Grecucci et al. applied for the first time a multivariate whole brain approach known as Source-based Morphometry (SBM). This method was used on ASD individuals and controls to detect maximally independent networks of gray matter. Group comparisons revealed a network comprising broad temporal and frontal regions differently expressed in ASD individuals that correlated with social and behavioral deficits.

Alterations in brain connectivity are explored in two papers. Chen et al. used a network logic to identify abnormal functional connectivity of resting state fMRI in ASD individuals. In another connectivity study, Lee et al. decompose the inter- and intra-hemispheric regions and compare the functional connectivity density (FCD) between ASD and controls, finding evidence of FCD decreases in subjects with ASD in the posterior cingulate cortex, lingual/parahippocampal gyrus, and postcentral gyrus.

Magnetoencephalography (MEG) has been used to find cortical activation differences in ASD individuals in two studies. Khan et al. applied a novel method that measured the spatio-temporal divergence of cortical activation. It was found that the ASD group, relative to controls, is characterized by an increase in the onset component of the cortical response, and a faster spread of local activity. In an attempt to integrate fMRI with Magnetoencephalography (MEG), Datko et al. explored the links between sources of MEG amplitude in various frequency bands and functional connectivity in resting state fMRI. Hypoconnectivity between many sources of low and high gamma activity was found. This may pave the way to study differences in functionally defined networks. These studies confirm and extend results using Electroencephalography (Murias et al., 2007; Coben et al., 2014; Boutros et al., 2015; Shou et al., 2017).

One of the main practical problems clinicians are faced with is the use of objective markers to diagnose autism. Three papers make relevant contributions to this problem. A useful approach that looks for informative biomarkers of pathology in the brain is a multivariate analysis techniques based on Support Vector Machines that has been explored by Retico et al. The authors used the One-Class Classification (OCC), a reliable method that could be used as a diagnostic tool looking at language and default mode network regions that contribute most to distinguishing individuals with ASD from controls. Carper et al. used for the first time Restriction Spectrum Imaging (RSI), a multi-shell diffusion-weighted imaging technique, to examine gray matter microstructure in ASD individuals and controls, making multi-shell diffusion imaging a promising technique to understand the underlying cytoarchitecture of ASD. Last but not least, Simas and Suckling in a short commentary discuss a graph theory approach, specifically a semi-metric analysis of the functional connectome that is both sensitive and specific to psychopathologies. This suggests that resting state data are a valuable measure on which several network connectivity analysis methods can be easily applied.

On the important issue of intervention, the paper by Sperdin and Schaer reviews the critical role of *orienting to speech* in ASD, as well as the neural substrates of human voice processing, and claim that aberrant voice processing could be a promising marker to identify ASD very early on. Calderoni et al. review the neural circuit modifications after non-pharmacological interventions and stress the importance of MRI evaluation for the detection of neural changes in response to treatment.

CONCLUSIONS AND FURTHER CONSIDERATIONS

The past 20 years witnessed a dramatic increase in the number of studies trying to uncover the pathophysiology of ASD. If it is true that neuroscience provided several proofs of abnormalities involved in autism, it is also true that this scientific endeavor failed in creating a coherent and clear picture of autism biology, so that the etiology of autism remains nowadays elusive. We suggest that in order to make progresses on this issue we need to (1) build explicit pathophysiologic models, (2) use advanced neuroimaging methods based on a whole brain and multivariate approaches; (3) integrate different neuroscientific methods (as well as other methodologies such as genetics, computational models, and other). About the first point, we believe that the practice of gathering new data not driven by explicit and testable models will not lead to a clear understanding of autism and will leave the field even more confused. Explicit pathological models are necessary to narrow down the number of factors to be taken into account. Computational methods like machine learning can find specific cerebral patterns for the disorder and classify them. For the second point, it is now clear that using a region of interest approach may obscure the importance of complex distributed networks. This is especially true for complex neuropsychiatric disorders such as autism. Third, we believe that every methodology is partial. We need to integrate data provided by different techniques in order to have a better understanding of how the brain creates autistic behavioral symptoms, and to increase the pace of a comprehensive view of autism.

AUTHOR CONTRIBUTIONS

AG wrote the editorial, RS and RJ significantly contributed to it.

ACKNOWLEDGMENTS

AG has been supported by a grant awarded by the The Neuropsychoanalysis Foundation, New York, USA.

REFERENCES

Boutros, N. N., Lajiness-O' Neill, R., Zillgitt, A., Richard, A. E., and Bowyer, S. M. (2015). EEG changes associated with autistic spectrum disorders. *Neuropsy. Electrophysiol.* 1:3. doi: 10.1186/s40810-014-0001-5

Christensen, D. L., Baio, J., Braun, K. V., Bilder, D., Charles, J., Constantino, J. N., et al. (2016). Prevalence and Characteristics of Autism Spectrum Disorder Among Children Aged 8 Years — Autism and Developmental Disabilities Monitoring Network, 11 Sites, United States, 2012. *MMWR Surveill Summ.* 65, 1–23. doi: 10.15585/mmwr.ss6503a1

Coben, R., Mohammad-Rezazadeh, I., and Cannon, R. L. (2014). Using quantitative and analytic EEG methods in the understanding of connectivity in autism spectrum disorders: a theory of mixed over- and under-connectivity. *Front. Hum. Neurosci.* 8:45. doi: 10.3389/fnhum.2014.00045

Murias, M., Webb, S. J., Greenson, J., and Dawson, G. (2007). Resting state cortical connectivity reflected in EEG coherence in individuals with autism. *Biol. Psychiatry* 62, 270–273. doi: 10.1016/j.biopsych.2006.11.012

Shou, G. F., Mosconi, M. W., Wang, J., Ethridge, L. E., Sweeney, J. A., and Ding, L. (2017). Electrophysiological signatures of atypical intrinsic brain connectivity networks in autism. *J. Neural Eng.* 14:046010. doi: 10.1088/1741-2552/aa6b6b

Conflict of Interest Statement: The authors declare that the research was conducted in the absence of any commercial or financial relationships that could be construed as a potential conflict of interest.

frontiers in Neuroscience

METHODS
published: 24 January 2017
doi: 10.3389/fnins.2017.00016

ANOCVA in R: A Software to Compare Clusters between Groups and Its Application to the Study of Autism Spectrum Disorder

Maciel C. Vidal[1], *João R. Sato*[2], *Joana B. Balardin*[3], *Daniel Y. Takahashi*[4] *and André Fujita*[1]*

[1] Department of Computer Science, Institute of Mathematics and Statistics, University of São Paulo, São Paulo, Brazil, [2] Center of Mathematics, Computation, and Cognition, Universidade Federal do ABC, Santo André, Brazil, [3] Hospital Israelita Albert Einstein, São Paulo, Brazil, [4] Deparment of Psychology and Princeton Neuroscience Institute, Princeton University, Princeton, NJ, USA

Understanding how brain activities cluster can help in the diagnosis of neuropsychological disorders. Thus, it is important to be able to identify alterations in the clustering structure of functional brain networks. Here, we provide an R implementation of Analysis of Cluster Variability (ANOCVA), which statistically tests (1) whether a set of brain regions of interest (ROI) are equally clustered between two or more populations and (2) whether the contribution of each ROI to the differences in clustering is significant. To illustrate the usefulness of our method and software, we apply the R package in a large functional magnetic resonance imaging (fMRI) dataset composed of 896 individuals (529 controls and 285 diagnosed with ASD—autism spectrum disorder) collected by the ABIDE (The Autism Brain Imaging Data Exchange) Consortium. Our analysis show that the clustering structure of controls and ASD subjects are different ($p < 0.001$) and that specific brain regions distributed in the frontotemporal, sensorimotor, visual, cerebellar, and brainstem systems significantly contributed ($p < 0.05$) to this differential clustering. These findings suggest an atypical organization of domain-specific function brain modules in ASD.

Keywords: Analysis of Cluster Variability, silhouette statistic, functional brain network, ABIDE, fMRI

OPEN ACCESS

Edited by:
Alessandro Grecucci, University of Trento, Italy

Reviewed by:
Munis Dundar, Erciyes University, Turkey
Baxter P. Rogers, Vanderbilt University, USA
Sydney Moirangthem, National Institute of Mental Health and Neurosciences, India

***Correspondence:**
André Fujita
fujita@ime.usp.br

Specialty section:
This article was submitted to Child and Adolescent Psychiatry, a section of the journal Frontiers in Neuroscience

Received: *27 July 2016*
Accepted: *09 January 2017*
Published: *24 January 2017*

Citation:
Vidal MC, Sato JR, Balardin JB, Takahashi DY and Fujita A (2017) ANOCVA in R: A Software to Compare Clusters between Groups and Its Application to the Study of Autism Spectrum Disorder. Front. Neurosci. 11:16. doi: 10.3389/fnins.2017.00016

INTRODUCTION

The brain activity is organized in clusters/modules that have different roles in our behavior (Tononi et al., 1999). Alterations in the clustering pattern can be associated with neurologic disorders (Grossberg, 2000; Sato et al., 2016). Thus, it is important to systematically discriminate the clustering structures among different populations. This leads to the problem of how to statistically test the equality of clustering structures of two or more populations and how to identify the features that contribute to the differential clustering structure. These statistical problems were recently solved for a large class of clustering algorithms by using the Analysis of Cluster Variability—ANOCVA (Fujita et al., 2014a).

Here, we provide an implementation of ANOCVA in R for a better dissemination of this technique in the scientific community. ANOCVA was designed to test whether the clustering structures of several populations are equal. Briefly, ANOCVA uses the silhouette statistic

(Rousseeuw, 1987) as a measure of variability of the clustering structure of each population and then compares the variability among populations using an idea similar to the classical analysis of variance (ANOVA). To calculate the statistical significance value, we use a bootstrap procedure that was previously shown to control the type I error.

We illustrate the step-by-step application of ANOCVA by analyzing a large functional magnetic resonance imaging (fMRI) data acquired under a resting-state protocol (ABIDE—The Autism Brain Imaging Data Exchange Consortium) composed of 529 controls and 285 patients diagnosed with autism. Subjects with Autism Spectrum Disorders (ASD) have significant differences in the resting state functional connectivity when compared to healthy subjects (for review, see Kana et al., 2011), suggesting that ASD is as a neural systems disorder with disruptions in several distributed neurocognitive networks of brain regions (Ecker et al., 2015). However, most studies describe integration (Washington et al., 2014; Sporns and Betzel, 2016) and segregation (Assaf et al., 2013) as separate processes. Instead, in this study we consider both processes simultaneously using the idea of clusters, where structures within are integrated and structures between are segregated.

MATERIALS AND METHODS

To formalize ANOCVA, we will first describe the silhouette statistic to define "clustering variability" and then we introduce the ANOCVA. Finally, we describe its implementation and application to ABIDE dataset.

The Silhouette Statistic

The silhouette statistic is a measure of how well an item (regions of interest—ROI in fMRI data) is clustered given a clustering algorithm. In other words, it can also be interpreted as a measure of clustering variability (Rousseeuw, 1987). Formally, let $\chi = \{x_1, .., x_N\}$ be the N ROIs of one subject that are clustered into $C = \{C_1, \ldots, C_r\}$ clusters by a clustering algorithm. Denote the dissimilarity between ROIs x and y by $d(x, y)$. Let $|C|$ be the number of ROIs of C. Then, define $d(x, C) = \frac{1}{|C|}\sum_{y\in C} d(x, y)$ as the average dissimilarity of x to all ROIs of cluster C. Denote $D_q \in C$ as the cluster to which x_q has been assigned by the clustering algorithm. Define $a_q = d(x_q, D_q)$ (the within dissimilarity of x_q) and $b_q = \min_{C_p \neq D_q} d(x_q, C_p)$ (the smallest between dissimilarity of x_q), for $q = 1, \ldots, N$. Then, we can measure how well each ROI x_q has been clustered by analyzing the silhouette statistic given by

$$s_q = \begin{cases} \frac{b_q - a_q}{\max\{b_q, a_q\}}, \text{ if } |D_q| > 1, \\ 0, \text{ if } |D_q| = 1. \end{cases}$$

The silhouette statistic s_q assumes values from -1 to $+1$ and its interpretation given by Rousseeuw (1987) is as follows. If $s_q \approx 1$, it means $a_q \ll b_q$, i.e., the ROI x_q has been assigned to an appropriate cluster because the second-best choice cluster is not as close as the actual cluster. If $s_q \approx 0$, then $a_q \approx b_q$. In this case, it is not clear whether ROI x_q should have been assigned to the actual cluster or to the second-best choice cluster because it is equally far away from both. If $s_q \approx -1$, then $a_q \gg b_q$. In other words, the ROI x_q should be assigned to the second-best choice cluster because it lies much closer to it than to the actual cluster. In summary, s_q is a measure of how well the clustering algorithm labeled ROI x_q.

ANOCVA

In the present section, we briefly describe the ANOCVA. For further details, refer to Fujita et al. (2014a). Let $T_1, T_2, \ldots, T_k$ be k types of populations (e.g., controls and ASD). For the j th population, n_j subjects are collected, for $j = 1, \ldots, k$. The items (e.g., ROIs) of the i th subject taken from the j th population are represented by the matrix $X_{i,j} = (x_{i,j,1}, \ldots, x_{i,j,N})$, where each ROI $x_{i,j,q}$ $(q = 1, .., N)$ is a vector containing a time series (the blood-oxygen-level dependent signal).

First, define the $(N \times N)$ matrix of dissimilarities among ROIs of each matrix $X_{i,j}$ by $A_{i,j} = \{d(x_{i,j,q}, x_{i,j,q'})\}$, for $i = 1, \ldots, n_j$, $j = 1, \ldots, k$. Second, let $n = \sum_{j=1}^{k} n_j$, then define the following average matrices of dissimilarities:

$$\bar{A}_j = \frac{1}{n_j}\sum\nolimits_{i=1}^{n_j} A_{i,j} = \frac{1}{n_j}\sum\nolimits_{i=1}^{n_j}\{d(x_{i,j,q}, x_{i,j,q'})\} \text{ and}$$

$$\bar{\bar{A}} = \frac{1}{n}\sum\nolimits_{j=1}^{k} n_j \bar{A}_j, \text{ where } q, q' = 1, \ldots, N.$$

Next, apply a clustering algorithm on the matrix of dissimilarities $\bar{\bar{A}}$, to determine the clustering labels $l_{\bar{\bar{A}}}$. Finally, compute the following silhouette statistics: $s_q^{(\bar{\bar{A}}, l_{\bar{\bar{A}}})}$ (the silhouette statistic of the qth ROI based on the dissimilarity matrix $\bar{\bar{A}}$ and the labeling $l_{\bar{\bar{A}}}$) and $s_q^{(\bar{A}_j, l_{\bar{\bar{A}}})}$ (the silhouette statistic of the qth ROI based on the dissimilarity matrix $\bar{A}_j$ and the labeling $l_{\bar{\bar{A}}}$), for $q = 1, \ldots, N$. The statistical test consists in verifying whether all k populations are equally clustered (present the same clustering structure) or if at least one is clustered in a different manner. If the ROIs from all populations $T_1, \ldots, T_k$ are equally clustered, then the quantities $s_q^{(\bar{\bar{A}}, l_{\bar{\bar{A}}})}$ and $s_q^{(\bar{A}_j, l_{\bar{\bar{A}}})}$ must be close for all $j = 1, \ldots, k$ and $q = 1, \ldots, N$.

Given a clustering algorithm and a distance metric, define the following vectors:

$$S = (s_1^{(\bar{\bar{A}}, l_{\bar{\bar{A}}})}, \ldots, s_N^{(\bar{\bar{A}}, l_{\bar{\bar{A}}})})^{\mathrm{T}} \text{ and } S_j = (s_1^{(\bar{A}_j, l_{\bar{\bar{A}}})}, \ldots, s_N^{(\bar{A}_j, l_{\bar{\bar{A}}})})^{\mathrm{T}}.$$

Define $\delta S_j = S - S_j$. We will use the statistic $\Delta S = \sum_{j=1}^{k} \delta S_j^{\mathrm{T}} \delta S_j$ to build the test statistic. Notice that under the null hypothesis, all N ROIs are equally clustered along the k populations, i.e., $s_q^{(\bar{\bar{A}}, l_{\bar{\bar{A}}})} \approx s_{q'}^{(\bar{\bar{A}}, l_{\bar{\bar{A}}})}$ for all $q = 1, \ldots, N$ and thus, we expect small ΔS. On the other hand, large ΔS suggests a rejection of the null hypothesis.

To test the contribution of each ROI for the differential clustering, define $\delta s_q = s_q^{(\bar{\bar{A}}, l_{\bar{\bar{A}}})} - \frac{1}{k}\sum_{j=1}^{k} s_q^{(\bar{A}_j, l_{\bar{\bar{A}}})}$, for $q = 1, \ldots, N$.

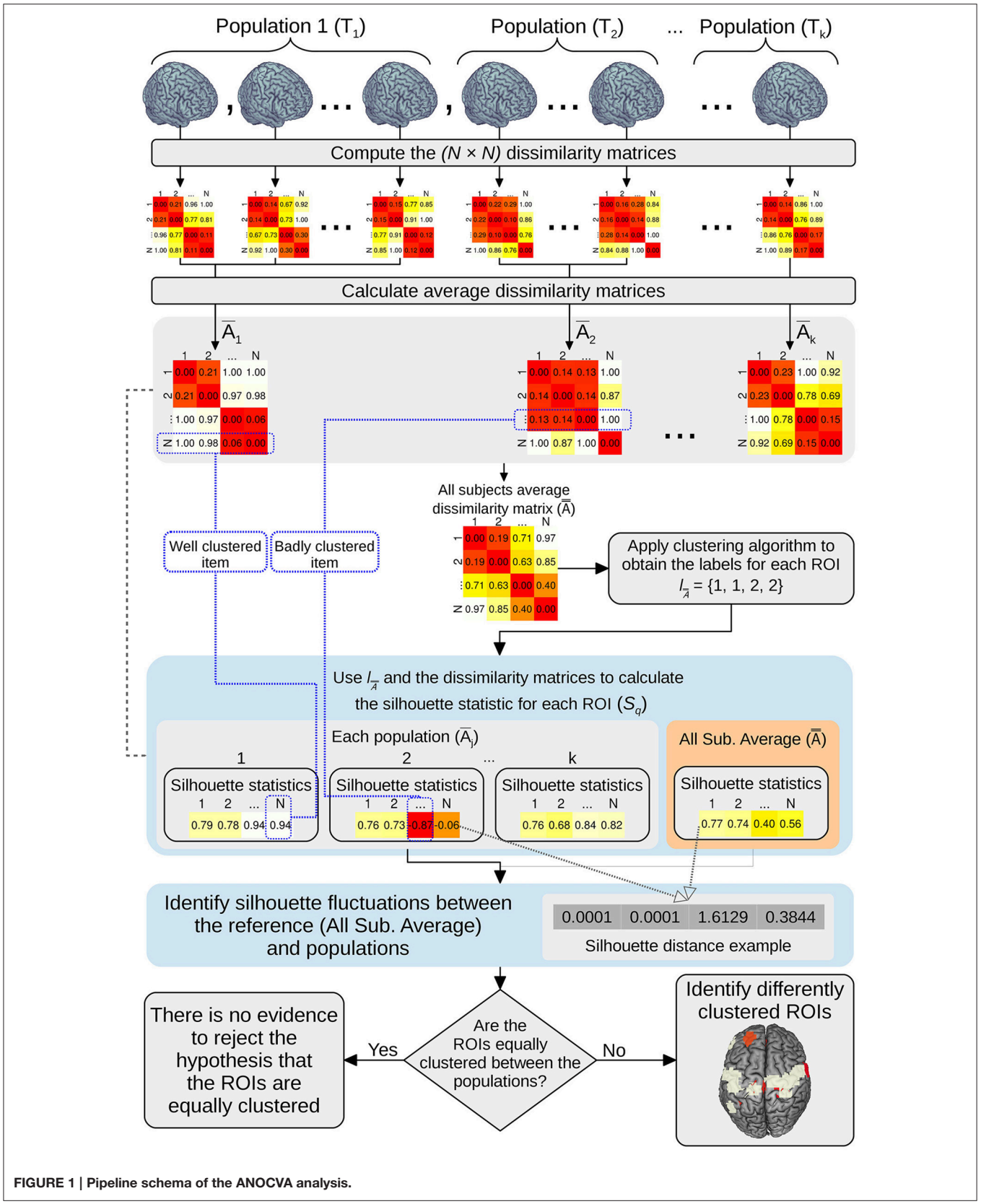

FIGURE 1 | Pipeline schema of the ANOCVA analysis.

This test consists in verifying whether the qth ROI ($q = 1, \ldots, N$) is equally clustered among populations. We will use the statistic $\Delta s_q = \delta s_q^2$, for $q = 1, \ldots, N$ to build the test statistic. Under the null hypothesis, we expect small Δs_q. On the other hand, large Δs_q suggests a rejection of the null hypothesis.

To compute distributions of ΔS and Δs_q under the null hypothesis, Fujita et al. (2014a) proposed a bootstrap procedure described as follows:

1. Resample with replacement n_j subjects from the entire dataset $\{T_1, T_2, \ldots, T_k\}$ in order to construct bootstrap samples T_j^*, for $j = 1, \ldots, k$.
2. Calculate $\bar{A}_j^*$, $\bar{\bar{A}}^*$, $s_q^{\left(\bar{A}, l=A\right)*}$ and $s_q^{\left(\bar{A}, l=A\right)*}$, for $q = 1, \ldots, N$, using the bootstrap samples T_j^*.
3. Calculate $\widehat{\Delta S}^*$ and $\widehat{\Delta s_q}^*$.
4. Repeat steps 1 to 3 until the desired number of bootstrap replications is obtained.
5. The p-values from the bootstrap tests based on the observed statistics ΔS and ΔS_q are the fraction of replicates of $\widehat{\Delta S}^*$ and $\widehat{\Delta s_q}^*$ on the bootstrap dataset T_j^*, respectively, that are at least as large as the observed statistics on the original dataset.

R Implementation

ANOCVA is implemented in R and is freely available at the R project website[1] (package "anocva").

This implementation requires as input, the functional brain networks (ROIs dissimilarity matrices), a vector of labels describing which individual belongs to which group, the number of clusters, and the number of bootstrap samples.

ANOCVA uses the spectral clustering algorithm to cluster the ROIs (Ng et al., 2002). Internal to the spectral clustering algorithm, we use the k -medoids procedure instead of the usual k -means because the former is more robust to outliers than the latter (Aggarwal and Reddy, 2013). If the number of clusters is not known a priori, the ANOCVA R package provides the option to estimate it by using the silhouette or the slope statistic (Fujita et al., 2014b). The slope criterion is the difference of the silhouette statistic as a function of the number of clusters. The difference between the slope and silhouette is the fact that by maximizing the silhouette statistic as described by Rousseeuw (1987) the number of clusters is estimated correctly only when the within-cluster variances are equal. The slope criterion is more robust than the silhouette when the within-cluster variances are unequal.

The output consists in one p-value, which represents whether there is at least one group that clusters in a different manner and a vector of p-values representing which ROI is differentially clustered among groups. The entire ANOCVA analysis pipeline can be visualized in **Figure 1**.

ABIDE Data Description and Pre-processing

The ABIDE Consortium dataset is a large resting state fMRI dataset that includes controls and ASD subjects. It can be downloaded from the ABIDE website[2]. This data was collected in 17 sites that compose the ABIDE Consortium. Data collection was conducted with local internal review board approval, and also in accordance with local internal review board protocols. For further details regarding this dataset, refer to the ABIDE Consortium website.

Data pre-processing and network construction (dissimilarity matrices) were carried out as our previous works (Sato et al., 2015, 2016) using the ABIDE dataset. The final dataset used here is composed of 529 controls (430 males, mean age ± standard deviation of 17.47 ± 7.81 years) and 285 autistic patients (255 males, 17.53 ± 7.13 years).

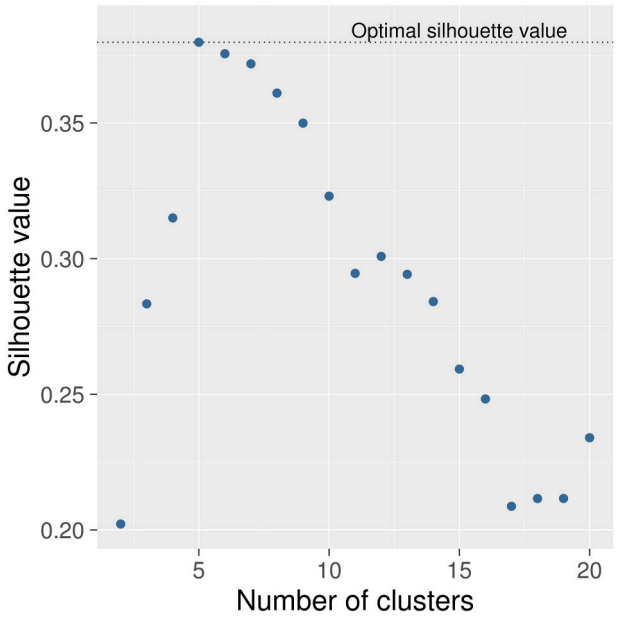

FIGURE 2 | Selection of the number of clusters. The number of clusters was selected by using the silhouette criterion. The number of clusters that presented the highest silhouette statistic is five. In other words, the silhouette criterion suggests that this dataset can be split into five sub-networks.

RESULTS

The problem that we want to solve is the following. Given k populations $T_1, T_2, \ldots, T_k$ where each population T_j ($j = 1, \ldots, k$) is composed of n_j subjects, and each subject has N items that are clustered, we would like to verify whether the clustering structures of the brain networks of the k populations are equal and, if not, which ROIs are differently clustered. In our case, we have $k = 2$ populations with T_1 and T_2 as controls and ASD, respectively. The number of subjects in each population is $n_1 = 529$ and $n_2 = 285$, for T_1 and T_2, respectively. The number of ROIs (items) to be clustered is $N = 316$. Since head movement during magnetic resonance scanning may affect statistical analysis, ANOCVA was

[1]www.r-project.org

[2]http://fcon_1000.projects.nitrc.org/indi/abide/

applied to both "scrubbed" and "not scrubbed" data (Power et al., 2012) with the number of bootstrap samples set to 1000.

The first step in ANOCVA analysis is the construction of the average dissimilarity matrix $\overline{\overline{A}}$ and its clustering. The estimated number of clusters by the silhouette criterion was five as depicted in **Figure 2**. Notice that the highest silhouette statistic was obtained when the number of clusters is five. The sub-networks obtained by applying the spectral clustering on the dissimilarity matrix $\overline{\overline{A}}$ can be visualized in **Figure 3** where each color represents one sub-network (cluster).

Then, ANOCVA calculates the silhouette statistic for each ROI by using the labels obtained by clustering the dissimilarity matrix $\overline{\overline{A}}$ and performs the test. We verified that in fact the entire clustering structure of subjects diagnosed with ASD differs from controls ($p < 0.001$). Next, we tested each ROI to identify which ones significantly contribute to the differential clustering between controls and subjects diagnosed with ASD. ROIs that presented a difference in $p > 5\%$ between "scrubbed" and "not scrubbed" datasets were excluded for subsequent analysis. Remaining p-values were corrected for multiple comparisons by the Bonferroni method. **Figure 4** illustrates the statistically significant ROIs at a p-value threshold of 0.05 after Bonferroni correction. The highlighted regions include portions of the cerebellum and middle frontal gyrus, pre- and post-central gyri, inferior temporal gyrus, and lateral occipital cortex.

DISCUSSION

In the current study, we combined spectral clustering analysis with ANOCVA implemented in R to investigate which brain regions are clustered in a different way between controls and ASD groups. Our results suggest that several regions distributed across different neurocognitive systems significantly contributed to the different clustering network structure observed in ASD. First we demonstrated that the spectral clustering method yielded partitions that were well-characterized as functional modules of the brain that have been consistently identified in previous studies using different approaches (Damoiseaux et al., 2006; Power et al., 2011), including the fronto-temporal, sensorimotor, visual, and cerebellar systems. This is consistent with the hypothesis that the spectral clustering algorithm groups anatomically contiguous and also spatially distributed areas with common brain functionalities in the same cluster. Then, using ANOCVA we showed that the superior division of the lateral parietal cortex, precentral, and postcentral gyri, anterior dorsal middle frontal gyrus, and a medial portion of the cerebellum and of the brainstem have a distinct cluster organization between ASD and controls. All these brain regions have been previously identified as presenting ASD-related differences in studies using functional MRI. For example, the recruitment of portions of the precentral and postcentral gyri as well as the cerebellum across sensorimotor tasks are atypical in ASD, and may underlie deficits in fine motor sequencing and visual motor learning observed in autistic individuals (Müller et al., 2001; Mostofsky et al., 2009).

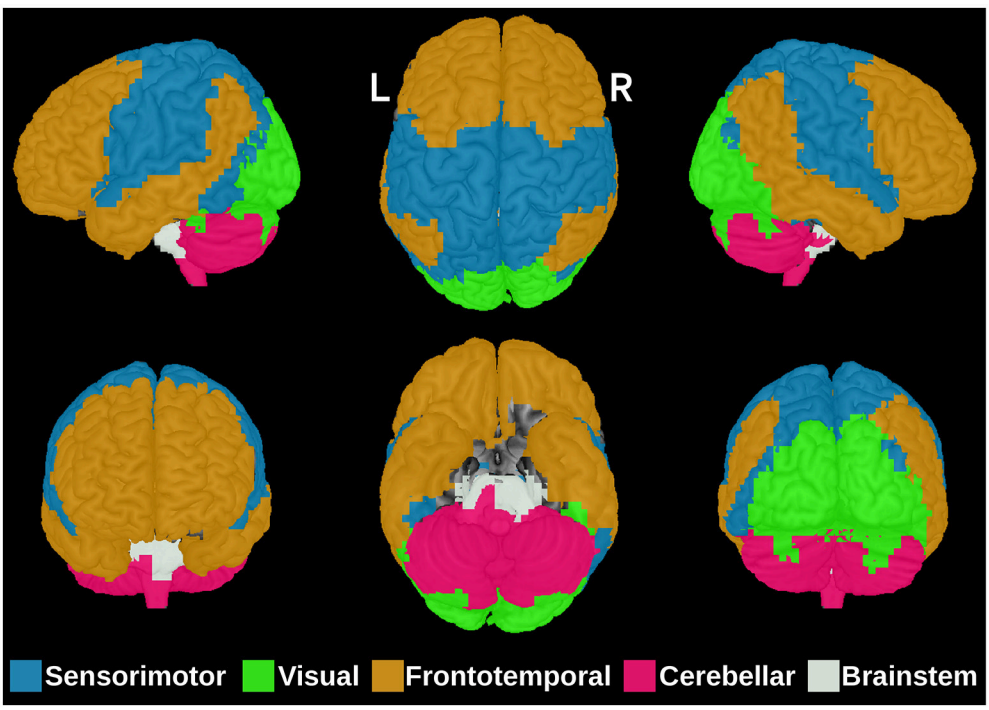

FIGURE 3 | The five brain sub-networks obtained by the spectral clustering algorithm on the dissimilarity matrix $\overline{\overline{A}}$. Each color represents one functional sub-network: sensorimotor (blue), visual (green), frontotemporal (orange), cerebellar (pink), and brainstem (white). R, right; L, Left.

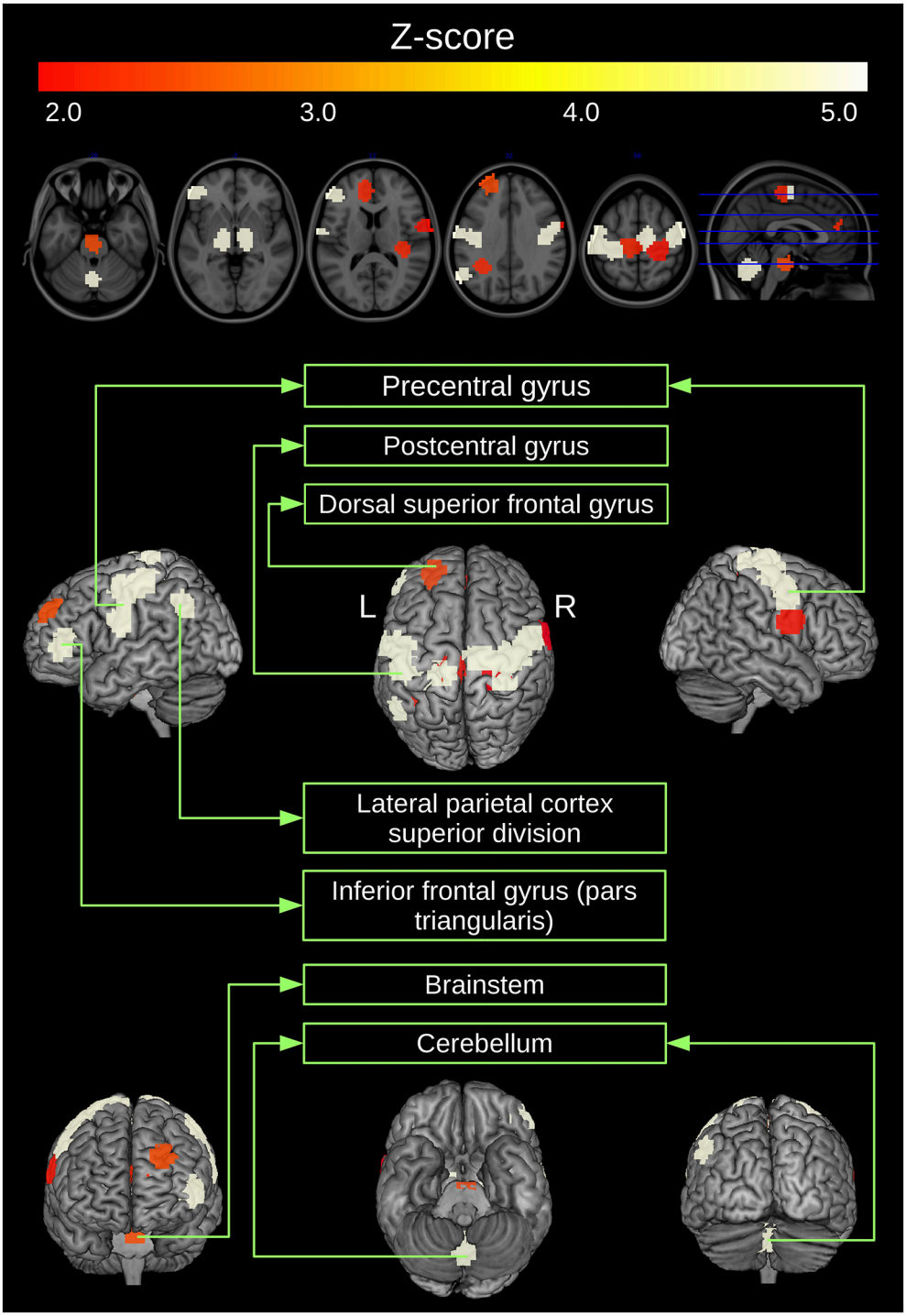

FIGURE 4 | ROIs clustered in a different manner between controls and ASD. ROIs that present a *p*-value (obtained by ANOCVA) lower than 5% after Bonferroni correction were converted to *z*-scores and highlighted.

Interestingly, these regions have also been implicated in cognitive process crucial for interpersonal interactions such as theory-of-mind (Martineau et al., 2010; Wang et al., 2014). This suggests that these areas are involved in the social communication deficits that are a core clinical feature of ASD. Moreover, the lateral parietal cortex is an important node of the default-mode network, and abnormalities in the connectivity between nodes of this network have been widely investigated in ASD (Kennedy and

Courchesne, 2008; Assaf et al., 2010; Weng et al., 2010) giving its associations with social cognition (Buckner et al., 2008). The identification of these regions by our study therefore confirms that they are key brain structures in ASD that may have a role in the development of sub-networks organization in this population.

Head motion is one of the most challenging obstacles in functional connectivity studies involving clinical populations, which usually present high levels of movement. Our attempt to handle this problem was to apply the scrubbing method proposed by Power et al. (2012), which discards scans acquired under excessive head motion. However, although this approach may reduce the influence of movement artifacts, they may still be present in the scrubbed data. Thus, we opted for a more conservative approach, which consisted in excluding the regions where the *p*-values were more sensitive to scrubbing. We assumed that the analyses of these regions were more vulnerable to artifacts and thus they were removed. This approach is also helpful to reduce the number of multiple comparisons, by excluding the less reliable tests. Another important limitation to be mentioned is that the ABIDE data is multicentric with heterogeneous acquisition parameters across sites. We minimized the site effect by removing it in the pre-processing stage of the data. Finally, all analyses are based on the CC400 atlas (Craddock et al., 2012), obtained by using a functional parcellation. Since other atlases are different on ROIs size, number of ROIs and spatial location, the parcellation choice is expected to influence our findings. However, this variability does not invalidate the results obtained with CC400 because the procedures adopted here are conservative (regarding type I error control). Finally, an important future question for the presented results is whether the contribution of these specific brain regions to a differential network clustering in ASD is static or may exhibit dynamic changes during rest (Hutchison et al., 2013).

AUTHOR CONTRIBUTIONS

MV, JS, DT, and AF designed the work. MV pre-processed and analyzed the data. JS and JB interpreted the results. All authors drafted the work, read, and approved the final version of the manuscript.

FUNDING

MV was supported by CAPES and CNPq Fellowships. JS was supported by State of São Paulo Research Foundation—FAPESP (#2013/10498-6). DT was partially supported by Pew Latin American Fellowship and Ciência sem Fronteiras Fellowship (CNPq #246778/2012-1). AF was partially supported by FAPESP (#2014/09576-5, #2013/01715-3, #2015/01587-0, #2016/13422-9, and #2013/03447-6), CNPq (#304020/2013-3 and #473063/2013-1), and NAP eScience—PRP—USP.

ACKNOWLEDGMENTS

The authors would like to thank the ABIDE Consortium for providing publicly available the fMRI database.

REFERENCES

Aggarwal, C. C., and Reddy C. K. (eds.). (2013). *Data Clustering: Algorithms and Applications*. Boca Raton, FL: CRC Press.

Assaf, M., Hyatt, C. J., Wong, C. G., Johnson, M. R., Schultz, R. T., Hendler, T., et al. (2013). Mentalizing and motivation neural function during social interactions in autism spectrum disorders. *Neuroimage Clin.* 3, 321–31. doi: 10.1016/j.nicl.2013.09.005

Assaf, M., Jagannathan, K., Calhoun, V. D., Miller, L., Stevens, M. C., Sahl, R., et al. (2010). Abnormal functional connectivity of default mode subnetworks in autism spectrum disorder patients. *NeuroImage* 53, 247–256. doi: 10.1016/j.neuroimage.2010.05.067

Buckner, R. L., Andrews-Hanna, J. R., Schacter, D. L. (2008). The brain's default network: anatomy, function, and relevance to disease. *Ann. N. Y. Acad. Sci.* 1124, 1–38. doi: 10.1196/annals.1440.011

Craddock, R. C., James, G. A., Holtzheimer, P. E., Hu, X. P., Mayberg, H. S. (2012). A whole brain fMRI Atlas generated via spatial constrained spectral clustering. *Hum. Brain Mapp.* 33, 1914–1928. doi: 10.1002/hbm.21333

Damoiseaux, J. S., Rombouts, S. A., Barkhof, F., Scheltens, P., Stam, C. J., Smith, S. M., et al. (2006). Consistent resting-state networks across healthy subjects. *Proc. Natl. Acad. Sci. U.S.A.* 103, 13848–13853. doi: 10.1073/pnas.0601417103

Ecker, C., Bookheimer, S. Y., Murphy, D. G. (2015). Neuroimaging in autism spectrum disorder: brain structure and function across the lifespan. *Lancet Neurol.* 14, 1121–1134. doi: 10.1016/S1474-4422(15)00050-2

Fujita, A., Takahashi, D. Y., Patriota, A. G. (2014b). A non-parametric method to estimate the number of clusters. *Comput. Stat. Data Anal.* 73, 27–39. doi: 10.1016/j.csda.2013.11.012

Fujita, A., Takahashi, D. Y., Patriota, A. G., Sato, J. R. (2014a). A non-parametric statistical test to compare clusters with applications in functional magnetic resonance imaging data. *Stat. Med.* 33, 4949–4962.

Grossberg, S. (2000). The complementary brain: unifying brain dynamics and modularity. *Trends Cogn. Sci.* 4, 233–246. doi: 10.1016/S1364-6613(00)01464-9

Hutchison, R. M., Womelsdorf, T., Allen, E. A., Bandettini, P. A., Calhoun, V. D., Corbetta, M., et al. (2013). Dynamic functional connectivity: promise, issues, and interpretations. *NeuroImage* 80, 360–378. doi: 10.1016/j.neuroimage.2013.05.079

Kana, R. K., Libero, L. E., Moore, M. S. (2011). Disrupted cortical connectivity theory as an explanatory model for autism spectrum disorders. *Phys. Life Rev.* 8, 410–437. doi: 10.1016/j.plrev.2011.10.001

Kennedy, D. P., and Courchesne, E. (2008). Functional abnormalities of the default network during self- and other-reflection in autism. *Soc. Cogn. Affect. Neurosci.* 3, 177–190. doi: 10.1093/scan/nsn011

Martineau, J., Andersson, F., Barthélémy, C., Cottier, J. P., and Destrieux, C. (2010). Atypical activation of the mirror neuron system during perception of hand motion in autism. *Brain Res.* 1320, 168–75. doi: 10.1016/j.brainres.2010.01.035

Mostofsky, S. H., Powell, S. K., Simmonds, D. J., Goldberg, M. C., Caffo, B., and Pekar, J. J. (2009). Decreased connectivity and cerebellar activity in autism during motor task performance. *Brain* 132, 2413–2425. doi: 10.1093/brain/awp088

Müller, R. A., Pierce, K., Ambrose, J. B., Allen, G., and Courchesne, E. (2001). Atypical patterns of cerebral motor activation in autism: a functional magnetic resonance study. *Biol. Psychiatry* 49, 665–676. doi: 10.1016/S0006-3223(00)01004-0

Ng, A., Jordan, M., and Weiss, Y. (2002). "On spectral clustering: analysis and an algorithm," in *Advances in Neural Information Processing Systems,* Vol. 14, eds T. Dietterich, S. Becker, and Z. Ghahramani (London: MIT Press), 849–856.

Power, J. D., Barnes, K. A., Snyder, A. Z., Schlaggar, B. L., Petersen, S. E. (2012). Spurious but systematic correlations in functional connectivity MRI networks arise from subject motion. *NeuroImage* 59, 2142–2154. doi: 10.1016/j.neuroimage.2011.10.018

Power, J. D., Cohen, A. L., Nelson, S. M., Wig, G. S., Barnes, K. A., Church, J. A., et al. (2011). Functional network organization of the human brain. *Neuron* 72, 665–78. doi: 10.1016/j.neuron.2011.09.006

Rousseeuw, P. (1987). Silhouettes: a graphical aid to the interpretation and validation of cluster analysis. *J. Comput. Appl. Math.* 20, 53–65. doi: 10.1016/0377-0427(87)90125-7

Sato, J. R., Balardin, J. B., Vidal, M. C., and Fujita, A. (2016). Identification of segregated regions in the functional brain connectome of autistic patients by a combination of fuzzy spectral clustering and entropy analysis. *J. Psychiatry Neurosci.* 41, 124–132. doi: 10.1503/jpn.140364

Sato, J. R., Vidal, M. C., de Siqueira Santos, S., Massirer, K. B., and Fujita, A. (2015). Complex networks measures in autism spectrum disorders. *IEEE/ACM Trans. Comput. Biol. Bioinform.* doi: 10.1109/TCBB.2015.2476787. [Epub ahead of print].

Sporns, O., and Betzel, R. (2016). Modular brain networks. *Annu. Rev. Psychol.* 67, 613–640. doi: 10.1146/annurev-psych-122414-033634

Tononi, G., Sporns, O., and Edelman, G. M. (1999). Measures of degeneracy and redundancy in biological networks. *Proc. Natl. Acad. Sci. U.S.A.* 96, 3257–3262. doi: 10.1073/pnas.96.6.3257

Wang, S. S., Kloth, A. D., and Badura, A. (2014). The cerebellum, sensitive periods, and autism. *Neuron* 83, 518–532. doi: 10.1016/j.neuron.2014.07.016

Washington, S. D., Gordon, E. M., Brar, J., Warburton, S., Sawyer, A. T., Wolfe, A., et al. (2014). Dysmaturation of the default mode network in autism. *Hum. Brain Mapp.* 35, 1284–1296. doi: 10.1002/hbm.22252

Weng, S. J., Wiggins, J. L., Peltier, S. J., Carrasco, M., Risi, S., Lord, C., et al. (2010). Alterations of resting state functional connectivity in the default network in adolescents with autism spectrum disorders. *Brain Res.* 1313, 202–14. doi: 10.1016/j.brainres.2009.11.057

Conflict of Interest Statement: The authors declare that the research was conducted in the absence of any commercial or financial relationships that could be construed as a potential conflict of interest.

frontiers in Neuroscience

METHODS
published: 23 August 2016
doi: 10.3389/fnins.2016.00371

Noise Reduction in Arterial Spin Labeling Based Functional Connectivity Using Nuisance Variables

Kay Jann[1], Robert X. Smith[1], Edgar A. Rios Piedra[1], Mirella Dapretto[2] and Danny J. J. Wang[1]*

[1] *Laboratory of FMRI Technology, Department of Neurology, University of California Los Angeles, Los Angeles, CA, USA,*
[2] *Department of Psychiatry and Biobehavioral Sciences, University of California Los Angeles, Los Angeles, CA, USA*

Arterial Spin Labeling (ASL) perfusion image series have recently been utilized for functional connectivity (FC) analysis in healthy volunteers and children with autism spectrum disorders (ASD). Noise reduction by using nuisance variables has been shown to be necessary to minimize potential confounding effects of head motion and physiological signals on BOLD based FC analysis. The purpose of the present study is to systematically evaluate the effectiveness of different noise reduction strategies (NRS) using nuisance variables to improve perfusion based FC analysis in two cohorts of healthy adults using state of the art 3D background-suppressed (BS) GRASE pseudo-continuous ASL (pCASL) and dual-echo 2D-EPI pCASL sequences. Five different NRS were performed in healthy volunteers to compare their performance. We then compared seed-based FC analysis using 3D BS GRASE pCASL in a cohort of 12 children with ASD (3f/9m, age 12.8 ± 1.3 years) and 13 typically developing (TD) children (1f/12m; age 13.9 ± 3 years) in conjunction with NRS. Regression of different combinations of nuisance variables affected FC analysis from a seed in the posterior cingulate cortex (PCC) to other areas of the default mode network (DMN) in both BOLD and pCASL data sets. Consistent with existing literature on BOLD-FC, we observed improved spatial specificity after physiological noise reduction and improved long-range connectivity using head movement related regressors. Furthermore, 3D BS GRASE pCASL shows much higher temporal SNR compared to dual-echo 2D-EPI pCASL and similar effects of noise reduction as those observed for BOLD. Seed-based FC analysis using 3D BS GRASE pCASL in children with ASD and TD children showed that noise reduction including physiological and motion related signals as nuisance variables is crucial for identifying altered long-range connectivity from PCC to frontal brain areas associated with ASD. This is the first study that systematically evaluated the effects of different NRS on ASL based FC analysis. 3D BS GRASE pCASL is the preferred ASL sequence for FC analysis due to its superior temporal SNR. Removing physiological noise and motion parameters is critical for detecting altered FC in neurodevelopmental disorders such as ASD.

Keywords: functional connectivity (FC), noise reduction, default mode network (DMN), arterial spin labeling (ASL), blood oxygenation level dependent (BOLD), cerebral blood flow (CBF)

OPEN ACCESS

Edited by:
Alessandro Grecucci, University of Trento, Italy

Reviewed by:
Roberto Viviani, University of Innsbruck, Austria
Weiying Dai, Binghamton University, USA

****Correspondence:***
Kay Jann
kay.jann@loni.usc.edu

Specialty section:
This article was submitted to Child and Adolescent Psychiatry, a section of the journal Frontiers in Neuroscience

Received: *29 January 2016*
Accepted: *29 July 2016*
Published: *23 August 2016*

Citation:
Jann K, Smith RX, Rios Piedra EA, Dapretto M and Wang DJJ (2016) Noise Reduction in Arterial Spin Labeling Based Functional Connectivity Using Nuisance Variables. Front. Neurosci. 10:371. doi: 10.3389/fnins.2016.00371

INTRODUCTION

Functional connectivity (FC) analysis to compute functionally connected networks (FCNs) has become a major imaging approach to investigate the brain's organization and function. Moreover, comparing different cohorts such as elderly subjects to young adults, or healthy control groups to psychiatric populations, have identified patterns of altered connectivity within specific FCNs. In the past few years, however, it has become evident that there are several potential confounding factors that may lead to spurious findings when not properly addressed. Physiological noise such as fluctuations in respiratory and cardiac cycles or head movements can influence BOLD signal intensities in fMRI. This is particularly relevant since different study cohorts could exhibit different patterns or amounts of such confounding factors (e.g., children, elderly, and psychiatric patients tend to have more difficulties to lay motionless inside the MR scanner). Accordingly, using nuisance variables to account for noise related signal fluctuations in BOLD-fMRI based FC analysis has been shown to be imperative to minimize or avoid potential confounding effects of motion or other physiological factors (e.g., respiration and heart rate) on network connectivity measures (Murphy et al., 2013).

Physiological fluctuations or changes in cardiac pulsation and respiratory cycles can cause changes in blood CO_2 pressure (Wise et al., 2004), which in turn influences the BOLD signal. Hence variability in respiration and cardiac pulsation could give rise to spuriously correlated signals in distributed brain areas (Birn, 2012). Furthermore, the set of brain areas affected by these physiological fluctuations could resemble the patterns associated with certain FCNs (Birn et al., 2008). Accordingly, separating physiological noise from BOLD signal fluctuations increases sensitivity for detecting neuronal related FCNs. While these variations in physiological parameters are ideally measured by concurrent recordings with pulse oximetry and respiration belt (Chang and Glover, 2009b), data driven techniques have been proposed to estimate nuisance regressors from the fMRI data itself. Furthermore, regions that are unlikely to exhibit neuronal related BOLD signal changes such as in cerebro-spinal fluid (CSF) or white matter (WM) have been used to efficiently remove these physiological variations (Birn et al., 2008; Weissenbacher et al., 2009).

In addition to physiological noise, recent observations indicate also that head movements during the MR acquisition can have detrimental effects on FC measures (Power et al., 2012; Satterthwaite et al., 2012; Van Dijk et al., 2012). Head motion in the magnetic field perturbs the spin history and can introduce spurious signal variances that tend to be more similar locally than between distant brain areas. This biases FC analyses toward increased local correlations and reduced long-range correlations, a critical issue when comparing subject cohorts that might differ in their ability to lie still (e.g., children or psychiatric patients). Indeed children and psychiatric cohorts have displayed this pattern of increased local but reduced long-range FC, raising the critical question as to whether and to what extent these findings reflect motion effects. A variety of approaches to deal with motion effects in FC analyses have since been proposed, most of which include nuisance variables to regress out potential signal fluctuations related to head movements by using motion parameters estimated from rigid body volume alignments (for review see Power et al., 2015). In summary, in BOLD fcMRI several confounding factors have been identified and strategies have been proposed to minimize their influences.

Besides BOLD fcMRI, Arterial Spin Labeling (ASL) datasets have been recently used to compute FCNs (Viviani et al., 2011; Liang et al., 2012; Jann et al., 2015a) (review Chen et al., 2015).This approach was made feasible by technical advances in state-of-the-art ASL pulse sequences resulting in improved signal-to-noise ratio (SNR) and temporal stability (Chen et al., 2011; Vidorreta et al., 2013). These technical advances include pseudo-continuous ASL (pCASL) (Wu et al., 2007; Dai et al., 2008), background suppression and three-dimensional (3D) fast imaging sequences such as GRASE (a hybrid of gradient and spin echo) or stack of spirals. In addition to improved acquisition techniques, physiological noise regression in ASL has been shown to increase temporal SNR (Wang, 2012). To date, however, no study has systematically investigated the effect of noise reduction, using the same nuisance variables as proposed for BOLD, on ASL based FC. Therefore, the primary purpose of this study was to investigate the effect of motion and physiological noise reduction on ASL based FC. A second goal of this study was to apply the optimal noise-reduction strategy for ASL based FC analysis in a cohort of children with autism spectrum disorders (ASD) and typically developing children.

METHODS

All adult neurotypical participants in this study gave written informed consent according to a research protocol approved by the UCLA Institutional Review Board. Inclusion criteria of healthy volunteers included no history of psychiatric or neurological disorders, and no contraindications to MRI scan. Scans were performed on a 3T Siemens TIM Trio scanner, using body coil as the transmitter and 12-ch head coil as the receiver. We acquired ASL and BOLD data in 10 healthy young participants (6f/4m; age [mean $\pm$ sd] $=$ 22 $\pm$ 3 years) with a 3D background-suppressed (BS: 85% suppression) GRASE pCASL sequence (60 label/control pairs, TR/TE/τ/PLD $=$ 4000/22/1200/1000 ms; 26 slices, 64 $\times$ 64 matrix, voxel-size 3.44 $\times$ 3.44 $\times$ 5 mm^3) and a standard 2D EPI BOLD sequence (240 Volumes, TR/TE $=$ 2000/30 ms, 30 slices, 64 $\times$ 64 matrix, slice thickness $=$ 4 mm with 1 mm gap). For comparison, a separate cohort of 10 healthy volunteers (7f/3m; age [mean $\pm$ sd] $=$ 25.7 $\pm$ 8 years) underwent resting state fMRI scans using a dual-echo 2D EPI pCASL sequence (128 label/control pairs, TR/TE1/TE2/τ/PLD $=$ 4000/10/25/1200/1500 ms; 18 slices, 64 $\times$ 64 matrix, voxel-size 3.44 $\times$ 3.44 $\times$ 6 mm^3) to simultaneously acquire ASL and BOLD data. All datasets were first realigned to account for spatial motion displacements (for ASL separately for label and control images). Five different regression models using

different sets of nuisance variables [here termed Noise Reduction Strategies (NRS)] were then performed:

- *NRS1*: no nuisance variables for noise reduction.
- *NRS2*: 6 motion parameters (3 translations x, y, z and 3 rotations α, β, γ) and their 1st derivatives.
- *NRS3*: same as NRS2 plus additional regressor for Framewise Displacement (FD). FD was computed following the procedure described by Power et al. (2012). Rotational displacements were recomputed to millimeters of displacement on a sphere with 5 cm radius. The volume by volume (framewise) head displacement in translational and recomputed rotational parameters were then calculated and summed up. Mean FD (±SD) in mm for the groups in each dataset were: 3D GRASE pCASL 0.244 (±0.065), standard BOLD 0.192 (±0.060), 2D dual-echo pCASL 0.179 (±0.066) and dual-echo BOLD 0.153 (±0.049). *T*-tests did not reveal a significant difference between ASL and BOLD within the groups ($t_{3D} = 1.81$; $p = 0.086/t_{2D} = 0.996$; $p = 0.333$), nor between groups for BOLD ($t = 1.612$; $p = 0.124$). There was a small difference showing slightly higher motion in 3D pCASL than 2D pCASL ($t = -2.194$; $p = 0.042$).
- *NRS4*: White matter and CSF fluctuations (mean signal fluctuations within brain segmentation tissue probability masks thresholded at 0.95 for WM and 0.85 for CSF and coregistered/resampled to functional images).
- *NRS5*: NRS3 + NRS4.

CBF images were computed for all NRSs (one compartment model, pair-wise subtraction of Label/Control images) (Alsop et al., 2015). BOLD and CBF images were coregistered to individual anatomical scans, normalized to MNI template and smoothed with an 8 mm FWHM Gaussian kernel.

Connectivity Analysis

FC analysis was performed with Seed Based Correlation Analysis (SBA) using the posterior cingulate cortex (PCC) as a seed (template seed from Shirer et al., 2012) to identify the Default Mode Network (DMN). DMN maps for each NRS in all four datasets as well as overall DMNs for the four datasets were calculated by one-sample *t*-tests to identify all areas with correlations significantly greater than zero across all subjects. We determined the similarity of the DMN maps derived using different NRSs between each other as well as to a template BOLD-DMN (Shirer et al., 2012) and template ASL-DMN (Jann et al., 2015a) using Dice Similarity Coefficients (Dice, 1945; Jann et al., 2015a), which compares the number of common voxels between two maps based on the formula $DSC(A,B) = 2(A \cap B)/(A + B)$, where A and B are the two maps.

To investigate the effect of NRS on the often-discussed long-range connectivity between PCC and anterior cingulate/medial prefrontal cortex (ACC/mPFC) (Power et al., 2012, 2015; Satterthwaite et al., 2012; Van Dijk et al., 2012), we calculated the correlation between those two ROIs based on the template DMN nodes (Shirer et al., 2012) using different NRSs. FC changes due to different NRSs were further investigated by a voxel-wise analysis on the individual subjects' SBA connectivity maps for each NRS by computing voxel-wise repeated-measures ANOVA and *post-hoc* ROI based paired *t*-tests.

Distance Related Effects of Motion

We further investigated the relationship between spatial distance, the use of head motion related nuisance variables and FC changes in BOLD and pCASL data, respectively. Specifically, we parcellated the brain into 264 spherical ROIs defined by the Power-Atlas (Power et al., 2012). For the parcellated data we then computed the cross-correlation matrix using data processed with NRS4 (WM/CSF regression only) and NRS5 (WM/CSF regression + motion regression), respectively. Subtraction of the two cross-correlation matrices provides the difference in connectivity between any two ROIs (ΔFC) between NRS5 and NRS4. Plotting these ΔFC values against the Euclidean distance between the respective ROIs and fitting a linear equation to these plots examined the presence of a relation between ΔFC and spatial distance (Power et al., 2014, 2015).

Effects on Temporal SNR and Global-CBF Quantification

Finally, we estimated tSNR within gray matter and performed an ANOVA on these values to test for significant improvements in tSNR following noise reduction. Global mean CBF was also compared to test whether NRS affects mean CBF quantification between the two pCASL sequences.

Application of NRS in Children with ASD

To investigate the effects of NRS on seed-based FC analysis in a clinical cohort, we compared FC differences between a group of 12 children with ASD (3f/9m, age 12.8 ± 1.3 years; IQ = 107.0 ± 14.9) and an age and IQ matched group of 13 typically developing (TD) children (1f/12m; age 13.9 ± 3 years; IQ = 104.8 ± 14.4). Subjects and parents provided written consent according to the guidelines specified by the UCLA Institutional Review Board. Clinical diagnosis of ASD was confirmed with the Autism Diagnostic Observation Schedule (ADOS; Lord et al., 2000), Autism Diagnostic Interview-Revised (ADI-R; Lord et al., 1994) and best clinical judgment. Mean ADOS severity score was 7.6 (range 6–10). Statistical tests to compare group characteristics were not significant: Mann-Whitney *U*-Test for age ($U = 44$, $z = 1.822$, $p = 0.068$) and IQ ($U = 73.5$, $z = -0.2178$, $p = 0.826$) and Chi-square test with Yates correction for small samples for gender (0.401, $p = 0.527$).

We used the 3D BS GRASE pCASL sequence to acquire CBF data in these two groups given its favorable temporal characteristics shown in the above analyses. Preprocessing was identical as described above and NRS4 and NRS5 were compared to NRS1 in these cohorts. FC from the PCC-seed was computed for each subject and NRS. Within group analyses included comparisons between NRSs using voxel-wise paired-sample *t*-tests. In addition, between-group comparisons were performed by voxel-wise two-sample *t*-tests (correction for multiple comparison at $\alpha < 0.05$ was done by cluster-size estimation, CSE for NRS0 = 133 voxels, NRS4 = 115 voxels and NRS5 = 114 voxels). This analysis will reveal the effects of different NRSs on the outcome of ASL-FC differences between

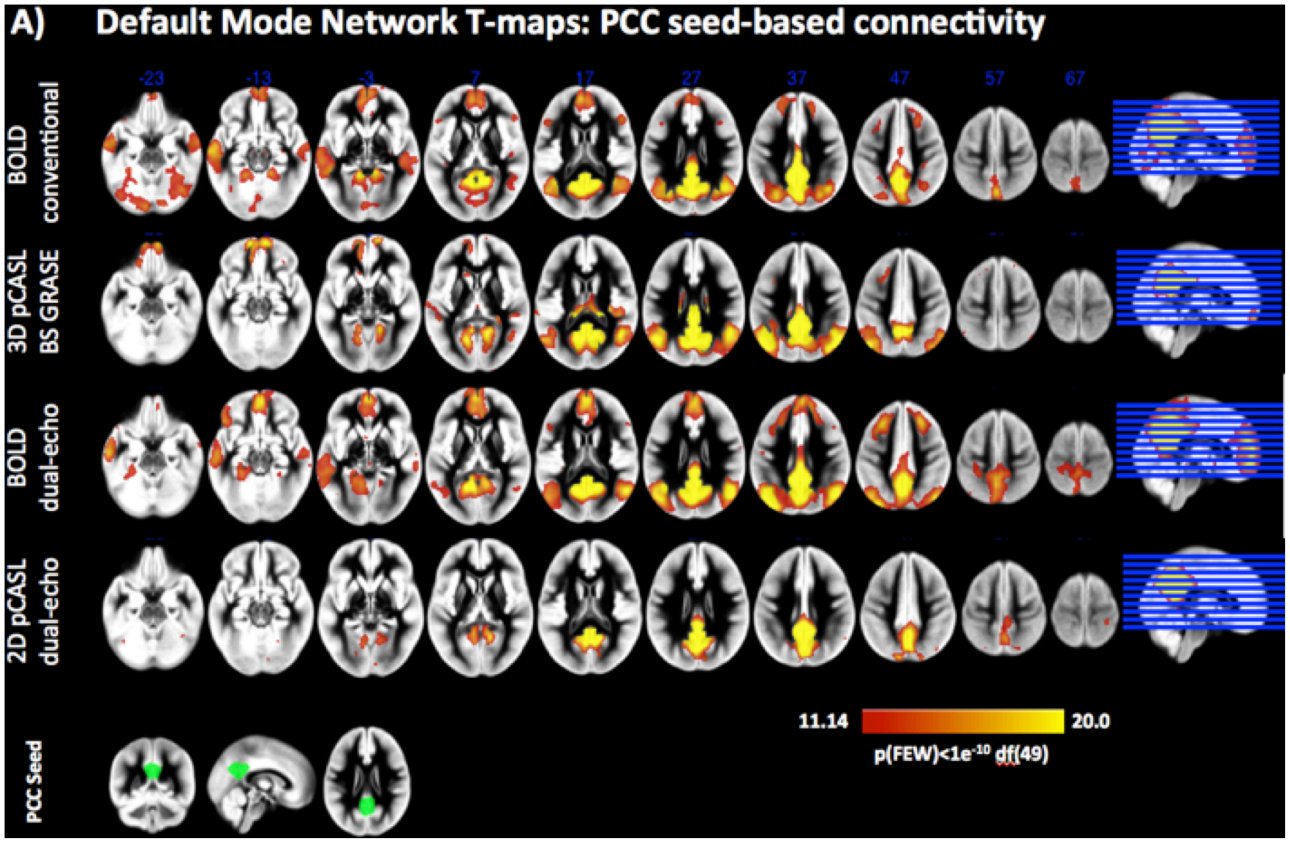

FIGURE 1 | Statistical t-maps displaying the spatial pattern of the DMNs as identified by Seed based Correlation analysis from a PCC seed (Lower left, green) on pCASL and BOLD datasets.

ASD and TD. To minimize the effects of differences in head motion between the groups, the ASD and TD groups were also matched for the amount of motion: mean frame-wise displacement (FD) for ASD was 0.453 ± 0.238 and TD 0.392 ± 0.241 (t-test $t = -0.641$, $p = 0.528$).

RESULTS

Both pCASL and BOLD data showed correlation maps using the PCC as the seed that resemble the DMN. **Figure 1** displays the PCC-Seed and the DMNs computed as t-maps across all NRSs for each dataset thresholded at family wise corrected $p < 1e^{-10}$. Dice Similarity Coefficients (DSCs) to the template BOLD-DMN (Shirer et al., 2012) and the template ASL-DMN (Jann et al., 2015a), respectively, are listed in **Table 1**. NRS1–3 showed low similarity while NRS4&5 showed greater overlap with the DMN templates. Furthermore, 2D pCASL showed the lowest DSC values, especially to the template ASL-DMN. **Figure 2** displays the cross-comparison of NRSs within each dataset to the template BOLD-DMN. Notably, DSC values between the separate NRS-DMNs showed that the DMN-maps without WM/CSF correction (NRS1–3) were highly similar to each other, while the DMNs with WM/CSF correction (NRS4, 5) showed high similarity to each other.

TABLE 1 | Dice Similarity Coefficients (DSCs) for all NRS in each condition to a template BOLD-DMN (Shirer et al., 2012) and a template ASL-DMN (Jann et al., 2015a), respectively.

	NRS1	NRS2	NRS3	NRS4	NRS5	Combined
TEMPLATE BOLD-DMN						
BOLD conventional	0.10	0.12	0.12	0.18	0.19	0.25
3D BS GRASE pCASL	0.12	0.11	0.11	0.19	0.19	0.17
BOLD dual-echo	0.09	0.09	0.09	0.28	0.39	0.39
2D pCASL	0.09	0.08	0.08	0.19	0.21	0.19
TEMPLATE ASL-DMN						
BOLD conventional	0.24	0.27	0.27	0.40	0.43	0.51
3D BS GRASE pCASL	0.36	0.40	0.40	0.51	0.49	0.55
BOLD dual-echo	0.24	0.23	0.23	0.51	0.55	0.58
2D pCASL	0.29	0.26	0.26	0.33	0.32	0.35

*The column termed combined represents the DMN t-maps across all subjects and NRSs as displayed in **Figure 1**.*

Effects of NRS on FC

Analysis of the connectivity between PCC and ACC/mPFC ROIs in both BOLD datasets showed a general decrease of FC after WM/CSF regression [$F_{BOLDconv(4,\ 9)} = 25.53$, $p < 1e\text{-}10$, $t_{NRS0vsNRS4} = 5.34$, $p = 0.0005$; $F_{BOLDdual-echo(4,\ 9)} = 12.49$,

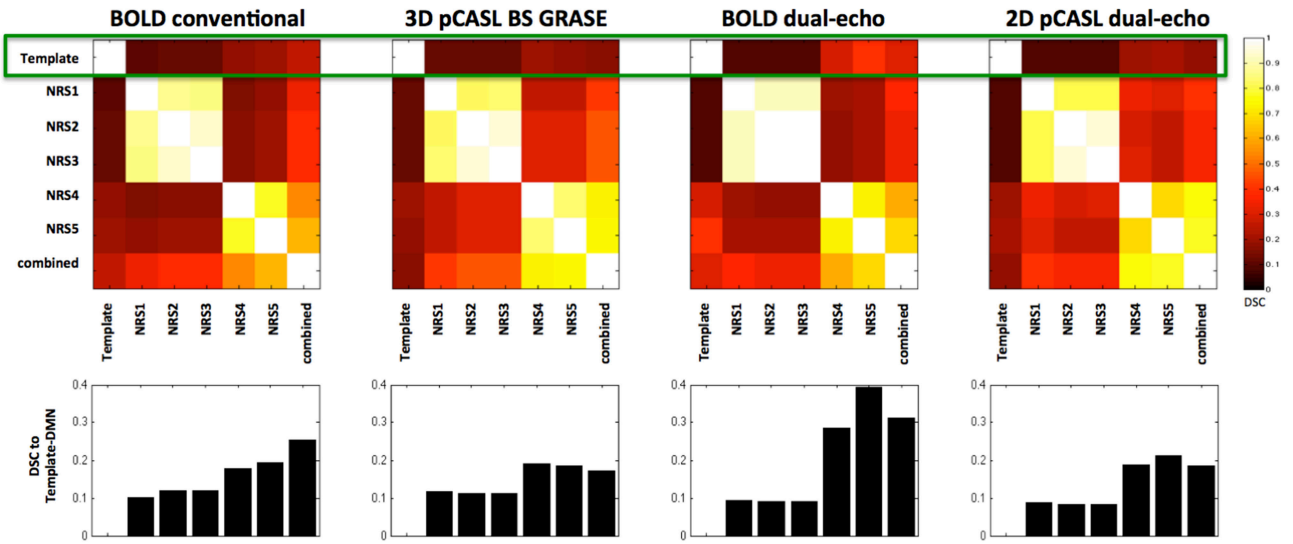

FIGURE 2 | Dice Similarity Coefficients (DSCs) between the spatial maps of the DMNs after different stages of noise reduction (NRS1–5). Template DMN derived from Shirer et al. (2012). Combined DMN computed as one-sample *t*-test across spatial correlation maps of all subjects and NRS. Clusters along the diagonal indicate that WM/CSF regression has large effect on similarity. Specifically after WM/CSF correction (NRS4/5) DSC values to the template DMN are increased (green rectangle and also bar-plots below cluster-plots), indicating increased spatial specificity of the DMN.

$p < 1e^{-10}$, $t_{NRS0vsNRS4} = 2.69$, $p = 0.025$], while motion parameter regression showed a tendency to slightly increase FC (*t*-test between NRS5 and NRS4 = $t_{BOLDconv} = 1.55$, $p = 0.155$; $t_{BOLDde} = 1.14$, $p = 0.284$). The same trend was observed for 3D GRASE pCASL [$F_{3DpCASL(4, 9)} = 75.5$, $p < 1e^{-10}$; $t_{NRS0vsNRS4} = 14.19$, $p < 0.0001$ and *t*-test NRS5 vs. NRS4: $t_{3DpCASL} = 1.51$, $p = 0.165$]; however, FC values were overall lower. For 2D pCASL there was little to no correlation between the two ROIs and no significant effect in the ANOVA ($F_{2DpCASL} = 1.4$, $p = 0.254$). Mean values of correlation coefficient across subjects for all NRSs and datasets are displayed in **Figure 3**.

A more detailed analysis of NRS effects throughout the DMN was performed by voxel-wise repeated-measures ANOVA (**Figure 4**). Results revealed that FC between PCC and mPFC/ACC were modified by NRS. Details for all ROIs including the results of the repeated-measures ANOVAs are listed in **Table 2**. For every ROI showing an effect of NRS, the boxplots represent the FC values (median and 75% interval across subjects) after different NRSs, revealing the directions of FC changes (i.e., increases or decreases). Moreover, the horizontal lines above the boxplots indicate the significance of *post-hoc* paired *t*-tests ($p < 0.05$) between any NRSs (*t* and *p* values for all *post-hoc t*-tests can be found in **Supplemental Table 1**). Similar to the analysis of connectivity between the PCC and ACC/mPFC ROIs, the voxel-wise ANOVA and *post-hoc t*-tests indicated that WM/CSF signal regression significantly reduces FC throughout the DMN. Furthermore, using head movement related nuisance variables in addition to WM/CSF (comparison between NRS5 and NRS4) tended to increase long-range FC from PCC to frontal areas while reducing local (within PCC) FC (**Table 2**). This distance-related effect was further investigated in a highly parcellated seed based approach.

Distance Dependence of Motion-Regression Effects

The scatter plots in **Figure 5** suggest a relationship between motion correction effects (after WM/CSF signal regression) and the distance between the connected ROIs. Specifically, ΔFC was increasingly positive the farther apart any two areas, thus yielding increased long-range connectivity and reduced or constant local short-range connectivity.

NRS Effects on Temporal SNR and Global CBF

Global tSNR in BOLD was expectedly higher than that of pCASL; furthermore, 3D pCASL showed 4.4 ± 0.4 times higher global tSNR than 2D pCASL. Differences in tSNR after NRS were observed for all modalities and with a similar behavior suggesting that motion regression increases tSNR and combining motion regression with WM/CSF regression results in highest increase in tSNR (**Figure 6**). This observation is supported by repeated-measures ANOVA analyses for both BOLD and 3D GRASE pCASL sequences: $F_{(4, 9)BOLD-S} = 7.5$, $p < 0.001$, $F_{BOLD-DE} = 21.92$, $p < 5e^{-10}$, $F_{ASL-3D-BS} = 7.78$, $p < 7.5e^{-5}$, whereas there was no significant effect for 2D dual-echo pCASL: $F_{ASL-2D-DE} = 0.73$, $p = 0.58$.

Along with the increase in temporal SNR for 3D GRASE pCASL, global mean CBF was also slightly higher for NRS4&5 than those observed for NRS1–3 [$F_{(4, 9)} = 63.36$, $p < 0.00001$]. An opposite effect was observed for 2D dual-echo pCASL where regression of WM/CSF signals (NRS4&5) slightly reduced global mean CBF [$F_{(4, 9)} = 3.36$, $p < 0.02$], as shown in **Table 3**.

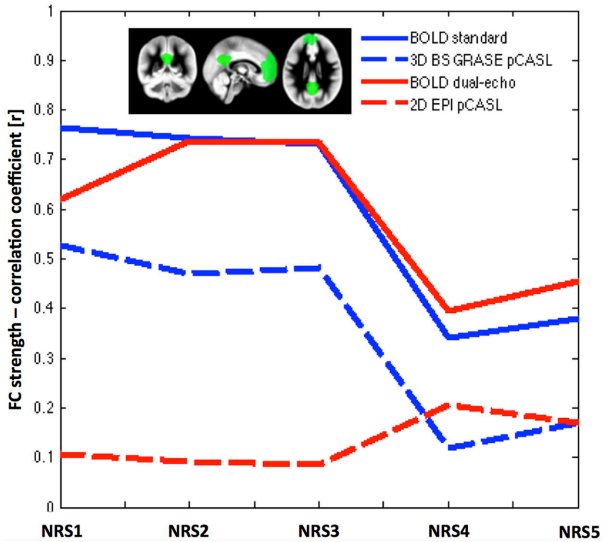

FIGURE 3 | Region-to-Region correlation between two template areas of the DMN: the PCC and the ACC/mPFC (shown in green in the small inlet figure). Overall BOLD exhibits stronger correlation values than ASL. Noise reduction shows similar behavior in FC changes for both BOLD datasets (solid lines) as well as the 3D BS GRASE pCASL data (blue dashed line), while showing little effect for 2D pCASL. A more regionally detailed analysis of these effects is displayed in **Figure 4**.

Results of NRS in Children with ASD vs. TD Children

Within-group

Comparing correlation maps seeded from the PCC revealed differences in long-range connections to the frontal cortex after noise reduction in both groups (TD and ASD children). Specifically, differences between NRS4 and NRS5 revealed increased long-range and decreased local correlations within the DMN, which are in accordance with the general observations of motion-regression effects (**Supplemental Figure 1**). In TD children, we found increased correlation to superior frontal gyri and to the hippocampi, as well as reduced local connectivity in PCC. In ASD children, we observed increased correlations with the orbitofrontal cortex (OFC) and similarly reductions in FC in PCC. Furthermore, we observed increases in anti-correlation to areas associated to other large-scale networks in autism: from PCC to the dorsal ACC, part of salience network, as well as regions of the motor network. Hence, in addition to within network effects (DMN), noise reduction might also increase the separation between networks.

Between-group

Direct comparisons between the TD and ASD groups revealed evidence highlighting the importance of noise reduction (**Figure 7**). While group differences without any noise-reduction (NRS1) showed decreased local FC in the precuneus and increased FC to lateral temporal areas bilaterally in the ASD group as compared to the TD group, group differences after noise regression (NRS4&5) revealed areas with reduced long-range FC from PCC to the dorsal portion of the prefrontal cortex and parahippocampal gyri in the ASD vs. the TD group. The areas showing reduced connectivity with the lateral temporal lobes in the ASD group were no longer evident.

DISCUSSION

FC analysis has become a major tool to assess the functional organization of brain networks as well as their integrity or alterations in clinical populations. However, to be clinically applicable, possible confounding factors for FC analysis need to be identified, understood and accounted for. For BOLD based FC such effects include physiological noise related to pulsatile fluctuations of the blood flow caused by heart beat (Shmueli et al., 2007; Chang et al., 2009) as well as changes in BOLD signal due to variations in rate and depth of respiration (Birn et al., 2006; Birn, 2012). More recently, it has been shown that even slight head movements can affect FC analysis outcomes (Power et al., 2012; Van Dijk et al., 2012).

By using different sets of nuisance variables (here termed Noise Reduction Strategies: NRS) representing noise from physiological noise sources and head movements in two separate BOLD and pCASL implementations, our study showed that accounting for physiological noise and motion-induced effects could indeed alter the connectivity strength and hence spatial maps of the DMN. For BOLD rs-fMRI, these effects have been described and were replicated in our study. For ASL, so far little has been known regarding how noise reduction affects ASL signal and ASL based FC analysis.

Noise Reduction Effects in Bold Based FC

Our findings generally align well with what has been described with regard to noise reduction effects in BOLD based FC analysis. First, regression of physiological noise related nuisance variables from WM and CSF signal fluctuations (Dagli et al., 1999; Windischberger et al., 2002; Birn et al., 2008; Weissenbacher et al., 2009; Jo et al., 2010) reduces connectivity in several brain areas but at the same time increases the spatial specificity of FC maps (Chang and Glover, 2009a; Birn, 2012; Power et al., 2015). The correlation maps generated by NRS4 and NRS5 are highly restricted to areas of the DMN while NRS1–3 display more widespread correlation maps that comprise areas affected by respiratory and heart rate pulsatility (Birn et al., 2008). Statistical comparisons using DCSs further demonstrated that the spatial maps for NRSs including physiological noise regression improved their similarity to the template DMN. A decrease in connectivity strength after removing physiological fluctuations is expected since noise induced spurious correlations are removed from the signal (Weissenbacher et al., 2009). Furthermore, temporal SNR was improved by noise reduction indicating reduced signal variance.

Using head motion nuisance regressors showed less pronounced effects. For conventional BOLD and dual-echo BOLD, frontal regions showed a trend of FC increases between NRS4 and NRS5 as well as FC decreases in the medial posterior cortex and PCC. Significant increases were only observed in ACC for the conventional BOLD dataset and the right angular gyrus for dual-echo BOLD (**Table 2**). However, the data overall

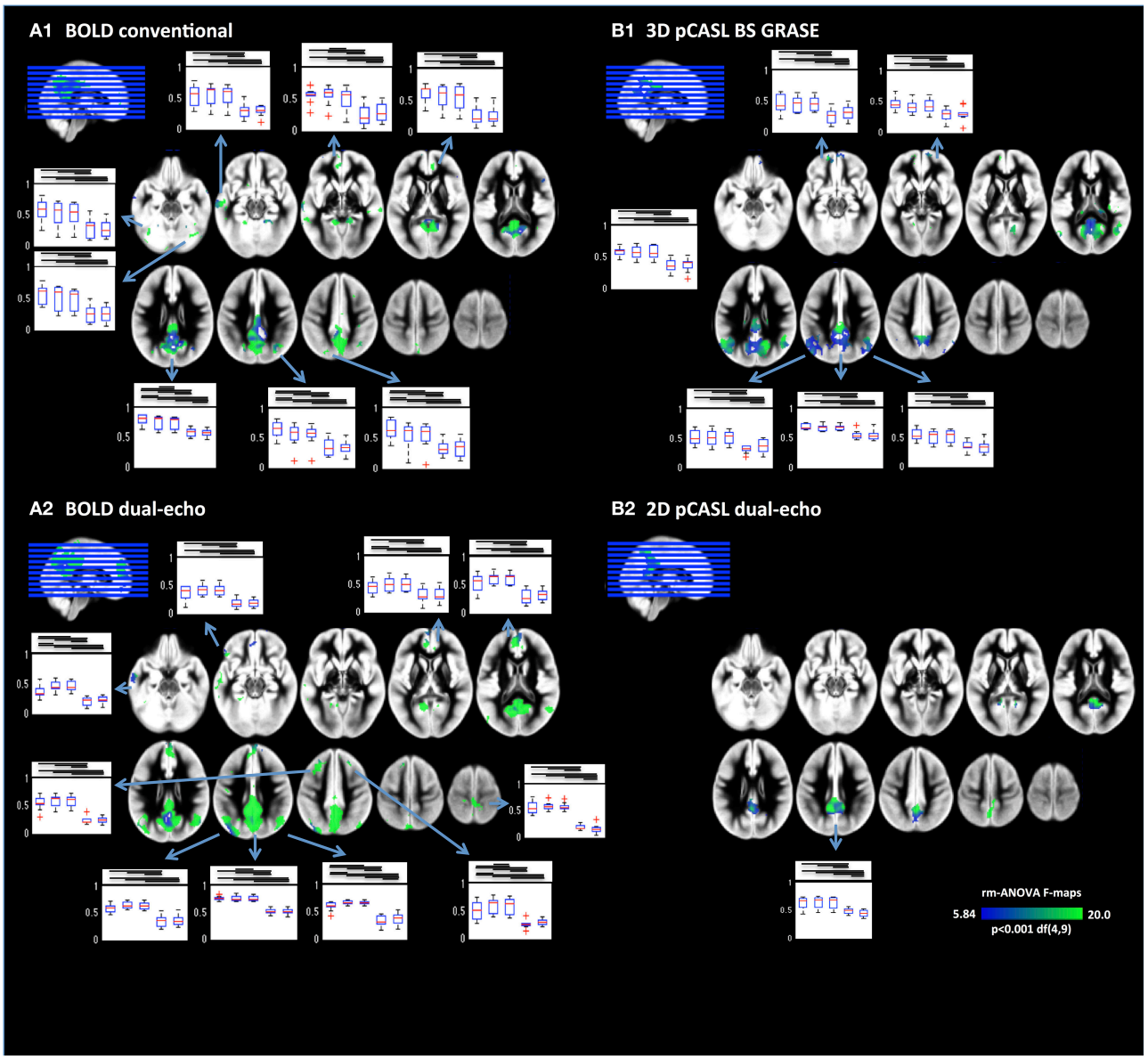

FIGURE 4 | Voxel-wise repeated-measures ANOVA F-maps highlighting the areas with significant FC changes after NRS. Results are limited to areas within the DMNs as displayed in **Figure 1**. Box plots display the regional FC values for NRS1–5. Generally physiological noise reduction (WM and CSF fluctuations) reduced FC significantly (bars above box plots indicate significance between NRS-FC values). Motion correction had more subtle effects on FC but nevertheless significant increases can be seen in several areas mainly in the frontal cortex.

suggest that reduction of head movement related signals improves FC strength between anterior and posterior areas. This effect has attracted wide interest in recent years since the head movement effects are subtle and can cause group differences between cohorts with different movement profiles (e.g., patient populations or children Van Dijk et al., 2010; Satterthwaite et al., 2012). Notably, in this study, there were no head movement differences within the neurotypical adult groups nor between the ASD and TD groups as evidenced by mean framewise displacement. Moreover, the spatial extent of DMN and regional effects of NRS onto FC within the DMN were compared within datasets separately (except for the between-group comparison of ASD vs. TD discussed below). Our participants further showed only small amount of motion hence changes were expected to be subtle. In a further analysis, we segregated the cortex into 264 regions and computed the distance dependence of FC due to reduction of head motion effects. This confirmed that long-range connections show proportionally larger increase in FC than connections between more proximal areas. This finding is in line with prior evidence that motion affects long- and short-range connections differently (Power et al., 2012, 2014; Van Dijk et al., 2012). Comparing our linear fitting results to recent work by Power et al. (2012, 2015) confirms that the distance dependency effects are in the same order of magnitude.

TABLE 2 | Clusters showing a change in functional connectivity across noise reduction strategies (NRS).

	Cluster size	Peak MNI coordinate			peak F	Anatomical area	BA	rm-ANOVA		Effects of motion regression	
Cluster	#voxels	*x*	*y*	*z*				$F_{(4, 9)}$	*P*	*Post-hoc t*-test NRS5-NRS4	*p*
3D BOLD											
1	91	34.0	−70.1	−23.9	47.3898	Fusiform_R	19	6.02	8.10E-04	−0.40	0.6996
2	329	−52.0	−14.1	−9.9	61.1242	Temporal_Mid_L	21	4.45	0.005	−0.01	0.9912
3	5290	0.0	−60.1	56.1	97.9045	Precuneus/posterior cingulate	(7/31)	15.95	1.34E-07	−1.20	0.2598
4	54	−18.0	−44.1	−11.9	38.5708	Fusiform_L	19	13.77	6.60E-07	−1.22	0.2534
5	53	−6.0	41.9	2.1	29.5438	Cingulum_Ant_L	32/10	4.03	0.0084	2.42	0.0386*
6	52	10.0	43.9	8.1	46.4137	Cingulum_Ant_R	32	11.14	5.56E-06	0.08	0.9390
7	259	28.0	−76.1	40.1	28.0085	Occipital_Sup_R	19	7.67	1.41E-04	−0.59	0.5716
8	86	−20.0	−62.1	38.1	42.1778	Parietal_Sup_L	7	4.37	0.0055	−0.72	0.4925
3D ASL											
1	129	14.0	63.9	6.1	23.8028	Frontal_Sup_Medial_R	(11/10)	6.67	4.03E-04	0.54	0.6032
2	184	−10.0	45.9	−3.9	44.5863	Cingulum_Ant_L	32	6.29	6.03E-04	3.34	0.0087*
3	4003	4.0	−44.1	46.1	37.23	Precuneus/posterior cingulate	7,31	3.17	0.0248	−0.61	0.5562
4	864	50.0	−46.1	28.1	28.0536	SupraMarginal_R	39	11.67	3.55E-06	0.11	0.9122
5	70	28.0	−34.1	12.1	33.0022	sub lobar		4.31	0.0059	−0.05	0.9604
6	1338	−56.0	−54.1	28.1	27.4496	SupraMarginal_L	39	6.06	7.78E-04	2.00	0.0770
2D BOLD											
1	333	−60.0	−24.1	−5.9	40.2981	Temporal_Mid_L	21	0.86	0.499	1.35	0.2113
2	81	−46.0	25.9	−9.9	50.8921	Frontal_Inf_Orb_L	47	4.32	0.0059	0.13	0.8987
3	91	−6.0	43.9	−3.9	19.2798	Cingulum_Ant_L	10.11	2.27	0.0805	0.59	0.5717
4	5609	4.0	−28.1	44.1	243.5297	Cingulum_Mid_R	31	0.85	0.5048	−1.46	0.1791
5	975	8.0	31.9	24.1	85.5258	Cingulum_Ant_R	10,32,9	2.74	0.0435	1.56	0.1521
6	833	48.0	−56.1	40.1	97.0885	Angular_R	39	2.97	0.0321	2.64	0.0268*
7	1014	−40.0	−54.1	34.1	66.9547	Angular_L	19,39	2.91	0.0347	0.99	0.3491
8	314	−22.0	15.9	44.1	251.0319	Frontal_Mid_L	8	4.41	0.0053	−0.15	0.8875
9	74	26.0	23.9	52.1	55.824	Frontal_Sup_R	8	3.12	0.0265	2.03	0.0735
10	188	8.0	−44.1	64.1	154.553	Paracentral_Lobule_R	6	0.49	0.745	−2.46	0.0363*
2D ASL											
1	2273	4.0	−36.1	58.1	72.8902	Posterior Cingulate	31,7	6.14	7.11E-04	−3.26	0.0099*

*Listed are cluster coordinates, size, and anatomical location as well as statistical test results for repeated measures ANOVA and post-hoc T-test between NRS5 vs. NRS4 (FC changes due to motion regression). *Indicate significant differences between NRS5 vs NRS4.*

TABLE 3 | Mean global CBF for both pCASL sequences and all NRSs.

Global CBF [ml/100g/min]	NRS1	NRS2	NRS3	NRS4	NRS5
2D EPI pCASL	59.66 ± 11.45	59.79 ± 11.45	59.79 ± 11.45	58.21 ± 9.77	58.17 ± 9.88
3D BS GRASE pCASL	59.99 ± 9.70	59.98 ± 9.68	59.99 ± 9.69	64.37 ± 10.78	64.37 ± 10.78

No differences were observed.

In summary, in both BOLD datasets the observed effects of noise reduction are in agreement with previous work, highlighting the importance of taking into account the effect of physiological and motion related confounds in FC analyses.

Noise Reduction Effects in ASL based FC

ASL based FC has recently gained interest in the research community (Chuang et al., 2008; Zou et al., 2009; Viviani et al., 2011; Jann et al., 2013; Dai et al., 2015; Jann et al., 2015a, for recent review see Chen et al., 2015) and in clinical studies (Orosz et al., 2012; Kindler et al., 2013; Jann et al., 2015b), since it provides not only assessments of functional brain networks but also a surrogate measure of metabolism, cerebral blood flow (CBF). Moreover, there appears to be a relation between connectivity strength and local CBF suggesting that increased connectivity of a region is more energy demanding (Liang et al., 2013; Tomasi et al., 2013; Jann et al., 2015a). While the feasibility of ASL based FC and the similarity of the identified networks to BOLD networks has been previously demonstrated (Chuang et al., 2008; Zou et al., 2009; Viviani et al., 2011; Jann et al., 2013, 2015a; Dai et al., 2015), it remains unknown how noise regression in ASL could benefit these analyses. Our results show that 3D GRASE pCASL with background suppression (BS) benefits from noise reduction as temporal SNR (tSNR) significantly increases in a similar manner as for BOLD (**Figure 6**). For 2D pCASL without BS there was a minor gain in tSNR (Wang et al., 2008; Wang, 2012) although this did not reach significance. Furthermore, we observed that 3D BS GRASE pCASL offers a four-times higher

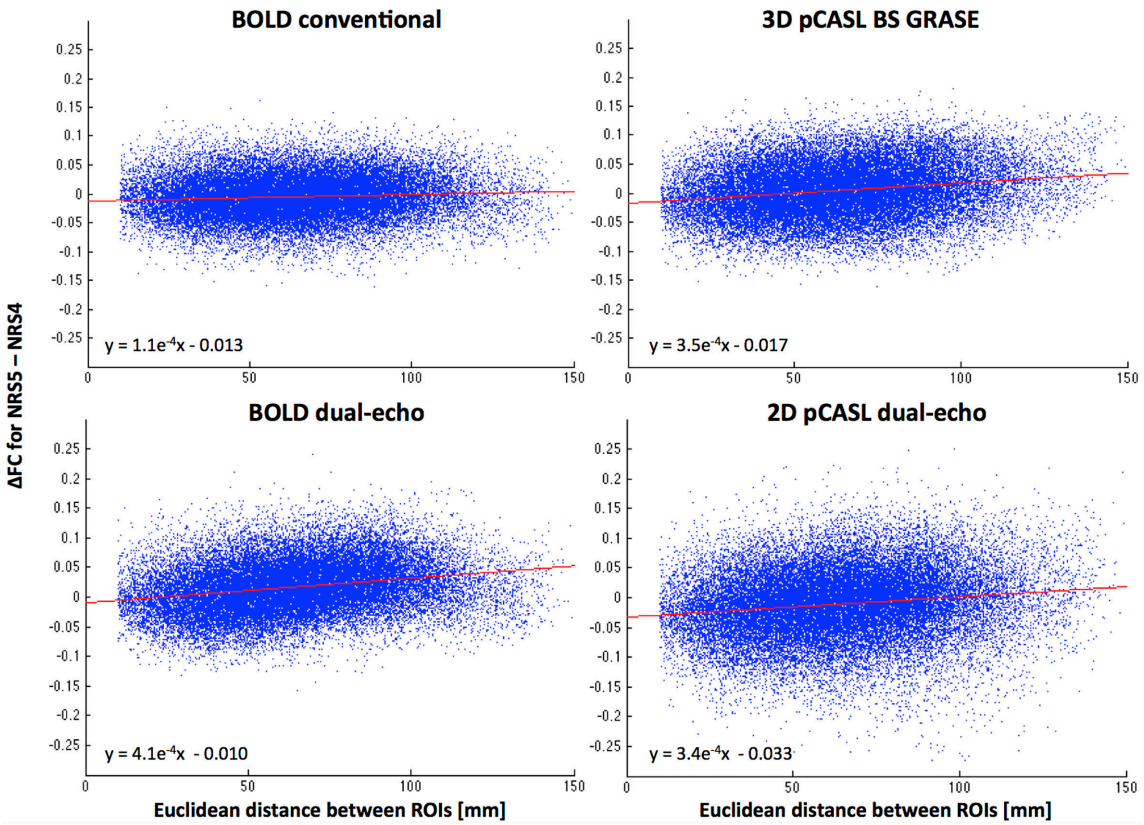

FIGURE 5 | Distance dependence of FC changes between NRS4 and NRS5 (indicating motion correction effects only, after correction for physiological noise). Scatter plots reveal that FC between more distant areas is increased more than for proximal areas. Red lines represent the linear fit between distance and ΔFC (see also equations).

tSNR than that of 2D pCASL. This higher tSNR across all NRSs can mainly be attributed to the background suppression (brain tissue signal suppressed by 85%), while the 3D readout mainly contributes to improved spatial SNR (Vidorreta et al., 2013; Chen et al., 2015; Wang et al., 2015). Based on tSNR measurements, 3D BS GRASE pCASL should be more suitable for CBF based FC analyses than 2D pCASL without BS.

The FC analysis on the CBF datasets demonstrated that the DMN can be detected in both pCASL implementations, albeit with less statistical power in the 2D pCASL due to lower tSNR and/or small sample size of this study. Removing WM and CSF fluctuations to minimize cardiac and respiration related noise prior to FC analysis resulted in reduced FC between PCC and ACC in the ROI based analysis for 3D BS GRASE pCASL whereas no significant effect was found for 2D pCASL. Notably, at the selected statistical threshold, 2D dual-echo pCASL did not show significant correlations between CBF signals in the seed area in the PCC and the anterior part of the DMN (i.e., the mPFC/ACC). It remains to be determined whether using larger samples or lower statistical thresholds will make 2D ASL based FC analysis feasible. Furthermore, as discussed above, the BOLD images acquired at the second echo of the dual echo ASL sequence used in our study showed highly similar network maps, correlation strength and behavior to NRS as the conventional BOLD sequence. On the other hand, the FC strength decrease between PCC and the frontal ROI in 3D BS GRASE pCASL mirrors the effects observed for BOLD. Not surprisingly, the CBF-FC was generally lower than that of BOLD in both ASL implementations, in agreement with other studies comparing ASL and BOLD FC (Viviani et al., 2011; Jann et al., 2015a). This globally decreased FC strength is a consequence of intrinsically lower tSNR in ASL and due to the subtraction of label and control images that generates shorter timeseries for FC analysis in CBF data. However, while FC strength is lower, comparison of the spatial maps using DSC analysis revealed that the DMNs were similar between CBF and BOLD datasets. Similar to BOLD rs-fMRI, physiological noise reduction by using WM and CSF derived nuisance variables in 3D BS GRASE pCASL also resulted in improved spatial specificity when compared to a template DMN. Including head movement related nuisance variables into the preprocessing pipeline resulted in slight improvements of FC in anterior-posterior connections in 3D BS GRASE pCASL. This effect again was similar to the effect observed in the BOLD data (Van Dijk et al., 2010, 2012; Power et al., 2012, 2015). The voxel-wise repeated-measures ANOVA across NRSs confirmed the template-ROI based analyses between PCC and frontal areas and revealed additional areas in the inferior parietal lobes (IPL) where noise reduction had effects on FC. Voxel-wise maps were dominated by effects from physiological noise reduction that generally reduced FC in all DMN areas. Furthermore, the two

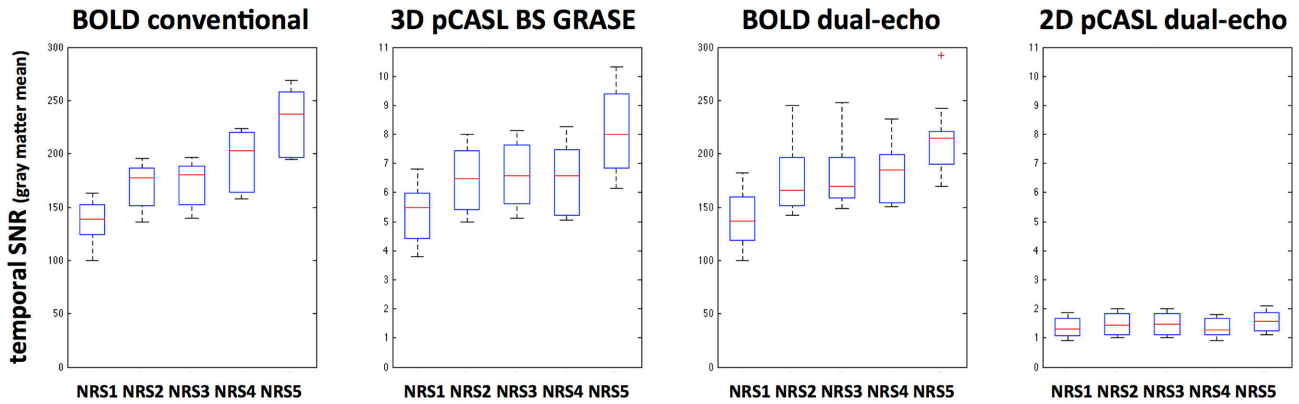

FIGURE 6 | Boxplots indicating tSNR increases after different noise reduction strategies (NRS1–5) in all analyzed MRI sequences. Significant effects were found for all but the 2D dual-echo pCASL datasets.

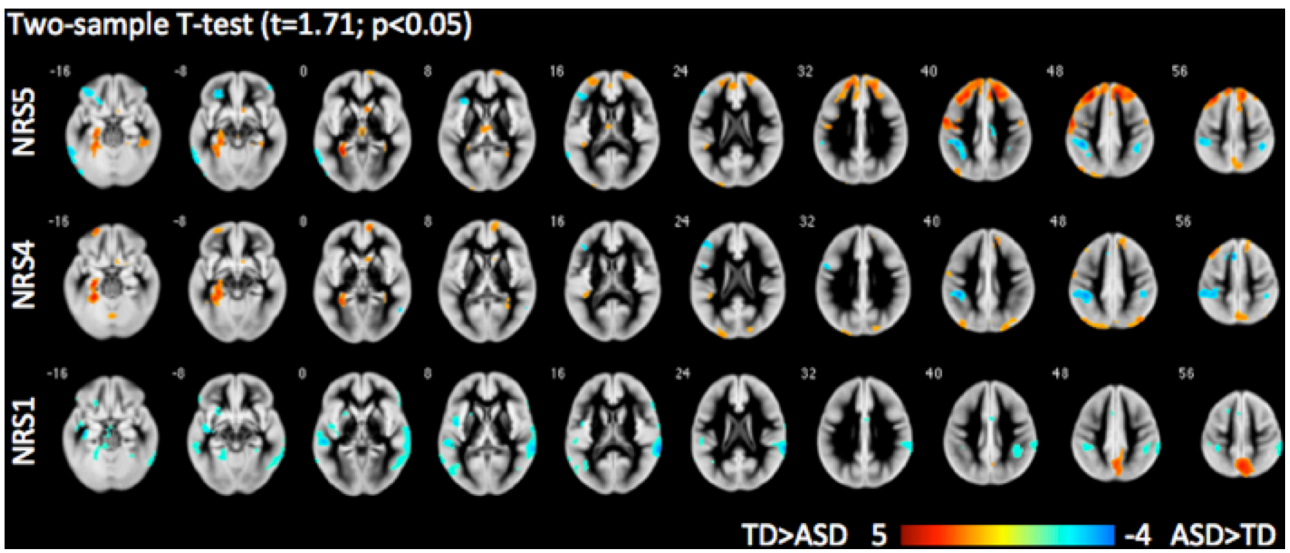

FIGURE 7 | Group differences between typically developing (TD) children and children with autism spectrum disorder (ASD) for different NRS in 3D BS GRASE pCASL data: NRS1 no noise reduction, NRS4 WM/CSF fluctuations removed, NRS5 WM/CSF and motion regression. While seed based FC (from PCC) in NRS1 did not reveal differences in frontal areas, NRS5 clearly delineates reduced long-range connections in ASD compared to TD.

frontal areas in 3D BS GRASE pCASL showed an increase in FC after motion correction although only the right mPFC ROI reached significance (**Figure 4B1**). The IPLs showed minor increases in FC whereas the PCC exhibited a minor reduction of local FC (**Table 1**). In 2D pCASL only the PCC was above the threshold for defining the DMN (compared to **Figure 1**). It showed significant decrease of local connectivity strength following motion regression in addition to physiological noise removal, and thus results are in agreement with the general observations of this study.

Finally, the whole brain parcellated connectivity analysis showed a similar motion related distance dependence of FC changes (**Figure 5**), with effects more pronounced for long-range than short-range connections. Notably, since this analysis was not limited to the DMN areas, the effect was observed in both the 3D BS GRASE and 2D dual-echo pCASL datasets. This suggests that although 2D pCASL shows low connectivity overall, on a less stringent threshold for connectivity results, it could still benefit from motion regression prior to FC analysis in the same fashion as the other datasets.

In summary, 3D BS GRASE pCASL revealed similar DMN maps at the same statistical threshold as BOLD, albeit with generally reduced FC strength. Moreover, 3D BS GRASE pCASL displayed similar FC changes as a function of different sets of nuisance variables used in the preprocessing, showing improved spatial specificity after physiological noise reduction and improved long-range connectivity with motion correction. In contrast, 2D dual-echo pCASL showed weak connectivity overall, which did not survive the same statistical threshold set for this study. This is most likely a problem of low tSNR for this

ASL implementation that has no background suppression or the small sample size.

Results for Clinical Cohort: Children with ASD vs. Matched TD Children

In both ASD and TD groups, motion regression reduced local connectivity in posterior DMN areas while it significantly increased connectivity with superior frontal areas in the TD group and with orbitofrontal areas in the ASD group. Furthermore, in ASD we observed an increased anti-correlation between PCC and areas of the anterior salience network as well as areas of the somatomotor network. This suggests that noise reduction might affect not only within network effects (DMN), it may also benefit the separation between functional networks in autism. These alterations in FC due to noise reduction were also observed in direct group comparisons, leading to marked changes in observed group differences, both in terms of hyper- and hypoconnectivity. While all NRS (NRS 1,4,5) yielded altered connectivity in somatomotor network in ASD, NRS4&5 revealed reduced long-range FC from PCC to the dorsal portion of the prefrontal cortex and parahippocampal gyri, with suppression of hyperconnectivity with lateral-temporal areas. Overall, noise reduction altered the pattern of temporal lobe hyperconnectivity highlighting instead long-range hypoconnections to frontal areas and the medial temporal lobes (i.e., parahippocampal gyri). Similar motion related effects on FC were found in a study using independent component analysis to identify BOLD-DMN subnetworks in ASD (Starck et al., 2013). They reported that after accounting for motion effects, group differences between posterior and anterior DMN subnetworks, as well as in a ventral subnetwork including the parahippocampal gyrus were accentuated. Moreover, altered connectivity from PCC to superior frontal and the parahippocampal gyri in ASD have also been related to deficits in social functioning (Monk et al., 2009; Weng et al., 2010).

Recently, an anterior-posterior gradient of hyper- and hypoconnectivity received considerable attention in neuroimaging studies of ASD (Keown et al., 2013; Rudie and Dapretto, 2013; Di Martino et al., 2014) and is discussed in the context of improved selective cognitive abilities (local hyperconnectivity) and impaired social functioning (long-range hypoconnectivity between frontal and posterior cortices) (Jann et al., 2015b).

CONCLUSION

Noise reduction affected FC analysis from a seed in the PCC to other brain areas of the DMN in all datasets (BOLD and pCASL). First, changes in FC strength and spatial maps of the DMN with regard to physiological nuisance variables (WM/CSF signals) and head movement related nuisance variables were replicated in two separate BOLD datasets, one with a conventional EPI implementation and another based on data acquired in a 2D dual-echo pCASL sequence. Second, analysis of NRS effects on FC analysis of CBF data demonstrated that 3D BS GRASE pCASL shows similar behavior as that observed for BOLD. The favorable noise properties of 3D BS GRASE pCASL as compared to 2D dual-echo pCASL and the improved tSNR after noise reduction render this pCASL implementation more suitable for CBF based FC analyses showing similar networks (Dai et al., 2015; Jann et al., 2015a) and dependence on noise reduction as BOLD. The dual-echo 2D pCASL used here provides perfusion and BOLD images with optimal contrasts, hence can provide proper BOLD based FC results and quantitative CBF (Zhu et al., 2013). FC analysis on the CBF timeseries of 2D pCASL should be treated with caution due to intrinsically low tSNRin conjunction with small sample size. However, a potential advantage of dual-echo ASL, that was not investigated here, is that the TE dependence of signal relaxation might be utilized to separate BOLD and non-BOLD signals (Kundu et al., 2012, 2013). The sensitivity of 2D pCASL can be improved in the future with optimized background suppression strategies in conjunction with multiband acquisitions (Shao et al., 2016).

Finally, applying the full spectrum of NRS in a cohort of children with ASD and typically developing controls we observed that 3D BS GRASE pCASL based FC analysis yielded results that are in accordance with effects of head motion and group differences between ASD and TD children observed in BOLD-DMNs. These findings underline the complex changes in functional organization in ASD and the impact that different preprocessing steps could have on the research findings (Nair et al., 2014).

AUTHOR CONTRIBUTIONS

KJ designed the experiment, performed the analyses and wrote the manuscript. ER analyzed the data and RS designed the experiment and contributed analysis tools. MD wrote the manuscript. DW conceptualized the study and wrote the manuscript.

ACKNOWLEDGMENTS

This work was supported by grants from NICHD (P50 HD055784), NIMH (1R01- MH080892), 5P50HD055784-07 sub#: 5845, R01-NS081077, R01-EB014922, the Garen and Shari Staglin and the International Mental Health Research Organization. KJ holds a fellowship of the Swiss National Science Foundation (SNF)/Swiss Foundation for Grants in Biology and Medicine (SFGBM) grant no.s142743 and 155345.

SUPPLEMENTARY MATERIAL

The Supplementary Material for this article can be found online at: http://journal.frontiersin.org/article/10.3389/fnins.2016.00371

Supplemental Table 1 | This table lists all *post-hoc t*-test (after ANOVA) *t* and *p*-values between all NRS in each brain area and for all 4 examined modalities.

Supplemental Figure 1 | Differences in group wise FC seeded from the PCC after motion regression. (A) Connectivity in Children with ASD for NRS4 and NRS5. **(B)** Difference between NRS4 and NRS5 in ASD. **(C)** Connectivity in TD children for NRS4 and NRS5. **(D)** Difference between NRS4 and NRS5 in TD.

REFERENCES

Alsop, D. C., Detre, J. A., Golay, X., Günther, M., Jeroen, H., Hernandez-Garcia, L., et al. (2015). Recommended Implementation of Arterial Spin Labeled Perfusion MRI for clinical applications: a consensus of the ISMRM Perfusion Study Group and the European Consortium for ASL in Dementia. *Magn. Reson. Med.* 73, 102–116. doi: 10.1002/mrm.25197

Birn, R. M. (2012). The role of physiological noise in resting-state functional connectivity. *Neuroimage* 62, 864–870. doi: 10.1016/j.neuroimage.2012.01.016

Birn, R. M., Diamond, J. B., Smith, M. A., and Bandettini, P. A. (2006). Separating respiratory-variation-related fluctuations from neuronal-activity-related fluctuations in fMRI. *Neuroimage* 31, 1536–1548. doi: 10.1016/j.neuroimage.2006.02.048

Birn, R. M., Murphy, K., and Bandettini, P. A. (2008). The effect of respiration variations on independent component analysis results of resting state functional connectivity. *Hum. Brain Mapp.* 29, 740–750. doi: 10.1002/hbm.20577

Chang, C., Cunningham, J. P., and Glover, G. H. (2009). Influence of heart rate on the BOLD signal: the cardiac response function. *Neuroimage* 44, 857–869. doi: 10.1016/j.neuroimage.2008.09.029

Chang, C., and Glover, G. H. (2009a). Effects of model-based physiological noise correction on default mode network anti-correlations and correlations. *Neuroimage* 47, 1448–1459. doi: 10.1016/j.neuroimage.2009.05.012

Chang, C., and Glover, G. H. (2009b). Relationship between respiration, end-tidal CO_2, and BOLD signals in resting-state fMRI. *Neuroimage* 47, 1381–1393. doi: 10.1016/j.neuroimage.2009.04.048

Chen, J. J., Jann, K., and Wang, D. J. (2015). Characterizing resting-state Brain function using Arterial Spin Labeling. *Brain Connect.* 5, 527–542. doi: 10.1089/brain.2015.0344

Chen, Y., Wang, D. J., and Detre, J. A. (2011). Test-retest reliability of arterial spin labeling with common labeling strategies. *J. Magn. Reson. Imaging* 33, 940–949. doi: 10.1002/jmri.22345

Chuang, K. H., van Gelderen, P., Merkle, H., Bodurka, J., Ikonomidou, V. N., Koretsky, A. P., et al. (2008). Mapping resting-state functional connectivity using perfusion MRI. *Neuroimage* 40, 1595–1605. doi: 10.1016/j.neuroimage.2008.01.006

Dagli, M. S., Ingeholm, J. E., and Haxby, J. V. (1999). Localization of cardiac-induced signal change in fMRI. *Neuroimage* 9, 407–415. doi: 10.1006/nimg.1998.0424

Dai, W., Garcia, D., de Bazelaire, C., and Alsop, D. (2008). Continuous flow-driven inversion for arterial spin labeling using pulsed radio frequency and gradient fields. *Magn. Reson. Med.* 60, 1488–1497. doi: 10.1002/mrm.21790

Dai, W., Varma, G., Scheidegger, R., and Alsop, D. C. (2015). Quantifying fluctuations of resting state networks using arterial spin labeling perfusion MRI. *J. Cereb. Blood Flow Metab.* 36, 463–473. doi: 10.1177/0271678X15615339

Dice, L. R. (1945). Measurment of the amount of ecologic association between species. *Ecology* 26, 297–302. doi: 10.2307/1932409

Di Martino, A., Yan, C. G., Li, Q., Denio, E., Castellanos, F. X., Alaerts, K., et al. (2014). The autism brain imaging data exchange: towards a large-scale evaluation of the intrinsic brain architecture in autism. *Mol. Psychiatry* 19, 659–667. doi: 10.1038/mp.2013.78

Jann, K., Gee, D. G., Kilroy, E., Schwab, S., Cannon, T. D., and Wang, D. J. (2015a). Functional connectivity in BOLD and CBF data: similarity and reliability of Resting Brain Networks. *Neuroimage* 106, 111–122. doi: 10.1016/j.neuroimage.2014.11.028

Jann, K., Hernandez, L. M., Beck-Pancer, D., McCarron, R., Smith, R. X., Dapretto, M., et al. (2015b). Altered resting perfusion and functional connectivity of default mode network in youth with autism spectrum disorder. *Brain Behav.* 5:e00358. doi: 10.1002/brb3.358

Jann, K., Orosz, A., Dierks, T., Wang, D. J., Wiest, R., and Federspiel, A. (2013). Quantification of network perfusion in ASL cerebral blood flow data with seed based and ICA approaches. *Brain Topogr.* 26, 569–580. doi: 10.1007/s10548-013-0280-3

Jo, H. J., Saad, Z. S., Simmons, W. K., Milbury, L. A., and Cox, R. W. (2010). Mapping sources of correlation in resting state FMRI, with artifact detection and removal. *Neuroimage* 52, 571–582. doi: 10.1016/j.neuroimage.2010.04.246

Keown, C. L., Shih, P., Nair, A., Peterson, N., Mulvey, M. E., and Muller, R. A. (2013). Local functional overconnectivity in posterior brain regions is associated with symptom severity in autism spectrum disorders. *Cell Rep.* 5, 567–572. doi: 10.1016/j.celrep.2013.10.003

Kindler, J., Jann, K., Homan, P., Hauf, M., Walther, S., Strik, W., et al. (2013). Static and dynamic characteristics of cerebral blood flow during the resting state in Schizophrenia. *Schizophr. Bull.* 41, 163–170. doi: 10.1093/schbul/sbt180

Kundu, P., Brenowitz, N. D., Voon, V., Worbe, Y., Vertes, P. E., Inati, S. J., et al. (2013). Integrated strategy for improving functional connectivity mapping using multiecho fMRI. *Proc. Natl. Acad. Sci. U.S.A.* 110, 16187–16192. doi: 10.1073/pnas.1301725110

Kundu, P., Inati, S. J., Evans, J. W., Luh, W. M., and Bandettini, P. A. (2012). Differentiating BOLD and non-BOLD signals in fMRI time series using multi-echo EPI. *Neuroimage* 60, 1759–1770. doi: 10.1016/j.neuroimage.2011.12.028

Liang, X. Y., Tournier, J. D., Masterton, R., Connelly, A., and Calamante, F. (2012). A k-space sharing 3D GRASE pseudocontinuous ASL method for whole-brain resting-state functional connectivity. *Int. J. Imaging Syst. Technol.* 22, 37–43. doi: 10.1002/ima.22006

Liang, X., Zou, Q., He, Y., and Yang, Y. (2013). Coupling of functional connectivity and regional cerebral blood flow reveals a physiological basis for network hubs of the human brain. *Proc. Natl. Acad. Sci. U.S.A.* 110, 1929–1934. doi: 10.1073/pnas.1214900110

Lord, C., Risi, S., Lambrecht, L., Cook, E. H. Jr., Leventhal, B. L., DiLavore, P. C., et al. (2000). The autism diagnostic observation schedule-generic: a standard measure of social and communication deficits associated with the spectrum of autism. *J. Autism Dev. Disord.* 30, 205–223. doi: 10.1023/A:1005592401947

Lord, C., Rutter, M., and Le Couteur, A. (1994). Autism Diagnostic Interview-Revised: a revised version of a diagnostic interview for caregivers of individuals with possible pervasive developmental disorders. *J. Autism Dev. Disord.* 24, 659–685. doi: 10.1007/BF02172145

Monk, C. S., Peltier, S. J., Wiggins, J. L., Weng, S. J., Carrasco, M., Risi, S., et al. (2009). Abnormalities of intrinsic functional connectivity in autism spectrum disorders. *Neuroimage* 47, 764–772. doi: 10.1016/j.neuroimage.2009.04.069

Murphy, K., Birn, R. M., and Bandettini, P. A. (2013). Resting-state fMRI confounds and cleanup. *Neuroimage* 80, 349–359. doi: 10.1016/j.neuroimage.2013.04.001

Nair, A., Keown, C. L., Datko, M., Shih, P., Keehn, B., and Muller, R. A. (2014). Impact of methodological variables on functional connectivity findings in autism spectrum disorders. *Hum. Brain Mapp.* 35, 4035–4048. doi: 10.1002/hbm.22456

Orosz, A., Jann, K., Federspiel, A., Horn, H., Hofle, O., Dierks, T., et al. (2012). Reduced cerebral blood flow within the default-mode network and within total gray matter in major depression. *Brain Connect.* 2, 303–310. doi: 10.1089/brain.2012.0101

Power, J. D., Barnes, K. A., Snyder, A. Z., Schlaggar, B. L., and Petersen, S. E. (2012). Spurious but systematic correlations in functional connectivity MRI networks arise from subject motion. *Neuroimage* 59, 2142–2154. doi: 10.1016/j.neuroimage.2011.10.018

Power, J. D., Mitra, A., Laumann, T. O., Snyder, A. Z., Schlaggar, B. L., and Petersen, S. E. (2014). Methods to detect, characterize, and remove motion artifact in resting state fMRI. *Neuroimage* 84, 32–341. doi: 10.1016/j.neuroimage.2013.08.048

Power, J. D., Schlaggar, B. L., and Petersen, S. E. (2015). Recent progress and outstanding issues in motion correction in resting state fMRI. *Neuroimage* 105, 536–551. doi: 10.1016/j.neuroimage.2014.10.044

Rudie, J. D., and Dapretto, M. (2013). Convergent evidence of brain overconnectivity in children with autism? *Cell Rep.* 5, 565–566. doi: 10.1016/j.celrep.2013.10.043

Satterthwaite, T. D., Wolf, D. H., Loughead, J., Ruparel, K., Elliott, M. A., Hakonarson, H., et al. (2012). Impact of in-scanner head motion on multiple measures of functional connectivity: relevance for studies of neurodevelopment in youth. *Neuroimage* 60, 623–632. doi: 10.1016/j.neuroimage.2011.12.063

Shao, X., Wang, Y., and Wang, D. J. (2016). "A constrained slice-dependent background suppression scheme for simultaneous multi-slice pseudo-continuous arterial spin labeling," in *International Society for Magnetic Resonance in Medicine, Program No 0286* (Singapore).

Shirer, W. R., Ryali, S., Rykhlevskaia, E., Menon, V., and Greicius, M. D. (2012). Decoding subject-driven cognitive states with whole-brain connectivity patterns. *Cereb. Cortex* 22, 158–165. doi: 10.1093/cercor/bhr099

Shmueli, K., van Gelderen, P., de Zwart, J. A., Horovitz, S. G., Fukunaga, M., Jansma, J. M., et al. (2007). Low-frequency fluctuations in the cardiac rate as a source of variance in the resting-state fMRI BOLD signal. *Neuroimage* 38, 306–320. doi: 10.1016/j.neuroimage.2007.07.037

Starck, T., Nikkinen, J., Rahko, J., Remes, J., Hurtig, T., Haapsamo, H., et al. (2013). Resting state fMRI reveals a default mode dissociation between retrosplenial and medial prefrontal subnetworks in ASD despite motion scrubbing. *Front. Hum. Neurosci.* 7:802. doi: 10.3389/fnhum.2013.00802

Tomasi, D., Wang, G. J., and Volkow, N. D. (2013). Energetic cost of brain functional connectivity. *Proc. Natl. Acad. Sci. U.S.A.* 110, 13642–13647. doi: 10.1073/pnas.1303346110

Van Dijk, K. R., Hedden, T., Venkataraman, A., Evans, K. C., Lazar, S. W., and Buckner, R. L. (2010). Intrinsic functional connectivity as a tool for human connectomics: theory, properties, and optimization. *J. Neurophysiol.* 103, 297–321. doi: 10.1152/jn.00783.2009

Van Dijk, K. R., Sabuncu, M. R., and Buckner, R. L. (2012). The influence of head motion on intrinsic functional connectivity MRI. *Neuroimage* 59, 431–438. doi: 10.1016/j.neuroimage.2011.07.044

Vidorreta, M., Wang, Z., Rodriguez, I., Pastor, M. A., Detre, J. A., and Fernandez-Seara, M. A. (2013). Comparison of 2D and 3D single-shot ASL perfusion fMRI sequences. *Neuroimage* 66, 662–671. doi: 10.1016/j.neuroimage.2012.10.087

Viviani, R., Messina, I., and Walter, M. (2011). Resting state functional connectivity in perfusion imaging: correlation maps with BOLD connectivity and resting state perfusion. *PLoS ONE* 6:e27050. doi: 10.1371/journal.pone.0027050

Wang, Y., Moeller, S., Li, X., Vu, A. T., Krasileva, K., Ugurbil, K., et al. (2015). Simultaneous multi-slice Turbo-FLASH imaging with CAIPIRINHA for whole brain distortion-free pseudo-continuous arterial spin labeling at 3 and 7 T. *Neuroimage* 113, 279–288. doi: 10.1016/j.neuroimage.2015.03.060

Wang, Z. (2012). Improving cerebral blood flow quantification for arterial spin labeled perfusion MRI by removing residual motion artifacts and global signal fluctuations. *Magn. Reson. Imaging* 30, 1409–1415. doi: 10.1016/j.mri.2012.05.004

Wang, Z., Aguirre, G. K., Rao, H., Wang, J., Fernandez-Seara, M. A., Childress, A. R., et al. (2008). Empirical optimization of ASL data analysis using an ASL data processing toolbox: *ASLtbx. Magn. Reson. Imaging* 26, 261–269. doi: 10.1016/j.mri.2007.07.003

Weissenbacher, A., Kasess, C., Gerstl, F., Lanzenberger, R., Moser, E., and Windischberger, C. (2009). Correlations and anticorrelations in resting-state functional connectivity MRI: a quantitative comparison of preprocessing strategies. *Neuroimage* 47, 1408–1416. doi: 10.1016/j.neuroimage.2009.05.005

Weng, S. J., Wiggins, J. L., Peltier, S. J., Carrasco, M., Risi, S., Lord, C., et al. (2010). Alterations of resting state functional connectivity in the default network in adolescents with autism spectrum disorders. *Brain Res.* 1313, 202–214. doi: 10.1016/j.brainres.2009.11.057

Windischberger, C., Langenberger, H., Sycha, T., Tschernko, E. M., Fuchsjager-Mayerl, G., Schmetterer, L., et al. (2002). On the origin of respiratory artifacts in BOLD-EPI of the human brain. *Magn. Reson. Imaging* 20, 575–582. doi: 10.1016/S0730-725X(02)00563-5

Wise, R. G., Ide, K., Poulin, M. J., and Tracey, I. (2004). Resting fluctuations in arterial carbon dioxide induce significant low frequency variations in BOLD signal. *Neuroimage* 21, 1652–1664. doi: 10.1016/j.neuroimage.2003.11.025

Wu, W.-C., Fernández-Seara, M., Detre, J. A., Wehrli, F. W., and Wang, J. (2007). A theoretical and experimental investigation of the tagging efficiency of pseudocontinuous arterial spin labeling. *Magn. Reson. Med.* 58, 1020–1027. doi: 10.1002/mrm.21403

Zhu, S., Fang, Z., Hu, S., Wang, Z., and Rao, H. (2013). Resting state brain function analysis using concurrent BOLD in ASL perfusion fMRI. *PLoS ONE* 8:e65884. doi: 10.1371/journal.pone.0065884

Zou, Q., Wu, C. W., Stein, E. A., Zang, Y., and Yang, Y. (2009). Static and dynamic characteristics of cerebral blood flow during the resting state. *Neuroimage* 48, 515–524. doi: 10.1016/j.neuroimage.2009.07.006

Conflict of Interest Statement: The authors declare that the research was conducted in the absence of any commercial or financial relationships that could be construed as a potential conflict of interest.

frontiers in Neuroscience

ORIGINAL RESEARCH
published: 02 June 2016
doi: 10.3389/fnins.2016.00237

Neuroanatomical Alterations in High-Functioning Adults with Autism Spectrum Disorder

Tehila Eilam-Stock[1,2,3], *Tingting Wu*[2], *Alfredo Spagna*[1,2], *Laura J. Egan*[1,2] and *Jin Fan*[1,2,3,4,5]*

[1] Department of Psychiatry, Icahn School of Medicine at Mount Sinai, New York, NY, USA, [2] Department of Psychology, Queens College, City University of New York, Flushing, NY, USA, [3] The Graduate Center, City University of New York, New York, NY, USA, [4] Department of Neuroscience, Icahn School of Medicine at Mount Sinai, New York, NY, USA, [5] Friedman Brain Institute, Icahn School of Medicine at Mount Sinai, New York, NY, USA

Autism spectrum disorder (ASD) is a pervasive neurodevelopmental condition, affecting cognition and behavior throughout the life span. With recent advances in neuroimaging techniques and analytical approaches, a considerable effort has been directed toward identifying the neuroanatomical underpinnings of ASD. While gray-matter abnormalities have been found throughout cortical, subcortical, and cerebellar regions of affected individuals, there is currently little consistency across findings, partly due to small sample-sizes and great heterogeneity among participants in previous studies. Here, we report voxel-based morphometry of structural magnetic resonance images in a relatively large sample of high-functioning adults with ASD ($n = 66$) and matched typically-developing controls ($n = 66$) drawn from multiple studies. We found decreased gray-matter volume in posterior brain regions, including the posterior hippocampus and cuneus, as well as increased gray-matter volume in frontal brain regions, including the medial prefrontal cortex, superior and inferior frontal gyri, and middle temporal gyrus in individuals with ASD. We discuss our results in relation to findings obtained in previous studies, as well as their potential clinical implications.

Keywords: autism, voxel-based morphometry, gray matter volume, autism brain imaging data exchange, ABIDE

OPEN ACCESS

Edited by:
Alessandro Grecucci, University of Trento, Italy

Reviewed by:
Vivek Agarwal, King George's Medical University, India
Alka Anand Subramanyam, TNMC & BYL Nair Ch. Hospital, India

***Correspondence:**
Jin Fan
jin.fan@qc.cuny.edu

Specialty section:
This article was submitted to Child and Adolescent Psychiatry, a section of the journal Frontiers in Neuroscience

Received: *29 March 2016*
Accepted: *12 May 2016*
Published: *02 June 2016*

Citation:
Eilam-Stock T, Wu T, Spagna A, Egan LJ and Fan J (2016) Neuroanatomical Alterations in High-Functioning Adults with Autism Spectrum Disorder. Front. Neurosci. 10:237. doi: 10.3389/fnins.2016.00237

INTRODUCTION

Autism spectrum disorder (ASD) is a neurodevelopmental condition characterized by abnormal social interactions and communication, repetitive behaviors, restricted interests, and atypical sensory processing (American Psychiatric Association, 2013). Advances in neuroimaging techniques and analyses over the past two decades have led to a burgeoning of structural studies aimed toward identifying the neuroanatomical underpinnings of ASD. Overall, findings suggest a complex neurodevelopmental trajectory, characterized by an early brain overgrowth (Courchesne et al., 2003; Zielinski et al., 2014; Zwaigenbaum et al., 2014), followed by arrested growth later in childhood and early adolescence (Courchesne et al., 2001; Mak-Fan et al., 2012), and accelerated neural atrophy later in adulthood (Courchesne et al., 2011; Lange et al., 2015). While studies were able to localize the neuroanatomical alterations in ASD to specific brain regions (Carper and Courchesne, 2005; Schumann et al., 2010; Scheel et al., 2011; Zielinski et al., 2014; Dierker et al., 2015; Libero et al., 2015), structures (Stanfield et al., 2008; Schumann et al., 2009; Via et al., 2011; Nickl-Jockschat et al., 2012; Maier et al., 2015) and networks (Ameis et al., 2011; Barttfeld et al., 2011; Solso et al., 2015), reports have been largely inconsistent.

The inconsistency in neuroanatomical findings of previous studies may have stemmed from several factors, including differences in methodology, data acquisition, analytical approaches, clinical and demographic characteristics of the samples, as well as small sample-sizes. As ASD is a complex condition with multiple etiologies, risk factors, and diverse clinical manifestations (Amaral et al., 2008; Ecker et al., 2013b; Chen et al., 2015), there is an inherent variability among individuals with ASD that is likely related to variations in neuroanatomical abnormalities. Indeed, ASD is linked to a great variety of gene mutations, each of which has the potential to affect neural development through different pathways and in different ways, including gene transcription, expression and regulation, protein synthesis and translation, synaptic formation and function, as well as cell migration (Persico and Bourgeron, 2006; Sahin and Sur, 2015). The clinical manifestation of ASD symptoms can also vary between affected individuals (Amaral et al., 2008), and there is an ongoing debate among scientists and clinicians regarding the inclusion of previously diagnostically-segregated groups (e.g., Asperger's syndrome vs. autism) under the unifying umbrella of the new guidelines for ASD diagnosis (Mcalonan et al., 2008; Toal et al., 2010; Mandy et al., 2012). In addition, intelligence quotient (IQ) scores vary significantly between individuals with ASD, with intellectual disability in the majority of affected individuals, but average or above-average scores in the high-functioning end of the spectrum (Toal et al., 2010).

In order to address the inconsistency in neuroanatomical reports of ASD, recent studies have used meta-analytic approaches (Cauda et al., 2011; Duerden et al., 2012; DeRamus and Kana, 2015), larger sample-sizes (Toal et al., 2010; Ecker et al., 2012; Haar et al., 2014; Itahashi et al., 2015; Sussman et al., 2015), and stricter inclusion criteria according to age (Raznahan et al., 2009; Toal et al., 2010; Greimel et al., 2013), gender (Ecker et al., 2012; Itahashi et al., 2015), IQ (Ecker et al., 2012; Itahashi et al., 2015; Maier et al., 2015), and diagnosis (Mcalonan et al., 2008; Toal et al., 2010; Via et al., 2011). Multivariate classification techniques were also used in an attempt to better characterize the complex patterns of neuroanatomical alterations in ASD (Ecker et al., 2010a,b; Jiao et al., 2010; Uddin et al., 2011; Haar et al., 2014). Only a few studies, however, investigated brain anatomy in large, matched samples of high-functioning adults with ASD and typically-developing controls (TDC) (e.g., Ecker et al., 2012).

To mitigate issues of sample variability and inconsistent findings, we conducted a neuromorphometric study in a relatively large sample of high-functioning adults with ASD ($n = 66$) and gender, age, and IQ-matched TDC ($n = 66$). The samples were selected from the Autism Brain Imaging Data Exchange (ABIDE) database (Di Martino et al., 2014), and included data from ASD and TDC participants collected in a previous study from our lab as well. We used voxel-based morphometry (VBM) (Ashburner and Friston, 2000), an automated, unbiased, and conservative approach, to investigate alterations in regional gray-matter (GM) volume of individuals with ASD. We also examined the possible contributions of gender, age, and ASD symptom severity by including them as regressors in our model.

MATERIALS AND METHODS

Participants

The samples were selected from the ABIDE database (Di Martino et al., 2014), which is a multicenter database containing anatomical MRI scans, clinical measures, and demographic data from approximately 1000 participants, with age range of 6–65 years. The ABIDE database offers a non-precedent opportunity for investigating neuroanatomical alterations in large samples of individuals with ASD. The MRI data selected for this study were collected from ASD and TDC adult participants in three different sites: New York University Langone Medical Center (NYU), Social Brain Lab at the Research School of Behavioral and Cognitive Neurosciences, NeuroImaging Center, University Medical Center Groeningen and Netherlands Institute for Neurosciences (SBL), and Katholieke Universiteit Leuven (KUL). Only participants with T1 images and sites that provided a relatively large number of adult participants (at least 12 in each group) were included. Participants who could not be matched according to their demographic data were excluded. MRI data from a previous study conducted in our lab at the Icahn School of Medicine at Mount Sinai (ISMMS; Eilam-Stock et al., 2014) were also used. The total number of participants was 66 in the ASD group and 66 in the TDC group (NYU $n = 19$; SBL $n = 15$; KUL $n = 14$; ISMMS $n = 18$). Demographic information for the combined samples are shown in **Table 1**.

Selected participants with ASD were all in the high-functioning end of the spectrum (IQ > 80), and received a DSM-IV-TR diagnosis of Autistic Disorder, Asperger's Disorder, or Pervasive Developmental Disorder Not-Otherwise-Specified. Detailed information regarding the diagnostic protocols for the ABIDE database at each site are publicly available on the ABIDE website (http://fcon_1000.projects.nitrc.org/indi/abide). After matching for gender, the ASD and TDC groups were matched on age across sites [$t_{(130)} = 0.2$; $p = 0.99$] and within each site separately [NYU $t_{(36)} = 0.23$; $p = 0.81$; SBL $t_{(28)} = 0.40$; $p = 0.69$; KUL $t_{(26)} = -1.10$; $p = 0.28$; ISMMS $t_{(34)} = 0.18$; $p = 0.86$]. The ASD and TDC groups were also matched on full score IQ (FSIQ) across sites [$t_{(113)} = 1.7$; $p = 0.9$] and within each site [NYU $t_{(36)} = -1.16$; $p = 0.25$; KUL $t_{(26)} = -0.72$; $p = 0.48$; ISMMS $t_{(34)} = 1.25$; $p = 0.22$], with the exception of participants from the SBL dataset for whom FSIQ scores were not available. Of note, however, all ASD and TDC participants from the SBL dataset were tested for FSIQ, and their scores were all within the normal range (http://fcon_1000.projects.nitrc.org/indi/abide/).

All sites contributing to the ABIDE database received approval from their local Institutional Review Boards for the acquisition of their data. In addition, all data retrieved from the ABIDE database are completely anonymous with no inclusion of protected health information, as required by the HIPAA guidelines (http://fcon_1000.projects.nitrc.org/indi/abide/). For the data acquired at ISMMS, all participants provided written informed consent, approved by the Institutional Review Board.

TABLE 1 | Demographic information.

Group	*n*	Age (years)				Gender		Full Scale IQ			
		Mean	SD	Max	Min	*M*	*F*	Mean	SD	Max	Min
TDC											
Total	66	27	7	43	18	60	6	114	12	143	89
SBL	15	34	7	42	20	15		–	–	–	–
KUL	14	23	3	29	18	14		113	10	134	98
NYU	19	25	5	32	18	15	4	113	12	139	91
ISMMS	18	28	7	43	20	16	2	117	15	143	89
ASD											
Total	66	27	8	64	18	60	6	110	14	143	80
SBL	15	35	10	64	22	15		–	–	–	–
KUL	14	22	4	32	18	14		109	13	128	89
NYU	19	25	6	39	18	15	4	108	13	137	80
ISMMS	18	28	6	42	19	16	2	111	17	143	87

TDC, typically-developed controls; ASD, autism spectrum disorder; SD, standard deviation; the two samples (TDC, ASD) did not differ in age [$t_{(130)} = 0.20$; $p = 0.99$] and in IQ [$t_{(113)} = 1.70$; $p = 0.90$].

Voxel-Based Morphometry Analysis

To measure differences in GM volume between the ASD and TDC groups, we conducted VBM analyses using the VBM8 toolbox (http://dbm.neuro.uni-jena.de/vbm) and Statistical Parametric Mapping (SPM8, Welcome Trust Centre for Neuroimaging, University College London, UK) in MATLAB R2012b (Mathworks Inc., Sherborn, MA). First, all T1-weighted images were manually reoriented to the anterior commissure—posterior commissure plane to improve the coregistration of T1 images to the template. Then, each image was segmented into six tissue classes (i.e., GM, white matter, cerebrospinal fluid, bone, non-brain soft tissue, and air outside of the head and in nose, sinus, and ears) using the SPM standard tissue probability map (Mazziotta et al., 1995) with default parameters. Segmented GM images were spatially normalized to the "IXI500_MNI152" template, using the DARTEL algorithm (Ashburner, 2007) with default parameters. Non-linear warping for the effect of spatial normalization was corrected to generate these modulated normalized images, which represent relative volume after correcting for brain size. Each image was then smoothed using an 8-mm full width at half maximum Gaussian kernel.

A two-sample *t*-test was conducted for smoothed GM volume images from the ASD and TDC groups using a random-effect general linear model (GLM), with gender and age as nuisance regressors. Because the scans were taken at multiple sites which may have different MRI scanners and scanning protocols, an inherent variability may exist within the data. Therefore, we included an equal number of ASD and TDC participants within each site. We also used the locations as a dummy variable in our model. As suggested by the VBM8 manual, an absolute threshold mask of 0.1 was used for all the second-level analyses. To test the relationship between autism symptom severity and GM volume, we conducted an additional second-level GLM analysis for ASD participants, using their Autism Diagnostic Observation Schedule (ADOS) scores (Lord et al., 2000) as a regressor. Higher ADOS scores are indicative of increased ASD severity. Forty ASD participants for whom the ADOS scores were available (ABIDE $n = 27$; ISMMS $n = 13$) were selected from the original sample for this analysis. The significance level for the height of each voxel was set to $p < 0.005$ (uncorrected), with a contiguous-voxel extent threshold k > 17 voxels, to correct for multiple voxel comparisons. This threshold was estimated by using 10,000 Monte Carlo simulations with a customized Matlab program (Slotnick et al., 2003). The corrected a priori height threshold was $p < 0.05$.

RESULTS

Between-Group Differences in Gray-Matter Volume

A between-group comparison of GM volume revealed increased volume in frontal, temporal, and cerebellar brain regions in the ASD group, compared to the TDC group. These regions included the medial prefrontal cortex (extending to the right), left superior frontal gyrus, left inferior frontal gyrus—pars opercularis (Broca's area), left inferior frontal gyrus—pars orbitalis, left middle temporal gyrus, and left cerebellum VIIb (**Figure 1** and **Table 2**). In addition, compared to the TDC group, decreased GM volume in posterior brain regions in the ASD group was found, including the left posterior hippocampus and the cuneus bilaterally (**Figure 1** and **Table 2**). These results remained consistent following an additional GLM analyses with age, gender, and site as nuisance regressors.

Neuroanatomical Correlations with ASD Symptom Severity

To assess the relationship between ASD symptom severity and GM volume, ADOS scores of 40 participants with ASD were used as a regressor in our GLM model. Results revealed negative correlations between symptom severity and GM volume in the right superior frontal gyrus, left middle frontal gyrus, inferior frontal gyri—pars orbitalis bilaterally, restrosplenial

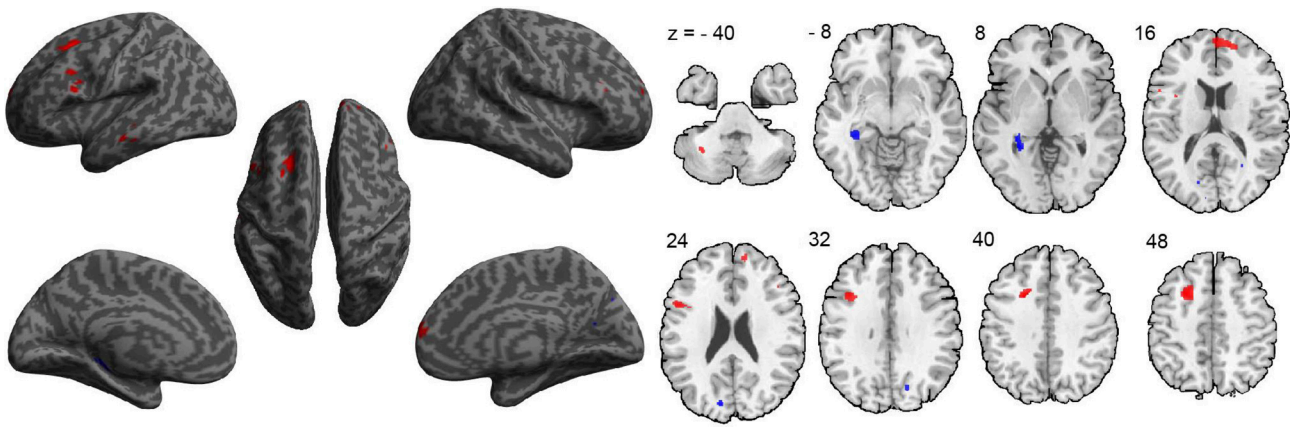

FIGURE 1 | Differences in gray-matter volume between the ASD and TDC groups. Red indicates areas of increased gray-matter volume in ASD (ASD > TDC). Blue indicates areas of decreased gray-matter volume in ASD (ASD < TDC).

TABLE 2 | Brain regions with abnormal gray-matter volume in ASD.

Region	L/R	BA	*x*	*y*	*z*	T	Z	K
ASD < TDC								
Posterior Hippocampus	L	36	−35	−36	−3	3.53	3.44	283
Cuneus	L	18/19	−12	−83	23	3.48	3.40	83
Cuneus	R	18	17	−72	32	2.82	2.77	31
ASD > TDC								
Superior frontal gyrus	L	8	−21	12	44	3.85	3.74	455
Superior frontal gyrus (medial)	R	10	2	54	11	3.50	3.41	634
Inferior frontal gyrus	L	44	−39	15	32	3.37	3.29	91
Inferior frontal gyrus	L	44	−51	11	26	3.35	3.27	196
Middle temporal gyrus	L	21	−62	−12	−14	3.12	3.06	86
Middle temporal gyrus	L	21	−59	−27	−12	3.06	3.00	35
Superior frontal gyrus (medial)	L	10	−18	62	21	2.97	2.91	28
Inferior frontal gyrus	R	45	44	29	26	2.92	2.87	18
Cerebellum VIIb	L		−33	−57	−41	2.91	2.86	24
Inferior frontal gyrus	L	47	−50	39	−15	2.87	2.82	34

Height threshold: T = 2.72, p < 0.005, Extent threshold: k > 17.

cortex bilaterally, supplementary motor area bilaterally, right middle cingulate cortex, thalamus bilaterally, and putamen bilaterally (**Figure 2** and **Table 3**), indicating that decreased GM volume in these regions is associated with more severe ASD symptoms. No significant positive correlations between symptom severity and GM volume were found.

DISCUSSION

Gray-Matter Volume Abnormalities along the Anterior-Posterior Axis

Our results show a general pattern of increased GM volume in anterior brain regions and decreased GM volume in posterior brain regions in the ASD group, relative to TDC. A few theoretical accounts for the lobular specificity of neuroanatomical abnormalities in ASD across development have emerged, and may shed light on the differences in GM volume found in our study. Research on brain development in ASD across the lifespan has demonstrated a complex neurodevelopmental trajectory in affected individuals, characterized by an early brain overgrowth (Courchesne et al., 2003; Zielinski et al., 2014; Zwaigenbaum et al., 2014), followed by arrested growth later in childhood and early adolescence (Courchesne et al., 2001; Mak-Fan et al., 2012), and accelerated neural atrophy in adulthood (Courchesne et al., 2011; Lange et al., 2015). Studies in very young individuals with ASD (i.e., 2–4 years old) observed an increase of 5–12% in brain volume that was specifically localized to the frontal and temporal lobes (Carper et al., 2002; Redcay and Courchesne, 2005; Courchesne et al., 2007). This significant enlargement in anterior brain regions is reduced in older ages, though

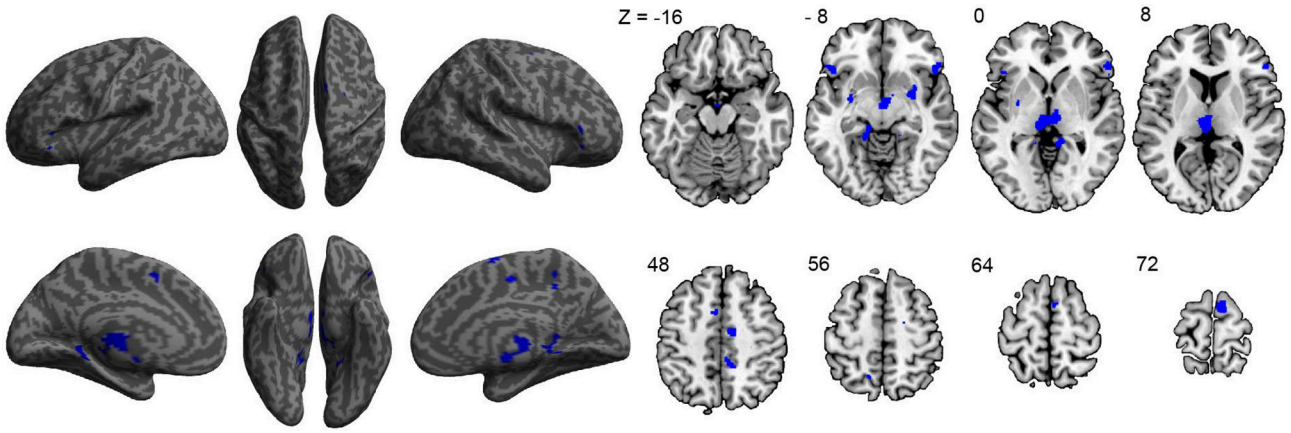

FIGURE 2 | Correlations between gray-matter volume and ASD symptom severity as indicated by the ADOS scores of each participant ($n = 40$). All significant correlations found were negative and are indicated in blue.

TABLE 3 | Correlations between gray-matter volume and ASD symptom severity.

Region	L/R	BA	*x*	*y*	*z*	T	Z	K
NEGATIVE								
Inferior frontal gyrus	R	47	54	24	−9	4.35	3.88	301
Inferior frontal gyrus	R	45	54	32	3	3.18	2.97	
Corpus mamillare	R		3	−12	−12	4.27	3.82	1342
Restrosplenial cortex	L	30	−15	−41	−6	3.67	3.36	
Thalamus	R		9	−18	−3	3.54	3.26	
Thalamus	L		6	−19	−3	3.33	3.09	
Mid cingulate cortex	R	6	14	−11	50	4.26	3.81	77
Restrosplenial cortex	R	30	8	−42	0	4.04	3.65	193
Inferior frontal gyrus	L	47	−47	23	−6	3.70	3.39	178
Supplementary motor area	R	6	6	0	74	3.69	3.38	198
Mid cingulate cortex	R	23	8	−39	48	3.24	3.02	139
Precuneus	L	7	−14	−59	56	3.22	3.00	19
Putamen	R		30	2	−9	3.10	2.90	143
Middle frontal gyrus	L	8/9	−32	36	44	3.07	2.87	20
Putamen	L		−30	−6	−6	2.97	2.79	95
Supplementary motor area	L	6	−9	9	51	2.96	2.78	79
Superior frontal gyrus	R	6	21	−6	59	2.90	2.73	25

n = 40, Height threshold: T = 2.72, p < 0.005, Extent threshold: k > 17. Structures listed below clusters with a K-value were within that same cluster with different local maxima.

GM volume in these regions continues to be greater in ASD participants relative to TDC throughout development (1–3% increase) (Redcay and Courchesne, 2005; Courchesne et al., 2007). By contrast, the occipital lobe is not enlarged in young children with ASD (Carper et al., 2002; Courchesne et al., 2007). The occipital lobe is phylogenetically older than the frontal and temporal lobes, and its maturation occurs earlier in development (Ecker et al., 2013b); while the frontal and temporal lobes continue to develop throughout the first years of life, the occipital lobe does not change dramatically across the life span in typically developing individuals (Gogtay and Thompson, 2010).

Models of ASD suggest that the frontal and temporal enlargements that characterize early brain development in ASD may be a result of increased numbers of excitatory pyramidal neurons in these regions (Courchesne and Pierce, 2005a; Courchesne et al., 2007, 2011; Santos et al., 2011). This localized overgrowth may damage the local connectivity patterns within these regions, as well as the large-scale connectivity between these regions and the rest of the brain (Courchesne and Pierce, 2005b; Courchesne et al., 2007; Geschwind and Levitt, 2007; Ecker et al., 2013b; Chen et al., 2015). In the typically-developing brain, the connectivity patterns that develop throughout the first years of life allow for the higher-level cognitive skills that develop at

the same time, including socio-emotional skills, language, and executive functions (Akshoomoff et al., 2002; Courchesne et al., 2007). Thus, it is reasonable to hypothesize that the aberrant connectivity patterns in ASD within the overgrowing frontal and temporal lobes, as well as between these regions and the rest of the brain, are at the core of the cognitive and behavioral deficits in ASD (Akshoomoff et al., 2002; Geschwind and Levitt, 2007). As individuals with ASD reach adulthood, processes of accelerated neuronal atrophy take place throughout the brain (Courchesne et al., 2011; Lange et al., 2015), perhaps to compensate for the early overgrowth in these individuals. The early localized enlargement of the anterior brain in ASD, together with the later broader neuronal atrophy in these individuals may, therefore, account for both our and others (e.g., Ecker et al., 2012) findings in adult ASD samples. The accelerated atrophy in adulthood may cause a GM volume decrease in both anterior parts of the brain, which are still greater relative to TDC though to a lesser extent, as well as in the posterior brain (mainly in the occipital cortex), which is now reduced relative to TDC.

Gray-Matter Volume Abnormalities in Cortical and Sub-Cortical Brain Regions

ASD is a complex disorder with multiple symptoms affecting both high-level (e.g., socio-emotional processing, self-referential processing, language) and low-level (e.g., sensory processing) functions. It is not surprising, therefore, that the extent of neuroanatomical alterations found in our study, as well as in previous empirical investigations, encompasses regions, structures, and neural networks throughout the brain. A hallmark of ASD is abnormal socio-emotional processing, including deficits in theory of mind (i.e., the ability to understand other's beliefs, intentions and perspectives; Baron-Cohen et al., 1985; Baron-Cohen, 2000; Pilowsky et al., 2000), affective evaluations (Hill et al., 2004; Dapretto et al., 2006), and empathy (Minio-Paluello et al., 2009; Fan et al., 2013; Hadjikhani et al., 2014; Gu et al., 2015). Theory of mind relies on several neural regions, including the medial prefrontal cortex, lateral orbitofrontal cortex, middle frontal gyrus, superior temporal gyrus, temporal pole, temporoparietal junction, and cuneus (Frith and Frith, 1999; Gallagher and Frith, 2003; Saxe and Kanwisher, 2003; Amodio and Frith, 2006; Völlm et al., 2006). In our study we found GM abnormalities in the medial prefrontal cortex (increased GM volume) and cuneus (decreased GM volume). We also found negative correlations between GM volume in the middle frontal gyrus and ASD symptom severity. These structural abnormalities may be related, therefore, to the commonly seen theory of mind deficits in individuals with ASD. Our finding of increased GM volume in the medial prefrontal cortex in ASD may also explain the emotional evaluation difficulties commonly seen in this disorder, as this region plays a role in that domain as well (Phan et al., 2002; Harris et al., 2007; Etkin et al., 2011).

Our results of GM abnormalities in the inferior frontal gyrus, but not the ventromedial prefrontal cortex, may be related to a specific deficit in emotional empathy (e.g., feeling another person's pain) but preserved cognitive empathy (e.g., understanding that another person is in pain) in ASD (Minio-Paluello et al., 2009; Fan et al., 2013; Hadjikhani et al., 2014). Indeed, a recent lesion study demonstrated an anatomical dissociation between the cognitive and emotional components of empathy, such that the ventromedial prefrontal cortex is necessary for cognitive empathy, while the inferior frontal gyrus is essential for emotional empathy (Shamay-Tsoory et al., 2009). Additionally, in a functional MRI study investigating brain regions associated with empathy for pain, we found abnormal brain activation in the inferior frontal gyrus in ASD, with no group differences in ventromedial prefrontal cortex activation (Gu et al., 2015).

Our findings also point to several GM abnormalities in ASD that may be related to limited self-referential processing (Lombardo et al., 2007, 2010; Uddin, 2011) and autobiographical memory (Bowler et al., 2000; Crane and Goddard, 2008; Lind and Bowler, 2010) in this disorder. Studies that investigated the neural substrates of self-referential processing in typically-developing samples found that these processes activate a set of regions along the medial axis of the brain, commonly termed cortical midline structures (Northoff et al., 2006), including the medial prefrontal cortex/pregenual anterior cingulate cortex, the dorsomedial prefrontal cortex/middle cingulate cortex, and the precuneus/posterior cingulate cortex (Kelley et al., 2002; Northoff et al., 2006; Lombardo et al., 2010). The left inferior frontal gyrus was also found to be activated during self-related judgments (Kelley et al., 2002). In addition, the posterior hippocampus is involved in the storage and retrieval of autobiographical memories (Fernández et al., 1998; Kim, 2015). Our results of increased GM volume in the medial prefrontal cortex and the left inferior frontal gyrus, decreased GM volume in the posterior hippocampus, and negative correlations between GM volume in the middle cingulate cortex and precuneus and ASD symptom severity, may be related, therefore, to aberrant self-referential processing and autobiographical memory in individuals with ASD.

The increased GM volume in the left inferior frontal gyrus and left middle temporal gyrus in the ASD group in the present study may be related to altered language functions in affected individuals, especially in the semantics domain. Although language abilities vary greatly across the ASD spectrum, ranging from a severe language delay to normal language development, there is empirical evidence suggesting that semantic processing is compromised even in high-functioning individuals with ASD who do not exhibit any language delay (Harris et al., 2006; Kamio et al., 2007). High-functioning adults with ASD also showed significantly reduced activation in the left inferior frontal gyrus (Broca's area) during semantic processing (Harris et al., 2006). Indeed, the left inferior frontal gyrus, together with the left middle temporal gyrus, is involved in semantic processing in the typically-developing brain (Goel and Dolan, 2001; Visser et al., 2012). In our study, both of these regions were identified as areas of increased GM volume in ASD, which may serve as neuroanatomical substrates for the abnormal semantic processing in this disorder.

Although we did not find GM alterations in the thalamus in ASD, we did find a significant negative correlation between

thalamic GM volume and ASD symptom severity. In addition, we observed decreased GM volume in the cuneus in the ASD group. The thalamus is a main hub for sensory processing across modalities, and it can affect sensory perception by integrating and relaying feedforward and feedback information between the sensory cortices and higher-order cortical regions (e.g., frontal lobe; Alitto and Usrey, 2003; Cudeiro and Sillito, 2006; Briggs and Usrey, 2008). The cuneus is a secondary visual area which may play a role in modulation of visual processing (Vanni et al., 2001). Abnormal sensory processing (both hyper-and-hypo-sensitivity) have been extensively documented in the ASD literature, especially in the visual modality (Behrmann et al., 2006; Vandenbroucke et al., 2008), and are now included in the ASD diagnostic criteria in the diagnostic and statistical manual of mental disorders (DSM-5) (American Psychiatric Association, 2013). Together, these findings may be related to the abnormal sensory processing commonly seen in individuals with ASD.

LIMITATIONS

Although our results are consistent with some previous reports, they did not replicate other findings of GM alterations in adults with ASD. For example, in a study that specifically examined between-group differences in the amygdala and hippocampus in 30 high-functioning (IQ $>$ 100) adults with ASD and gender, age, and IQ matched control participants (Maier et al., 2015), increased hippocampal volume bilaterally was found in ASD, opposite to our results. Yet, other studies failed to find any significant differences in GM volume between adults with ASD and TDC (Haar et al., 2014; Riedel et al., 2014; Riddle et al., 2016). This variability in structural findings may be due to relatively small sample sizes (Riedel et al., 2014; Maier et al., 2015) or differences in methodology and sample characteristics (Haar et al., 2014; Riddle et al., 2016). Thus, large-sample studies of different sub-groups within the ASD spectrum will likely promote a better characterization of neuroanatomical alterations that contribute to ASD symptomatology.

The current study took advantage of the relatively large sample of participants with ASD provided by the ABIDE database, and limited the inclusion criteria (i.e., high-functioning adults) to increase statistical power and reduce variability. However, as ASD is a complex condition with multiple contributing factors and etiologies, it is possible that our sample was not sufficiently homogeneous. While we attempted to control for different variables that may have contributed to the previously reported inconsistent findings, such as age and IQ, there are many other factors we did not take into account, such as genetic factors or clinical presentations. On the other hand, when using stricter inclusion criteria, the generalizability of the data is inevitably reduced. For example, it is possible that our findings represent neuroanatomical alterations in high-functioning adults with ASD only, and are less applicable to the majority of the ASD population, which has lower level of functioning and greater symptom severity. Studies with more individuals across the spectrum and higher severity of autism may shed a different light on the matter entirely. Future studies that continue to investigate neuroanatomy in large samples of affected individuals from different clinical and demographic subgroups, will, therefore, significantly contribute to our understanding of neuroanatomical alterations in individuals with ASD.

We measured GM volume using voxel-based morphometry, as this is one of the most informative and commonly used measures in the study of neuroanatomical abnormalities in clinical populations. However, other neuroanatomical measures were used in previous studies of ASD, which may also be useful indicators of structural abnormalities. These include measures of cortical folding and sulcal depth (Nordahl et al., 2007), cortical thickness (Hyde et al., 2010), cortical surface area (Ecker et al., 2013a), local gyrification index (Wallace et al., 2013), as well as diffusion tensor imaging for white-matter tract (Ameis et al., 2011; see Ecker et al., 2015 for review). Multivariate classification techniques were also recently used as a viable method for identifying complex patterns of neuroanatomical alterations in ASD (Ecker et al., 2010a,b; Jiao et al., 2010; Uddin et al., 2011; Haar et al., 2014). It would be valuable, therefore, to conduct studies with large samples that look at other structural measures as well.

CLINICAL IMPLICATIONS

Our study adds to the growing literature investigating neuroanatomical abnormalities in ASD. The research endeavor to characterize the profile of brain anatomy in ASD across development may have clinical implications, as it may facilitate identification of biomarkers for different subgroups within the ASD spectrum (Ecker et al., 2013b, 2015). While the behavioral markers of ASD have been extensively investigated and are relatively defined and agreed upon by researchers and clinicians, the neuroanatomical, neurofunctional and genetic profiles of ASD still warrant rigorous research. Once our knowledge of the different markers of ASD has been sufficiently advanced, the different pieces of the puzzle will come together to create a clear picture of this currently ill-understood disorder. This will allow for better diagnosis and treatment for ASD, which may be more specific to individuals or subgroups within the spectrum.

AUTHOR CONTRIBUTIONS

All authors (TE, TW, AS, LE, and JF) contributed to data analysis and report writing.

FUNDING

JF and AS were supported by the grant from Simons Foundation Autism Research Initiative (SFARI) 330704. JF was also supported by the National Institute of Mental Health of the National Institutes of Health under Award Number of and R21 MH083164. The content is solely the responsibility of the authors. The funders had no role in study design, data collection and analysis, decision to publish, or preparation of the manuscript.

ACKNOWLEDGMENTS

We thank the numerous contributors to the ABIDE database for their effort in the collection, organization and sharing of their datasets, the NITRC (http://www.nitrc.org) for providing the data sharing platform for the ABIDE initiative, and the other informatics databases for providing additional platforms (see http://fcon_1000.projects.nitrc.org/indi/abide).

REFERENCES

Akshoomoff, N., Pierce, K., and Courchesne, E. (2002). The neurobiological basis of autism from a developmental perspective. *Dev. Psychopathol.* 14, 613–634. doi: 10.1017/S0954579402003115

Alitto, H. J., and Usrey, W. M. (2003). Corticothalamic feedback and sensory processing. *Curr. Opin. Neurobiol.* 13, 440–445. doi: 10.1016/S0959-4388(03)00096-5

Amaral, D. G., Schumann, C. M., and Nordahl, C. W. (2008). Neuroanatomy of autism. *Trends Neurosci.* 31, 137–145. doi: 10.1016/j.tins.2007.12.005

Ameis, S. H., Fan, J., Rockel, C., Voineskos, A. N., Lobaugh, N. J., Soorya, L., et al. (2011). Impaired structural connectivity of socio-emotional circuits in autism spectrum disorders: a diffusion tensor imaging study. *PLoS ONE* 6:e28044. doi: 10.1371/journal.pone.0028044

American Psychiatric Association (2013). *Diagnostic and Statistical Manual of Mental Disorders: DSM-5.* Arlington: American Psychiatric Association.

Amodio, D. M., and Frith, C. D. (2006). Meeting of minds: the medial frontal cortex and social cognition. *Nat. Rev. Neurosci.* 7, 268–277. doi: 10.1038/nrn1884

Ashburner, J. (2007). A fast diffeomorphic image registration algorithm. *Neuroimage* 38, 95–113. doi: 10.1016/j.neuroimage.2007.07.007

Ashburner, J., and Friston, K. J. (2000). Voxel-based morphometry–the methods. *Neuroimage* 11, 805–821. doi: 10.1006/nimg.2000.0582

Baron-Cohen, S. (2000). *Theory of Mind and Autism: A Fifteen Year Review*. New York, NY: Oxford University Press.

Baron-Cohen, S., Leslie, A. M., and Frith, U. (1985). Does the autistic child have a "theory of mind"? *Cognition* 21, 37–46. doi: 10.1016/0010-0277(85)90022-8

Barttfeld, P., Wicker, B., Cukier, S., Navarta, S., Lew, S., and Sigman, M. (2011). A big-world network in ASD: dynamical connectivity analysis reflects a deficit in long-range connections and an excess of short-range connections. *Neuropsychologia* 49, 254–263. doi: 10.1016/j.neuropsychologia.2010.11.024

Behrmann, M., Thomas, C., and Humphreys, K. (2006). Seeing it differently: visual processing in autism. *Trends Cogn. Sci.* 10, 258–264. doi: 10.1016/j.tics.2006.05.001

Bowler, D. M., Gardiner, J. M., and Grice, S. J. (2000). Episodic memory and remembering in adults with asperger syndrome. *J. Autism Dev. Disord.* 30, 295–304. doi: 10.1023/A:1005575216176

Briggs, F., and Usrey, W. M. (2008). Emerging views of corticothalamic function. *Curr. Opin. Neurobiol.* 18, 403–407. doi: 10.1016/j.conb.2008.09.002

Carper, R. A., and Courchesne, E. (2005). Localized enlargement of the frontal cortex in early autism. *Biol. Psychiatry* 57, 126–133. doi: 10.1016/j.biopsych.2004.11.005

Carper, R. A., Moses, P., Tigue, Z. D., and Courchesne, E. (2002). Cerebral lobes in autism: early hyperplasia and abnormal age effects. *Neuroimage* 16, 1038–1051. doi: 10.1006/nimg.2002.1099

Cauda, F., Geda, E., Sacco, K., D'agata, F., Duca, S., Geminiani, G., et al. (2011). Grey matter abnormality in autism spectrum disorder: an activation likelihood estimation meta-analysis study. *J. Neurol. Neurosurg. Psychiatry* 82, 1304–1313. doi: 10.1136/jnnp.2010.239111

Chen, J. A., Peñagarikano, O., Belgard, T. G., Swarup, V., and Geschwind, D. H. (2015). The Emerging Picture of Autism Spectrum Disorder: genetics and pathology. *Annu. Rev. Pathol. Mech. Dis.* 10, 111–144. doi: 10.1146/annurev-pathol-012414-040405

Courchesne, E., Campbell, K., and Solso, S. (2011). Brain growth across the life span in autism: age-specific changes in anatomical pathology. *Brain Res.* 1380, 138–145. doi: 10.1016/j.brainres.2010.09.101

Courchesne, E., Carper, R., and Akshoomoff, N. (2003). Evidence of brain overgrowth in the first year of life in autism. *JAMA* 290, 337–344. doi: 10.1001/jama.290.3.337

Courchesne, E., Karns, C., Davis, H., Ziccardi, R., Carper, R., Tigue, Z., et al. (2001). Unusual brain growth patterns in early life in patients with autistic disorder an MRI study. *Neurology* 57, 245–254. doi: 10.1212/WNL.57.2.245

Courchesne, E., and Pierce, K. (2005a). Brain overgrowth in autism during a critical time in development: implications for frontal pyramidal neuron and interneuron development and connectivity. *Int. J. Dev. Neurosci.* 23, 153–170. doi: 10.1016/j.ijdevneu.2005.01.003

Courchesne, E., and Pierce, K. (2005b). Why the frontal cortex in autism might be talking only to itself: local over-connectivity but long-distance disconnection. *Curr. Opin. Neurobiol.* 15, 225–230. doi: 10.1016/j.conb.2005.03.001

Courchesne, E., Pierce, K., Schumann, C. M., Redcay, E., Buckwalter, J. A., Kennedy, D. P., et al. (2007). Mapping early brain development in autism. *Neuron* 56, 399–413. doi: 10.1016/j.neuron.2007.10.016

Crane, L., and Goddard, L. (2008). Episodic and semantic autobiographical memory in adults with autism spectrum disorders. *J. Autism Dev. Disord.* 38, 498–506. doi: 10.1007/s10803-007-0420-2

Cudeiro, J., and Sillito, A. M. (2006). Looking back: corticothalamic feedback and early visual processing. *Trends Neurosci.* 29, 298–306. doi: 10.1016/j.tins.2006.05.002

Dapretto, M., Davies, M. S., Pfeifer, J. H., Scott, A. A., Sigman, M., Bookheimer, S. Y., et al. (2006). Understanding emotions in others: mirror neuron dysfunction in children with autism spectrum disorders. *Nat. Neurosci.* 9, 28–30. doi: 10.1038/nn1611

DeRamus, T. P., and Kana, R. K. (2015). Anatomical likelihood estimation meta-analysis of grey and white matter anomalies in autism spectrum disorders. *Neuroimage Clin.* 7, 525–536. doi: 10.1016/j.nicl.2014.11.004

Dierker, D. L., Feczko, E., Pruett, J. R., Petersen, S. E., Schlaggar, B. L., Constantino, J. N., et al. (2015). Analysis of cortical shape in children with simplex autism. *Cereb. Cortex* 25, 1042–1051. doi: 10.1093/cercor/bht294

Di Martino, A., Yan, C.-G., Li, Q., Denio, E., Castellanos, F. X., Alaerts, K., et al. (2014). The autism brain imaging data exchange: towards a large-scale evaluation of the intrinsic brain architecture in autism. *Mol. Psychiatry* 19, 659–667. doi: 10.1038/mp.2013.78

Duerden, E. G., Mak-Fan, K. M., Taylor, M. J., and Roberts, S. W. (2012). Regional differences in grey and white matter in children and adults with autism spectrum disorders: an activation likelihood estimate (ALE) meta-analysis. *Autism Res.* 5, 49–66. doi: 10.1002/aur.235

Ecker, C., Bookheimer, S. Y., and Murphy, D. G. (2015). Neuroimaging in autism spectrum disorder: brain structure and function across the lifespan. *Lancet Neurol.* 14, 1121–1134. doi: 10.1016/S1474-4422(15)00050-2

Ecker, C., Ginestet, C., Feng, Y., Johnston, P., Lombardo, M. V., Lai, M. C., et al. (2013a). Brain surface anatomy in adults with autism: the relationship between surface area, cortical thickness, and autistic symptoms. *JAMA Psychiatry* 70, 59–70. doi: 10.1001/jamapsychiatry.2013.265

Ecker, C., Marquand, A., Mourao-Miranda, J., Johnston, P., Daly, E. M., Brammer, M. J., et al. (2010a). Describing the brain in autism in five dimensions–magnetic resonance imaging-assisted diagnosis of autism spectrum disorder using a multiparameter classification approach. *J. Neurosci.* 30, 10612–10623. doi: 10.1523/JNEUROSCI.5413-09.2010

Ecker, C., Rocha-Rego, V., Johnston, P., Mourao-Miranda, J., Marquand, A., Daly, E. M., et al. (2010b). Investigating the predictive value of whole-brain structural MR scans in autism: a pattern classification approach. *Neuroimage* 49, 44–56. doi: 10.1016/j.neuroimage.2009.08.024

Ecker, C., Spooren, W., and Murphy, D. G. (2013b). Translational approaches to the biology of autism: false dawn or a new era? *Mol. Psychiatry* 18, 435–442. doi: 10.1038/mp.2012.102

Ecker, C., Suckling, J., Deoni, S. C., Lombardo, M. V., Bullmore, E. T., Baron-Cohen, S., et al. (2012). Brain anatomy and its relationship to behavior in adults with autism spectrum disorder: a multicenter

magnetic resonance imaging study. *Arch. Gen. Psychiatry* 69, 195–209. doi: 10.1001/archgenpsychiatry.2011.1251

Eilam-Stock, T., Xu, P., Cao, M., Gu, X., Van Dam, N. T., Anagnostou, E., et al. (2014). Abnormal autonomic and associated brain activities during rest in autism spectrum disorder. *Brain* 137, 153–171. doi: 10.1093/brain/awt294

Etkin, A., Egner, T., and Kalisch, R. (2011). Emotional processing in anterior cingulate and medial prefrontal cortex. *Trends Cogn. Sci.* 15, 85–93. doi: 10.1016/j.tics.2010.11.004

Fan, Y. T., Chen, C., Chen, S. C., Decety, J., and Cheng, Y. (2013). Empathic arousal and social understanding in individuals with autism: evidence from fMRI and ERP measurements. *Soc. Cogn. Affect Neurosci.* 9, 1203–1213. doi: 10.1093/scan/nst101

Fernández, G., Weyerts, H., Schrader-Bolsche, M., Tendolkar, I., Smid, H. G., Tempelmann, C., et al. (1998). Successful verbal encoding into episodic memory engages the posterior hippocampus: a parametrically analyzed functional magnetic resonance imaging study. *J. Neurosci.* 18, 1841–1847.

Frith, C. D., and Frith, U. (1999). Interacting minds–a biological basis. *Science* 286, 1692–1695. doi: 10.1126/science.286.5445.1692

Gallagher, H. L., and Frith, C. D. (2003). Functional imaging of 'theory of mind'. *Trends Cogn. Sci.* 7, 77–83. doi: 10.1016/S1364-6613(02)00025-6

Geschwind, D. H., and Levitt, P. (2007). Autism spectrum disorders: developmental disconnection syndromes. *Curr. Opin. Neurobiol.* 17, 103–111. doi: 10.1016/j.conb.2007.01.009

Goel, V., and Dolan, R. J. (2001). The functional anatomy of humor: segregating cognitive and affective components. *Nat. Neurosci.* 4, 237–238. doi: 10.1038/85076

Gogtay, N., and Thompson, P. M. (2010). Mapping gray matter development: implications for typical development and vulnerability to psychopathology. *Brain Cogn.* 72, 6–15. doi: 10.1016/j.bandc.2009.08.009

Greimel, E., Nehrkorn, B., Schulte-Rüther, M., Fink, G. R., Nickl-Jockschat, T., Herpertz-Dahlmann, B., et al. (2013). Changes in grey matter development in autism spectrum disorder. *Brain Struct. Funct.* 218, 929–942. doi: 10.1007/s00429-012-0439-9

Gu, X., Eilam-Stock, T., Zhou, T., Anagnostou, E., Kolevzon, A., Soorya, L., et al. (2015). Autonomic and brain responses associated with empathy deficits in autism spectrum disorder. *Hum. Brain Mapp.* 36, 3323–3338. doi: 10.1002/hbm.22840

Haar, S., Berman, S., Behrmann, M., and Dinstein, I. (2014). Anatomical abnormalities in autism? *Cereb. Cortex* 26, 1440–1452. doi: 10.1093/cercor/bhu242

Hadjikhani, N., Zürcher, N. R., Rogier, O., Hippolyte, L., Lemonnier, E., Ruest, T., et al. (2014). Emotional contagion for pain is intact in autism spectrum disorders. *Transl. Psychiatry* 4, e343. doi: 10.1038/tp.2013.113

Harris, G. J., Chabris, C. F., Clark, J., Urban, T., Aharon, I., Steele, S., et al. (2006). Brain activation during semantic processing in autism spectrum disorders via functional magnetic resonance imaging. *Brain Cogn.* 61, 54–68. doi: 10.1016/j.bandc.2005.12.015

Harris, L. T., Mcclure, S. M., Van Den Bos, W., Cohen, J. D., and Fiske, S. T. (2007). Regions of the MPFC differentially tuned to social and nonsocial affective evaluation. *Cogn. Affect. Behav. Neurosci.* 7, 309–316. doi: 10.3758/CABN.7.4.309

Hill, E., Berthoz, S., and Frith, U. (2004). Brief report: cognitive processing of own emotions in individuals with autistic spectrum disorder and in their relatives. *J. Autism Dev. Disord.* 34, 229–235. doi: 10.1023/B:JADD.0000022613.41399.14

Hyde, K. L., Samson, F., Evans, A. C., and Mottron, L. (2010). Neuroanatomical differences in brain areas implicated in perceptual and other core features of autism revealed by cortical thickness analysis and voxel-based morphometry. *Hum. Brain Mapp.* 31, 556–566. doi: 10.1002/hbm.20887

Itahashi, T., Yamada, T., Nakamura, M., Watanabe, H., Yamagata, B., Jimbo, D., et al. (2015). Linked alterations in gray and white matter morphology in adults with high-functioning autism spectrum disorder: a multimodal brain imaging study. *Neuroimage Clin.* 7, 155–169. doi: 10.1016/j.nicl.2014.11.019

Jiao, Y., Chen, R., Ke, X., Chu, K., Lu, Z., and Herskovits, E. H. (2010). Predictive models of autism spectrum disorder based on brain regional cortical thickness. *Neuroimage* 50, 589–599. doi: 10.1016/j.neuroimage.2009.12.047

Kamio, Y., Robins, D., Kelley, E., Swainson, B., and Fein, D. (2007). Atypical lexical/semantic processing in high-functioning autism spectrum disorders without early language delay. *J. Autism Dev. Disord.* 37, 1116–1122. doi: 10.1007/s10803-006-0254-3

Kelley, W. M., Macrae, C. N., Wyland, C. L., Caglar, S., Inati, S., and Heatherton, T. F. (2002). Finding the self? An event-related fMRI study. *J. Cogn. Neurosci.* 14, 785–794. doi: 10.1162/08989290260138672

Kim, H. (2015). Encoding and retrieval along the long axis of the hippocampus and their relationships with dorsal attention and default mode networks: the HERNET model. *Hippocampus* 25, 500–510. doi: 10.1002/hipo.22387

Lange, N., Travers, B. G., Bigler, E. D., Prigge, M. B., Froehlich, A. L., Nielsen, J. A., et al. (2015). Longitudinal volumetric brain changes in autism spectrum disorder ages 6–35 years. *Autism Res.* 8, 82–93. doi: 10.1002/aur.1427

Libero, L. E., Deramus, T. P., Lahti, A. C., Deshpande, G., and Kana, R. K. (2015). Multimodal neuroimaging based classification of autism spectrum disorder using anatomical, neurochemical, and white matter correlates. *Cortex* 66, 46–59. doi: 10.1016/j.cortex.2015.02.008

Lind, S. E., and Bowler, D. M. (2010). Episodic memory and episodic future thinking in adults with autism. *J. Abnorm. Psychol.* 119, 896–905. doi: 10.1037/a0020631

Lombardo, M. V., Barnes, J. L., Wheelwright, S. J., and Baron-Cohen, S. (2007). Self-referential cognition and empathy in autism. *PLoS ONE* 2:e883. doi: 10.1371/journal.pone.0000883

Lombardo, M. V., Chakrabarti, B., Bullmore, E. T., Sadek, S. A., Pasco, G., Wheelwright, S. J., et al. (2010). Atypical neural self-representation in autism. *Brain* 133, 611–624. doi: 10.1093/brain/awp306

Lord, C., Risi, S., Lambrecht, L., Cook E. H., Jr, Leventhal, B. L., Dilavore, P. C., et al. (2000). The autism diagnostic observation schedule—generic: a standard measure of social and communication deficits associated with the spectrum of autism. *J. Autism Dev. Disord.* 30, 205–223. doi: 10.1023/A:1005592401947

Maier, S., Van Elst, L. T., Beier, D., Ebert, D., Fangmeier, T., Radtke, M., et al. (2015). Increased hippocampal volumes in adults with high functioning autism spectrum disorder and an IQ> 100: a manual morphometric study. *Psychiatry Res.* 234, 152–155. doi: 10.1016/j.pscychresns.2015.08.002

Mak-Fan, K. M., Taylor, M. J., Roberts, W., and Lerch, J. P. (2012). Measures of cortical grey matter structure and development in children with autism spectrum disorder. *J. Autism Dev. Disord.* 42, 419–427. doi: 10.1007/s10803-011-1261-6

Mandy, W. P., Charman, T., and Skuse, D. H. (2012). Testing the construct validity of proposed criteria for DSM-5 autism spectrum disorder. *J. Am. Acad. Child Adolesc. Psychiatry* 51, 41–50. doi: 10.1016/j.jaac.2011.10.013

Mazziotta, J. C., Toga, A. W., Evans, A., Fox, P., and Lancaster, J. (1995). A probabilistic atlas of the human brain: theory and rationale for Its development. *Neuroimage* 2, 89–101. doi: 10.1006/nimg.1995.1012

Mcalonan, G. M., Suckling, J., Wong, N., Cheung, V., Lienenkaemper, N., Cheung, C., et al. (2008). Distinct patterns of grey matter abnormality in high-functioning autism and Asperger's syndrome. *J. Child Psychol. Psychiatry* 49, 1287–1295. doi: 10.1111/j.1469-7610.2008.01933.x

Minio-Paluello, I., Baron-Cohen, S., Avenanti, A., Walsh, V., and Aglioti, S. M. (2009). Absence of embodied empathy during pain observation in Asperger syndrome. *Biol. Psychiatry* 65, 55–62. doi: 10.1016/j.biopsych.2008.08.006

Nickl-Jockschat, T., Habel, U., Maria Michel, T., Manning, J., Laird, A. R., Fox, P. T., et al. (2012). Brain structure anomalies in autism spectrum disorder—a meta−analysis of VBM studies using anatomic likelihood estimation. *Hum. Brain Mapp.* 33, 1470–1489. doi: 10.1002/hbm.21299

Nordahl, C. W., Dierker, D., Mostafavi, I., Schumann, C. M., Rivera, S. M., Amaral, D. G., et al. (2007). Cortical folding abnormalities in autism revealed by surface-based morphometry. *J. Neurosci.* 27, 11725–11735. doi: 10.1523/JNEUROSCI.0777-07.2007

Northoff, G., Heinzel, A., De Greck, M., Bermpohl, F., Dobrowolny, H., and Panksepp, J. (2006). Self-referential processing in our brain–a meta-analysis of imaging studies on the self. *Neuroimage* 31, 440–457. doi: 10.1016/j.neuroimage.2005.12.002

Persico, A. M., and Bourgeron, T. (2006). Searching for ways out of the autism maze: genetic, epigenetic and environmental clues. *Trends Neurosci.* 29, 349–358. doi: 10.1016/j.tins.2006.05.010

Phan, K. L., Wager, T., Taylor, S. F., and Liberzon, I. (2002). Functional neuroanatomy of emotion: a meta-analysis of emotion activation studies in PET and fMRI. *Neuroimage* 16, 331–348. doi: 10.1006/nimg.2002.1087

Pilowsky, T., Yirmiya, N., Arbelle, S., and Mozes, T. (2000). Theory of mind abilities of children with schizophrenia, children with autism, and normally developing children. *Schizophr. Res.* 42, 145–155. doi: 10.1016/S0920-9964(99)00101-2

Raznahan, A., Toro, R., Daly, E., Robertson, D., Murphy, C., Deeley, Q., et al. (2009). Cortical anatomy in autism spectrum disorder: an *in vivo* MRI study on the effect of age. *Cereb. Cortex* 20, 1332–1340. doi: 10.1093/cercor/bhp198

Redcay, E., and Courchesne, E. (2005). When is the brain enlarged in autism? A meta-analysis of all brain size reports. *Biol. Psychiatry* 58, 1–9. doi: 10.1016/j.biopsych.2005.03.026

Riddle, K., Cascio, C. J., and Woodward, N. D. (2016). Brain structure in autism: a voxel-based morphometry analysis of the Autism Brain Imaging Database Exchange (ABIDE). *Brain Imaging Behav.* doi: 10.1007/s11682-016-9534-5. [Epub ahead of print].

Riedel, A., Maier, S., Ulbrich, M., Biscaldi, M., Ebert, D., Fangmeier, T., et al. (2014). No significant brain volume decreases or increases in adults with high-functioning autism spectrum disorder and above average intelligence: a voxel-based morphometric study. *Psychiatry Res.* 223, 67–74. doi: 10.1016/j.pscychresns.2014.05.013

Sahin, M., and Sur, M. (2015). Genes, circuits, and precision therapies for autism and related neurodevelopmental disorders. *Science* 350:aab3897. doi: 10.1126/science.aab3897

Santos, M., Uppal, N., Butti, C., Wicinski, B., Schmeidler, J., Giannakopoulos, P., et al. (2011). Von Economo neurons in autism: a stereologic study of the frontoinsular cortex in children. *Brain Res.* 1380, 206–217. doi: 10.1016/j.brainres.2010.08.067

Saxe, R., and Kanwisher, N. (2003). People thinking about thinking people. the role of the temporo-parietal junction in "theory of mind". *Neuroimage* 19, 1835–1842. doi: 10.1016/S1053-8119(03)00230-1

Scheel, C., Rotarska-Jagiela, A., Schilbach, L., Lehnhardt, F. G., Krug, B., Vogeley, K., et al. (2011). Imaging derived cortical thickness reduction in high-functioning autism: key regions and temporal slope. *Neuroimage* 58, 391–400. doi: 10.1016/j.neuroimage.2011.06.040

Schumann, C. M., Barnes, C. C., Lord, C., and Courchesne, E. (2009). Amygdala enlargement in toddlers with autism related to severity of social and communication impairments. *Biol. Psychiatry* 66, 942–949. doi: 10.1016/j.biopsych.2009.07.007

Schumann, C. M., Bloss, C. S., Barnes, C. C., Wideman, G. M., Carper, R. A., Akshoomoff, N., et al. (2010). Longitudinal magnetic resonance imaging study of cortical development through early childhood in autism. *J. Neurosci.* 30, 4419–4427. doi: 10.1523/JNEUROSCI.5714-09.2010

Shamay-Tsoory, S. G., Aharon-Peretz, J., and Perry, D. (2009). Two systems for empathy: a double dissociation between emotional and cognitive empathy in inferior frontal gyrus versus ventromedial prefrontal lesions. *Brain* 132, 617–627. doi: 10.1093/brain/awn279

Slotnick, S. D., Moo, L. R., Segal, J. B., and Hart, J. (2003). Distinct prefrontal cortex activity associated with item memory and source memory for visual shapes. *Cogn. Brain Res.* 17, 75–82. doi: 10.1016/S0926-6410(03)00082-X

Solso, S., Xu, R., Proudfoot, J., Hagler, D. J. Jr, Campbell, K., Venkatraman, V., et al. (2015). Diffusion tensor imaging provides evidence of possible axonal overconnectivity in frontal lobes in autism spectrum disorder toddlers. *Biol. Psychiatry* 79, 676–684. doi: 10.1016/j.biopsych.2015.06.029

Stanfield, A. C., Mcintosh, A. M., Spencer, M. D., Philip, R., Gaur, S., and Lawrie, S. M. (2008). Towards a neuroanatomy of autism: a systematic review and meta-analysis of structural magnetic resonance imaging studies. *Eur. Psychiatry* 23, 289–299. doi: 10.1016/j.eurpsy.2007.05.006

Sussman, D., Leung, R., Vogan, V., Lee, W., Trelle, S., Lin, S., et al. (2015). The autism puzzle: diffuse but not pervasive neuroanatomical abnormalities in children with ASD. *Neuroimage Clin.* 8, 170–179. doi: 10.1016/j.nicl.2015.04.008

Toal, F., Daly, E. M., Page, L., Deeley, Q., Hallahan, B., Bloemen, O., et al. (2010). Clinical and anatomical heterogeneity in autistic spectrum disorder: a structural MRI study. *Psychol. Med.* 40, 1171–1181. doi: 10.1017/S0033291709991541

Uddin, L. Q. (2011). The self in autism: an emerging view from neuroimaging. *Neurocase* 17, 201–208. doi: 10.1080/13554794.2010.509320

Uddin, L. Q., Menon, V., Young, C. B., Ryali, S., Chen, T., Khouzam, A., et al. (2011). Multivariate searchlight classification of structural magnetic resonance imaging in children and adolescents with autism. *Biol. Psychiatry* 70, 833–841. doi: 10.1016/j.biopsych.2011.07.014

Vandenbroucke, M. W., Scholte, H. S., Van Engeland, H., Lamme, V. A., and Kemner, C. (2008). A neural substrate for atypical low-level visual processing in autism spectrum disorder. *Brain* 131, 1013–1024. doi: 10.1093/brain/awm321

Vanni, S., Tanskanen, T., Seppä, M., Uutela, K., and Hari, R. (2001). Coinciding early activation of the human primary visual cortex and anteromedial cuneus. *Proc. Natl. Acad. Sci. U.S.A.* 98, 2776–2780. doi: 10.1073/pnas.041600898

Via, E., Radua, J., Cardoner, N., Happé, F., and Mataix-Cols, D. (2011). Meta-analysis of gray matter abnormalities in autism spectrum disorder: should Asperger disorder be subsumed under a broader umbrella of autistic spectrum disorder? *Arch. Gen. Psychiatry* 68, 409–418. doi: 10.1001/archgenpsychiatry.2011.27

Visser, M., Jefferies, E., Embleton, K. V., and Lambon Ralph, M. A. (2012). Both the middle temporal gyrus and the ventral anterior temporal area are crucial for multimodal semantic processing: distortion-corrected fMRI evidence for a double gradient of information convergence in the temporal lobes. *J. Cogn. Neurosci.* 24, 1766–1778. doi: 10.1162/jocn_a_00244

Völlm, B. A., Taylor, A. N., Richardson, P., Corcoran, R., Stirling, J., Mckie, S., et al. (2006). Neuronal correlates of theory of mind and empathy: a functional magnetic resonance imaging study in a nonverbal task. *Neuroimage* 29, 90–98. doi: 10.1016/j.neuroimage.2005.07.022

Wallace, G. L., Robustelli, B., Dankner, N., Kenworthy, L., Giedd, J. N., and Martin, A. (2013). Increased gyrification, but comparable surface area in adolescents with autism spectrum disorders. *Brain* 136, 1956–1967. doi: 10.1093/brain/awt106

Zielinski, B. A., Prigge, M. B., Nielsen, J. A., Froehlich, A. L., Abildskov, T. J., Anderson, J. S., et al. (2014). Longitudinal changes in cortical thickness in autism and typical development. *Brain* 137, 1799–1812. doi: 10.1093/brain/awu083

Zwaigenbaum, L., Young, G. S., Stone, W. L., Dobkins, K., Ozonoff, S., Brian, J., et al. (2014). Early head growth in infants at risk of autism: a baby siblings research consortium study. *J. Am. Acad. Child Adolesc. Psychiatry* 53, 1053–1062. doi: 10.1016/j.jaac.2014.07.007

Conflict of Interest Statement: The authors declare that the research was conducted in the absence of any commercial or financial relationships that could be construed as a potential conflict of interest.

frontiers in Neuroscience

ORIGINAL RESEARCH
published: 31 August 2016
doi: 10.3389/fnins.2016.00388

Uncovering the Social Deficits in the Autistic Brain. A Source-Based Morphometric Study

Alessandro Grecucci[1], Danilo Rubicondo[1,2], Roma Siugzdaite[3], Luca Surian[1] and Remo Job[1]*

[1] Department of Psychology and Cognitive Sciences, University of Trento, Trento, Italy, [2] Center for Mind/Brain Sciences, University of Trento, Trento, Italy, [3] Department of Experimental Psychology, Faculty of Psychological and Pedagogical Sciences, Ghent University, Ghent, Belgium

Autism is a neurodevelopmental disorder that mainly affects social interaction and communication. Evidence from behavioral and functional MRI studies supports the hypothesis that dysfunctional mechanisms involving social brain structures play a major role in autistic symptomatology. However, the investigation of anatomical abnormalities in the brain of people with autism has led to inconsistent results. We investigated whether specific brain regions, known to display functional abnormalities in autism, may exhibit mutual and peculiar patterns of covariance in their gray-matter concentrations. We analyzed structural MRI images of 32 young men affected by autistic disorder (AD) and 50 healthy controls. Controls were matched for sex, age, handedness. IQ scores were also monitored to avoid confounding. A multivariate Source-Based Morphometry (SBM) was applied for the first time on AD and controls to detect maximally independent networks of gray matter. Group comparison revealed a gray-matter source that showed differences in AD compared to controls. This network includes broad temporal regions involved in social cognition and high-level visual processing, but also motor and executive areas of the frontal lobe. Notably, we found that gray matter differences, as reflected by SBM, significantly correlated with social and behavioral deficits displayed by AD individuals and encoded via the Autism Diagnostic Observation Schedule scores. These findings provide support for current hypotheses about the neural basis of atypical social and mental states information processing in autism.

Keywords: autism, morphometric analysis, social deficits, neuroscience, developmental disabilities

OPEN ACCESS

Edited by:
Ahmet O. Caglayan, Yale University, USA

Reviewed by:
Munis Dundar, Erciyes University, Turkey
Chiara Nosarti, King's College London, UK

****Correspondence:***
Alessandro Grecucci
alessandro.grecucci@unitn.it

Specialty section:
This article was submitted to Child and Adolescent Psychiatry, a section of the journal Frontiers in Neuroscience

Received: *11 May 2016*
Accepted: *09 August 2016*
Published: *31 August 2016*

Citation:
Grecucci A, Rubicondo D, Siugzdaite R, Surian L and Job R (2016) Uncovering the Social Deficits in the Autistic Brain. A Source-Based Morphometric Study. Front. Neurosci. 10:388. doi: 10.3389/fnins.2016.00388

INTRODUCTION

Autism Spectrum Disorder (ASD) is a category of pervasive developmental disorders (PDD) that affect 1 in 150 children (Rapin and Tuchman, 2008). Autistic symptomatology is characterized by severe impairments that mainly affect social interaction, communication, while sparing basic cognitive skills (Misra, 2014), and not implying emotional disturbance (Rapin and Tuchman, 2008). The term ASD was introduced by Allen (1988) and included: autistic disorder (AD), Asperger syndrome (AS), and PDD not otherwise specified (Levy et al., 2009; Pina-Camacho et al., 2012). Recently, the DSM V revised the conceptualization of those disorders and currently diagnostic classifications only include Autism Spectrum Disorders (ASD) (Lord and Bishop, 2015). Nevertheless, the diagnostic criteria adopted in the current study still refer to DSM IV, and we

focused primarily on autism disorder (AD). Consequently, we use the words "autism" and "autistic" to specifically refer to AD.

The mind-blindness theory proposed that characteristic problem in social interaction arises because AD have difficulties in mentalizing and understanding psychological dynamics in other people and in oneself (Baron-Cohen et al., 1985; Frith et al., 1991). Support for this model comes from behavioral studies showing that autistics poorly perform on tasks that require theory of mind (ToM) abilities (Baron-Cohen et al., 1985; Misra, 2014). The poor performance of people with autism on ToM task is thought to be due to a conceptual deficit or to processing peculiarities. In normally developing children ToM tasks elicit intuitive social insights into people. In contrast, autistic children treat these tasks as logical-reasoning problems relying on language and non-social cognitive functions (Tager-Flusberg et al., 2009). In line with this hypothesis, functional MRI investigations of AD have highlighted reduced responses in cortical areas related to social interaction (Frith, 2003; Di Martino et al., 2009; Lombardo et al., 2011; Gliga et al., 2014), and the engagement of areas associated with general problem solving abilities (Frith, 2003). Moreover, functional connectivity in a group with autism shows abnormal pattern in areas mediating ToM and in the mirror neuron system (MNS) as well (Fishman et al., 2014; Cheng et al., 2015; Kana et al., 2015).

On the other hand, studies of volumetric changes in the autistic brain resulted in inconsistent brain structures across studies: prefrontal cortex (Courchesne et al., 2011b), cerebellum (Sparks et al., 2002), temporal lobe (Palmen et al., 2006), both the frontal (Herbert et al., 2004; Jiao et al., 2010) and parietal lobes (Courchesne et al., 1993) and amygdala (Schumann et al., 2004). Some inconsistencies in the structural MRI literature may be attributed to differences in methodology, age, heterogeneity of the disorder (Geschwind, 2009), or diffuse structural abnormalities. Diffuse structural abnormalities in autism could reflect impairment of many, if not most, brain networks (Müller, 2007).

Recently, predictive models of autism based on pattern recognition in structural MR images have been successfully developed. Ecker et al. (2010) adopted a support vector machine (SVM) method to discriminate ASD individuals from controls. Brain areas in the temporal lobe, precuneus, hippocampal, and fusiform gyri were crucial for discrimination. Neural abnormalities discovered with such methodologies, however, rarely correlate with clinical criteria, or correlate only with generic total scores, and not with specific subscales (Eliez and Reiss, 2000; Lord et al., 2000; Hardan et al., 2006a,b; Ecker et al., 2010; Griebling et al., 2010). In other words, these correlations may refer more to a general severity of pathology than to specific deficits.

We suggest that neuroanatomical markers of autism disorder may be better understood by studying large-scale anatomical networks (Minshew and Williams, 2007; Schaer et al., 2013). SBM is a data-driven multivariate alternative to the standard Voxel-Based Morphometry (VBM), and it may be particularly suitable to the investigation of anatomical changes in autism. SBM takes into account information across different voxels and identifies unpredicted, naturally occurring patterns of covariance across brain regions (Xu et al., 2009). Notably, such anatomical covariance has been shown to reflect functional connectivity (Evans, 2013). For these reasons, we expect SBM to individuate large anatomical networks of gray-matter which show aberrant patterns of covariance in AD, as compared to control. We also expect those networks to include brain areas that previous studies showed to be anatomically or functionally abnormal.

Given the heterogeneity of AD and the need for large-scale samples of MR and clinical measures, the present study utilizes the ABIDE (Autism Brain Imaging Data Exchange) database.

METHODS

Participants

Structural MRI of 82 participants (32 AD and 50 controls) were extracted from Autism Brain Imaging Data Exchange (ABIDE). Details of acquisition, informed consent, site-specific protocols, specific diagnostic criteria for each data set can be found at http://fcon_1000.projects.nitrc.org/indi/abide/index.html. The following committees approved the protocols of each site: the Human Subjects Protection Committee of the California Institute of Technology (CAL), the Institutional Review Board at the University of Pittsburgh (PBG) and the University of Utah School of Medicine (USM).

From around 3000 subjects available, we carefully selected participants by gender (males), age (range: 18–39 years old), as well as parameters of the MR scanners (image type: T1; magnetic field strength: 3T). This first selection resulted in a dataset composed by structural MRI of 283 subject acquired with 12 different MRI scanners. Next, the 283 subjects were screened on the basis of the DSV-IV for either the absence of any neuropsychiatric disorders (control group), or the diagnosis of Autism (AD) (patients group). Further inclusion criteria were: (a) the indication of the IQ score computed on the basis of Wechsler abbreviated scale of intelligence (WASI); (b) scores on at least three specific subscales of the Autism diagnostic observation schedule (ADOS) for AD participants. Finally, individuals with any other pathology or comorbidity were rejected. An in house made Dori script iteratively sampled the database until controls and AD group were balanced for age and there was no association between groups and a particular scanner.

This procedure yielded a dataset comprising 82 participants (32 AD and 50 controls) tested on one of the two MR scanners, with the same MR sequence (Table 1 in Supplementary Material). The scanners belonged to the same vendor (i.e., Siemens MAGNETOM TrioTim, Siemens MAGNETOM Allegra), and participants were equally distributed between scanners (See Table 1 in Supplementary Material). The two groups did not differed for age [$t_{(31)} = 0.2953$, $p = 0.7728$]. However, there was a difference in IQ scores [$t_{(31)} = 2.9586$, $p = 0.0041$]. See Table 1 in Supplementary Material. This is in line with previous observations for which the prevalence of mental retardation in autism is ∼60% groups, and AD naturally differ from normal controls for IQ (Amaral et al., 2008).

Data Analysis

Source-based morphometry (SBM) is a multivariate technique that takes advantage of independent component analysis (ICA) (Lee, 1998; Xu et al., 2009). ICA is a statistical technique that

is widely used in many fields of biomedical research for signal analysis. In the field of neuroscience ICA has found important application in EEG/MEG/fMRI data analyses to isolate noisy artifacts.

Pulling images from different MR scanners is known to lead to confounding, even though MR sequences are the same (Han et al., 2006). This is especially true for a massive univariate analysis, such as VBM. However, SBM can decompose the MR signal in several maximally independent sources, or independent components (ICs). In this study, few sources may reflect signal differences among MR scanners, while the majority of ICs individuate networks of gray-matter that share patterns of covariance among subjects (Xu et al., 2009; Kaspárek et al., 2010; Kubera et al., 2014). Artifactual components are usually easy to detect because are asymmetric, do not follow the anatomical organization of the brain, and do not exhibit any coherent patterns. In addition, the distribution of subjects throughout scanners is similar in both controls and AD, and this should guarantee that group differences are not due to artifact components.

The preprocessing of images is identical to the procedure adopted for classical VBM analyses. Brain extraction and robust center estimation was automatically carried out using FSL Brain extraction tool (BET) (Smith, 2002). For normalization and segmentation we used the SPM toolbox VBM8. Images were spatially normalized to the 152 average T1 MNI (Montreal Neurological Institute) template, and segmented into gray-matter (GM), white-matter (WM), and cerebrospinal fluid (CSF). The normalized gray-matter images were smoothed with 8-mm full width at half-maximum (FWHM) Gaussian kernel to establish spatial correspondence between the different brains.

Source-based morphometry analysis was carried out using the GIFT toolbox (http://icatb.sourceforge.net) (Xu et al., 2009). The minimum description length (MDL) principle was used to estimate a number of independent components. MDL found eight reliable ICs. We performed ICA using a neural network algorithm (Infomax) that attempts to minimize the mutual information of the network outputs to identify naturally grouping and maximally independent sources (Bell and Sejnowski, 1995). ICA was repeated 20 times in ICASSO (http://research.ics.aalto.fi/ica/icasso/) and the resulting components were clustered to ensure the consistency and reliability of the results. Reliability is quantified using a quality index Iq, ranging from 0 to 1 and reflecting the difference between intra-cluster and extra-cluster similarity (Himberg et al., 2004). All the 8 components extracted from the GM images were found to be associated with an Iq > 0.97 indicating a highly stable ICA decomposition.

SBM involves converting each gray-matter volume into a vector. As a result, we obtained a matrix where the 82 rows represent the 82 subjects (the first 50 rows represent controls, while the other 32 AD), and each column indicates a voxel. This matrix was decomposed into two matrices by ICA. The first matrix is named "mixing matrix" and it is composed by a subject per row and an IC per column. Therefore, the mixing matrix indicates how much a subject expresses a given component. For this reason, values in the mixing matrix are called "loading coefficients." The second matrix is named source matrix and it specifies the relation between the ICs and the voxels. For gray-matter volume component visualization the source matrix was reshaped back to a three-dimensional image, scaled to unit standard deviations (Z maps) and thresholded at $Z > 2.5$.

We used the mixing matrix to verify whether components are differently expressed between controls and AD. A two sample t-test without assuming equal variances (F-test revealed unequal variances) was used to test whether all the ICs are similarity expressed by either of the groups. Similarly, we used the loading coefficients in the mixing matrix to test a linear relation among ADOS scores and the level of components' expression. All the results were thresholded at $p < 0.05$ corrected for Family Wise Error (FWE).

RESULTS

We extracted eight independent components (**Figure 1**). However, only the 7th component was significantly different [$t_{(31)} = 2.9482$, $p_{(\mathrm{FWE})} = 0.0042$] between AD and controls. We call this component "autism-specific structural network" (ASN). Anatomical labels of the regions composing ASN were obtained using the WFU PickAtlas (Tzourio-Mazoyer et al., 2002). Among regions that differ between AD and controls we found: inferior, middle, superior temporal gyri, fusiform gyrus, parahippocampal gyrus, paracentral lobule, precuneus, cerebellar tonsil, and portions of the inferior, middle, and superior frontal gyri (**Figure 2**). All the gray-matter regions of ASN are presented in Table 2 in Supplementary Material, and in **Figure 2**.

To ensure that differences in IQ (see Table 1 in Supplementary Material) did not account for brain differences we correlated ASN loading coefficients (i.e., 7th column of the mixing matrix) against IQ values. The correlation was not significant ($p = 0.6336$), thus excluding the relevance of IQ on this component.

Notably, ASN significantly correlated with the total scores of ADOS, and also with two ADOS subscales measuring highly relevant impairments in AD, i.e., difficulties in social interactions and stereotyped behavior. Both variables show significant correlation with the loading coefficient of ASN, after Bonferroni correction for multiple comparisons. Classic Total ADOS Score: $r = 0.4708$, $p_{(\mathrm{FWE})} = 0.0065$. Social Total subscore: $r = 0.4269$, $p_{(\mathrm{FWE})} = 0.0148$. Stereotyped behaviors and restricted interest: $r = 0.4152$, $p_{(\mathrm{FWE})} = 0.0181$. See **Figure 2**.

DISCUSSION

In this study we presented for the first time a whole brain morphometric method (SBM), based on independent component analysis, which shows alterations in gray-matter between AD individuals and controls. This innovative multivariate procedure was applied to detect brain networks that exhibit abnormal pattern of gray-matter covariance in AD. We showed that morphometric changes in autism, as detected by SBM, are significantly associated with observable social and behavioral deficits (ADOS scores).

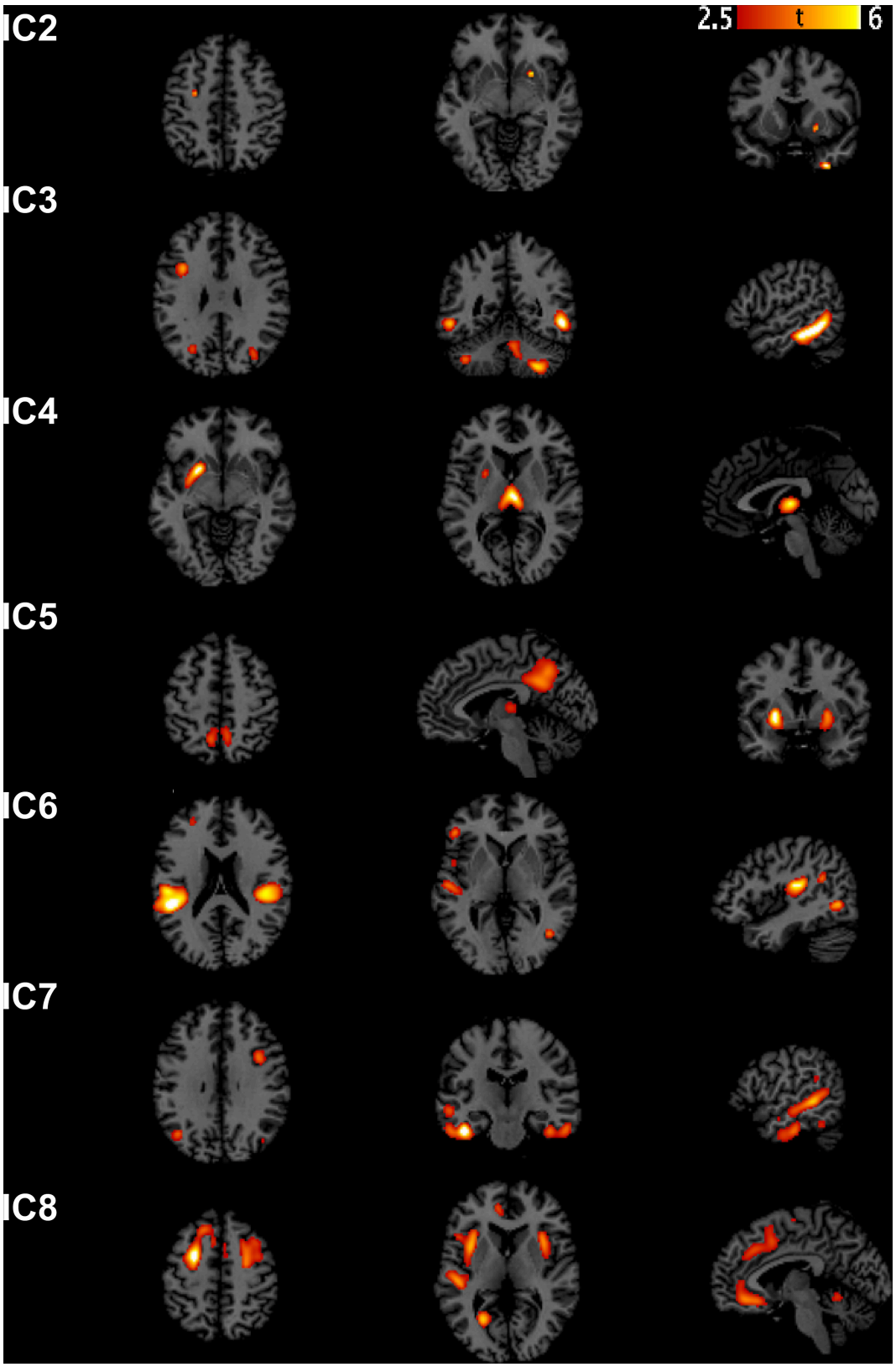

FIGURE 1 | Sources discovered by SBM. According to the estimation of the number of components, eight independent components were extracted. Note that IC1 is not graphically represented because no voxel survived after thresholding for $Z > 2.5$.

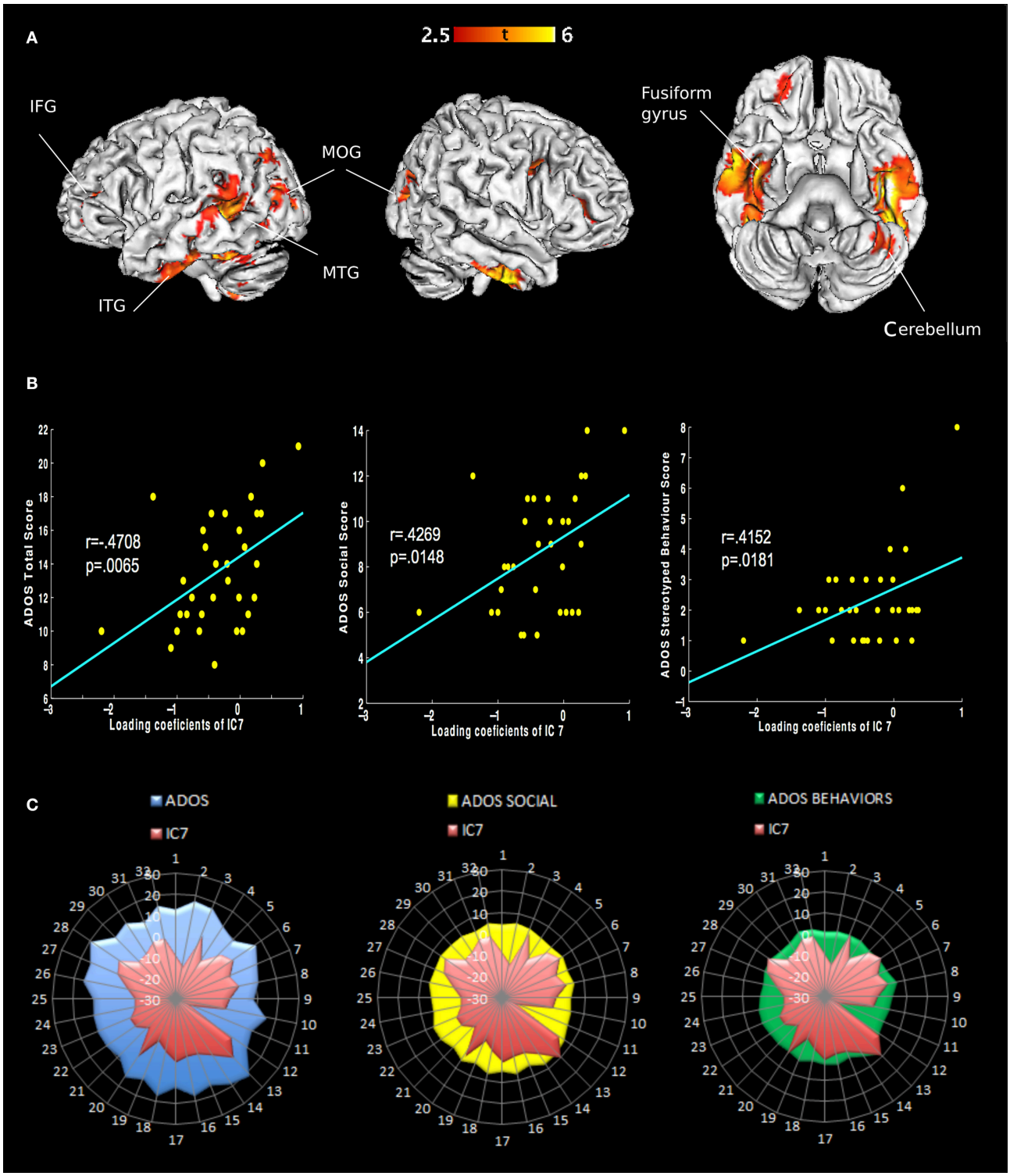

FIGURE 2 | Representation of ASN in the brain and behavior in AD. (A) Only the seventh component shows different loading coefficient between ASD and controls. The regions involved are: inferior frontal gyrus, middle frontal gyrus, superior frontal gyrus, inferior temporal gyrus, middle temporal gyrus and superior temporal gyrus, fusiform gyrus, parahippocampal gyrus, paracentral lobule, precuneus and cerebellar tonsil (Table 2 in Supplementary Material). **(B)** Correlations of behavioral measures with loading coeficients values in IC 7: Classic Total ADOS Score (communication subscore + social interaction subscore); Social Total subscore: Stereotyped behaviors and restricted interest. **(C)** Covariance plots showing each subjects' ADOS scores and individual ASN loading coefficients.

SBM addresses a different question in comparison with massive univariate approaches to morphological changes, as Voxel-Base-Morphometry (VBM) or ROI differences between groups. Univariate approaches detect voxel- or ROI-based changes in gray-matter concentrations, while SBM individuates different levels of expression in maximally independent gray-matter networks. Differences in network expression in turn implicate differences in gray-matter concentrations, distributed along patterns of voxel-covariation. SBM is particularly suitable to study autism as spectrum disorder, since anatomical changes are likely to be distributed along networks of brain regions. In this scenario, such anatomical changes may not be locally detectable by univariate approaches.

In the present study we found an autism-specific structural network (ASN) which covers brain regions found to exhibit functional and structural abnormalities in previous studies compared with controls (Castelli et al., 2002; Saxe and Wexler, 2005; Amaral et al., 2008; Courchesne et al., 2011b; Ecker et al., 2012; Nickl-Jockschat et al., 2012; Pappaianni et al., 2016).

Autism-Specific Structural Network (ASN)

Temporal Lobe

The core of ASN is localized in temporal regions involved in processing and integrating social stimuli, such as faces and intention-related movements.

ASN is centered in vast portions of the temporal lobes, suggesting that the temporal lobe may have particular relevance in the autistic disorder. ASN includes parts of the inferior, medial and superior temporal sulci, the fusiform gyrus, and the parahippocampal gyrus. Temporal lobe regions are implicated in social perception, auditory processing, language, and theory of mind. These abilities were shown to be the most damaged in autism (Gendry Meresse et al., 2005). In the present study inferior temporal and fusiform gyri are the brain regions which disclosed the greatest differences between AD and controls. These are the areas involved in high-level visual processing and object recognition, in particular face recognition (Rossion et al., 2003). Furthermore, the posterior superior temporal sulcus (STS) is a core region for perception of social acts (Zilbovicius et al., 2006). STS appears to respond also to biological motion and to how another person's motion is related to his/her intentions (Vander Wyk et al., 2009). Pelphrey et al. (2007) individuated a functional deficit in ASD regarding neural mechanisms for processing emotional facial expressions and biological motion. This system of regions referring to the deficit includes the amygdala, posterior STS and fusiform gyrus. This evidence provides further support for the idea that autism disorder relates to an impairment in processing social-relevant information (Baron-Cohen et al., 1985).

Frontal Lobe

ASN includes bilateral clusters in both the superior frontal gyrus (BA6) and in the precentral gyrus (BA4). Those areas correspond to premotor, supplementary, and primary motor cortices. Action processing impairments and repetitive movements are commonly observed among subjects affected by autism. Even though motor impairments are not considered one of the main symptoms of ASD, recently increasing attention has been directed to motor aspects aiming to improve a diagnostic process (Torres et al., 2013).

Our results also showed abnormalities in the inferior part of the frontal gyrus, a brain region implied in executive processes and language (Gotts et al., 2012; Libero et al., 2014). Since AD are largely characterized by deficits in imitation, language, ToM and empathy, a theory known as "broken mirror" hypothesis of ASD, has suggested that a dysfunctional MNS is an important factor in AD pathogenesis (Oberman et al., 2005). Sustaining this hypothesis, some recent studies have found abnormal pattern of functional connectivity in networks believed to underlie social abilities, as MNS and ToM systems (Fishman et al., 2014). However, the role of the mirror system in understanding AD symptomatology is still controversial (Grecucci et al., 2013; Hamilton, 2013; Enticott et al., 2014).

Other Areas Implicated in Autism

Cerebellar pathology is usually reported in autism (Courchesne et al., 1994, 2011a; Cauda et al., 2011; Rogers et al., 2013), both at structural and functional level (Fatemi et al., 2012). We also found cerebellum to be a part of the autism-specific structural network. Evidence suggests that the cerebellum supports cognitive functions, including language and executive functions (Becker and Stoodley, 2013), which are typically damaged in autism.

Previous meta-analyses of VBM in ASD have proposed that the amygdala and the insula are two brain regions frequently associated with abnormalities in autism (Cauda et al., 2011). In our study, we did not find structural changes in those regions. Our interpretation is that the amygdala and the insula are likely to play a role in autism, though these areas belong to a broader limbic system that, considered as a whole, may be sufficiently preserved in AD. Therefore, the neurostructural configuration of the limbic system was not markedly different between AD and controls.

Correlations with Behavioral Deficits

Finally, we found that the autism-specific structural network (ASN loading coefficients) significantly correlates with ADOS social and ADOS stereotypic behavior scores. Such evidence further supports the relation between the structural differences in ASN and the behavioral deficits displayed by AD individuals. These findings provide support for current hypotheses about the neural basis of atypical social and mental states information processing in autism.

CONCLUSION

Autism is a behaviorally diagnosed pathology, although evidence of brain abnormalities in AD, such as atypical neural "connectivity" (Ecker et al., 2012), are increasing. MRI investigation is a precious tool for shedding light on both the neurological causes and the neurodevelopment of AD. This knowledge is needed to get fast and objective diagnosis, but also for developing appropriate treatments. The present study,

along with increasing evidence (Ecker et al., 2010; Jiao et al., 2010), suggests that structural MRI may become a diagnostic instrument useful to improve the traditional behavior-based diagnosis.

AUTHOR CONTRIBUTIONS

AG: Experimental design, data collection and writing. DR: Experimental design, data collection, analyses and writing. RS: Experimental design, data collection, analyses, and writing. LS: writing of the paper. RJ: writing of the paper.

ACKNOWLEDGMENTS

We would like to thank the Comune of Rovereto and the Neuropsychoanalysis Foundation for grants that supported the present study. Special thanks go to Aidas Aglinskas for precious advice.

SUPPLEMENTARY MATERIAL

The Supplementary Material for this article can be found online at: http://journal.frontiersin.org/article/10.3389/fnins.2016.00388

REFERENCES

Allen, D. A. (1988). Austistic spectrum disorders: clinical presentation in preschool children. *J. Child Neurol.* 3(Suppl.), S48–S56. doi: 10.1177/088307388800300110

Amaral, D. G., Schumann, C. M., and Nordahl, C. W. (2008). Neuroanatomy of autism. *Trends Neurosci.* 31, 137–145. doi: 10.1016/j.tins.2007.12.005

Baron-Cohen, S., Leslie, A. M., and Frith, U. (1985). Does the autistic child have a "theory of mind"? *Cognition* 21, 37–46.

Becker, E. B. E., and Stoodley, C. J. (2013). Autism spectrum disorder and the cerebellum. *Int. Rev. Neurobiol.* 113, 1–34. doi: 10.1016/B978-0-12-418700-9.00001-0

Bell, A. J., and Sejnowski, T. J. (1995). An information-maximization approach to blind separation and blind deconvolution. *Neural Comput.* 7, 1129–1159.

Castelli, F., Frith, C., Happé, F., and Frith, U. (2002). Autism, Asperger syndrome and brain mechanisms for the attribution of mental states to animated shapes. *Brain* 125(Pt 8), 1839–1849. doi: 10.1093/brain/awf189

Cauda, F., Geda, E., Sacco, K., D'Agata, F., Duca, S., Geminiani, G., et al. (2011). Grey matter abnormality in autism spectrum disorder: an activation likelihood estimation meta-analysis study. *J. Neurol. Neurosurg. Psychiatr.* 82, 1304–1313. doi: 10.1136/jnnp.2010.239111

Cheng, W., Rolls, E. T., Gu, H., Zhang, J., and Feng, J. (2015). Autism: reduced connectivity between cortical areas involved in face expression, theory of mind, and the sense of self. *Brain* 138(Pt 5), 1382–1393. doi: 10.1093/brain/awv051

Courchesne, E., Campbell, K., and Solso, S. (2011a). Brain growth across the life span in autism: age-specific changes in anatomical pathology. *Brain Res.* 1380, 138–145. doi: 10.1016/j.brainres.2010.09.101

Courchesne, E., Mouton, P. R., Calhoun, M. E., Semendeferi, K., Ahrens-Barbeau, C., Hallet, M. J., et al. (2011b). Neuron number and size in prefrontal cortex of children with autism. *JAMA* 306, 2001–2010. doi: 10.1001/jama.2011.1638

Courchesne, E., Press, G. A., and Yeung-Courchesne, R. (1993). Parietal lobe abnormalities detected with MR in patients with infantile autism. *Am. J. Roentgenol.* 160, 387–393. doi: 10.2214/ajr.160.2.8424359

Courchesne, E., Townsend, J., Akshoomoff, N. A., Saitoh, O., Yeung-Courchesne, R., Lincoln, A. J., et al. (1994). Impairment in shifting attention in autistic and cerebellar patients. *Behav. Neurosci.* 108, 848–865. doi: 10.1037/0735-7044.108.5.848

Di Martino, A., Ross, K., Uddin, L. Q., Sklar, A. B., Castellanos, F. X., and Milham, M. P. (2009). Functional brain correlates of social and nonsocial processes in autism spectrum disorders: an activation likelihood estimation meta-analysis. *Biol. Psychiatry* 65, 63–74. doi: 10.1016/j.biopsych.2008.09.022

Ecker, C., Rocha-Rego, V., Johnston, P., Mourao-Miranda, J., Marquand, A., Daly, E. M., et al. (2010). Investigating the predictive value of whole-brain structural MR scans in autism: a pattern classification approach. *Neuroimage* 49, 44–56. doi: 10.1016/j.neuroimage.2009.08.024

Ecker, C., Suckling, J., Deoni, S. C., Lombardo, M. V., Bullmore, E. T., Baron-Cohen, S., et al. (2012). Brain anatomy and its relationship to behavior in adults with autism spectrum disorder: a multicenter magnetic resonance imaging study. *Arch. Gen. Psychiatry* 69, 195–209. doi: 10.1001/archgenpsychiatry.2011.1251

Eliez, S., and Reiss, A. L. (2000). MRI neuroimaging of childhood psychiatric disorders: a selective review. *J. Child Psychol. Psychiatry* 41, 679–694. doi: 10.1111/1469-7610.00656

Enticott, P. G., Kennedy, H. A., Johnston, P. J., Rinehart, N. J., Tonge, B. J., Taffe, J. R., et al. (2014). Emotion recognition of static and dynamic faces in autism spectrum disorder. *Cogn. Emot.* 28, 1110–1118. doi: 10.1080/02699931.2013.867832

Evans, A. C. (2013). Networks of anatomical covariance. *Neuroimage* 80, 489–504. doi: 10.1016/j.neuroimage.2013.05.054

Fatemi, S. H., Aldinger, K. A., Ashwood, P., Bauman, M. L., Blaha, C. D., Blatt, G. J., et al. (2012). Consensus paper: pathological role of the cerebellum in autism. *Cerebellum* 11, 777–807. doi: 10.1007/s12311-012-0355-9

Fishman, I., Keown, C. L., Lincoln, A. J., Pineda, J. A., and Müller, R.-A. (2014). Atypical cross talk between mentalizing and mirror neuron networks in autism spectrum disorder. *JAMA Psychiatry* 71, 751–760. doi: 10.1001/jamapsychiatry.2014.83

Frith, C. (2003). What do imaging studies tell us about the neural basis of autism? *Novartis Found. Symp.* 251, 149–66; discussion 166–76, 281–97.

Frith, U., Morton, J., and Leslie, A. M. (1991). The cognitive basis of a biological disorder: autism. *Trends Neurosci.* 14, 433–438.

Gendry Meresse, I., Zilbovicius, M., Boddaert, N., Robel, L., Philippe, A., Sfaello, I., et al. (2005). Autism severity and temporal lobe functional abnormalities. *Ann. Neurol.* 58, 466–469. doi: 10.1002/ana.20597

Geschwind, D. H. (2009). Advances in autism. *Annu. Rev. Med.* 60, 367–380. doi: 10.1146/annurev.med.60.053107.121225

Gliga, T., Jones, E. J. H., Bedford, R., Charman, T., and Johnson, M. H. (2014). From early markers to neuro-developmental mechanisms of autism. *Dev. Rev.* 34, 189–207. doi: 10.1016/j.dr.2014.05.003

Gotts, S. J., Simmons, W. K., Milbury, L. A., Wallace, G. L., Cox, R. W., and Martin, A. (2012). Fractionation of social brain circuits in autism spectrum disorders. *Brain* 135(Pt 9), 2711–2725. doi: 10.1093/brain/aws160

Grecucci, A., Brambilla, P., Siugzdaite, R., Londero, D., Fabbro, F., and Rumiati, R. I. (2013). Emotional resonance deficits in autistic children. *J. Autism Dev. Disord.* 43, 616–628. doi: 10.1007/s10803-012-1603-z

Griebling, J., Minshew, N. J., Bodner, K., Libove, R., Bansal, R., Konasale, P., et al. (2010). Dorsolateral prefrontal cortex magnetic resonance imaging measurements and cognitive performance in autism. *J. Child Neurol.* 25, 856–863. doi: 10.1177/0883073809351313

Hamilton, A. F. (2013). Reflecting on the mirror neuron system in autism: a systematic review of current theories. *Dev. Cogn. Neurosci.* 3, 91–105. doi: 10.1016/j.dcn.2012.09.008

Han, X., Jovicich, J., Salat, D., van der Kouwe, A., Quinn, B., Czanner, S., et al. (2006). Reliability of MRI-derived measurements of human cerebral cortical thickness: the effects of field strength, scanner upgrade and manufacturer. *Neuroimage* 32, 180–194. doi: 10.1016/j.neuroimage.2006.02.051

Hardan, A. Y., Girgis, R. R., Adams, J., Gilbert, A. R., Keshavan, M. S., and Minshew, N. J. (2006a). Abnormal brain size effect on the thalamus in autism. *Psychiatry Res.* 147, 145–151. doi: 10.1016/j.pscychresns.2005.12.009

Hardan, A. Y., Girgis, R. R., Lacerda, A. L. T., Yorbik, O., Kilpatrick, M., Keshavan, M. S., et al. (2006b). Magnetic resonance imaging study of the orbitofrontal cortex in autism. *J. Child Neurol.* 21, 866–871.

Herbert, M. R., Ziegler, D. A., Makris, N., Filipek, P. A., Kemper, T. L., Normandin, J. J., et al. (2004). Localization of white matter volume increase in autism and developmental language disorder. *Ann. Neurol.* 55, 530–540. doi: 10.1002/ana.20032

Himberg, J., Hyvärinen, A., and Esposito, F. (2004). Validating the independent components of neuroimaging time series via clustering and visualization. *Neuroimage* 22, 1214–1222. doi: 10.1016/j.neuroimage.2004.03.027

Jiao, Y., Chen, R., Ke, X., Chu, K., Lu, Z., and Herskovits, E. H. (2010). Predictive models of autism spectrum disorder based on brain regional cortical thickness. *Neuroimage* 50, 589–599. doi: 10.1016/j.neuroimage.2009.12.047

Kana, R. K., Maximo, J. O., Williams, D. L., Keller, T. A., Schipul, S. E., Cherkassky, V. L., et al. (2015). Aberrant functioning of the theory-of-mind network in children and adolescents with autism. *Mol. Autism* 6, 59. doi: 10.1186/s13229-015-0052-x

Kaspárek, T., Marecek, R., Schwarz, D., Prikryl, R., Vanícek, J., Mikl, M., et al. (2010). Source-based morphometry of gray matter volume in men with first-episode schizophrenia. *Hum. Brain Mapp.* 31, 300–310. doi: 10.1002/hbm.20865

Kubera, K. M., Sambataro, F., Vasic, N., Wolf, N. D., Frasch, K., Hirjak, D., et al. (2014). Source-based morphometry of gray matter volume in patients with schizophrenia who have persistent auditory verbal hallucinations. *Prog. Neuropsychopharmacol. Biol. Psychiatry* 50, 102–109. doi: 10.1016/j.pnpbp.2013.11.015

Lee, T.-W. (1998). "Independent component analysis," in *Independent Component Analysis* (Boston, MA: Springer US), 27–66. doi: 10.1007/978-1-4757-2851-4_2

Levy, S. E., Mandell, D. S., and Schultz, R. T. (2009). Autism. *Lancet* 374, 1627–1638. doi: 10.1016/S0140-6736(09)61376-3

Libero, L. E., Maximo, J. O., Deshpande, H. D., Klinger, L. G., Klinger, M. R., and Kana, R. K. (2014). The role of mirroring and mentalizing networks in mediating action intentions in autism. *Mol. Autism* 5:50. doi: 10.1186/2040-2392-5-50

Lombardo, M. V., Chakrabarti, B., Bullmore, E. T., and Baron-Cohen, S. (2011). Specialization of right temporo-parietal junction for mentalizing and its relation to social impairments in autism. *Neuroimage* 56, 1832–1838. doi: 10.1016/j.neuroimage.2011.02.067

Lord, C., and Bishop, S. L. (2015). Recent advances in autism research as reflected in DSM-5 criteria for autism spectrum disorder. *Annu. Rev. Clin. Psychol.* 11, 53–70. doi: 10.1146/annurev-clinpsy-032814-112745

Lord, C., Cook, E. H., Leventhal, B. L., and Amaral, D. G. (2000). Autism spectrum disorders. *Neuron* 28, 355–363.

Minshew, N. J., and Williams, D. L. (2007). The new neurobiology of autism: cortex, connectivity, and neuronal organization. *Arch. Neurol.* 64, 945–950. doi: 10.1001/archneur.64.7.945

Misra, V. (2014). The social brain network and autism. *Ann. Neurosci.* 21, 69–73. doi: 10.5214/ans.0972.7531.210208

Müller, R.-A. (2007). The study of autism as a distributed disorder. *Ment. Retard. Dev. Disabil. Res. Rev.* 13, 85–95. doi: 10.1002/mrdd.20141

Nickl-Jockschat, T., Habel, U., Michel, T. M., Manning, J., Laird, A. R., Fox, P. T., et al. (2012). Brain structure anomalies in autism spectrum disorder–a meta-analysis of VBM studies using anatomic likelihood estimation. *Hum. Brain Mapp.* 33, 1470–1489. doi: 10.1002/hbm.21299

Oberman, L. M., Hubbard, E. M., McCleery, J. P., Altschuler, E. L., Ramachandran, V. S., and Pineda, J. A. (2005). EEG evidence for mirror neuron dysfunction in autism spectrum disorders. *Brain Res. Cogbrainres.* 24, 190–198. doi: 10.1016/j.cogbrainres.2005.01.014

Palmen, S. J. M. C., Durston, S., Nederveen, H., and Van Engeland, H. (2006). No evidence for preferential involvement of medial temporal lobe structures in high-functioning autism. *Psychol. Med.* 36, 827–834. doi: 10.1017/S0033291706007215

Pappaianni, E., Siugzdaite, R., and Grecucci, A. (2016). An abnormal cerebellar network in children with autistic spectrum disorder: a morphometric study. *Autism Open Access* 6:178. doi: 10.4172/2165-7890.1000178

Pelphrey, K. A., Morris, J. P., McCarthy, G., and Labar, K. S. (2007). Perception of dynamic changes in facial affect and identity in autism. *Soc. Cogn. Affect Neurosci.* 2, 140–149. doi: 10.1093/scan/nsm010

Pina-Camacho, L., Villero, S., Fraguas, D., Boada, L., Janssen, J., Navas-Sánchez, F. J., et al. (2012). Autism spectrum disorder: does neuroimaging support the DSM-5 proposal for a symptom dyad? A systematic review of functional magnetic resonance imaging and diffusion tensor imaging studies. J. Autism Dev. Disord. 42, 1326–1341. doi: 10.1007/s10803-011-1360-4

Rapin, I., and Tuchman, R. F. (2008). Autism: definition, neurobiology, screening, diagnosis. *Pediatr. Clin. North Am.* 55, 1129–1146, viii. doi: 10.1016/j.pcl.2008.07.005

Rogers, T. D., McKimm, E., Dickson, P. E., Goldowitz, D., Blaha, C. D., and Mittleman, G. (2013). Is autism a disease of the cerebellum? An integration of clinical and pre-clinical research. Front. Syst. Neurosci. 7:15. doi: 10.3389/fnsys.2013.00015

Rossion, B., Caldara, R., Seghier, M., Schuller, A.-M., Lazeyras, F., and Mayer, E. (2003). A network of occipito-temporal face-sensitive areas besides the right middle fusiform gyrus is necessary for normal face processing. *Brain* 126(Pt 11), 2381–2395. doi: 10.1093/brain/awg241

Saxe, R., and Wexler, A. (2005). Making sense of another mind: the role of the right temporo-parietal junction. *Neuropsychologia* 43, 1391–1399. doi: 10.1016/j.neuropsychologia.2005.02.013

Schaer, M., Ottet, M.-C., Scariati, E., Dukes, D., Franchini, M., Eliez, S., et al. (2013). Decreased frontal gyrification correlates with altered connectivity in children with autism. *Front. Hum. Neurosci.* 7:750. doi: 10.3389/fnhum.2013.00750

Schumann, C. M., Hamstra, J., Goodlin-Jones, B. L., Lotspeich, L. J., Kwon, H., Buonocore, M. H., et al. (2004). The amygdala is enlarged in children but not adolescents with autism; the hippocampus is enlarged at all ages. *J. Neurosci.* 24, 6392–6401. doi: 10.1523/JNEUROSCI.1297-04.2004

Smith, S. M. (2002). Fast robust automated brain extraction. *Hum. Brain Mapp.* 17, 143–155. doi: 10.1002/hbm.10062

Sparks, B. F., Friedman, S. D., Shaw, D. W., Aylward, E. H., Echelard, D., Artru, A. A., et al. (2002). Brain structural abnormalities in young children with autism spectrum disorder. *Neurology* 59, 184–192. doi: 10.1212/WNL.59.2.184

Tager-Flusberg, H., Rogers, S., Cooper, J., Landa, R., Lord, C., Paul, R., et al. (2009). Defining spoken language benchmarks and selecting measures of expressive language development for young children with autism spectrum disorders. *J. Speech Lang. Hear. Res.* 52, 643–652. doi: 10.1044/1092-4388(2009/08-0136)

Torres, E. B., Isenhower, R. W., Yanovich, P., Rehrig, G., Stigler, K., Nurnberger, J., et al. (2013). Strategies to develop putative biomarkers to characterize the female phenotype with autism spectrum disorders. *J. Neurophysiol.* 110, 1646–1662. doi: 10.1152/jn.00059.2013

Tzourio-Mazoyer, N., Landeau, B., Papathanassiou, D., Crivello, F., Etard, O., Delcroix, N., et al. (2002). Automated anatomical labeling of activations in SPM using a macroscopic anatomical parcellation of the MNI MRI single-subject brain. *NeuroImage* 15, 273–289. doi: 10.1006/nimg.2001.0978

Vander Wyk, B. C., Hudac, C. M., Carter, E. J., Sobel, D. M., and Pelphrey, K. A. (2009). Action understanding in the superior temporal sulcus region. *Psychol. Sci.* 20, 771–777. doi: 10.1111/j.1467-9280.2009.02359.x

Xu, L., Groth, K. M., Pearlson, G., Schretlen, D. J., and Calhoun, V. D. (2009). Source-based morphometry: the use of independent component analysis to identify gray matter differences with application to schizophrenia. *Hum. Brain Mapp.* 30, 711–724. doi: 10.1002/hbm.20540

Zilbovicius, M., Meresse, I., Chabane, N., Brunelle, F., Samson, Y., and Boddaert, N. (2006). Autism, the superior temporal sulcus and social perception. *Trends Neurosci.* 29, 359–366. doi: 10.1016/j.tins.2006.06.004

Conflict of Interest Statement: The authors declare that the research was conducted in the absence of any commercial or financial relationships that could be construed as a potential conflict of interest.

frontiers in Neuroscience

ORIGINAL RESEARCH
published: 21 March 2017
doi: 10.3389/fnins.2017.00125

Latent and Abnormal Functional Connectivity Circuits in Autism Spectrum Disorder

Shuo Chen[1]*, *Yishi Xing*[1] and *Jian Kang*[2]

[1] Department of Epidemiology and Biostatistics, University of Maryland, College Park, MD USA, [2] Department of Biostatistics, University of Michigan, Ann Arbor, MI, USA

Autism spectrum disorder (ASD) is associated with disrupted brain networks. Neuroimaging techniques provide noninvasive methods of investigating abnormal connectivity patterns in ASD. In the present study, we compare functional connectivity networks in people with ASD with those in typical controls, using neuroimaging data from the Autism Brain Imaging Data Exchange (ABIDE) project. Specifically, we focus on the characteristics of intrinsic functional connectivity based on data collected by resting-state functional magnetic resonance imaging (rs-fMRI). Our aim was to identify disrupted brain connectivity patterns across all networks, instead of in individual edges, by using advanced statistical methods. Unlike many brain connectome studies, in which networks are prespecified before the edge connectivity in each network is compared between clinical groups, we detected the latent differentially expressed networks automatically. Our network-level analysis identified abnormal connectome networks that (i) included a high proportion of edges that were differentially expressed between people with ASD and typical controls; and (ii) showed highly-organized graph topology. These findings provide new insight into the study of the underlying neuropsychiatric mechanism of ASD.

Keywords: Autism spectrum disorder, biomarker, brain connectivity, fMRI, graph topology, network

OPEN ACCESS

Edited by:
Alessandro Grecucci, University of Trento, Italy

Reviewed by:
Kathleen Susan Franco, Case Western Reserve University School of Medicine, USA
Don Hong, Middle Tennessee State University, USA
Keith Maurice Kendrick, University of Electronic Science and Technology of China, China

***Correspondence:**
Shuo Chen
shuochen@umd.edu

Specialty section:
This article was submitted to Child and Adolescent Psychiatry, a section of the journal Frontiers in Neuroscience

Received: *04 May 2016*
Accepted: *28 February 2017*
Published: *21 March 2017*

Citation:
Chen S, Xing Y and Kang J (2017) Latent and Abnormal Functional Connectivity Circuits in Autism Spectrum Disorder. Front. Neurosci. 11:125. doi: 10.3389/fnins.2017.00125

1. INTRODUCTION

Autism spectrum disorder (ASD) is a neurodevelopmental disorder whose clinical symptoms include impaired social communication and language abilities, and repetitive behaviors (American Psychiatric Association, 2013). Its prevalence is increasing; one in 68 children were diagnosed with ASD in the United States in 2014 (CDC reports, 2014). However, the etiology of ASD remains unclear. Many recent studies have focused on the neural pathophysiology of brain structures and functions associated with ASD symptoms.

Neuroimaging techniques provide noninvasive methods of studying the neuropathology of ASD by learning about abnormal connectivity patterns. Mounting evidence suggests that ASD is associated with disturbances of neural connectivity rather than solely local neural activities (Di Martino et al., 2014; Hahamy et al., 2015). Resting-state functional magnetic resonance imaging (rs-fMRI) has become widely used to measure the functional connectivity between brain regions by calculating the correlations between time series of spontaneous low-frequency fluctuations in cerebral blood flow. The Autism Brain Imaging Data Exchange (ABIDE) consortium has contributed a publicly available set of existing rs-fMRI data from more than 1000 subjects, with the aim of improving the quality and reliability of functional connectivity research in ASD (Di Martino et al., 2014; Cheng et al., 2015). Many studies have yielded interesting, yet controversial, findings

of altered connectivity patterns (Shih et al., 2010; Vissers et al., 2012; Chen et al., 2015a; Ecker et al., 2015; Ha et al., 2015; Hahamy et al., 2015). For example, hypoconnectivity is associated with ASD, particularly in long-range and cross-hemispheric connections, such as those between the left and right insula and left and right parieto-occipital regions, which are known as the default mode network (DMN) (Broyd et al., 2009; Anderson et al., 2010; Schipul et al., 2011; Just et al., 2012; Di Martino et al., 2014). However, these claims have been challenged by findings reporting hyperconnectivity within networks (including the DMN, and frontostriatal, frontotemporal, motor, visual, and salience networks), as well as between the striatum, insula, and superior temporal gyrus, in children with ASD compared with typical children (Di Martino et al., 2011; Müller et al., 2011; Keown et al., 2013; Lynch et al., 2013; Supekar et al., 2013; Uddin et al., 2013).

The conflicting evidence regarding differentially expressed connectome features may arise for many possible reasons, such as demographic variation between subjects recruited in the studies, preprocessing steps, network selection methods, and statistical analysis methods. Recently, Cheng et al. (2015) report reduced connectivity in ASD based on the ABIDE data (418 autism and 509 matched healthy controls) using a voxel-wise meta-analysis, and more importantly they also report that the reduced connectivity is significantly correlated with symptom severity. Building on these findings, we aim to further investigate whether the disrupted brain connections in ASD are systematically organized from a network perspective. However, the disrupted networks in ASD are not known prior to the experiment, making it even more challenging to examine them with statistical rigor.

Conventionally, seed voxel analysis, descriptive statistics and mass univariate analysis are used for group-level brain connectivity analyses (Yeo et al., 2011; Craddock et al., 2013; Sporns, 2014; Smith et al., 2015). Descriptive graph metrics denote brain regions as nodes, and connections between them as edges, and have yielded many interesting findings (Bullmore and Sporns, 2009; Rubinov and Sporns, 2010; Biswal et al., 2010; Achard et al., 2012; Crossley et al., 2013, 2014; Fornito et al., 2013, 2015; van den Heuvel and Sporns, 2013; Stam, 2014). However, such metrics (i.e., modularity, clustering coefficients, and rich-club coefficients) summarize all edges as individual measures and lose localized connectivity (edge-specific) information. Thus, they may lack specificity and sensitivity, making it difficult to interpret such data clinically (Simpson et al., 2015). Mass univariate analysis (e.g., network-based statistics—NBS and family-wise error control; Zalesky et al., 2010), based on the connectome of the whole brain or prespecified brain regions, retains localized information about differentially expressed features but is subject to the trade-off between false positives and a lack of statistical power, and does not account for organized or complex network properties.

Our goal is to detect the latent and abnormal networks that (i) exhibit well-organized topology; and (ii) have a high proportion of differentially expressed edges (hypo- and/or hyperconnections). This approach integrates topological, differentially expressed, and localized edge features, to identify altered connectivity patterns. Recently, network object-oriented algorithms have been developed to detect and test these hidden disease-related brain connectivity networks (Chen et al., 2015b, 2016).

Here, we apply these recently developed statistical techniques to the ABIDE rs-fMRI data sets. Using these new statistical graph methods, our aim was to ASD related abnormal connectivity networks by automatically detecting latent networks with well-organized topological structures. Our resulting edgewise findings converge with previous studies using ABIDE data sets (Cheng et al., 2015). Moreover, we detect networks showing idiosyncratic distortion (Hahamy et al., 2015), which may help uncover the underlying mechanisms responsible for the joint hypo- *and* hyperconnectivity observed in ASD in many topological organization studies. Our findings may improve the understanding of neuropathological machinery and identify biomarkers that assist with disease diagnosis and treatment selection.

2. MATERIALS AND METHODS

2.1. Data Sets and Preprocessing

The data set was collected at the University of Michigan, one of the ABIDE data collection sites (Monk et al., 2009; Weng et al., 2010; Di Martino et al., 2014). The publicly available data set comprises data from 48 people with ASD and 65 TCs, with no significant differences in demographics between the two groups. For example, the mean age of the people with ASD at scan was 13.85 years (standard deviation (sd) = 2.31; range, 9.2–18.6); the mean age of the TCs was 15.03 (sd = 3.66; range, 8.2–28.8). Thirty-nine of the 48 people in the ASD group were male, compared with 49 of the 65 TCs. The p values from the Wilcoxon rank sum test (age) and Pearson χ^2 test (sex) were both greater than the α level at 0.05. The study was approved by the local institutional review boards, and data were fully de-identified by removing all 18 Health Insurance Portability and Accountability (HIPAA)-protected health information identifiers as well as facial information from structural images, and data were carefully examined before release to the public (Di Martino et al., 2014). TCs had no behavioral or mental concerns; inclusion and exclusion criteria for TCs are described on the ABIDE project website (http://fcon_1000.projects.nitrc.org/indi/abide/), Typical controls (TCs) were included by the criteria that either verbal or non-verbal IQ was $\geq$ 85 and were aged at least 7 years, whereas TCs were excluded for those who received a score of 10 or higher on the Social Communication Questionnaire 14 or a score of 6 or higher on the Obsessive/Compulsive subscale of the Spence Children's Anxiety Scale (SCAS) 16.

Imaging was performed on a 3 Tesla GE Signa scanner. Data were obtained using a gradient echo T2*-weighted echo planar imaging sequence, echo time = 30 ms, repetition time = 2,000 ms, 64 × 64 matrix with 40 slices, each 4.0 mm thick, no skip, resulting in whole brain coverage with a voxel size of 3.4 × 3.4 × 3.0 mm. During the scan, all subjects were asked to lie as still as possible, keep their eyes open, look at a fixation cross, and to try not to think about anything in particular.

On these rs-fMRI data we performed preprocessing based on the Configurable Pipeline for the Analysis of Connectomes

(C-PAC, http://fcp-indi.github.io). The images were slice-time and motion corrected. The data were then registered to a standard Montreal Neurological Institute (MNI) space with voxel size 2 mm^3 and converted to percent signal change. Masks of white matter, gray matter and cerebrospinal fluid (CSF) were created in the standard MNI space. The mean time series of the white matter, CSF and the six movement parameters were regressed from the gray matter. The linear trend was removed from the signal, and the fMRI time series were bandpass filtered (0.009–0.08 Hz) and spatially smoothed with a 6 mm full width at half maximum Gaussian kernel. Using automated anatomical labeling (AAL), we then used the first 90 regions of interest (ROIs) as nodes (Tzourio-Mazoyer et al., 2002), and took the weighted average of the temporal profiles of all voxels within each ROI as the region level signal for all subjects. The Pearson correlation coefficients were calculated between the 90 nodes and then Fisher's Z transformation was performed on each correlation. In our analysis, we focused on detecting and testing alterations in connectivity networks by comparing connectivity matrices between TCs and people with ASD.

2.2. Group Level Analysis

The goal of group-level functional connectivity analysis is to examine whether different groups (or individuals) show differences in connectivity. Conventional brain connectivity and network methods are conducted from two distinct perspectives: testing which edges are differentially expressed, or whether the global graph descriptive metrics differ (Simpson and Laurienti, 2016). Hybrid analyses are more attractive because they enable the identification of well-organized (systematic) networks (subgraphs) where most contained edges are differentially expressed. Such findings may provide insight into systematic disruptions of the brain connectome in people with ASD. To achieve this goal, we used network object-oriented algorithms (Chen et al., 2015b, 2016).

We first compared the TC and ASD data by performing two-sample t tests on each of the 4005 edges. Whole-brain results were denoted as a graph, $G = (V, E)$, where the node set V represents a brain region, and an edge $e_{ij} \in E$ connects regions i and j. For each edge (e_{ij}) we assigned the weight as $W_{ij} = -\log(p_{ij})$. The greater the W_{ij} value, the greater the difference in this edge between the TC and ASD data. Thus, the weighted adjacency matrix **W** is our input data for the detection of altered networks.

Next, we applied parsimonious differential brain connectivity network detection (Pard, for community detection) and k-partite algorithms (Chen et al., 2015b, 2016). The joint use of these algorithms enabled the automatic detection of latent abnormal networks with organized clique and k-partite graph topology. For each altered network detected, we performed a permutation test to obtain the statistical significance (network-level p-value).

We specified null and alternative hypotheses for testing differentially expressed connectivity networks (Chen et al., 2016). H_0: There is no altered connectivity network when comparing the connectivity matrices across clinical subpopulations; this is equivalent to: (i) there are no differentially expressed edges (C1), or (ii) there *are* differentially expressed edges but they are randomly distributed in the graph G (C2). H_1: There are altered connectivity networks; this is equivalent to: (i) there are differentially expressed edges, or (ii) the differentially expressed edges are *not* distributed randomly in the graph G, but in an organized pattern.

Therefore, the statistical significance of an altered connectivity network is determined by two factors: (1) the significance levels of all individual edges within the network; (2) the distribution of the differentially expressed edges in G. If C2 in the null hypothesis is true and differentially expressed edges are distributed randomly in G, then the detected network/subgraph $G_k \subset G$ is expected to contain a similar proportion of differentially expressed edges in G. Thus, based on the combinatorics and graph theory, the probability that the detected subgraph includes a much larger proportion of differentially expressed edges is extremely low, so we reject the null hypothesis. In theory, there are numerous possible subgraphs with various topological structures in G and thus testing detected networks is subject to multiplicity. We accounted for this multiple testing issue by using permutation testing techniques (Nichols and Holmes, 2002). In each permutation, we recorded the detected network with the maximum test statistic, and then calculated the percentiles of observed networks among the maximum test statistics from all permutations. We collected the suprathreshold networks as our resulting object-oriented altered connectivity networks. We set the α level of the permutation test as 0.05.

3. RESULTS

We applied the above network analysis procedure to the ABIDE data sets. Below is a summary of the latent differentially expressed networks we identified.

We compared the connectivity metrics (i.e., Fisher's Z-transformed correlation coefficients) on each edge between TC and ASD data using two-sample t tests, and stored the p value as $W_{ij} = -\log(p_{ij})$ where i and j were the first 90 AAL brain region indices ($i \neq j \in \{1, \cdots, 90\}$). **Figure 1A** displays the input data: a 90×90 pairwise connectivity testing result matrix (**W**) with the entry $W_{ij} = -\log(p_{ij})$. The ROIs in the heatmap of **Figure 1B** are listed in ascending order of regions in the AAL atlas. Next, we applied the Pard algorithm to determine whether the informative edges were distributed in communities, to capture the most differentially expressed edges in parsimonious (clique) networks. We then implemented the k-partite graph detection algorithm to obtain multi-partite subgraphs. In the heatmap of **Figure 1B**, we list the ROIs in order of identified networks and highlight three diagonal blocks, each representing one network. We then performed the permutation test on these networks, which revealed that the first two were significantly different (both $p < 0.001$) whereas the third was not ($p = 0.068$). Therefore, the differentially expressed edges were not randomly distributed in the 90×90 graph, but instead they were clustered within well-organized subgraphs.

Next, we investigated the two significant networks in detail. **Figure 2** shows the altered connections in the first network in an enlarged heatmap and as 3D images. The region names and corresponding information are listed in **Tables 1**, **2**. The heatmap

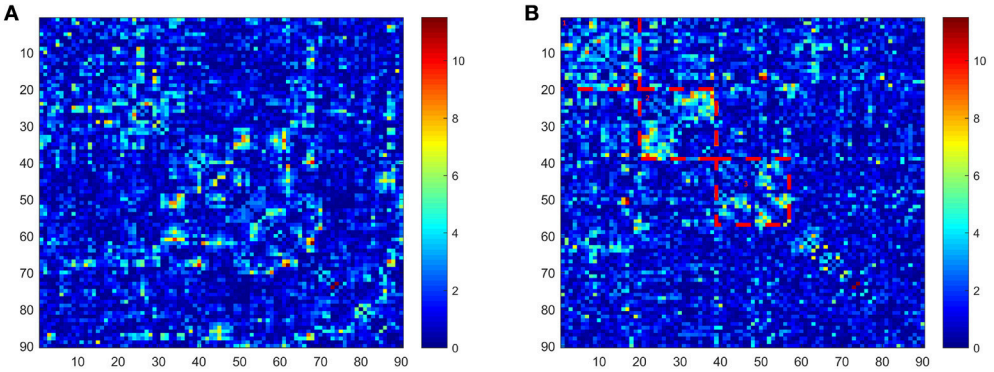

(a) Input bipartite $\mathbf{W}$ (b) Detected altered networks

FIGURE 1 | (A) Heatmap of $-\log(p_{ij})$ values in the original order of the first 90 AAL regions; **(B)** heatmap of $-\log(p_{ij})$ values reordered to list the detected networks first.

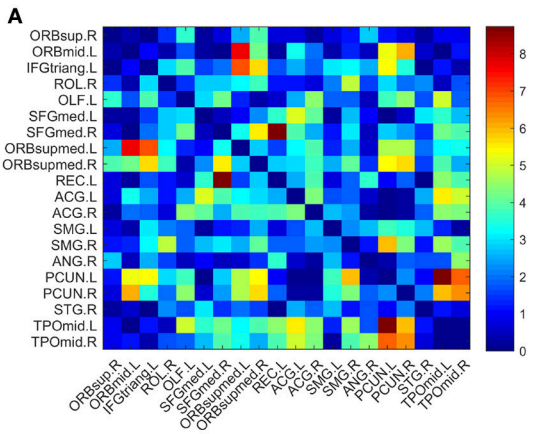

Altered network 1: clique topology

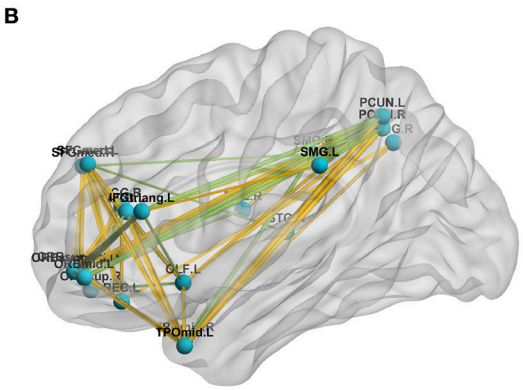

3D sagittal view

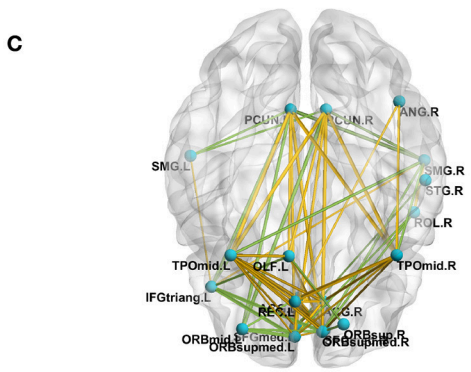

3D horizontal view

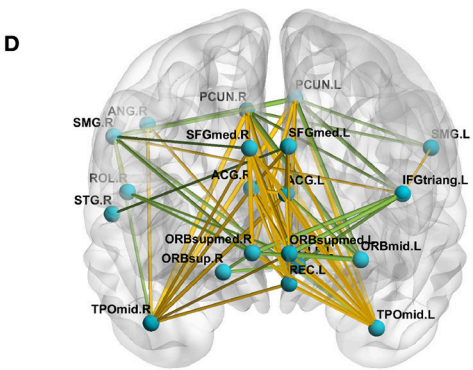

3D coronal view

FIGURE 2 | (A) Enlarged heatmap showing altered connections between brain regions. **(B–D)** 3D images showing altered connections within the identified network. Yellow edge, TC > ASD; green edge, ASD > TC. The width of an edge reflects the statistical significance of the difference between TC and ASD data.

TABLE 1 | Altered network 1 with clique topology.

AAL region name	Abbreviation	Index	*x*	*y*	*z*
Superior frontal gyrus, orbital part Right	ORBsup.R	6	18	48	−14
Middle frontal gyrus, orbital part, Left	ORBmid.L	9	−31	50	−10
Inferior frontal gyrus, triangular part,Left	IFGtriang.L	13	−46	30	14
Rolandic operculum,Right	ROL.R	18	53	−6	15
Olfactory cortex, Left	OLF.L	21	−8	15	−11
Superior frontal gyrus, medial, Left	SFGmed.L	23	−5	49	31
Superior frontal gyrus, medial, Right	SFGmed.R	24	9	51	30
Superior frontal gyrus, medial orbital, Left	ORBsupmed.L	25	−5	54	−7
Superior frontal gyrus, medial orbital, Right	ORBsupmed.R	26	8	52	−7
Gyrus rectus, Left	REC.L	27	−5	37	−18
Anterior cingulate and paracingulate gyri, Left	ACG.L	31	−4	35	14
Anterior cingulate and paracingulate gyri, Right	ACG.R	32	8	37	16
Supramarginal gyrus, Left	SMG.L	63	−56	−34	30
Supramarginal gyrus, Right	SMG.R	64	58	−32	34
Angular gyrus, Right	ANG.R	66	46	−60	39
Precuneus, Left	PCUN.L	67	−7	−56	48
Precuneus, Right	PCUN.R	68	10	−56	44
Superior temporal gyrus, Right	STG.R	82	58	−22	7
Temporal pole: middle temporal gyrus, Left	TPOmid.L	87	−36	15	−34
Temporal pole: middle temporal gyrus, Right	TPOmid.R	88	44	15	−32

TABLE 2 | Altered network 2 with bipartite topology.

AAL region name	Abbreviation	Index	*x*	*y*	*z*	set
Precentral gyrus, Left	PreCG.L	1	−39	−6	51	2
Olfactory cortex, Right	OLF.R	22	10	16	−11	2
Median cingulate and paracingulate gyri, Left	DCG.L	33	−5	−15	42	1
Median cingulate and paracingulate gyri, Right	DCG.R	34	8	−9	40	1
Posterior cingulate gyrus, Left	PCG.L	35	−5	−43	25	1
Posterior cingulate gyrus, Right	PCG.R	36	7	−42	22	1
Superior occipital gyrus, Left	SOG.L	49	−17	−84	28	2
Superior occipital gyrus, Right	SOG.R	50	24	−81	31	2
Middle occipital gyrus, Left	MOG.L	51	−32	−81	16	2
Middle occipital gyrus, Right	MOG.R	52	37	−80	19	2
Inferior occipital gyrus, Left	IOG.L	53	−36	−78	−8	1
Inferior occipital gyrus, Left	IOG.R	54	38	−82	−8	1
Postcentral gyrus, Right	PoCG.R	58	41	−25	53	2
Superior parietal gyrus, Left	SPG.L	59	−23	−60	59	2
Superior parietal gyrus, Right	SPG.R	60	26	−59	62	2
Inferior parietal, but supramarginal and angular gyri, Left	IPL.L	61	−43	−46	47	2
Angular gyrus, Left	ANG.L	65	−44	−61	36	1
Paracentral lobule, Right	PCL.R	70	7	−32	68	2
Inferior temporal gyrus, Right	ITG.R	90	54	−31	−22	1

(**Figure 2A**) shows the symmetric brain regions related to the altered connections; these include the left and right precuneus (involved in self-consciousness; Margulies et al., 2009), middle temporal gyri (face recognition; Acheson and Hagoort, 2013), supramarginal gyri (empathy; Silani, 2013), superior frontal gyri (self-awareness; Goldberg et al., 2006), and anterior cingulate cortices (emotion Decety and Jackson, 2004). Therefore, the systematic differences may provide a more comprehensive image for us to compare connectomes between TCs and people with ASD. Generally, there are more over-connections across hemispheres in TCs than in people with ASD. Patients with ASD have hypoconnections for most edges linked with right and left middle temporal gyri and precuneus, consistent with that reported by Cherkassky et al. (2006), Anderson et al. (2010),

and Lynch et al. (2013). Edgewise comparisons are shown in Supplementary Table 1.

We further validate the detected subnetwork features by performing classification analysis. We employ the support vector machine with radial basis function kernel and linear kernel as our classifier. The leave-one-out cross-validation results show that the accuracy rates are 89 and 84% correspondingly.

By implementing network detection and testing algorithms, we were able to conclude that the differentially expressed edges in the second abnormal connectivity network exhibited a k-partite topological structure (the algorithm selected $k = 2$ for this data set). The abnormal connectivity network is shown with a bipartite graph topological structure in **Figure 3**. In a bipartite graph there two disjoint sets of nodes; edges within each set are less differentially expressed than those between the two sets (**Figure 3A**). The first set of nodes includes lingual gyri, cingulate gyri, and the left angular gyrus, whereas the second set contains regions from the occipital, parietal, and frontal lobes. Interestingly, the brain regions in the second network are also fairly symmetric. The results suggest that people with ASD have hyperconnections for edges associated with the posterior cingulate gyrus (left and right), and hypoconnections for edges associated with the inferior occipital gyrus (left and right). In addition, all hyperconnections in our ASD group were associated with the angular and cingulate gyrus nodes. The hypo- and hyperconnected edges are in a well-organized topological structure and these results seem to be consistent with those of Monk et al. (2009), Just et al. (2012), Supekar et al. (2013), Uddin et al. (2013), Keown et al. (2013), and Di Martino et al. (2014). Overall, the findings may suggest that the coordination between the visual network (set two) and part of the DMN (set one) may be disrupted. A detailed edgewise comparison table and 3D video are presented as Supplementary Material.

4. DISCUSSION

Evidence of abnormal functional connectivity patterns in people with ASD has, to date, been inconsistent. The aim

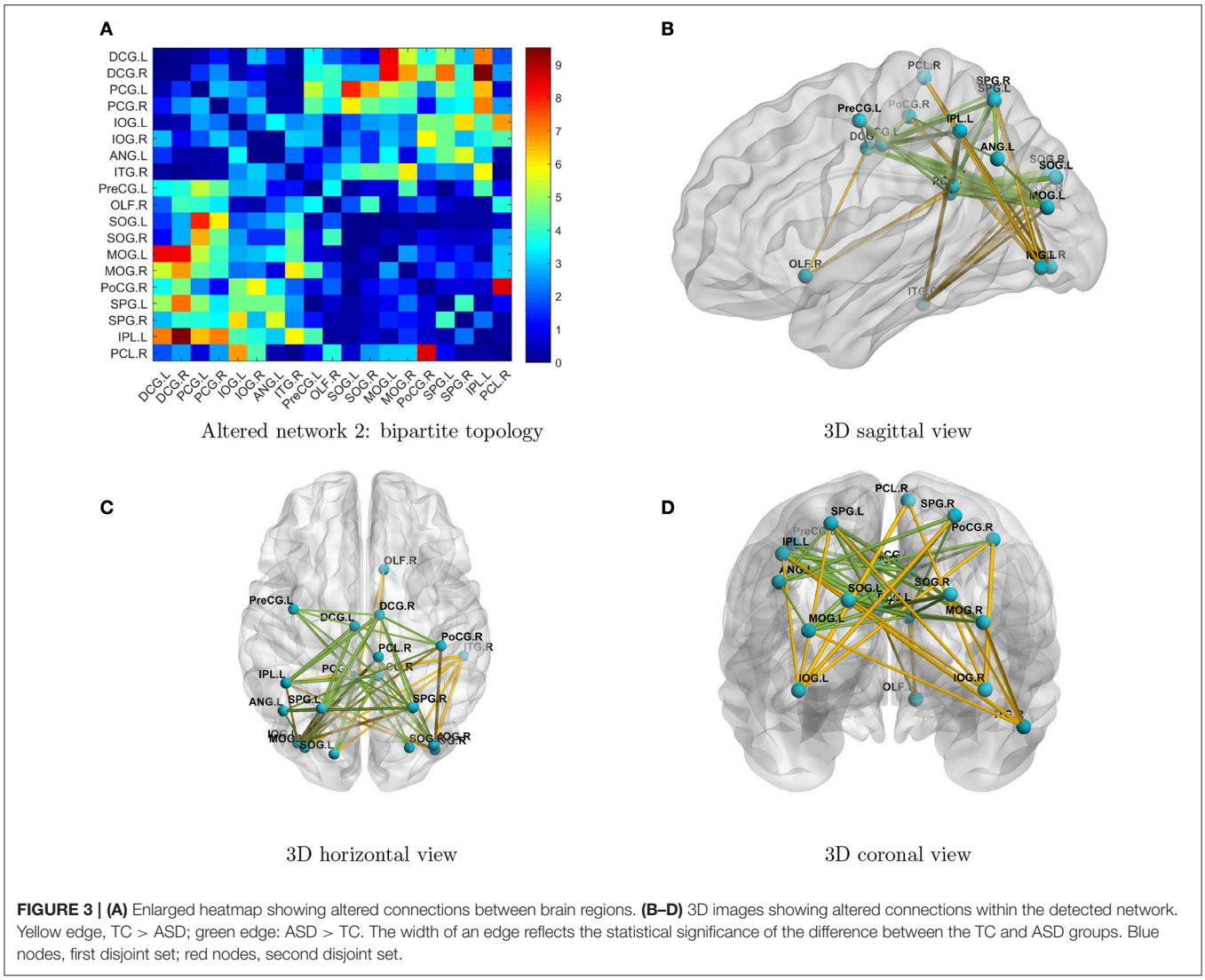

FIGURE 3 | (A) Enlarged heatmap showing altered connections between brain regions. **(B–D)** 3D images showing altered connections within the detected network. Yellow edge, TC > ASD; green edge: ASD > TC. The width of an edge reflects the statistical significance of the difference between the TC and ASD groups. Blue nodes, first disjoint set; red nodes, second disjoint set.

of the present study was to provide a novel strategy for brain connectivity analysis: to simultaneously uncover altered connectivity metrics and network structures. The findings of the present study suggest that unknown, systematic, and organized brain connectivity networks are disrupted in people with ASD. Within these aberrant networks, most edges are differentially expressed between TCs and people with ASD, and these differentially expressed edges show highly organized graph topology. Therefore, in the present study, we consider the altered connectivity as a network unit, rather than as individual edges or global graph summary metrics. This approach has several advantages: (i) the new statistical methods reveal specific nodes and edges within the abnormal networks; (ii) the statistical power is greatly increased while carefully controlling for multiple testing; and (iii) the topology of hypo- and hyperconnections in the abnormal networks could provide insight into the complex machinery underlying ASD. We used advanced graphical statistical methods to detect these hidden disease-related connectivity networks, and performed statistical tests to provide formal inferences.

From a statistical point of view, brain connectivity matrices are intercorrelated, high-throughput data. However, established statistical methods, including multiple-testing adjustment techniques (such as family error and false-positive discovery rate control) and shrinkage techniques (such as least absolute shrinkage and selection operator (Lasso) and elastic net) may not be directly applicable to connectivity analysis. The main reason is that connectivity edges are subject to spatial constraints and are thus dependent on each other in a highly complex, organized, yet unknown, topological structure. Without appropriately accounting for such a dependency structure, we risk a loss of statistical power and possible masking of significant findings. These new network-level connectivity analysis methods (Chen et al., 2015b, 2016) avoid the long-term trade-off between false positive findings and statistical power that arises from the universal cut-off in conventional statistical methods, because the edges borrow statistical strengths from each other through the topological structure. The latent topology provides additional information for statistical modeling and as a result we gain statistical power without increasing false positive error rates.

The topology of detected networks may reveal important underlying neuropathological mechanisms and provide valuable insight for future biological studies. In the networks we identified, most nodes were symmetric across hemispheres, and edges of hypo- and hyperconnections also seemed to be well organized. If we were to perform individual edge statistical analysis, only a small proportion of differentially expressed edges would pass the multiple testing adjustment threshold and no topological patterns would be detected. Interestingly, the two networks we identified include the functional hub nodes of the DMN, such as the posterior cingulate cortex, medial prefrontal cortex, and angular gyri, and the nodes from the dorsomedial subsystem, such as the temporoparietal junction (e.g., inferior parietal lobule and superior temporal gyrus; STG), lateral temporal cortex (e.g., inferior temporal gyrus), and anterior temporal pole (e.g., left and right middle temporal gyri). The first network also involved bilateral anterior, median, and posterior cingulate gyri and the occipital lobes. Our findings largely overlap with previously reported abnormalities in DMN, visual, and motor networks (Di Martino et al., 2011; Just et al., 2012; Uddin et al., 2013; Lynch et al., 2013; Ha et al., 2015; Cheng et al., 2015). The first network is mainly involved in the functional hubs of the DMN and is related to self-consciousness and emotion. The second network reflects the abnormal pattern of connections between parts of the DMN and the visual network. The first and second networks are jointly involved in many features of ASD including those related to receptive language, social cognition, joint attention, action observation, and empathy/emotion. The networks do not identify any consistent hypo- or hyperconnectivity in ASD; instead, the (significant) aberrant connectivities are organized systematically in topological structures. The organized topology of the altered connectivity networks identified here provides further evidence that these findings are promising clinical biomarker candidates.

Throughout this study, we limited our topological structure detection methods to clique and multipartite subgraphs. We are extending these methods to identify various other organized topological structures. We also focused on cross-sectional imaging data and did not address developmental changes of the brain connectome. Although we applied our methods only to fMRI data here, we may further extend these new network-based connectivity analysis tools to various other types of data including functional connectivity data (e.g., from EEG and fMRI) and structural connectivity data (e.g., from diffusion-weighted imaging) to investigate multimodal altered connectivity networks in ASD. The only requirements of the input data are an undirected graph, and that there is no restriction by the choice of connectivity metrics (such as in functional connectivity analysis correlation coefficients, maximum information coefficient, or spectral coherence). In addition, we only utilize a subset of ABIDE data base, and we plan to compare results from different study sites and perform meta-analysis in future work. We also plan to perform multivariate regression analysis to investigate association between brain connectivity and symptom severity at the network level.

We plan to develop more sophisticated algorithms for the automatic detection of complex latent topological structures that have explicit neurological significance, such as rich-club and hyper-graph topology. These new topological structure detection and statistical testing tools have the potential to become important research techniques for understanding the human connectome and its association with neuropsychiatric disorders.

5. AUTHOR CONTRIBUTIONS

SC and JK designed this work. SC, JK, and YX performed the data preprocessing and analysis. SC drafted the manuscript.

ACKNOWLEDGMENTS

We would thank the ABIDE initiative for aggregating and sharing the imaging and clinical data. Kang's work is supported by NIH 1R01MH105561-01.

SUPPLEMENTARY MATERIAL

The Supplementary Material for this article can be found online at: http://journal.frontiersin.org/article/10.3389/fnins.2017.00125/full#supplementary-material

REFERENCES

Achard, S., Delon-Martin, C., Vrtes, P. E., Renard, F., Schenck, M., Schneider, F., et al. (2012). Hubs of brain functional networks are radically reorganized in comatose patients. *Proc. Natl. Acad. Sci. U.S.A.* 109, 20608–20613. doi: 10.1073/pnas.1208933109

Acheson, D., and Hagoort, P. (2013). Stimulating the brain's language network: syntactic ambiguity resolution after TMS to the inferior frontal gyrus and middle temporal gyrus. *J. Cogn. Neurosci.* 25, 1664–1677. doi: 10.1162/jocn_a_00430

American Psychiatric Association. (2013). *Diagnostic and Statistical Manual of Mental Disorders, 5th Edn.* Washington, DC: American Psychiatric Association.

Anderson, J. S., Druzgal, T. J., Froehlich, A., DuBray, M. B., Lange, N., Alexander, A. L., et al. (2010). Decreased interhemispheric functional connectivity in autism. *Cereb. Cortex* 21, 1134–1146. doi: 10.1093/cercor/bhq190

Biswal, B. B., Mennes, M., Zuo, X. N., Gohel, S., Kelly, C., Smith, S. M., et al. (2010). Toward discovery science of human brain function. *Proc. Natl. Acad. Sci. U.S.A.* 107, 4734–4739. doi: 10.1073/pnas.0911855107

Bullmore, E., and Sporns, O. (2009). Complex brain networks: graph theoretical analysis of structural and functional systems. *Nat. Rev. Neurosci.* 10, 186–198. doi: 10.1038/nrn2575

Broyd, S. J., Demanuele, C., Debener, S., Helps, S. K., James, C. J., and Sonuga-Barke, E. J. (2009). Default-mode brain dysfunction in mental disorders: a systematic review. *Neurosci. Biobehav. Rev.* 33, 279–296. doi: 10.1016/j.neubiorev.2008.09.002

CDC reports, (2014). *Centers for Disease Control and Prevention (CDC) Report.* Available online at: http://www.cdc.gov/media/releases/2014/p0327-autism-spectrum-disorder.html

Chen, S., Kang, J., and Wang, G. (2015a). An empirical Bayes normalization method for connectivity metrics in resting state fMRI. *Front. Neurosci.* 9:316. doi: 10.3389/fnins.2015.00316

Chen, S., Kang, J., Xing, Y., and Wang, G. (2015b). A parsimonious statistical method to detect groupwise differentially expressed functional connectivity networks. *Hum. Brain Mapp.* 36, 5196–5206. doi: 10.1002/hbm.23007

Chen, S., Bowman, F. D., and Xing, Y., (2016). *Differentially Expressed Functional Connectivity Networks with K-partite Graph Topology.* arXiv:1603.07211.

Cheng, W., Rolls, E. T., Gu, H., Zhang, J., and Feng, J. (2015). Autism: reduced connectivity between cortical areas involved in face expression, theory of mind, and the sense of self. *Brain* 138, 1382–1393. doi: 10.1093/brain/awv051

Cherkassky, V. L., Kana, R. K., Keller, T. A., and Just, M. A. (2006). Functional connectivity in a baseline resting-state network in autism. *Neuroreport* 17, 1687–1690. doi: 10.1097/01.wnr.0000239956.45448.4c

Craddock, R. C., Jbabdi, S., Yan, C. G., Vogelstein, J. T., Castellanos, F. X., Di Martino, A., et al. (2013). Imaging human connectomes at the macroscale. *Nat. Methods* 10, 524–539. doi: 10.1038/nmeth.2482

Crossley, N. A., Mechelli, A., Vrtes, P. E., Winton-Brown, T. T., Patel, A. X., Ginestet, C. E., et al. (2013). Cognitive relevance of the community structure of the human brain functional coactivation network. *Proc. Natl. Acad. Sci. U.S.A.* 110, 11583–11588. doi: 10.1073/pnas.1220826110

Crossley, N. A., Mechelli, A., Scott, J., Carletti, F., Fox, P. T., McGuire, P., et al. (2014). The hubs of the human connectome are generally implicated in the anatomy of brain disorders. *Brain* 137, 2382–2395. doi: 10.1093/brain/awu132

Decety, J., and Jackson, P. L. (2004). The functional architecture of human empathy. *Behav. Cogn. Neurosci. Rev.* 3, 71–100. doi: 10.1177/1534582304267187

Di Martino, A., Kelly, C., Grzadzinski, R., Zuo, X. N., Mennes, M., Mairena, M. A., et al. (2011). Aberrant striatal functional connectivity in children with autism. *Biol. Psychiatry* 69, 847–856. doi: 10.1016/j.biopsych.2010.10.029

Di Martino, A., Yan, C. G., Li, Q., Denio, E., Castellanos, F. X., Alaerts, K., et al. (2014). The autism brain imaging data exchange: towards a large-scale evaluation of the intrinsic brain architecture in autism. *Mol. Psychiatry* 19, 659–667. doi: 10.1038/mp.2013.78

Ecker, C., Bookheimer, S. Y., and Murphy, D. G. (2015). Neuroimaging in autism spectrum disorder: brain structure and function across the lifespan. *Lancet Neurol.* 14, 1121–1134.. doi: 10.1016/S1474-4422(15)00050-2

Margulies, D. S., Vincent, J. L., Kelly, C., Lohmann, G., Uddin, L. Q., Biswal, B. B., et al. (2009). Precuneus shares intrinsic functional architecture in humans and monkeys. *Proc. Natl. Acad. Sci. U.S.A.* 106, 20069–20074. doi: 10.1073/pnas.0905314106

Monk, C. S., Peltier, S. J., Wiggins, J. L., Weng, S. J., Carrasco, M., Risi, S., et al. (2009). Abnormalities of intrinsic functional connectivity in autism spectrum disorders. *Neuroimage* 47, 764–772. doi: 10.1016/j.neuroimage.2009.04.069

Fornito, A., Zalesky, A., and Breakspear, M. (2013). Graph analysis of the human connectome: promise, progress, and pitfalls. *Neuroimage* 80, 426–444. doi: 10.1016/j.neuroimage.2013.04.087

Fornito, A., Zalesky, A., and Breakspear, M. (2015). The connectomics of brain disorders. *Nat. Rev. Neurosci.* 16, 159–172. doi: 10.1038/nrn3901

Goldberg, I., Harel, M., and Malach, R. (2006). When the brain loses its self: prefrontal inactivation during sensorimotor processing. *Neuron* 50, 329–339. doi: 10.1016/j.neuron.2006.03.015

Ha, S., Sohn, I. J., Kim, N., Sim, H. J., and Cheon, K. A. (2015). Characteristics of Brains in Autism Spectrum Disorder: structure, function and connectivity across the Lifespan. *Exp. Neurobiol.* 24, 273–284. doi: 10.5607/en.2015.24.4.273

Hahamy, A., Behrmann, M., and Malach, R. (2015). The idiosyncratic brain: distortion of spontaneous connectivity patterns in autism spectrum disorder. *Nat. Neurosci.* 18, 302–309. doi: 10.1038/nn.3919

Just, M. A., Keller, T. A., Malave, V. L., Kana, R. K., and Varma, S. (2012). Autism as a neural systems disorder: a theory of frontal-posterior underconnectivity. *Neurosci. Biobehav. Rev.* 36, 1292–1313. doi: 10.1016/j.neubiorev.2012.02.007

Keown, C. L., Shih, P., Nair, A., Peterson, N., Mulvey, M. E., and Mller, R. A. (2013). Local functional overconnectivity in posterior brain regions is associated with symptom severity in autism spectrum disorders. *Cell Reports* 5, 567–572. doi: 10.1016/j.celrep.2013.10.003

Lynch, C. J., Uddin, L. Q., Supekar, K., Khouzam, A., Phillips, J., and Menon, V. (2013). Default mode network in childhood autism: posteromedial cortex heterogeneity and relationship with social deficits. *Biol. Psychiatry* 74, 212–219. doi: 10.1016/j.biopsych.2012.12.013

Müller, R. A., Shih, P., Keehn, B., Deyoe, J. R., Leyden, K. M., and Shukla, D. K. (2011). Underconnected, but how? A survey of functional connectivity MRI studies in autism spectrum disorders. *Cereb. Cortex* 21, 2233–2243. doi: 10.1093/cercor/bhq296

Nichols, T. E., and Holmes, A. P. (2002). Nonparametric permutation tests for functional neuroimaging: a primer with examples. *Hum. Brain Mapp.* 15, 1–25. doi: 10.1002/hbm.1058

Rubinov, M., and Sporns, O. (2010). Complex network measures of brain connectivity: uses and interpretations. *Neuroimage* 52, 1059–1069. doi: 10.1016/j.neuroimage.2009.10.003

Schipul, S. E., Keller, T. A. and Just, M. A. (2011). Inter-regional brain communication and its disturbance in autism. *Front. Syst. Neurosci.* 5:10. doi: 10.3389/fnsys.2011.00010

Shih, P., Shen, M., Öttl, B., Keehn, B., Gaffrey, M. S., and Müller, R. A. (2010). Atypical network connectivity for imitation in autism spectrum disorder. *Neuropsychologia* 48, 2931–2939. doi: 10.1016/j.neuropsychologia.2010.05.035

Silani, G., Lamm, C., Ruff, C. C., and Singer, T. (2013). Right supramarginal gyrus is crucial to overcome emotional egocentricity bias in social judgments. *J. Neurosci.* 33, 15466–15476. doi: 10.1523/JNEUROSCI.1488-13.2013

Simpson, S. L., Burdette, J. H., and Laurienti, P. J. (2015). The brain science interface. *Significance* 12, 34–39. doi: 10.1111/j.1740-9713.2015.00843.x

Simpson, S. L., and Laurienti, P. J. (2016). Disentangling brain graphs: a note on the conflation of network and connectivity analyses. *Brain Connect.* 6, 95–98. doi: 10.1089/brain.2015.0361

Smith, S. M., Nichols, T. E., Vidaurre, D., Winkler, A. M., Behrens, T. E., Glasser, M. F., et al. (2015). A positive-negative mode of population covariation links brain connectivity, demographics and behavior. *Nat. Neurosci.* 18, 1565–1567. doi: 10.1038/nn.4125

Sporns, O. (2014). Contributions and challenges for network models in cognitive neuroscience. *Nat. Neurosci.* 17, 652–660. doi: 10.1038/nn.3690

Supekar, K., Uddin, L. Q., Khouzam, A., Phillips, J., Gaillard, W. D., Kenworthy, L. E., et al. (2013). Brain hyperconnectivity in children with autism and its links to social deficits. *Cell Reports* 5, 738–747. doi: 10.1016/j.celrep.2013.10.001

Stam, C. J. (2014). Modern network science of neurological disorders. *Nat. Rev. Neurosci.* 15, 683–695. doi: 10.1038/nrn3801

Tzourio-Mazoyer, N., Landeau, B., Papathanassiou, D., Crivello, F., Etard, O., Delcroix, N., et al. (2002). Automated anatomical labeling of activations in SPM using a macroscopic anatomical parcellation of the MNI MRI single-subject brain. *Neuroimage* 15, 273–289. doi: 10.1006/nimg.2001.0978

Uddin, L. Q., Supekar, K., Lynch, C. J., Khouzam, A., Phillips, J., Feinstein, C., et al. (2013). Salience networkbased classification and prediction of symptom severity in children with autism. *JAMA Psychiatry* 70, 869–879. doi: 10.1001/jamapsychiatry.2013.104

van den Heuvel, M. P., and Sporns, O. (2013). Network hubs in the human brain. *Trends Cogn. Sci.* 17, 683–696. doi: 10.1016/j.tics.2013.09.012

Vissers, M. E., Cohen, M. X., and Geurts, H. M. (2012). Brain connectivity and high functioning autism: a promising path of research that needs refined models, methodological convergence, and stronger behavioral links. *Neurosci. Biobehav. Rev.* 36, 604–625. doi: 10.1016/j.neubiorev.2011.09.003

Weng, S. J., Wiggins, J. L., Peltier, S. J., Carrasco, M., Risi, S., Lord, C., et al. (2010). Alterations of resting state functional connectivity in the default network in adolescents with autism spectrum disorders. *Brain Res.* 1313, 202–214. doi: 10.1016/j.brainres.2009.11.057

Yeo, B. T., Krienen, F. M., Sepulcre, J., Sabuncu, M. R., Lashkari, D., Hollinshead, M., et al. (2011). The organization of the human cerebral cortex estimated by intrinsic functional connectivity. *J. Neurophysiol.* 106, 1125–1165. doi: 10.1152/jn.00338.2011

Zalesky, A., Fornito, A., and Bullmore, E. T. (2010). Network-based statistic: identifying differences in brain networks. *Neuroimage* 53, 1197–1207. doi: 10.1016/j.neuroimage.2010.06.041

Conflict of Interest Statement: The authors declare that the research was conducted in the absence of any commercial or financial relationships that could be construed as a potential conflict of interest.

frontiers in Neuroscience

ORIGINAL RESEARCH
published: 03 May 2016
doi: 10.3389/fnins.2016.00191

Abnormalities of Inter- and Intra-Hemispheric Functional Connectivity in Autism Spectrum Disorders: A Study Using the Autism Brain Imaging Data Exchange Database

Jung Min Lee[1†], Sunghyun Kyeong[2†], Eunjoo Kim[3] and Keun-Ah Cheon[3]*

[1] Division of Computational Mathematics, National Institute for Mathematical Sciences, Daejeon, South Korea, [2] Severance Biomedical Science Institute, Yonsei University College of Medicine, Seoul, South Korea, [3] Division of Child and Adolescent Psychiatry, Department of Psychiatry and Institute of Behavioral Science in Medicine, Yonsei University College of Medicine, Seoul, South Korea

OPEN ACCESS

Edited by:
Roma Siugzdaite, Ghent University, Belgium

Reviewed by:
David Cochran, University of Massachusetts Medical Center, USA
Suhash Chakraborty, Hindustan Aeronautics Limited Hospital, India

***Correspondence:**
Keun-Ah Cheon
kacheon@yuhs.ac

[†] These authors have contributed equally to this work.

Specialty section:
This article was submitted to Child and Adolescent Psychiatry, a section of the journal Frontiers in Neuroscience

Received: *25 December 2015*
Accepted: *18 April 2016*
Published: *03 May 2016*

Citation:
Lee JM, Kyeong S, Kim E and Cheon K-A (2016) Abnormalities of Inter- and Intra-Hemispheric Functional Connectivity in Autism Spectrum Disorders: A Study Using the Autism Brain Imaging Data Exchange Database. Front. Neurosci. 10:191. doi: 10.3389/fnins.2016.00191

Recently, the Autism Brain Imaging Data Exchange (ABIDE) project revealed decreased functional connectivity in individuals with Autism Spectrum Disorders (ASD) relative to the typically developing controls (TDCs). However, it is still questionable whether the source of functional under-connectivity in subjects with ASD is equally contributed by the ipsilateral and contralateral parts of the brain. In this study, we decomposed the inter- and intra-hemispheric regions and compared the functional connectivity density (FCD) between 458 subjects with ASD and 517 TDCs from the ABIDE database. We quantified the inter- and intra-hemispheric FCDs in the brain by counting the number of functional connectivity with all voxels in the opposite and same hemispheric brain regions, respectively. Relative to TDCs, both inter- and intra-hemispheric FCDs in the posterior cingulate cortex, lingual/parahippocampal gyrus, and postcentral gyrus were significantly decreased in subjects with ASD. Moreover, in the ASD group, the restricted and repetitive behavior subscore of the Autism Diagnostic Observation Schedule (ADOS-RRB) score showed significant negative correlations with the average inter-hemispheric FCD and contralateral FCD in the lingual/parahippocampal gyrus cluster. Also, the ADOS-RRB score showed significant negative correlations with the average contralateral FCD in the default mode network regions such as the posterior cingulate cortex and precuneus. Taken together, our findings imply that a deficit of non-social functioning processing in ASD such as restricted and repetitive behaviors and sensory hypersensitivity could be determined via both inter- and intra-hemispheric functional disconnections.

Keywords: Autism Spectrum Disorder (ASD), inter-hemisphere, intra-hemisphere, functional connectivity, resting state fMRI

INTRODUCTION

Autism Spectrum Disorder (ASD) is characterized by impairments in social interaction and communication, and restrictive and repetitive behaviors (American Psychiatric Association, 2013). ASD is caused by genetic and neurobiological factors (Frith and Happe, 1993; Bogdashina, 2006; Hughes, 2009; Amaral, 2011). Among the neurobiological mechanisms, the prevailing theory is that ASD is caused by abnormalities in the neuronal system and social brain network (Bogdashina, 2006; Minshew and Keller, 2010; Nebel et al., 2014). In functional neuroimaging studies, researchers have investigated the functional connectivity in subjects with ASD (Just et al., 2007), and the under-connectivity theory of ASD has been supported by many previous studies (Muller et al., 2011; Rudie et al., 2012; Vissers et al., 2012; Di Martino et al., 2014). A neuronal network study using electroencephalography showed long-range under-connectivity and short-range over-connectivity in patients with ASD (Barttfeld et al., 2011). The white matter integrity of the brain network has been examined with diffusion tensor imaging analysis. Furthermore, a decreased size of the corpus callosum was observed in the ASD group in a structural magnetic resonance imaging (MRI) study (Keary et al., 2009). Because the corpus callosum is the biggest part of the transcallosal connectivity in the human brain, a decreased corpus callosum size has been argued as an indication of long-range under-connectivity. Moreover, decreased volumes and abnormal integrity of the corpus callosum have been observed in diffusion tensor imaging studies (Alexander et al., 2007; Keller et al., 2007; Cheon et al., 2011).

Many researchers utilized the resting state functional MRI and found atypical brain activities in ASD (Cherkassky et al., 2006; Di Martino et al., 2014). Due to the restricted computational power, studies in the neuroimaging, and psychiatric research areas predominantly used a seed-based analysis by considering a default network alteration (Monk et al., 2009; Weng et al., 2010). Recently, voxel-wise data-driven functional connectivity density (FCD) mapping method was proposed (Tomasi and Volkow, 2010), in which all voxels in the whole brain region would be examined rather than using a specific seed region of interest for a connectivity analysis. The FCD method has been applied successfully to analyze the sex differences in functional connectivity in both healthy control subjects (Tomasi and Volkow, 2012b) and subjects with attention deficit hyperactivity disorder (ADHD) using large samples (Tomasi and Volkow, 2012a).

Due to the diverse symptoms and complexity of ASD, a large dataset is needed to investigate the characteristic features of ASD. Recently, the Autism Brain Imaging Data Exchange (ABIDE) collected 1112 resting state functional MRI datasets of subjects with ASD and typically developing control (TDC) subjects from 17 international sites. Previously, large datasets from multiple centers have been successfully analyzed to identify features of the functional human brain (Lord et al., 2000; Biswal et al., 2010; Tomasi and Volkow, 2012a). In particular, the FCD method was applied successfully to the ADHD-200 dataset to identify differences in the functional hubs among children with ADHD (Tomasi and Volkow, 2012a). A deeper understanding of the connectivity abnormalities in ASD has been achieved with the worldwide neuroimaging data sharing initiative. Di Martino et al. analyzed brain connectivity in 1000 subjects using global connectivity measures, and revealed over- and under-connectivity in the ASD group (Di Martino et al., 2014).

Several studies have examined the regional inter-hemispheric under-connectivity in ASD by evaluating the correlation between a voxel and its opposite hemispheric counterpart on a symmetric template (Anderson et al., 2011; Di Martino et al., 2014). However, the whole-brain inter- and intra-hemispheric functional under-connectivity studies have been rarely investigated to uncover the deficit of social and non-social functioning in ASD. Because the global FCD was originally proposed to identify the functional hub regions, the ipsilateral FCD and contralateral FCD measure the intra-hemispheric and inter-hemispheric functional hub regions, respectively. A recently published study using the ABIDE datasets examined both intra-hemispheric and inter-hemispheric connectivity in participants with ASD, and revealed both increased and decreased connectivity in the ASD groups in comparison to the control groups, depending on the different types of brain connectivity and distortions in connectivity patterns examined at the individual level (Hahamy et al., 2015). In the current study, we aimed to examine both inter- and inter-hemispheric connectivity in the brains of participants with ASD by decomposing the functional connectivity into ipsilateral and contralateral parts. These approaches would allow us to investigate how connectivity abnormalities in the ASD group would be determined by interactions between the intra- and inter-hemispheric functional connectivity. The results would also confirm that the abnormal regions of the resting state functional connectivity in ASD are related to the default mode network (Raichle and Snyder, 2007; Assaf et al., 2010; Weng et al., 2010; Lynch et al., 2013) and brain regions implicated in the non-social functioning processes such as restricted and repetitive behaviors (Di Martino et al., 2009; Supekar et al., 2013; von dem Hagen et al., 2013; Fishman et al., 2014).

MATERIALS AND METHODS

Dataset

We used resting state fMRI data of 458 subjects with ASD and 517 TDCs (see **Table 1** for additional demographic information) among 1112 datasets from the ABIDE datasets (http://fcon_1000.projects.nitrc.org/indi/abide). To minimize the institution dependent variability, our study included data from research centers that contributed to both the ASD and TDC groups. Therefore, the present study included neuroimaging datasets from California Institute of Technology (CALTECH), Kennedy Krieger Institute (KKI), Ludwig Maximilians University, Munich (MAX_MUM), New York University Langone Medical Center (NYU), Olin Institute of Living at Hartford Hospital (OLIN), Oregon Health & Science University (OHSU), University of Pittsburgh School of Medicine (PITT), San Diego State University (SDSU), Stanford University (STANFORD), Trinity Center for Health Sciences (TRINITY), University of California,

Los Angeles (UCLA), University of Leuven (LEUVEN), University of Michigan (UM), University of Utah School of Medicine (USM), and Yale Child Study Center (YALE). All experimental protocols were in compliance with the policies of site-specific institutional review boards. The demographic variables and scanning parameters are summarized in **Table 1**. The graphical illustration of the demographic variables can be found in elsewhere (Di Martino et al., 2014). We excluded datasets from the social brain Lab BCN NIC UMC Groningen and Netherlands Institute for Neurosciences due to the missing information of a full-scale intelligence quotient (IQ) for many subjects. After preprocessing, we found that a large part of the cerebellum was missing in the imaging dataset of Carnegie Mellon University, and all datasets from Carnegie Mellon University were excluded. To control for potential confounding effects of IQ in our analysis, we decided to exclude five datasets that included some subjects with IQ lower than 70. Finally, we performed voxel-wise group comparisons with 975 imaging datasets.

Image Preprocessing

Datasets were preprocessed with SPM8 (http://www.fil.ion.ucl.ac.uk/spm/software/spm8/). The first step was realignment for head motion correction. Images were realigned to the first image and a mean echo planar image (EPI) was created during this step. Subsequently, structural T1 images were coregistered to their mean EPI data. Registered EPI data of each subject were normalized to Montreal Neurological Institute (MNI) template and spatially smoothed with 8 mm of full-width at half-maximum. Then, in the temporal domain, the linearly increasing trend due to heat absorption was removed at each voxel, and the effects of the head motion, white matter, cerebrospinal fluid, and global signal were regressed out. Lastly, temporal band-pass filtering was applied (0.01–0.08 Hz).

Functional Connectivity Density Mapping

Preprocessed resting state fMRI data were normalized into the MNI template space with a voxel size of $2 \times 2 \times 2$ mm. At each voxel, we applied a voxel-wise data-driven FCD mapping method to calculate the global FCD, which was introduced by Tomasi and Volkow (2010). In this study, we divided the global functional connectivity density into two parts. One is the contralateral FCD and another is the ipsilateral FCD (**Figure 1**). The global FCD is the number of functional edges connected with all other voxels. For a given voxel i, a voxel j is said to be connected to the voxel i if the correlation coefficient between i-th and j-th time series is larger than 0.6 (Tomasi and Volkow, 2010, 2012a,b,c). Then the degree between the two voxels is defined to be 1 ($S_{ij} = 1$); and otherwise, the degree is zero ($S_{ij} = 0$). Likewise, we could obtain the degree from other voxels and the sum of all degrees at a given voxel i is defined as the global FCD at that voxel. At a voxel i, the global FCD is calculated as,

$$\text{global FCD}_i = \sum_{j=1}^{N} S_{ij},$$

where N is the number of voxels (or nodes) in the gray matter regions.

The contralateral (or inter-hemispheric) FCD is evaluated by counting the number of functional connectivity with all voxels in the opposite hemispheric brain regions as follows:

$$\text{contralateral FCD}_i = \sum_{j=1}^{N} h_{ij} S_{ij},$$

where h_{ij} is 1 if j-th voxels are in the opposite hemispheres and 0 otherwise.

Lastly, the ipsilateral (or intra-hemispheric) FCD was computed by subtracting the number of contra-lateral functional connectivity from the total number of functional connectivity as follows:

$$\text{ipsilateral FCD}_i = \text{global FCD}_i - \text{contralateral FCD}_i.$$

The graphical illustrations of global, contralateral, and ipsilateral functional connectivity densities are presented in **Figure 1**. Finally, the normalized contralateral FCD (cFCD), normalized ipsilateral FCD (iFCD), and normalized global FCD (gFCD) were obtained by normalizing the number of functional connections at each voxel with respect to the average value of the global functional connectivity of each subject.

$$\text{iFCD}_i = \frac{\text{ipsilateral FCD}_i}{mean\left(\text{global FCD}\right)}, \text{cFCD}_i = \frac{\text{contralateral FCD}_i}{mean\left(\text{global FCD}\right)},$$
$$\text{and gFCD}_i = \frac{\text{global FCD}_i}{mean\left(\text{global FCD}\right)},$$

where *mean*(global FCD) is the average of the global FCD for all voxels.

The use of the normalized functional connectivity density minimizes the individual variability of the overall connectivity and makes it easier to detect the fractionally increased or decreased connectivity. Consequently, the average of the gFCD becomes one.

Statistical Analysis

The images of the gFCD, cFCD, and iFCD were used for a second-level analysis, comparing the subjects with ASD and TDCs using SPM8, in which a 2-tailed t-test design with two covariates of age and sex was used to compute the statistical significance of the FCD differences between the two groups. Statistical significance was based on the false discovery rate corrected $P < 0.05$ together with requiring 20 voxels for the minimum continuous voxel size within a cluster (corrected $P < 0.05$). For brain regions showing significantly decreased FCDs, we computed the partial correlations between the averages (or regional maximum) of the FCD values for each cluster and the scores from symptom severity scales while controlling for effects of age and sex. The Benjamini-Hochberg procedure was applied to control multiple comparison corrections (Benjamini and Hochberg, 1995). The significances of the correlation analysis were set at a threshold of (Benjamini–Hochberg) corrected $P < 0.05$.

TABLE 1 | Demographic variables and imaging parameters for the selected resting-state functional MRI datasets from Autism Brain Imaging Data Exchange database.

Center	No. of scans	TR(ms)	TDC			ASD		
			M/F	Age	FIQ	M/F	Age	FIQ
PITT	200	1500	23/4	18.9 ± 6.5	110.1 ± 9.2	26/4	18.9 ± 7.1	110.0 ± 14.1
OLIN	210	1500	14/2	16.9 ± 3.6	114.9 ± 16.0	16/2	16.3 ± 3.0	113.0 ± 17.4
OHSU	82	2500	15/0	10.1 ± 1.0	115.7 ± 10.7	10/0	10.9 ± 1.8	109.7 ± 18.4
SDSU	180	2000	16/6	14.2 ± 1.9	108.1 ± 10.3	13/1	14.7 ± 1.7	111.4 ± 17.4
TRINITY	150	2000	25/0	17.1 ± 3.7	110.9 ± 12.0	24/0	17.3 ± 3.5	109.3 ± 14.7
UM	300	2000	56/17	14.6 ± 3.6	108.0 ± 9.7	50/9	13.2 ± 2.5	107.3 ± 16.8
USM	240	2000	43/0	21.4 ± 7.6	115.1 ± 13.6	57/0	22.4 ± 7.5	100.9 ± 15.2
YALE	200	2000	20/8	12.7 ± 2.7	105.0 ± 17.1	18/8	12.7 ± 3.0	97.9 ± 17.8
LEUVEN	250	1667	15/0	23.3 ± 2.8	114.8 ± 12.4	14/0	21.9 ± 4.0	109.4 ± 12.6
KKI	156	2500	23/9	10.1 ± 1.2	113.8 ± 8.9	16/4	10.0 ± 1.5	97.8 ± 16.4
NYU	180	2000	79/26	15.8 ± 6.2	113.2 ± 13.1	68/10	14.5 ± 7.0	108.1 ± 16.5
STANDFORD	180	2000	16/4	10.0 ± 1.6	112.1 ± 15.0	16/3	9.9 ± 1.5	113.3 ± 17.5
UCLA	120	3000	38/6	13.0 ± 1.9	106.3 ± 10.8	46/6	13.1 ± 2.4	100.9 ± 13.2
MAX_MUN	120	3000	29/4	26.2 ± 9.7	111.5 ± 8.7	16/3	22.9 ± 14.1	107.6 ± 13.7
CALTECH	150	2000	15/4	28.9 ± 10.9	114.2 ± 9.4	14/4	27.8 ± 10.2	108.2 ± 12.2
Total			427/90	16.5 ± 7.3	111.2 ± 12.4	404/54	16.2 ± 7.4	106.0 ± 16.3

ASD, autism spectrum disorder; CALTECH, California Institute of Technology; F, female; FIQ, full scale IQ standard score; KKI, Kennedy Krieger Institute; M, Male; MAX_MUM, Ludwig Maximilians University Munich; NYU, New York University Langone Medical Center; OLIN, Olin Institute of Living at Hartford Hospital; OHSU, Oregon Health and Science University; PITT, University of Pittsburgh School of Medicine; SDSU, San Diego State University; STANFORD, Stanford University; TDC, Typically developed control group; TRINITY, Trinity Center for Health Sciences; UCLA, University of California, Los Angeles; LEUVEN, University of Leuven; UM, University of Michigan; USM, University of Utah School of Medicine; YALE, Yale Child Study Center.

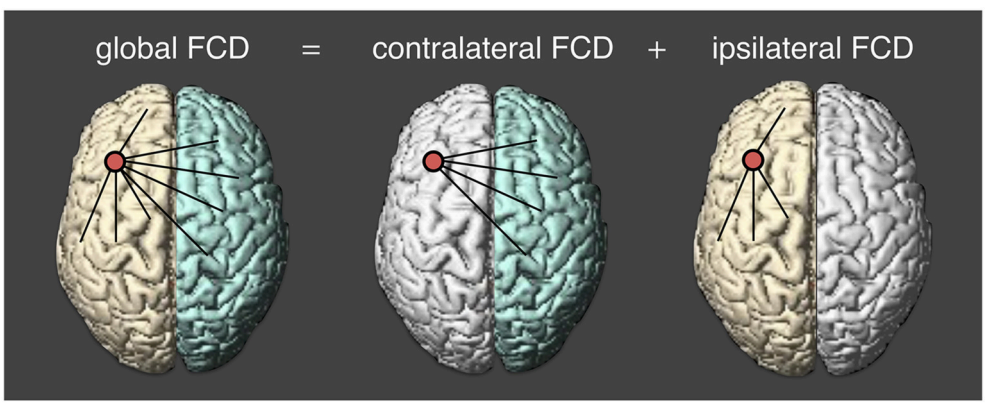

FIGURE 1 | Calculating three measures of functional connectivity density. cFCD (contralateral functional connectivity density) is the number of functional connectivity from the opposite hemisphere; iFCD (ipsilateral functional connectivity density) is from the same hemisphere; gFCD (global functional connectivity density) is computed as the sum of cFCD and iFCD.

RESULTS

Demographic Variables and Clinical Measures

We included data from 458 subjects (54 females) with ASD and 517 TDCs (90 females) in the data analysis. The two-sample *t*-test showed that the age distribution of subjects with ASD were not significantly different from that of TDCs, but the full-scale IQ score was significantly lower in the ASD group than that in the TDC group ($P < 0.05$).

Functional Connectivity Density

For both the ASD and TDC groups, the average values of gFCD, iFCD, and cFCD are presented (**Figure 2**), and the distribution of the functional connectivity density were bilateral. For each measure of the normalized gFCDs, iFCDs, and cFCDs, the two-sample *t*-test with covariates of age and sex found significantly decreased functional connectivity in multiple regions in the ASD group, but no significantly increased functional connectivity was detected (**Figure 3** and **Table 2**). For example, in the comparisons of gFCD, the ASD group showed a significantly decreased

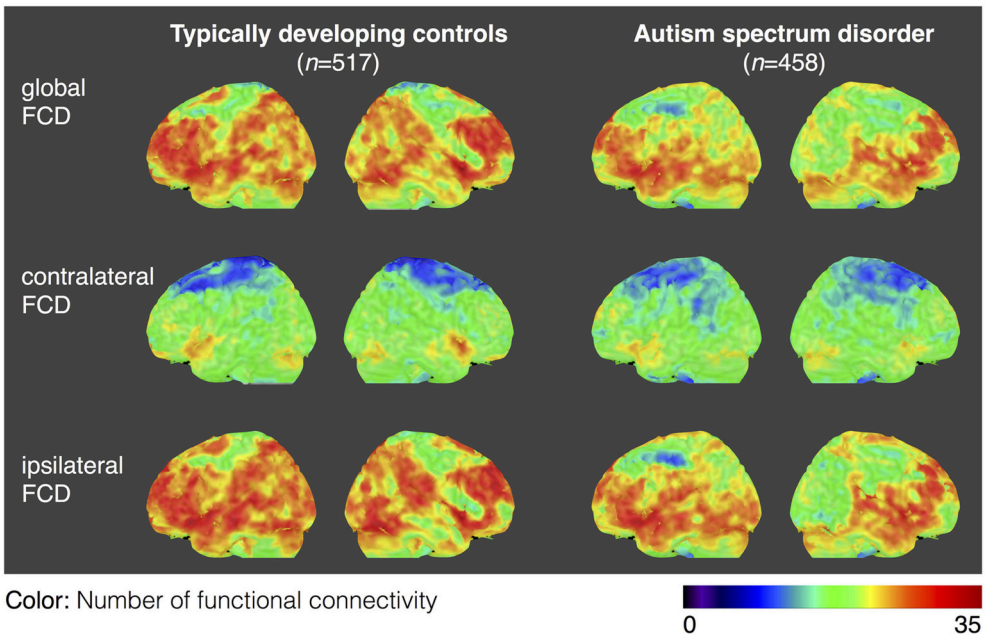

FIGURE 2 | Average maps of functional connectivity densities for the typically developing controls (TDCs) and autism spectrum disorders (ASDs). Distribution of gFCD, cFCD, and iFCD are averaged over 458 patients with ASDs and 517 TDCs. The color bar represents the number of functional connectivities.

functional connectivity in the default mode network regions including the medial prefrontal cortex, posterior cingulate cortex, and inferior parietal lobule, and the sensorimotor regions including the bilateral postcentral gyri, paracentral lobule, and parahippocampal gyrus (corrected $P < 0.05$; **Table 2** gFCD; **Figure 3**). The group differences in the iFCD showed similar patterns to that of the gFCD. Furthermore, iFCDs of the right inferior frontal gyrus, left superior frontal gyrus, and precuneus were significantly decreased in the ASD group (corrected $P < 0.05$; **Table 2** iFCD, **Figure 3**). Finally, the comparison of cFCD revealed regional under-connectivity of the ASD group in the posterior cingulate cortex, parahippocampal gyrus, precentral gyrus, and right angular gyrus (corrected $P < 0.05$; **Table 2** cFCD, **Figure 3**).

In particular, common brain regions showing under-connectivity in ASD across different institutions were the default mode network regions, such as the medial prefrontal cortex, posterior cingulate cortex, precuneus, and lingual/parahippocampal gyrus. The extent of regional overlaps in the normalized global, contralateral, and ipsilateral FCDs are presented in **Figure 4**.

Correlation between Clinical Data and FCD

In several sites, the datasets contained clinical information such as the Autism Diagnostic Interview-Revised (ADI-R), the restricted and repetitive behavior subscore of the Autism Diagnostic Observation Schedule (ADOS-RRB), and communication subscore of the ADOS (ADOS-COM). The average values of FCDs in each region of interest showed meaningful correlations with the ADI-R scores (Lord et al., 1994) and ADOS scores (Lord et al., 2000). **Figure 5** shows the significant correlations between the FCDs and the ADOS-RRB score. In the ASD group, the ADOS-RRB score showed significant negative correlations with the average gFCD ($\rho = -0.24$, corrected $P = 0.003$, $df = 217$), iFCD ($\rho = -0.23$, corrected $P = 0.006$, $df = 217$), and cFCD ($\rho = -0.24$, corrected $P = 0.003$, $df = 217$) in the lingual/parahippocampal gyrus cluster. Also, the ADOS-RRB score showed significant negative correlations with the average cFCD in the PCC ($\rho = -0.18$, corrected $P = 0.03$, and $df = 217$) and precuneus ($\rho = -0.15$, corrected $P = 0.05$, and $df = 217$). Moreover, significances of those correlations were preserved if we use a regional maximum value of FCDs instead of a regional mean within each region of interest (corrected $P < 0.05$).

DISCUSSION

Abnormalities in the neuronal systems of individuals with ASD have been reported in many studies over the last two decades, using small sample ASD groups. We used data from 517 TDCs and 458 patients with ASD from the ABIDE database to examine the abnormalities of functional connectivity in the ASD group relative to TDCs. We used a data-driven voxel-wise method, which examined all voxels in the entire brain. We computed the FCD maps by calculating the connectivity degree of each voxel with all other voxels. The FCD maps were used to compare the functional connectivity between the ASD and TDC groups. A group difference analysis showed regional under-connectivity in the ASD group relative to the TDC group. The abnormal

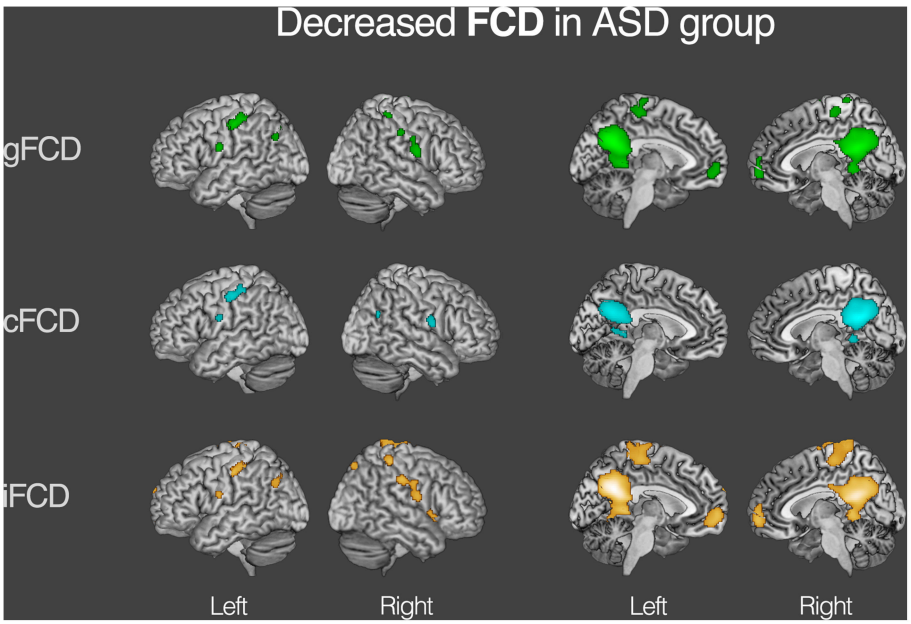

FIGURE 3 | Decreased functional connectivity density (FCD) in autism spectrum disorder (ASD) group. Group differences in the normalized global, contralateral, and ipsilateral FCDs were visualized with the statistical significance at corrected $P < 0.05$. Detailed information on each cluster is written in **Table 2**.

regions of intrinsic functional connectivity in the ASD group were the lingual/parahippocampal gyrus, posterior cingulate cortex, precuneus, postcentral gyrus, paracentral lobule, medial prefrontal cortex, precentral gyrus, angular gyrus, inferior frontal gyrus, superior frontal gyrus, and supplementary motor area, which are related to the default mode network and social functioning processes.

To the best of our knowledge, the present study is the first attempt to decompose the functional connectivity into ipsilateral and contralateral parts to explore abnormalities in the intrinsic neural networks of ASD. Inter-hemispheric connectivity in ASD was examined previously in several studies (Anderson et al., 2011), in which a correlation between each voxel and a corresponding voxel in the opposite hemisphere was calculated. The present study used all voxels in the opposite hemisphere to calculate the inter-hemispheric connectivity. Consequently, inter-hemispheric FCD is somewhat analogous to long distance connectivity. Intra-hemispheric FCD was used to identify the characteristics of the short distance connectivity. Global functional connectivity density was obtained by combining the inter- and intra-hemispheric FCDs.

Functional Under-Connectivity vs. Over-Connectivity

Neuroimaging studies have shown abnormal brain networks in ASD, but the issue of over-connectivity or under-connectivity in those findings remains controversial (Muller et al., 2011). Children with ASD showed both over-and under-connectivity (Lynch et al., 2013). The precuneus was underconnected with other brain regions, as we observed in this study, but the posterior cingulate cortex was overconnected, which was the opposite result from our study. For adolescents with ASD, functional connectivity between the medial prefrontal cortex and precuneus (theory of mind regions) and some regions in the mirror neuron system have been found to be overconnected (Northoff et al., 2006; Fishman et al., 2014). However, when the brains of adults with ASD were examined, the medial prefrontal cortex and precuneus were underconnected. This result may be explained by two reasons. First, including adult subjects may change the overall result from over-connectivity to under-connectivity. However, it is unlikely that the inclusion of adult subjects may change the connectivity pattern of subjects with ASD because the majority of subjects with ASD in our study were children and adolescents. Second, the medial prefrontal cortex and precuneus were overconnected with some regions in the mirror neuron system but underconnected with a majority of other brain regions. In summary, the medial prefrontal cortex and precuneus may appear underconnected in some specific brain regions.

In a prior study where the posterior cingulate cortex had been used as a single seed (Monk et al., 2009), the ASD group showed under-connectivity in the right superior frontal gyrus and over-connectivity in the right temporal pole and right parahippocampal gyrus, compared to the TDC group. In our results using the voxel-wise data-driven method, both the posterior cingulate cortex and parahippocampal gyrus in the ASD group showed reduced functional connectivity compared to TDCs. This result is consistent with the result from prior studies showing a weaker connectivity between the posterior cingulate cortex and precuneus in the ASD group compared to that of the TDC group (Cherkassky et al., 2006).

TABLE 2 | Group differences in the normalized global, contralateral, and ipsilateral FCDs (gFCD, cFCD, and iFCD) between the ASDs and TDCs.

Cluster Name	BA	gFCD	cFCD	iFCD
		Cluster Size (MNI)	Cluster Size (MNI)	Cluster Size (MNI)
Lt. Medial prefrontal cortex*	10	303 (0, 62, −6)		538 (0, 62, −6)
Lt. Superior frontal gyrus	10			58 (−14, 72, 28)
Rt. Inferior frontal gyrus	22			60 (54, 16, −4)
Lt. Supplementary motor area	6			49 (0, −6, 76)
Lt. Precentral gyrus	4	51 (−64, −4, 22)	29 (−62, −4, 22)	25 (−64, −4, 22)
Lt. Postcentral gyrus	2	648 (−64, −20, 50)	751 (−60, −18, 48)	387 (−64, −20, 48)
Rt. Postcentral gyrus	2	136 (40, −36, 58)	91 (66, −2, 16)	234 (44, −34, 60)
Rt. Lingual/parahippocampal gyrus	30		74 (12, −44, −2)	
Lt. Cerebellum (Culmen)	29	4014 (−6, −56, 28)	113 (−6, −44, 2)	4190 (−6, −56, 28)
Rt. Posterior cingulate cortex*	23		2682 (6, −50, 22)	
Rt. Precuneus	7			127 (24, −76, 56)
Lt. Angular gyrus*	39	43 (−54, −68, 32)		176 (−46, −78, 46)
Lt. Inferior parietal lobule*	39	46 (−48, −76, 46)		
Rt. Angular gyrus	39		29 (50, −62, 26)	
Rt. Supramarginal gyrus	40	24 (62, −22, 42)		224 (62, −22, 40)
Lt. Paracentral lobule	6	333 (0, −24, 60)		1338 (0, −24, 60)
Rt. Paracentral lobule	6	56 (8, −38, 76)		

The number of voxels and the corresponding center of mass in MNI for each cluster were described accordingly.
Cortical clusters that cover wide range of brain areas were highlighted in dark gray.
Asterisk(*) indicates the default mode network regions.
BA, Brodmann areas; Lt, left; Rt, right.

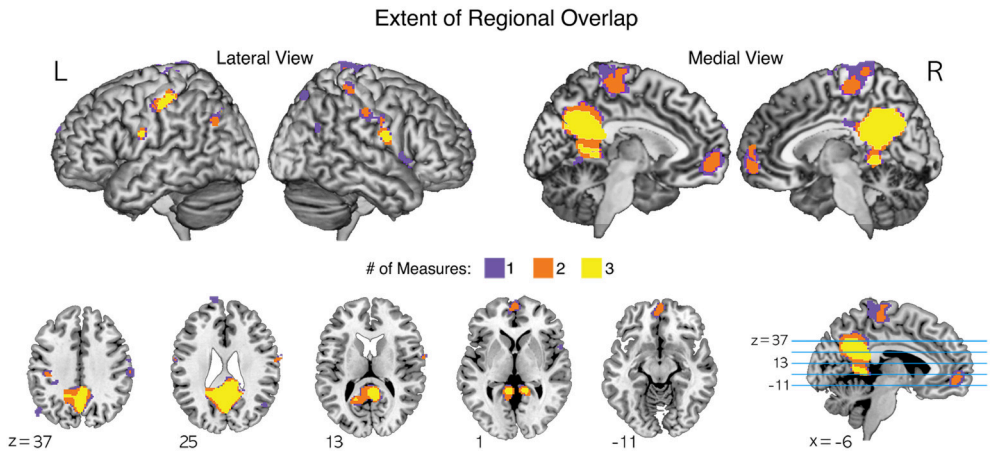

FIGURE 4 | The extent of regional overlaps for functional underconnectivities in the normalized global, contralateral, and ipsilateral FCDs (gFCD, cFCD, and iFCD). Yellow color represents the overlapping areas for functional underconnectivities observed in gFCD, cFCD, and iFCD. Orange color represents the overlapping areas of functional underconnectivities observed in any pairs of FCDs: gFCD and cFCD, gFCD and iFCD, or cFCD and iFCD. Purple color represents functional underconnectivities observed in gFCD, cFCD, or iFCD without overlapping areas.

Hypofunctional Connectivity Density

Functional connectivity differences between the ASD and TDC groups were found in the medial prefrontal cortex, posterior cingulate cortex, precuneus, and parahippocampal gyrus. The medial prefrontal cortex, posterior cingulate cortex, and precuneus have been reported to be an important parts of the default mode network, and abnormalities in the default mode network have been reported in subjects with ASD

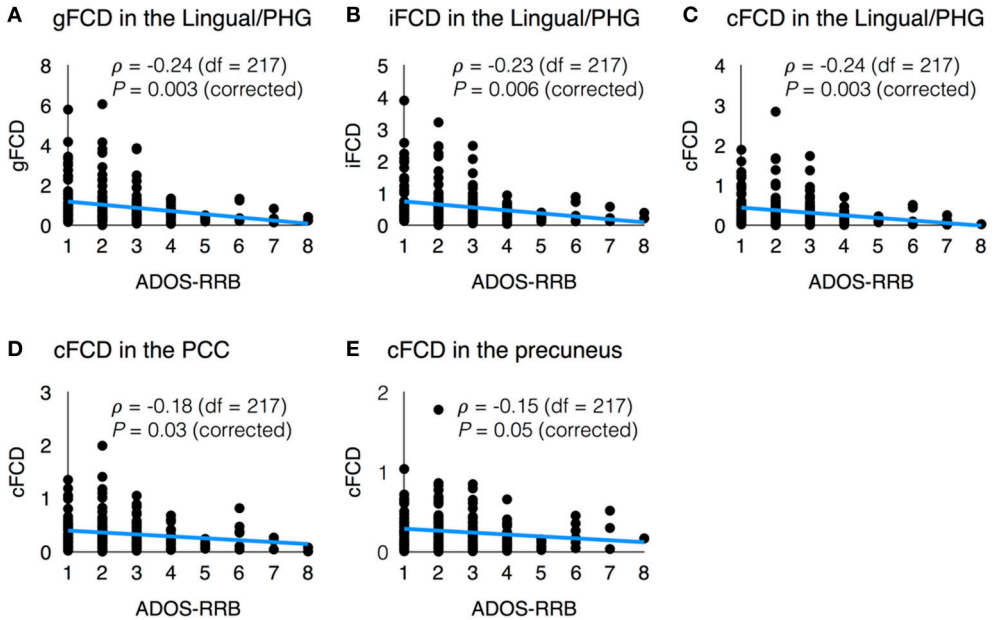

FIGURE 5 | Scatter plots of functional connectivity density (FCD) vs. clinical variable. (A) gFCD in the Lingual/PHG and ADOS-RRB score; **(B)** iFCD in the Lingual/PHG and ADOS-RRB score; **(C)** cFCD in the Lingual/PHG and ADOS-RRB score; **(D)** cFCD in the PCC and ADOS-RRB score; and **(E)** cFCD in the precuneus and ADOS-RRB score.

(Ochsner et al., 2005; Northoff et al., 2006). The above-mentioned brain regions are involved in many impaired mental functions seen in the ASD group, such as difficulty in decision making (Luke et al., 2012), lack of identification with self (Northoff et al., 2006), cognitive deficits (Baron-Cohen et al., 1985) and problems in self-referential thought (Ochsner et al., 2005) and mentalizing (Frith and Happe, 1993; Frith and Frith, 1999; Gallagher and Frith, 2003; Kana et al., 2009; Gotts et al., 2012; Schurz et al., 2014). Especially, the medial prefrontal cortex and posterior cingulate cortex are implicated in the theory of mind network, a key symptomatic feature of patients with ASD. Therefore, we assert that the under-connectivity in the medial prefrontal cortex and posterior cingulate cortex may cause the social functioning impairments in ASD.

Inter- and Intra-Hemispheric Connectivity

Using inter-hemispheric correlation, Anderson et al. showed a lower inter-hemispheric correlation in the sensorimotor cortex, superior parietal lobule, and frontal insula in subjects with ASD compared to that in controls (Anderson et al., 2011). Moreover, the mean corpus callosum volume in the ASD group was significantly smaller than that of TDCs. Although, both corpus callosum volume and gray matter inter-hemispheric functional connectivity were significantly reduced in autism, no direct relationship was observed between them, suggesting that the structural and functional imaging measure different aspects of inter-hemispheric connectivity (Anderson et al., 2011).

In our study, the inter-hemispheric differences between the two groups were computed by the difference in cFCDs between the two groups. Regions showing lower cFCD in the ASD group were the posterior cingulate/precuneus, somatosensory areas, parahippocampal gyrus, and angular gyrus. However, the mean cFCD in the ASD group was not significantly different from that of TDCs and the mean cFCD in the ASD group was even higher than that of TDCs after normalization. On the contrary, the examination of the mean iFCD showed that it is significantly reduced in the ASD group compared to that of TDCs. As intra-hemispheric under-connectivity contributed more to the overall results of our study, global under-connectivity in patients with autism may be a result of intra-hemispheric under-connectivity rather than inter-hemispheric under-connectivity. This result is consistent with that of a prior study showing altered intra-hemispheric connectivity in the autistic brains (Minshew and Williams, 2007). In reality, intra-hemispheric connectivity has been less studied than inter-hemispheric connectivity, due to the complex and time-consuming processes needed to calculate these values. However, our results suggest that the models of under-connectivity in autism should consider intra-hemispheric as well as inter-hemispheric connectivity for more sophisticated understanding of how connectivity abnormalities would be determined by interactions between the intra- and inter-hemispheric functional connectivity in the ASD group.

Correlation between Connectivity and Clinical Measures

We found that there were significant correlations between the average of gFCD, cFCD, and iFCD values in the

lingual/parahippocampal gyrus and ADOS-RRB scores (**Figure 5**). The lingual/parahippocampal gyrus is connected with the amygdala and limbic structure in the brain, and is believed to play an important role in the processing of visual information about parts of the human faces (McCarthy et al., 1999) and processing high-emotion words or images, identifying visual scene and social context, and paralinguistic communication (Epstein and Kanwisher, 1998). These functions are the main areas in which individuals with ASD suffers from severe impairment, and the abnormality in the lingual/parahippocampal gyrus has been reported in individuals with autism (Weng et al., 2010). The significant correlation between gFCD and iFCD in the lingual/parahippocampal and ADOS-RRB scores can be explained by a theoretical framework provided by the salience landscape theory (Ramachandran and Oberman, 2006). Although autism is mainly considered a social disability, it also has non-social features, such as restricted and repetitive behavior/interests and sensory hypersensitivity. The salience landscape theory provides a compelling explanation for this symptom dimension of autism, suggesting that the altered connections between the limbic system and the sensory areas could cause extreme emotional responses and autonomic hyperactivity to the surrounding environment in patients with ASD, and repetitive behavior has a compensatory calming effect by reducing the child's autonomic arousal. The lingual/parahippocampal area is adjacent to, or a part of the limbic system. Therefore, our result suggests that the functional connectivity of this area might be altered in a different way in individuals with ASD, and these alterations may explain the restricted and repetitive behaviors in the ASD group.

Differences in a Recent Study Using ABIDE Dataset

Recently, a study using a large dataset from ABIDE was published with 360 male subjects with ASD and 403 male TDCs (Di Martino et al., 2014). They used four different imaging analysis methods. Among the four methods, the degree centrality was similar to gFCD used in this study. However, their results using the degree centrality were different from our results, in that the ASD group showed over-connectivity in the right middle frontal gyrus. In the right posterior cingulate cortex, no difference was observed between the two groups according to the degree centrality analysis, but in our analysis, the ASD group showed under-connectivity in the posterior cingulate cortex. Even though the degree centrality method and FCD methods are both data-driven voxel-wise methods, several factors may explain such different results. The degree centrality method used eight times lower resolutions in voxel dimensions ($4 \times 4 \times 4$ mm) (Zuo et al., 2012) than our method ($2 \times 2 \times 2$ mm). Their sample size was smaller than our sample size; they used only male subjects, whereas we used all subjects, including females and adults.

LIMITATIONS

There are several potential limitations in this study. First, the age of the subjects with ASD and TDCs are widely distributed from childhood through adolescence to adulthood. We considered only the average FCDs of all subjects from these broad age groups. Although we found average patterns of functional connectivity in the ASD group compared to those in the TDC group after setting age as a covariate, we may have missed age-related changes in the functional connectivity of the ASD group. Brain structure changes during human development (Sowell et al., 1999, 2003). In particular, adolescence is a time of human brain maturation as remarkable physical and behavioral changes occur (Paus et al., 2008; Koyama et al., 2011). Thus, future research should focus on the age effects on the neural system in ASD. The second limitation is that the FCD mapping analytical method found cortical hubs, but we did not examine which regions were strongly connected with those hubs after group comparison. This approach may require higher computational power. Third, the inconsistent findings regarding over- vs. under-connectivity in the brains of patients with ASD might be due to individualized alterations in the functional connectivity patterns, and the group comparison study like ours may not have taken functional idiosyncrasy into consideration as a possible source of these discrepant findings in functional connectivity (Hahamy et al., 2015).

CONCLUSIONS

In conclusion, we observed abnormalities of global functional connectivity in ASD by applying FCD mapping on data from 517 TDC subjects and 458 patients with ASD from the ABIDE datasets. We found regional under-connectivity in ASD by comparing of intra-hemispheric, inter-hemispheric, and global functional connectivity. Our findings suggest that a deficit of non-social functioning process in ASD, such as restricted and repetitive behaviors and sensory hypersensitivity, might be determined by both the inter- and intra-hemispheric functional disconnections in the posterior limbic and sensorimotor regions.

AUTHOR CONTRIBUTIONS

Equally contributed first authors: JL, SK. Conceived and designed the experiments: JL, SK, KC. Performed the experiments: JL, SK, KC. Analyzed the data: JL, SK. Contributed reagents/materials/analysis tools: JL, SK, EK, KC. Wrote the manuscript: JL, SK, EK, KC.

ACKNOWLEDGMENTS

This work was supported by the research grant from Korean Health Technology R&D Project of Ministry of health & welfare, Republic of Korea (Grant number: HI12C0021-A120029, HI12C0245).

REFERENCES

Alexander, A. L., Lee, J. E., Lazar, M., Boudos, R., DuBray, M. B., Oakes, T. R., et al. (2007). Diffusion tensor imaging of the corpus callosum in Autism. *Neuroimage* 34, 61–73. doi: 10.1016/j.neuroimage.2006.08.032

Amaral, D. G. (2011). The promise and the pitfalls of autism research: an introductory note for new autism researchers. *Brain Res.* 1380, 3–9. doi: 10.1016/j.brainres.2010.11.077

American Psychiatric Association (2013). *Diagnostic and Statistical Manual of Mental Disorders, 5th Edn.* Arlington, VA.

Anderson, J. S., Druzgal, T. J., Froehlich, A., DuBray, M. B., Lange, N., Alexander, A. L., et al. (2011). Decreased interhemispheric functional connectivity in autism. *Cereb. Cortex* 21, 1134–1146. doi: 10.1093/cercor/bhq190

Assaf, M., Jagannathan, K., Calhoun, V. D., Miller, L., Stevens, M. C., Sahl, R., et al. (2010). Abnormal functional connectivity of default mode sub-networks in autism spectrum disorder patients. *Neuroimage* 53, 247–256. doi: 10.1016/j.neuroimage.2010.05.067

Baron-Cohen, S., Leslie, A. M., and Frith, U. (1985). Does the autistic child have a "theory of mind"? *Cognition* 21, 37–46.

Barttfeld, P., Wicker, B., Cukier, S., Navarta, S., Lew, S., and Sigman, M. (2011). A big-world network in ASD: dynamical connectivity analysis reflects a deficit in long-range connections and an excess of short-range connections. *Neuropsychologia* 49, 254–263. doi: 10.1016/j.neuropsychologia.2010.11.024

Benjamini, Y., and Hochberg, Y. (1995). Controlling the false discovery rate: a practical and powerful approach to multiple testing. *J. R. Statist. Soc. Ser. B* 57, 289–300.

Biswal, B. B., Mennes, M., Zuo, X. N., Gohel, S., Kelly, C., Smith, S. M., et al. (2010). Toward discovery science of human brain function. *Proc. Natl. Acad. Sci. U.S.A.* 107, 4734–4739. doi: 10.1073/pnas.0911855107

Bogdashina, O. (2006). *Theory of Mind and the Triad of Perspectives on Autism and Asperger Syndrome.* Philadelphia, PA: Jessica Kingsley Publishers.

Cheon, K.-A., Kim, Y.-S., Oh, S.-H., Park, S.-Y., Yoon, H.-W., Herrington, J., et al. (2011). Involvement of the anterior thalamic radiation in boys with high functioning autism spectrum disorders: a diffusion tensor imaging study. *Brain Res.* 1417, 77–86. doi: 10.1016/j.brainres.2011.08.020

Cherkassky, V. L., Kana, R. K., Keller, T. A., and Just, M. A. (2006). Functional connectivity in a baseline resting-state network in autism. *Neuroreport* 17, 1687–1690. doi: 10.1097/01.wnr.0000239956.45448.4c

Di Martino, A., Ross, K., Uddin, L. Q., Sklar, A. B., Castellanos, F. X., and Milham, M. P. (2009). Functional brain correlates of social and nonsocial processes in autism spectrum disorders: an activation likelihood estimation meta-analysis. *Biol. Psychiatry* 65, 63–74. doi: 10.1016/j.biopsych.2008.09.022

Di Martino, A., Yan, C. G., Li, Q., Denio, E., Castellanos, F. X., Alaerts, K., et al. (2014). The autism brain imaging data exchange: towards a large-scale evaluation of the intrinsic brain architecture in autism. *Mol. Psychiatry* 19, 659–667. doi: 10.1038/mp.2013.78

Epstein, R., and Kanwisher, N. (1998). A cortical representation of the local visual environment. *Nature* 392, 598–601. doi: 10.1038/33402

Fishman, I., Keown, C. L., Lincoln, A. J., Pineda, J. A., and Müller, R. (2014). Atypical cross talk between mentalizing and mirror neuron networks in autism spectrum disorder. *JAMA Psychiatry* 71, 751–760. doi: 10.1001/jamapsychiatry.2014.83

Frith, C. D., and Frith, U. (1999). Interacting minds–a biological basis. *Science* 286, 1692–1695. doi: 10.1126/science.286.5445.1692

Frith, U., and Happe, F. (1993). Autism: beyond "theory of mind". *Cognition* 50, 115–132. doi: 10.1016/0010-0277(94)90024-8

Gallagher, H. L., and Frith, C. D. (2003). Functional imaging of 'theory of mind'. *Trends Cogn. Sci.* 7, 77–83. doi: 10.1016/S1364-6613(02)00025-6

Gotts, S. J., Simmons, W. K., Milbury, L. A., Wallace, G. L., Cox, R. W., and Martin, A. (2012). Fractionation of social brain circuits in autism spectrum disorders. *Brain* 135, 2711–2725. doi: 10.1093/brain/aws160

Hahamy, A., Behrmann, M., and Malach, R. (2015). The idiosyncratic brain: distortion of spontaneous connectivity patterns in autism spectrum disorder. *Nat. Neurosci.* 18, 302–309. doi: 10.1038/nn.3919

Hughes, J. R. (2009). Update on autism: a review of 1300 reports published in 2008. *Epilepsy Behav.* 16, 569–589. doi: 10.1016/j.yebeh.2009.09.023

Just, M. A., Cherkassky, V. L., Keller, T. A., Kana, R. K., and Minshew, N. J. (2007). Functional and anatomical cortical underconnectivity in autism: evidence from an FMRI study of an executive function task and corpus callosum morphometry. *Cereb. Cortex* 17, 951–961. doi: 10.1093/cercor/bhl006

Kana, R. K., Keller, T. A., Cherkassky, V. L., Minshew, N. J., and Just, M. A. (2009). Atypical frontal-posterior synchronization of theory of mind regions in autism during mental state attribution. *Soc. Neurosci.* 4, 135–152. doi: 10.1080/17470910802198510

Keary, C. J., Minshew, N. J., Bansal, R., Goradia, D., Fedorov, S., Keshavan, M. S., et al. (2009). Corpus callosum volume and neurocognition in autism. *J. Autism Dev. Disord.* 39, 834–841. doi: 10.1007/s10803-009-0689-4

Keller, T. A., Kana, R. K., and Just, M. A. (2007). A developmental study of the structural integrity of white matter in autism. *Neuroreport* 18, 23–27. doi: 10.1097/01.wnr.0000239965.21685.99

Koyama, M. S., Di Martino, A., Zuo, X. N., Kelly, C., Mennes, M., Jutagir, D. R., et al. (2011). Resting-state functional connectivity indexes reading competence in children and adults. *J. Neurosci.* 31, 8617–8624. doi: 10.1523/JNEUROSCI.4865-10.2011

Lord, C., Risi, S., Lambrecht, L., Cook, E. H. Jr., Leventhal, B. L., DiLavore, P. C., et al. (2000). The autism diagnostic observation schedule-generic: a standard measure of social and communication deficits associated with the spectrum of autism. *J. Autism Dev. Disord.* 30, 205–223. doi: 10.1023/A:1005592401947

Lord, C., Rutter, M., and Le Couteur, A. (1994). Autism Diagnostic Interview-Revised: a revised version of a diagnostic interview for caregivers of individuals with possible pervasive developmental disorders. *J. Autism Dev. Disord.* 24, 659–685. doi: 10.1007/BF02172145

Luke, L., Clare, I. C., Ring, H., Redley, M., and Watson, P. (2012). Decision-making difficulties experienced by adults with autism spectrum conditions. *Autism* 16, 612–621. doi: 10.1177/1362361311415876

Lynch, C. J., Uddin, L. Q., Supekar, K., Khouzam, A., Phillips, J., and Menon, V. (2013). Default mode network in childhood autism: posteromedial cortex heterogeneity and relationship with social deficits. *Biol. Psychiatry* 74, 212–219. doi: 10.1016/j.biopsych.2012.12.013

McCarthy, G., Puce, A., Belger, A., and Allison, T. (1999). Electrophysiological studies of human face perception. II: response properties of face-specific potentials generated in occipitotemporal cortex. *Cereb. Cortex* 9, 431–444. doi: 10.1093/cercor/9.5.431

Minshew, N. J., and Keller, T. A. (2010). The nature of brain dysfunction in autism: functional brain imaging studies. *Curr. Opin. Neurol.* 23, 124–130. doi: 10.1097/WCO.0b013e32833782d4

Minshew, N. J., and Williams, D. L. (2007). The new neurobiology of autism: cortex, connectivity, and neuronal organization. *Arch. Neurol.* 64, 945–950. doi: 10.1001/archneur.64.7.945

Monk, C. S., Peltier, S. J., Wiggins, J. L., Weng, S.-J., Carrasco, M., Risi, S., et al. (2009). Abnormalities of intrinsic functional connectivity in autism spectrum disorders. *Neuroimage* 47, 764–772. doi: 10.1016/j.neuroimage.2009.04.069

Muller, R. A., Shih, P., Keehn, B., Deyoe, J. R., Leyden, K. M., and Shukla, D. K. (2011). Underconnected, but how? A survey of functional connectivity MRI studies in autism spectrum disorders. *Cereb. Cortex* 21, 2233–2243. doi: 10.1093/cercor/bhq296

Nebel, M. B., Joel, S. E., Muschelli, J., Barber, A. D., Caffo, B. S., Pekar, J. J., et al. (2014). Disruption of functional organization within the primary motor cortex in children with autism. *Hum. Brain Mapp.* 35, 567–580. doi: 10.1002/hbm.22188

Northoff, G., Heinzel, A., de Greck, M., Bermpohl, F., Dobrowolny, H., and Panksepp, J. (2006). Self-referential processing in our brain—A meta-analysis of imaging studies on the self. *Neuroimage* 31, 440–457. doi: 10.1016/j.neuroimage.2005.12.002

Ochsner, K. N., Beer, J. S., Robertson, E. R., Cooper, J. C., Gabrieli, J. D., Kihsltrom, J. F., et al. (2005). The neural correlates of direct and reflected self-knowledge. *Neuroimage* 28, 797–814. doi: 10.1016/j.neuroimage.2005.06.069

Paus, T., Keshavan, M., and Giedd, J. N. (2008). Why do many psychiatric disorders emerge during adolescence? *Nat. Rev. Neurosci.* 9, 947–957. doi: 10.1038/nrn2513

Raichle, M. E., and Snyder, A. Z. (2007). A default mode of brain function: a brief history of an evolving idea. *Neuroimage* 37, 1083–1090. doi: 10.1016/j.neuroimage.2007.02.041

Ramachandran, V. S., and Oberman, L. M. (2006). Broken mirrors: a theory of autism. *Sci. Am.* 295, 62–69. doi: 10.1038/scientificamerican1106-62

Rudie, J. D., Brown, J. A., Beck-Pancer, D., Hernandez, L. M., Dennis, E. L., Thompson, P. M., et al. (2012). Altered functional and structural brain network organization in autism. *Neuroimage* 2, 79–94. doi: 10.1016/j.nicl.2012.11.006

Schurz, M., Radua, J., Aichhorn, M., Richlan, F., and Perner, J. (2014). Fractionating theory of mind: a meta-analysis of functional brain imaging studies. *Neurosci. Biobehav. Rev.* 42, 9–34. doi: 10.1016/j.neubiorev.2014.01.009

Sowell, E. R., Peterson, B. S., Thompson, P. M., Welcome, S. E., Henkenius, A. L., and Toga, A. W. (2003). Mapping cortical change across the human life span. *Nat. Neurosci.* 6, 309–315. doi: 10.1038/nn1008

Sowell, E. R., Thompson, P. M., Holmes, C. J., Batth, R., Jernigan, T. L., and Toga, A. W. (1999). Localizing age-related changes in brain structure between childhood and adolescence using statistical parametric mapping. *Neuroimage* 9, 587–597. doi: 10.1006/nimg.1999.0436

Supekar, K., Uddin, L. Q., Khouzam, A., Phillips, J., Gaillard, W. D., Kenworthy, L. E., et al. (2013). Brain hyperconnectivity in children with autism and its links to social deficits. *Cell Rep.* 5, 738–747. doi: 10.1016/j.celrep.2013.10.001

Tomasi, D., and Volkow, N. D. (2010). Functional connectivity density mapping. *Proc. Natl. Acad. Sci. U.S.A.* 107, 9885–9890. doi: 10.1073/pnas.1001414107

Tomasi, D., and Volkow, N. D. (2012a). Abnormal functional connectivity in children with attention-deficit/hyperactivity disorder. *Biol. Psychiatry* 71, 443–450. doi: 10.1016/j.biopsych.2011.11.003

Tomasi, D., and Volkow, N. D. (2012b). Gender differences in brain functional connectivity density. *Hum. Brain Mapp.* 33, 849–860. doi: 10.1002/hbm.21252

Tomasi, D., and Volkow, N. D. (2012c). Laterality patterns of brain functional connectivity: gender effects. *Cereb. Cortex* 22, 1455–1462. doi: 10.1093/cercor/bhr230

Vissers, M. E. X., Cohen, M., and Geurts, H. M. (2012). Brain connectivity and high functioning autism: a promising path of research that needs refined models, methodological convergence, and stronger behavioral links. *Neurosci. Biobehav. Rev.* 36, 604–625. doi: 10.1016/j.neubiorev.2011.09.003

von dem Hagen, E. A., Stoyanova, R. S., Baron-Cohen, S., and Calder, A. J. (2013). Reduced functional connectivity within and between 'social' resting state networks in autism spectrum conditions. *Soc. Cogn. Affect. Neurosci.* 8, 694–701. doi: 10.1093/scan/nss053

Weng, S. J., Wiggins, J. L., Peltier, S. J., Carrasco, M., Risi, S., Lord, C., et al. (2010). Alterations of resting state functional connectivity in the default network in adolescents with autism spectrum disorders. *Brain Res.* 1313, 202–214. doi: 10.1016/j.brainres.2009.11.057

Zuo, X. N., Ehmke, R., Mennes, M., Imperati, D., Castellanos, F. X., Sporns, O., et al. (2012). Network centrality in the human functional connectome. *Cereb. Cortex* 22, 1862–1875. doi: 10.1093/cercor/bhr269

Conflict of Interest Statement: The authors declare that the research was conducted in the absence of any commercial or financial relationships that could be construed as a potential conflict of interest.

frontiers in Neuroscience

ORIGINAL RESEARCH
published: 08 June 2016
doi: 10.3389/fnins.2016.00255

Altered Onset Response Dynamics in Somatosensory Processing in Autism Spectrum Disorder

Sheraz Khan[1,2,3,4], *Javeria A. Hashmi*[1,2,3†], *Fahimeh Mamashli*[1,2,3], *Hari M. Bharadwaj*[1,2,3], *Santosh Ganesan*[1,2], *Konstantinos P. Michmizos*[5], *Manfred G. Kitzbichler*[1,2,3†], *Manuel Zetino*[1,2], *Keri-Lee A. Garel*[1,2], *Matti S. Hämäläinen*[2,3,6,7] *and Tal Kenet*[1,2,3*]

[1] Department of Neurology, Massachusetts General Hospital, Boston, MA, USA, [2] Athinoula A. Martinos Center for Biomedical Imaging, MGH/MIT/Harvard, Boston, MA, USA, [3] Harvard Medical School, Boston, MA, USA, [4] McGovern Institute for Brain Research, Massachusetts Institute of Technology, Cambridge, MA, USA, [5] Department of Computer Science, Rutgers University, Piscataway, NJ, USA, [6] Department of Radiology, Massachusetts General Hospital, Boston, MA, USA, [7] Department of Neuroscience and Biomedical Engineering, Aalto University School of Science, Espoo, Finland

Abnormalities in cortical connectivity and evoked responses have been extensively documented in autism spectrum disorder (ASD). However, specific signatures of these cortical abnormalities remain elusive, with data pointing toward abnormal patterns of both increased and reduced response amplitudes and functional connectivity. We have previously proposed, using magnetoencephalography (MEG) data, that apparent inconsistencies in prior studies could be reconciled if functional connectivity in ASD was reduced in the feedback (top-down) direction, but increased in the feedforward (bottom-up) direction. Here, we continue this line of investigation by assessing abnormalities restricted to the onset, feedforward inputs driven, component of the response to vibrotactile stimuli in somatosensory cortex in ASD. Using a novel method that measures the spatio-temporal divergence of cortical activation, we found that relative to typically developing participants, the ASD group was characterized by an increase in the initial onset component of the cortical response, and a faster spread of local activity. Given the early time window, the results could be interpreted as increased thalamocortical feedforward connectivity in ASD, and offer a plausible mechanism for the previously observed increased response variability in ASD, as well as for the commonly observed behaviorally measured tactile processing abnormalities associated with the disorder.

Keywords: autism spectrum disorders (ASD), magnetoencephalography (MEG), somatosensory cortex, feedforward, feedback, tactile sensing, cortical connectivity, biomarker

OPEN ACCESS

Edited by:
Roma Siugzdaite, Ghent University, Belgium

Reviewed by:
Tatiana Alexandrovna Stroganova, Moscow State University of Psychology and Education, Russia
Bharat B. Biswal, University of Medicine and Dentistry of New Jersey (UMDNJ), USA

***Correspondence:**
Tal Kenet
tal@nmr.mgh.harvard.edu

***Present Address:**
Javeria A. Hashmi, Department of Anesthesia, Dalhousie University, Halifax, NS, Canada; Manfred G. Kitzbichler, Behavioural and Clinical Neuroscience Institute, University of Cambridge, Cambridge, UK

Specialty section:
This article was submitted to Child and Adolescent Psychiatry, a section of the journal Frontiers in Neuroscience

Received: *29 January 2016*
Accepted: *23 May 2016*
Published: *08 June 2016*

Citation:
Khan S, Hashmi JA, Mamashli F, Bharadwaj HM, Ganesan S, Michmizos KP, Kitzbichler MG, Zetino M, Garel K-LA, Hämäläinen MS and Kenet T (2016) Altered Onset Response Dynamics in Somatosensory Processing in Autism Spectrum Disorder. Front. Neurosci. 10:255. doi: 10.3389/fnins.2016.00255

INTRODUCTION

Autism spectrum disorder (ASD) is diagnosed by hallmark abnormalities in social behavior, and has a complex genetic basis (Berg and Geschwind, 2012; Skafidas et al., 2014; Pramparo et al., 2015) with no clear disease etiology. The neural correlates of ASD have been extensively explored, using a wide range of paradigms and non-invasive neuroimaging methods. One of the more consistent findings in ASD is that the connectivity between different brain areas is abnormal in ASD (Khan et al., 2013). This has been explored using both anatomical connectivity measures

(Wolff et al., 2012; Mueller et al., 2013; Peeva et al., 2013) and functional connectivity measures (Kana et al., 2011; Müller et al., 2011; Wass, 2011; Vissers et al., 2012).

The prevailing hypothesis in the field (Rubenstein and Merzenich, 2003; Just et al., 2004), has been that long-range functional connectivity is reduced and local functional connectivity is increased in ASD (Belmonte et al., 2004; Minshew and Williams, 2007). However, evidence for this dual hypothesis is inconclusive. In particular, the hypothesis that long-range functional connectivity, i.e., connectivity between two spatially distinct brain regions, is universally reduced in ASD has been challenged by recent studies showing instances of both increased (Cerliani et al., 2015) and normal (Tyszka et al., 2014) long-range functional connectivity in ASD.

Previously, we proposed that the inconsistencies in long-range functional connectivity studies in ASD might be reconciled if the directionally of the connectivity, i.e., the direction in which two areas are connected, would be considered. Specifically, we proposed that long-range feedforward (bottom-up along the cortical hierarchy) connectivity would be abnormally increased in ASD, while feedback (top-down along the cortical hierarchy) long-range connectivity would be abnormally reduced (Khan et al., 2015; Kitzbichler et al., 2015). In particular, in our recent study of cortical responses to vibrotactile stimuli in ASD, we showed that long-range functional connectivity was indeed significantly increased in the ASD group in the feedforward direction, from the primary somatosensory cortex (S1), upwards toward the secondary somatosensory cortex (S2) (Khan et al., 2015).

In that same study, we also found a significantly increased onset response in S1 in the ASD group. While the response in S1 was significantly increased at onset in the ASD group, it was not possible to determine, based on our prior analysis, whether this increase was generated locally, or via abnormal long-range connectivity, such as reduced feedforward functional connectivity from the thalamus for instance. This question is important, because increased local connectivity and increased long-range functional connectivity might have a similar final signature in the cortex, but would be generated and mediated by substantially different neural mechanisms, and thus different neural abnormalities. Thus, delineating the neural mechanisms that underlie the observed abnormal response in ASD is absolutely essential for understanding the abnormal neurophysiology of ASD.

To address this question, we focused here on the transient component of the response, and specifically on the rising edge of the evoked response. This transient response window, 30–70 ms immediately following the onset of the cortical response, has not been previously studied in relation to abnormal tactile processing in ASD. Given its timing, this part of the response is most likely generated at least in part by feedforward inputs from the thalamus. However, the mere observation of an increased response amplitude during that period is not sufficient to indicate whether the processes leading to that increase are local, or generated by long-range connections. Here, to test our hypothesis, that the increase in the transient evoked response observed in ASD is due to feedforward inputs from subcortical regions, we applied a novel measure that indicates how activation of a small neural population spreads in adjoining areas to become locally synchronized (Khan et al., 2009). This method, which is referred to as Spatio-Temporal Divergence (S-T Div), uses techniques based on the concept of optical flow, and was recently adapted to map the time-course of spatiotemporal propagation of brain activity across different cortical region (Khan et al., 2011).

RESULTS

Spatial Localization of Evoked Response to Tactile Vibrations

As expected and as described previously (Khan et al., 2015), the cortical evoked responses to the 25 Hz vibrotactile stimulus (**Figure 1A**) localized to the contralateral (left) S1 and S2 (**Figure 1B**).

Sharper Evoked Response in ASD

There was no group difference in the latency of the response. The amplitude of the evoked transient response was slightly increased in the ASD group relative to the TD group, but this difference was not statistically significant (**Figure 2A**). In contrast, when the cortical response was examined over the onset time window in the time-frequency domain, i.e., with spectral specificity rather than averaging over the frequency domain as for the standard evoked response shown in **Figure 2A**, significant group differences emerged (**Figure 2B**, $p = 0.0470$, corrected). The difference arose primarily from the higher frequencies, at the 25–60 Hz range.

Increased Onset Response Divergence in ASD

We computed the spatio-temporal divergence (S-T Div) at the onset component of the response, and specifically at the rising edge of the first peak (30–70 ms). This was done by selecting the latency for each subject individually, computing S-T Div for that particular subject at their latency, and then averaging the results at the group level. At this time window, the ASD groups demonstrated significantly increased S-T Div in S1 (**Figure 3**, $p = 0.034$, corrected). As a control, we also examined S-T Div during the steady state component of the response ($t = 250$–550 ms). As expected, there were no significant group differences in this later time window.

Correlations with Behavioral Measures and Prior Neurophysiological Measures

The neurophysiologically derived S-T Div was negatively correlated with the behaviorally derived ADOS (ASD group, $P < 0.002$, $r = 0.74$, **Figure 4A**) and touch perception score (TD group, $P < 0.008$, $r = -0.58$; ASD group, $P < 0.02$, $r = -0.63$, **Figure 4B**). Because the participants are identical to those in our prior study (Khan et al., 2015), we also assessed whether the onset derived S-T Div correlated with the steady-state derived neurophysiological measures from our prior study. Our steady state measures consisted of the LFCi ("Local Functional Connectivity index"), which estimated local functional connectivity in S1 during the steady state component

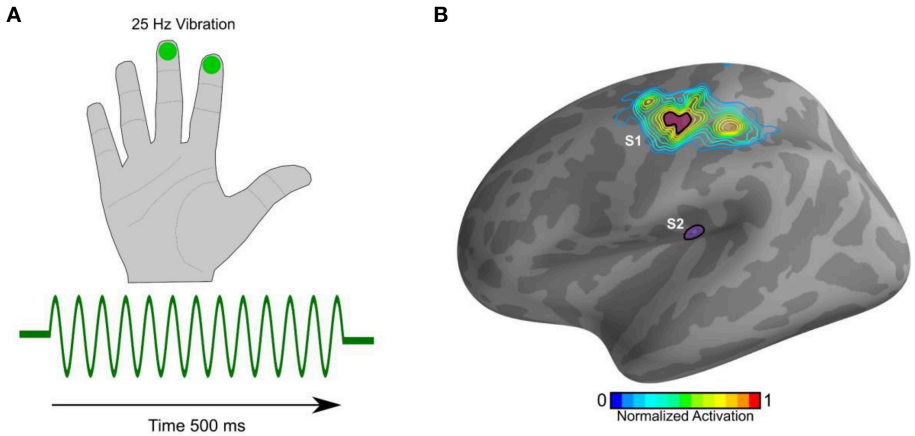

FIGURE 1 | Stimulus and source localization. (A) 500 ms train of pulses at 25 Hz (green trace) was delivered via a pneumatic stimulator and experienced as gentle vibrations on the index and middle right fingers. **(B)** The estimated cortical sources showing activation in S1 and S2. The contour plot represents average activation on the cortical manifold. The distance between adjacent contours is 10%.

of the response, and the GCS (Granger Causality score), which estimated the strength of feedforward connectivity from S1 to S2 during the steady state component of the response. Both were abnormal in the ASD group, with LFCi abnormally decreased, and the GCS abnormally increased. Our correlation analysis showed that LFCi was correlated with S-T Div for both the TD (**Figure 4C**, $P < 0.002$, $r = -0.66$) and ASD ($P < 0.007$, $r = -0.67$) groups. In contrast, S-T Div was not correlated with the GCS (**Figure 4D**).

Statistical Classification

Lastly, we tested whether S-T Div could be used to blindly classify participants with ASD (neuroimaging Biomarker) from TD participants, using a Linear Discriminant Analysis classifier (LDA). This approach evaluates the sensitivity and specificity, and thus the relevance, of the assessed neurophysiological measure to the behavioral phenotype. Using S-T Div alone, the classifier had 83.3% accuracy (80% sensitivity, 90% specificity). We then repeated the classifier computations using S-T Div alongside our two previously derived neurophysiological measures, LFCi, and GCS. The combination of these three neurophysiological features yielded a mean classification accuracy of 91.6%, with 95% specificity and 90% sensitivity (**Figure 5**, **Figure S1** and **Movie M1**). In our prior work the accuracy of the classifier was 89.7%. To assess whether adding the S-T Div measure significantly improved the classifier, the prior model (using LFCi, GCA) and the current model (using LFCi, GCA, S-T Div) were compared using the Akaike Information Criterion (AIC). The AIC score was −79.98 for the first model, and −92.17 for the second model. These scores, with a greater than 12-point difference, indicate that adding S-T Div significantly improved the model.

DISCUSSION

In the vast majority of studies, abnormal functional connectivity in ASD and abnormal evoked responses in ASD have been addressed separately. It is clear that functional connectivity and evoked responses are not independent from one another, but instead are tightly coupled. In our prior study using the same paradigm (Khan et al., 2015), we showed that the observed increases in steady state responses in the ASD group at 25 Hz in S2, were due to increased feedforward connectivity from S1. We also hypothesized that the observed increased onset response in S1 was due to increased feedforward connectivity from the thalamus, but were not able to test this hypothesis at the time.

The current method (S-T Div) allowed us to test this hypothesis indirectly, since it measures the flow (magnitude and velocity of spread) of neural activation in a given region and time window. The velocity at the onset of the response in S1, at the rising edge of the response, before local connections are strongly activated through recurrent loops, is likely to arise entirely or nearly entirely from feedforward connections into S1, primarily from the thalamus. While an increase in magnitude might arise from local recurrent connections, an increase in the velocity of spread can be attributed with relatively high certainty to an increase in feedforward inputs (Papadelis et al., 2012). Indeed, we found that at rising edge of the transient response in S1, this flow was greatly and significantly increased in ASD relative to TD.

Interestingly, as is evident from the time-frequency plots presented in **Figure 2B**, the evoked response in S1 in ASD is abnormally increased not only at the 25 Hz component of the response, but also at higher frequencies, including the 50 Hz component of the response. This seemingly contradicts our prior results. In our prior study (Khan et al., 2015), using a computational model and prior literature, we argued that only the 25 Hz component of the response, which was increased in ASD, is generated via feedforward connectivity, while the steady state of the 50 Hz component of the response, which was reduced in ASD, is generated via local connectivity within S1 and its immediate vicinity, i.e., horizontal connections across layers II/III. Simply put, why would the response in higher frequencies, and specifically around 50 Hz, be increased in ASD in the transient component immediately following the

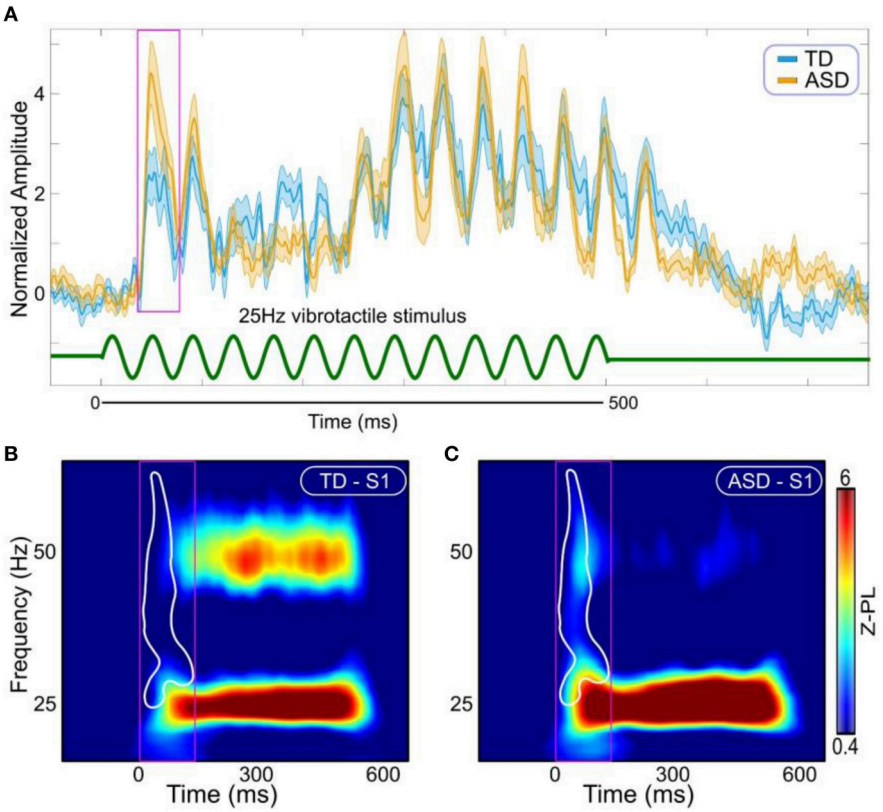

FIGURE 2 | Evoked responses. (A) Evoked responses in S1 (Orange ASD; Cyan TD). Stimulus is represented with green curve at the bottom. Magenta box shows the window for the first transient peak [30–70 ms]. **(B)** Time-frequency representations of Z-scored phase locking (Z-PL) at S1 in the TD group. **(C)** Time-frequency representations of Z-scored phase locking (Z-PL) at S1 in the ASD group. White contour outlines the region where the response was significantly increased in the ASD group ($p = 0.0470$, cluster corrected). Magenta boxes show time window for the transient response in the time-frequency domain [0–140 ms].

onset, but decreased during the steady state component of the response? If both the transient onset component and the steady state component of the cortical response were generated by the same neural mechanisms (local recurrent connections), the interpretation of the 50 Hz component of the response we proposed earlier would be inconsistent with the current proposed interpretation.

The logical resolution of this apparent conflict emerges from a line of studies affirming the fundamentally different nature of the onset component of the response relative to the steady state component (Nangini et al., 2006). For instance, somatosensory inputs from the thalamus to area 3b have been shown to evoke fast and slow adapting response patterns in non-human primates where one set of cortical cells respond only to stimulus onset and offset, while the other module respond throughout stimulus presentation (Sur et al., 1984). In contrast, the steady state response serves to more linearly convey detailed information about attended stimulus features (Ramcharan et al., 2005; Sherman, 2012). Furthermore, the corticothalamic pathways that would be most active during the onset component of the response, are largely distinct from the interareal corticocortical pathways that would be most active during the steady state component of the response (Petrof et al., 2012). Thus, the opposite patterns we observed in ASD for the onset component and the steady state components of the response around 50 Hz are not contradictory, as they are probably generated by at least partially independent neuronal assemblies.

That said, it is worthwhile to note that the strong correlation we observed between S-T Div and LFCi suggests that while these two temporally differentiated components of the response are distinct, they are not independent. However, from the current data, it is not possible to determine to what extent the abnormal response in ASD during the steady state component of the response is influenced by the initial abnormality in the onset component of the response. Since the two measures, S-T Div and LFCi, are correlated but not perfectly so, it is plausible that the reduced steady state response in ASD is a result both of the state of the neuronal assemblies following the increased onset response, alongside the previously discussed (Khan et al., 2015) inherent abnormalities in the local networks that mediate the steady state component of the response. Furthermore, the results from our classifier analysis indicate that the S-T Div analysis of the onset period adds independent information to the prior analyses of the steady state component of the response.

The differentiation proposed here between the feedforward dependent onset component of the response and the local

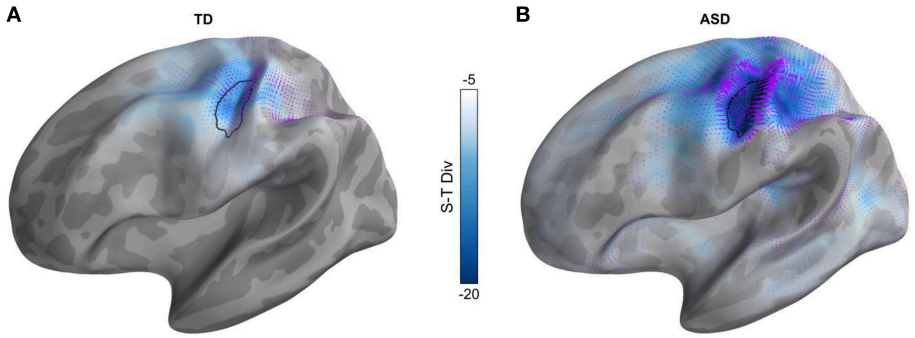

FIGURE 3 | S-T Div during the onset of the transient tactile response. S-T DIV in **(A)** The TD group, **(B)** The ASD group. The colormap represents the magnitude of divergence, and the purple vectors represent the velocity of the divergence. Black outline represents the area that is statistically significantly different ($p = 0.034$, cluster corrected) between the TD and ASD groups.

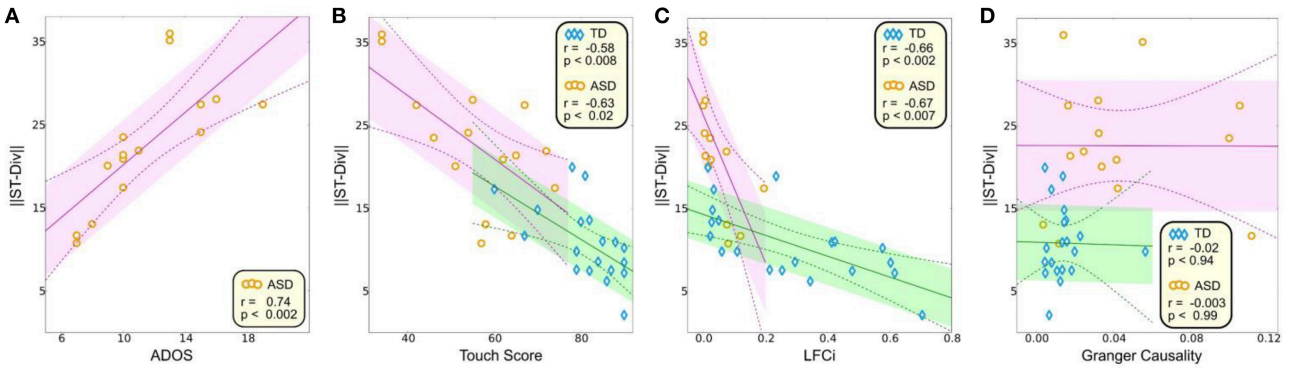

FIGURE 4 | Correlations between S-T Div and other measures. Correlation between S-T Div and: **(A)** ADOS score, **(B)** Touch score, **(C)** LFCi, and **(D)** GCS. The shaded areas (TD in green, ASD in purple) delineate the standard error, and the dashed lines encompass 95% of the confidence interval for the correlation.

feedback dependent steady state component of the response, is in line with studies of ASD that indirectly infer increased bottom-up perceptual processing tendencies in ASD (Neumann et al., 2006; Jarvinen-Pasley et al., 2008; Cook et al., 2012; Amso et al., 2014; Robertson et al., 2014). They are also in line with prior fMRI-based studies finding increased thalamocortical connectivity in ASD, in paradigms that were more likely to activate feedforward networks (Mizuno et al., 2006; Cerliani et al., 2015). These results are also intriguing in the context of a recent finding of increased inter-trial variability in ASD (Dinstein et al., 2012). Unmodulated, i.e., inconsistently gain controlled, feedforward inputs, as observed previously in ASD (Peiker et al., 2015), would likely result in more variable trial to trial onset responses. Lastly, these results are also relevant in the context of the high prevalence of behavioral sensory hypo- and hyper- sensitivities in ASD (Tommerdahl et al., 2007; Marco et al., 2011, 2012). Increased feedforward inputs and flow of sensory information would naturally result in hyper-sensitive behavior. It is possible that the observed hypo-sensitivities are due to generalized down regulation, as a compensatory strategy to the increased input intensities. Such a compensatory strategy would likely result in hypo-sensitivities.

An important limitation of the study is that this method does not directly measure thalamocortical feedforward connectivity from the specific thalamic nuclei, since no thalamic activation has been observed directly. Thus, the proposed interpretation, while relying strongly on known properties of response onset in early sensory cortex, and while fitting well with other studies, remains an indirect interpretation. Alternatively, other processes may also impact the observed abnormal dynamics of the onset response. For instance, it has been suggested that excitatory feedforward drive and feedback input from higher-order cortex or non-specific thalamic nuclei might also contribute to the onset component of the response (Cauller and Kulics, 1991; Jones et al., 2009). In addition, local interactions between excitatory and inhibitory circuits that occur before the M70 peak (Peterson et al., 1995) may also impact the abnormal dynamics observed here.

In summary, in our previous studies (Khan et al., 2015; Kitzbichler et al., 2015), we found increased forward cortical functional connectivity in ASD during the steady state component of the cortical response, from S1 to S2. We also found an increased onset response in S1 in the ASD group. In the present investigation we used the novel S-T Div measure to assess the dynamics of the onset response in S1. The observed

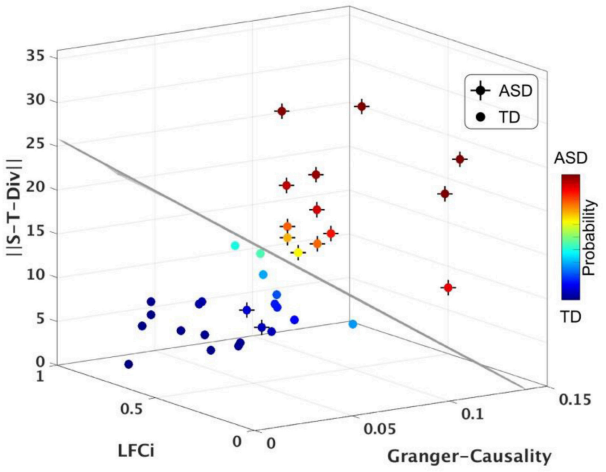

FIGURE 5 | Classifier results, using S-T Div, LFCi and Granger Causality. Visualization of LDA analysis using the full dataset. Each axis corresponds to each neurophysiological imaging feature. The probability of a participant having a diagnosis of ASD is shown as color of the sphere. Plain sphere represents the TD participants, while sphere with a cross represent ASD participants. The black line represents classification boundary (see also, **Figure S1** and **Movie M1**).

dynamics are consistent with an interpretation of increased feedforward thalamocortical connectivity. The interpretation proposed here of the result of the S-T Div measure, is consistent with the conjecture that stronger feedforward connectivity is likely characteristic of ASD, andmay underlie the behaviorally observed aberrant somatosensory and vibrotactile processing in ASD.

MATERIALS AND METHODS

Participants

Participants were 15 males diagnosed with ASD and 20 age-matched TD males, ages 8–18 (11.6 mean age). ASD participants had a prior clinically verified ASD diagnosis, met a cutoff of > 15 on the SCQ, Lifetime Version, and were assessed with either Module 3 ($n = 3$) or 4 ($n = 12$) of the ADOS (ADOS, Lord et al., 1999), administered by trained research personnel who had established inter-rater reliability. Individuals with autism-related medical conditions, e.g., Fragile-X syndrome, tuberous sclerosis, and other known risk factors, e.g., premature birth, were excluded from the study. All TD participants were below threshold on the SCQ and were confirmed to be free of any comorbid neurological or psychiatric conditions, and of substance use for the past 6 months, via parent and self-reports. The ASD and TD groups did not differ in verbal or nonverbal IQ, as measured with the Kaufman Brief Intelligence Test—II (Kaufman and Kaufman, 2004). Handedness information was collected using the Dean Questionnaire (Piro, 1998). Only right-handed participants were included in the study. Additional details on the participants are provided in **Table T1**. Participants overlapped in full with those studied in our prior publication on this paradigm (Khan et al., 2015). All the experimental protocols were approved by The Massachusetts General Hospital (MEG) Institutional Review Board and all procedures were carried out in accordance with the approved guidelines. Written informed consent was obtained from all subjects.

Experimental Paradigms and MEG Data Acquisition

Vibrotactile stimulation in the MEG consisted of pulses applied to the index and middle right fingers at 25 Hz using a custom made pneumatic tactile stimulator with latex tactor tips, based on a published design (Briggs et al., 2004). The duration of each stimulus train was 500 ms with an inter-stimulus interval of 3 s with a 500 ms jitter. The stimuli were presented while participants were watching a movie. Participants were instructed to not pay attention to the stimulation and not move their hands. Hands were kept still using an armrest, and a blanket positioned over the arm. The sequence of stimuli was presented using the psychophysics toolbox (www.psychtoolbox.org). A total of 100 trials were collected. The total recording time was 6 min per subject.

MEG data were acquired inside a magnetically shielded room (IMEDCO, Hagendorf, Switzerland) (Khan and Cohen, 2013) using a whole-head VectorView MEG system (Elekta-Neuromag, Helsinki, Finland), comprised of 306 sensors arranged in 102 triplets of two orthogonal planar gradiometers and one magnetometer. The MEG signals were acquired at 600 Hz, with a hardware bandpass filter set between 0.1 and 200 Hz. The position and orientation of the head with respect to the MEG sensor array was recorded continuously with help of four Head Position Indicator coils (Uutela et al., 2001; Zaidel et al., 2009). To allow co-registration of the MEG and MRI data, the locations of three fiduciary points (nasion and auricular points) that define a head-based coordinate system, a set of points from the head surface, and the sites of the four HPI coils were digitized using a Fastrak digitizer (Polhemus, Colchester, VT, USA) integrated with the Vectorview system. The ECG and EOG signals were recorded simultaneously to identify epochs containing heartbeats as well as vertical and horizontal eye-movement and blink artifacts. During data acquisition, on-line averages were computed from artifact-free trials to monitor data quality in real time. All off-line analysis was based on the saved raw data. In addition, 5 min of data were recorded from the room void of a subject before each experimental session for noise estimation purposes.

Structural MRI Data Acquisition and Processing

T1-weighted high-resolution magnetization-prepared rapid gradient echo (MPRAGE) structural images were acquired using a 3.0 T Siemens Trio whole body MR scanner (Siemens Medical Systems, Erlangen, Germany) and a 32 channel head coil. The in-plane resolution was 1×1 mm^2, slice thickness 1.3 mm with no gaps, and a TR/TI/TE/Flip Angle 2530 ms/1100 ms/3.39 ms/7°. Cortical reconstructions and parcellations for each subject were generated using FreeSurfer (Dale et al., 1999; Fischl et al., 1999a). After correcting for topological defects, cortical surfaces were

triangulated with dense meshes with ∼130,000 vertices in each hemisphere. For visualization, the surfaces were inflated, thereby exposing the sulci (Dale et al., 1999).

MEG Data Pre-Processing

Cleaning and Motion Correction

The data were spatially filtered using the SSS method (Elekta-Neuromag Maxfilter software) to suppress noise generated by sources outside the brain (Taulu et al., 2004; Taulu and Simola, 2006). SSS also corrects for head motion between and within runs (Taulu et al., 2004). Cardiac and ocular artifacts were removed by signal space projection (Gramfort et al., 2013). The MEG data were then further low-pass filtered at 145 Hz to remove the HPI coil signals. The filtered data were then used for all further analyses.

Epoching

The data were epoched into single trials lasting 2.5 s, from 1000 ms prior to stimulus onset to 1500 ms following it. Epochs were rejected if the peak-to-peak amplitude during the epoch exceeded 1000 fT and 3000 fT/cm in any of the magnetometer and gradiometer channels, respectively. This resulted in the loss of 2–20 trials per participant. To maintain a constant signal to noise ratio across conditions and participants, the number of trials per condition per participant was fixed at 80, the minimum number of accepted trials that we had for each condition and participant. For participants that had more than 80 good trials, we selected 80 trials randomly from the available trials.

Transient Response Time Window Selection

For the standard evoked response (**Figure 2A**), we selected the first transient peak in the time window between 30 and 70 ms from stimulus onset, to evaluate latency and amplitude. For the response in the time-frequency domain, we needed to account for smoothing due to the convolution of the seven cycles complex Morlet wavelet with the data. Therefore, the time window of interest was 0–140 ms from stimulus onset.

Data Quality

There were no group differences in overall quality of the data, and the number of good (un-rejected) trials per condition was similar between groups and across conditions. For each participant, the same set of trials was used for all analyses.

Mapping MEG Data Onto Cortical Space

Source Estimation

The cortical source space consisted of 10,242 dipoles per hemisphere, corresponding to a spacing of approximately 3 mm between adjacent source locations. The forward solution was computed using a single-compartment boundary-element model (Hämäläinen and Sarvas, 1989). The individual inner skull surface triangulations for this model were generated with the watershed algorithm in FreeSurfer. The current distribution was estimated using the minimum-norm estimate by fixing the source orientation to be perpendicular to the cortex (Gramfort et al., 2014). The noise covariance matrix was estimated from data acquired in the absence of a subject prior to each session. We employed depth weighting to reduce the bias of the minimum norm estimates toward superficial currents (Lin et al., 2006).

Inter-Subject Cortical Surface Registration for Group Analysis

A morphing map to optimally align the cortical surface of each participant to an average cortical representation (FsAverage in FreeSurfer) was computed in FreeSurfer (Fischl et al., 1999b).

Data Analysis

Phase Locking

Inter Trial Phase Locking (PL) is a method to quantify phase synchrony across multiple trials. To compute PL, we convolved the epoched time series with a dictionary of complex Morlet wavelets (each spanning seven cycles). We then normalized the resulting complex coefficients by dividing by their absolute magnitude and averaging the unit-norm phasors across trials for each time-frequency bin. We then took their absolute value so that each number ranged between 0 and 1, with 0 representing a uniform distribution of phase angles and 1 representing perfectly synchronized phase angles, across trials (Tallon-Baudry et al., 1996; Makeig et al., 2002). Mathematically PL is defined as:

$$PL(f, t) = \frac{1}{N}\left|\sum_{n=1}^{N} e^{\phi^{k(f,t)}}\right|$$

Where $\emptyset^{K}$ represent instantaneous phase resulting from convolution of the trial with the complex Morlet wavelet, and N is the numbers of trials.

Z-PL (Normalized Phase Locking)

To compute Z-PL (**Figure 2**), we compared each PL value to a set of surrogate null distributions, to correct for statistical biases proportional to the number of epochs. This approach is non-parametric, and makes no a-priori assumptions besides the independence across the trials in the experimental data. The independence across trials was motivated by the fact that there was an average 3 s time interval between trials, and anticipation effects were eliminated because our experimental paradigm had a 500 ms jitter in Stimulus-Onset Asynchrony. Z-PL was computed as follows: each trial was first circularly shifted by a random lag ($\tau\epsilon(0, T]$, where T = period (1/f) in samples) and PL was computed on the shifted epoched data. This process was repeated 500 times. Z-PL was then computed by subtracting the mean and dividing by the standard deviation of the null distributions from the actual PL values.

S-T Div Decomposition

S-T Div is composed of two components. The first is the scalar component of the extent of divergence of the source estimates, i.e. the magnitude of the divergence, illustrated in **Figure 3** as a colormap. The second is the velocity of this divergence, illustrated in **Figure 3** with purple vectors, to represent both direction and magnitude. The S-T Div decomposition involves two steps: (i) The optical flow of distributed MEG/EEG MNE normalized estimates, where the relative maximum is set to be one unit for each individual subject, is computed on the cortical manifold. This step ensures that amplitude does not impact the result, so that different data sets where signal to noise may not be constant, can nonetheless be directly compared. (ii) Helmholtz-Hodge decomposition is then applied to the optical flow computed

previously. The details and mathematics of the approach were published previously (Khan et al., 2011). Briefly, optical flow V is a vector field which defines the motion of scalar quantity *I*, defined on a surface *M* and at time *t*, such that:

$$\partial_t + \mathbf{g}(\mathbf{V}, \nabla_M I) = 0$$

Where $g(.,.)$ is the scalar product, modified by the local curvature of *M*. Given optical flow vector field **V** defined on a surface *M*, there exists: a scalar field U, a rotational vector field A, and a harmonic vector field **H** such that:

$\mathsf{V} = \nabla_{\mathrm{M}}\mathrm{U} + \nabla \times \mathsf{A} + \mathsf{H}$ The scalar field U is the divergnce of the scalar field *I,* and $\mathbf{V}_{div} = \nabla_{\mathrm{M}}\mathrm{U}$ is the divergence vector field component of vector field **V** defined on a surface *M* and at time *t*. Optical flow and S-T Div are availaible as part of open-source MEG/EEG toolboxes; Brainstorm (Tadel et al., 2011) and MNE-Python (Gramfort et al., 2013).

Lastly, it is important to note that S-T Div is not affected by the point spread of MNE solution. This is because S-T div is computed by taking the gradient in space and time. The point spread of MNE results from the regularization of the ill-posed inverse solution. Therefore, for a particular location in space, the spread is "constant" across different time points. Thus, because it is constant, taking the gradient cancels the impact of the point spread. This is discussed at length in prior publications on the topic (Khan et al., 2011).

Correlations Analyses

All correlation coefficients and the corresponding *P*-values were computed using Pearson correlation (**Figure 4**). Correlations resulting in significant *P*-values were then tested using Robust Correlation (Pernet et al., 2012), which strictly checks for false positive correlations using bootstrap resampling and 6 correlation tests (bootstrap Pearson correlation, bootstrap Spearman correlation, bootstrap Bend correlation, bootstrap Pearson skipped correlation and bootstrap Spearman skipped correlation). Significant correlations were further tested for survival of multiple comparison correction by controlling for family-wise error rate using maximum statistics through permutation testing (Groppe et al., 2011).

Linear Discriminant Analysis (LDA)

The performance of LDA was evaluated using 10-fold cross validation (a model validation technique for assessing how the results of a model will generalize to an independent data set). To perform this cross validation, both TD and ASD Subjects (35 total) were randomly partitioned into 10 equal size subsamples. Of the 10 subsamples, 9 subsamples were used as training data for model learning and then applied on the remaining subsample to test the validity of the model. The cross-validation process was then repeated 10 times, with each of the subsamples used once as the validation data. Scikit-learn Machine Learning in Python (Pedregosa et al., 2011) was used for the above analysis.

Akaike Information Criterion (AIC)

Given a set of models for the data, the Akaike Information Criterion (AIC) is a measure that assesses the quality of each model, relative to the remaining models in the set. The chosen model minimizes the Kullback-Leibler distance between the model and the ground truth. AIC takes into account both descriptive accuracy and parsimony, since it carries a penalty for increasing the number of free parameters. The model with the lowest AIC is considered the best model among all models specified for the data at hand. The absolute AIC values are not particularly meaningful since they are specific to the data set being modeled. The relative AIC value ($\Delta AIC_i = AIC_i - \min\{AIC_p\}$) is used to rank models: $\Delta AIC_i < 2$ suggest that models are basically equivalent, whereas a $\Delta AIC_i > 10$ indicates that the model with the minimum AIC ($\min\{AIC_p\}$) is significantly better than the alternative model (Akaike, 1992).

Statistical Analyses on Cortical Surface

Our statistical analyses (**Figure 3**) were based on cluster-based statistics which is a non-parametric method (Maris and Oostenveld, 2007; Maris et al., 2007) that also corrects for multiple comparisons. We used 1000 permutations and the test statistics used were Wilcoxon Rank Sum test.

AUTHOR CONTRIBUTIONS

SK and TK designed research; SK, FM, HB, SG, KG collected the data; SK, JH, FM, KM, MK, and MH analyzed the data; and SK, JH, MH, and TK wrote the paper. All authors reviewed the manuscript.

FUNDING

This work was supported by grants from the Nancy Lurie Marks Family Foundation (TK, SK, MK), Autism Speaks (TK), The Simons Foundation (SFARI 239395, TK), The National Institute of Child Health and Development (R01HD073254, TK), The National Center for Research Resources (P41EB015896, MH), National Institute for Biomedical Imaging and Bioengineering (5R01EB009048, MH), and the Cognitive Rhythms Collaborative: A Discovery Network (NFS 1042134, MH).

SUPPLEMENTARY MATERIAL

The Supplementary Material for this article can be found online at: http://journal.frontiersin.org/article/10.3389/fnins.2016.00255

Figure S1 | ROCs showing performance of statistical classifier. We evaluated the performance of the classifier using the standard approach of measuring the area under the curve (AUC), where an AUC of 0.5 represents chance (dashed blacked line). Orange line, represent average ROC curve for 10-fold validation, standard error of the folds is represented as shaded area around the line. (AUC = 0.95).

Movie M1 | Rotating visualization of the 4D depiction of the LDA shown in Figure 5.

Table T1 | Participants in experimental paradigm. As expected, only ADOS scores and Touch scores were significantly different between the groups.

REFERENCES

Akaike, H. (1992). Data analysis by statistical models. *No To Hattatsu* 24, 127–133.

Amso, D., Haas, S., Tenenbaum, E., Markant, J., and Sheinkopf, S. J. (2014). Bottom-up attention orienting in young children with autism. *J. Autism Dev. Disord.* 44, 664–673. doi: 10.1007/s10803-013-1925-5

Belmonte, M. K., Allen, G., Beckel-Mitchener, A., Boulanger, L. M., Carper, R. A., and Webb, S. J. (2004). Autism and abnormal development of brain connectivity. *J. Neurosci.* 24, 9228–9231. doi: 10.1523/JNEUROSCI.3340-04.2004

Berg, J. M., and Geschwind, D. H. (2012). Autism genetics: searching for specificity and convergence. *Genome Biol.* 13, 247. doi: 10.1186/gb-2012-13-7-247

Briggs, R. W., Dy-Liacco, I., Malcolm, M. P., Lee, H., Peck, K. K., Gopinath, K. S., et al. (2004). A pneumatic vibrotactile stimulation device for fMRI. *Magn. Res. Med.* 51, 640–643. doi: 10.1002/mrm.10732

Cauller, L. J., and Kulics, A. (1991). The neural basis of the behaviorally relevant N1 component of the somatosensory-evoked potential in SI cortex of awake monkeys: evidence that backward cortical projections signal conscious touch sensation. *Exp. Brain Res.* 84, 607–619. doi: 10.1007/BF00230973

Cerliani, L., Mennes, M., Thomas, R. M., Di Martino, A., Thioux, M., and Keysers, C. (2015). Increased functional connectivity between subcortical and cortical resting-state networks in autism spectrum disorder. *JAMA Psychiatry* 72, 767–777. doi: 10.1001/jamapsychiatry.2015.0101

Cook, J., Barbalat, G., and Blakemore, S. J. (2012). Top-down modulation of the perception of other people in schizophrenia and autism. *Front. Hum. Neurosci.* 6:175. doi: 10.3389/fnhum.2012.00175

Dale, A. M., Fischl, B., and Sereno, M. I. (1999). Cortical surface-based analysis. I. Segmentation and surface reconstruction. *Neuroimage* 9, 179–194. doi: 10.1006/nimg.1998.0395

Dinstein, I., Heeger, D. J., Lorenzi, L., Minshew, N. J., Malach, R., and Behrmann, M. (2012). Unreliable evoked responses in autism. *Neuron* 75, 981–991. doi: 10.1016/j.neuron.2012.07.026

Fischl, B., Sereno, M. I., and Dale, A. M. (1999a). Cortical surface-based analysis. II: Inflation, flattening, and a surface-based coordinate system. *Neuroimage* 9, 195–207.

Fischl, B., Sereno, M. I., Tootell, R. B., and Dale, A. M. (1999b). High-resolution intersubject averaging and a coordinate system for the cortical surface. *Hum. Brain Mapp.* 8, 272–284.

Gramfort, A., Luessi, M., Larson, E., Engemann, D. A., Strohmeier, D., Brodbeck, C., et al. (2013). MEG and EEG data analysis with MNE-Python. *Front. Neurosci.* 7:267. doi: 10.3389/fnins.2013.00267

Gramfort, A., Luessi, M., Larson, E., Engemann, D. A., Strohmeier, D., Brodbeck, C., et al. (2014). MNE software for processing MEG and EEG data. *Neuroimage* 86, 446–460. doi: 10.1016/j.neuroimage.2013.10.027

Groppe, D. M., Urbach, T. P., and Kutas, M. (2011). Mass univariate analysis of event-related brain potentials/fields I: a critical tutorial review. *Psychophysiology* 48, 1711–1725. doi: 10.1111/j.1469-8986.2011.01273.x

Hämäläinen, M. S., and Sarvas, J. (1989). Realistic conductivity geometry model of the human head for interpretation of neuromagnetic data. *IEEE Trans. Biomed. Eng.* BME-36, 165–171. doi: 10.1109/10.16463

Jarvinen-Pasley, A., Wallace, G. L., Ramus, F., Happe, F., and Heaton, P. (2008). Enhanced perceptual processing of speech in autism. *Dev. Sci.* 11, 109–121. doi: 10.1111/j.1467-7687.2007.00644.x

Jones, S. R., Pritchett, D. L., Sikora, M. A., Stufflebeam, S. M., Hamalainen, M., and Moore, C. I. (2009). Quantitative analysis and biophysically realistic neural modeling of the MEG mu rhythm: rhythmogenesis and modulation of sensory-evoked responses. *J. Neurophysiol.* 102, 3554–3572. doi: 10.1152/jn.00535.2009

Just, M. A., Cherkassky, V. L., Keller, T. A., and Minshew, N. J. (2004). Cortical activation and synchronization during sentence comprehension in high-functioning autism: evidence of underconnectivity. *Brain* 127, 1811–1821. doi: 10.1093/brain/awh199

Kana, R. K., Libero, L. E., and Moore, M. S. (2011). Disrupted cortical connectivity theory as an explanatory model for autism spectrum disorders. *Phys. Life Rev.* 8, 410–437. doi: 10.1016/j.plrev.2011.10.001

Kaufman, A. S., and Kaufman, N. L. (2004). *Kaufman Brief Intelligence Test, 2nd Edn*. Circle Pines, MN: AGS Publishing.

Khan, S., and Cohen, D. (2013). Note: Magnetic noise from the inner wall of a magnetically shielded room. *Rev. Sci. Instrum.* 84, 056101. doi: 10.1063/1.4802845

Khan, S., Gramfort, A., Shetty, N. R., Kitzbichler, M. G., Ganesan, S., Moran, J. M., et al. (2013). Local and long-range functional connectivity is reduced in concert in autism spectrum disorders. *Proc. Natl. Acad. Sci. U.S.A.* 110, 3107–3112. doi: 10.1073/pnas.1214533110

Khan, S., Lefevre, J., Ammari, H., and Baillet, S. (2011). Feature detection and tracking in optical flow on non-flat manifolds. *Pattern Recognit. Lett.* 32, 2047–2052. doi: 10.1016/j.patrec.2011.09.017

Khan, S., Lefevre, J., and Baillet, S. (2009). Feature extraction from time-resolved cortical current maps using the Helmholtz-Hodge decomposition. *Neuroimage* 47(Suppl. 1), S79. doi: 10.1016/S1053-8119(09)70547-6

Khan, S., Michmizos, K., Tommerdahl, M., Ganesan, S., Kitzbichler, M. G., Zetino, M., et al. (2015). Somatosensory cortex functional connectivity abnormalities in autism show opposite trends, depending on direction and spatial scale. *Brain* 138, 1394–1409. doi: 10.1093/brain/awv043

Kitzbichler, M. G., Khan, S., Ganesan, S., Vangel, M. G., Herbert, M. R., Hämäläinen, M. S., et al. (2015). Altered development and multifaceted band-specific abnormalities of resting state networks in autism. *Biol. Psychiatry* 77, 794–804. doi: 10.1016/j.biopsych.2014.05.012

Lin, F. H., Witzel, T., Ahlfors, S. P., Stufflebeam, S. M., Belliveau, J. W., and Hämäläinen, M. S. (2006). Assessing and improving the spatial accuracy in MEG source localization by depth-weighted minimum-norm estimates. *Neuroimage* 31, 160–171. doi: 10.1016/j.neuroimage.2005.11.054

Lord, C., Rutter, M., Dilavore, P. C., and Risi, S. (1999). *Autism Diagnostic Observation Schedule—WPS (ADOS-WPS)*. Los Angeles, CA: Western Psychological Services.

Makeig, S., Westerfield, M., Jung, T. P., Enghoff, S., Townsend, J., Courchesne, E., et al. (2002). Dynamic brain sources of visual evoked responses. *Science* 295, 690–694. doi: 10.1126/science.1066168

Marco, E. J., Hinkley, L. B., Hill, S. S., and Nagarajan, S. S. (2011). Sensory processing in autism: a review of neurophysiologic findings. *Pediatric Res.* 69, 48R–54R. doi: 10.1203/PDR.0b013e3182130c54

Marco, E. J., Khatibi, K., Hill, S. S., Siegel, B., Arroyo, M. S., Dowling, A. F., et al. (2012). Children with autism show reduced somatosensory response: an MEG study. *Autism Res.* 5, 340–351. doi: 10.1002/aur.1247

Maris, E., and Oostenveld, R. (2007). Nonparametric statistical testing of EEG- and MEG-data. *J. Neurosci. Methods* 164, 177–190. doi: 10.1016/j.jneumeth.2007.03.024

Maris, E., Schoffelen, J. M., and Fries, P. (2007). Nonparametric statistical testing of coherence differences. *J. Neurosci. Methods* 163, 161–175. doi: 10.1016/j.jneumeth.2007.02.011

Minshew, N. J., and Williams, D. L. (2007). The new neurobiology of autism: cortex, connectivity, and neuronal organization. *Arch. Neurol.* 64, 945–950. doi: 10.1001/archneur.64.7.945

Mizuno, A., Villalobos, M. E., Davies, M. M., Dahl, B. C., and Müller, R. A. (2006). Partially enhanced thalamocortical functional connectivity in autism. *Brain Res.* 1104, 160–174. doi: 10.1016/j.brainres.2006.05.064

Mueller, S., Keeser, D., Samson, A. C., Kirsch, V., Blautzik, J., Grothe, M., et al. (2013). Convergent findings of altered functional and structural brain connectivity in individuals with high functioning autism: a multimodal MRI study. *PLoS ONE* 8:e67329. doi: 10.1371/journal.pone.0067329

Müller, R. A., Shih, P., Keehn, B., Deyoe, J. R., Leyden, K. M., and Shukla, D. K. (2011). Underconnected, but how? A survey of functional connectivity MRI studies in autism spectrum disorders. *Cereb. Cortex* 21, 2233–2243. doi: 10.1093/cercor/bhq296

Nangini, C., Ross, B., Tam, F., and Graham, S. J. (2006). Magnetoencephalographic study of vibrotactile evoked transient and steady-state responses in human somatosensory cortex. *Neuroimage* 33, 252–262. doi: 10.1016/j.neuroimage.2006.05.045

Neumann, D., Spezio, M. L., Piven, J., and Adolphs, R. (2006). Looking you in the mouth: abnormal gaze in autism resulting from impaired top-down modulation of visual attention. *Soc. Cogn. Affect. Neurosci.* 1, 194–202. doi: 10.1093/scan/nsl030

Papadelis, C., Leonardelli, E., Staudt, M., and Braun, C. (2012). Can magnetoencephalography track the afferent information flow along

white matter thalamo-cortical fibers? *Neuroimage* 60, 1092–1105. doi: 10.1016/j.neuroimage.2012.01.054

Pedregosa, F., Varoquaux, G., Gramfort, A., Michel, V., Thirion, B., Grisel O., et al. (2011). Scikit-learn: machine learning in python. *J. Mach. Learn. Res.* 12, 2825–2830.

Peeva, M. G., Tourville, J. A., Agam, Y., Holland, B., Manoach, D. S., and Guenther, F. H. (2013). White matter impairment in the speech network of individuals with autism spectrum disorder. *Neuroimage Clin* 3, 234–241. doi: 10.1016/j.nicl.2013.08.011

Peiker, I., Schneider, T. R., Milne, E., Schottle, D., Vogeley, K., Munchau, A., et al. (2015). Stronger neural modulation by visual motion intensity in autism spectrum disorders. *PLoS ONE* 10:e0132531. doi: 10.1371/journal.pone.0132531

Pernet, C. R., Wilcox, R., and Rousselet, G. A. (2012). Robust correlation analyses: false positive and power validation using a new open source matlab toolbox. *Front. Psychol.* 3:606. doi: 10.3389/fpsyg.2012.00606

Peterson, N. N., Schroeder, C. E., and Arezzo, J. C. (1995). Neural generators of early cortical somatosensory evoked potentials in the awake monkey. *Electroencephalogr. Clin. Neurophysiol.* 96, 248–260.

Petrof, I., Viaene, A. N., and Sherman, S. M. (2012). Two populations of corticothalamic and interareal corticocortical cells in the subgranular layers of the mouse primary sensory cortices. *J. Comp. Neurol.* 520, 1678–1686. doi: 10.1002/cne.23006

Piro, J. M. (1998). Handedness and intelligence: patterns of hand preference in gifted and nongifted children. *Dev. Neuropsychol.* 14, 619–630. doi: 10.1080/87565649809540732

Pramparo, T., Pierce, K., Lombardo, M. V., Carter Barnes, C., Marinero, S., Ahrens-Barbeau, C., et al. (2015). Prediction of autism by translation and immune/inflammation coexpressed genes in toddlers from pediatric community practices. *JAMA Psychiatry* 72, 386–394. doi: 10.1001/jamapsychiatry.2014.3008

Ramcharan, E. J., Gnadt, J. W., and Sherman, S. M. (2005). Higher-order thalamic relays burst more than first-order relays. *Proc. Natl. Acad. Sci. U.S.A.* 102, 12236–12241. doi: 10.1073/pnas.0502843102

Robertson, C. E., Thomas, C., Kravitz, D. J., Wallace, G. L., Baron-Cohen, S., Martin, A., et al. (2014). Global motion perception deficits in autism are reflected as early as primary visual cortex. *Brain* 137, 2588–2599. doi: 10.1093/brain/awu189

Rubenstein, J. L., and Merzenich, M. M. (2003). Model of autism: increased ratio of excitation/inhibition in key neural systems. *Genes Brain Behav.* 2, 255–267. doi: 10.1034/j.1601-183X.2003.00037.x

Sherman, S. M. (2012). Thalamocortical interactions. *Curr. Opin. Neurobiol.* 22, 575–579. doi: 10.1016/j.conb.2012.03.005

Skafidas, E., Testa, R., Zantomio, D., Chana, G., Everall, I. P., and Pantelis, C. (2014). Predicting the diagnosis of autism spectrum disorder using gene pathway analysis. *Mol. Psychiatry* 19, 504–510. doi: 10.1038/mp.2012.126

Sur, M., Wall, J. T., and Kaas, J. H. (1984). Modular distribution of neurons with slowly adapting and rapidly adapting responses in area 3b of somatosensory cortex in monkeys. *J. Neurophysiol.* 51, 724–744.

Tadel, F., Baillet, S., Mosher, J. C., Pantazis, D., and Leahy, R. M. (2011). Brainstorm: a user-friendly application for MEG/EEG analysis. *Comput. Intell. Neurosci.* 2011, 879716. doi: 10.1155/2011/879716

Tallon-Baudry, C., Bertrand, O., Delpuech, C., and Pernier, J. (1996). Stimulus specificity of phase-locked and non-phase-locked 40 Hz visual responses in human. *J. Neurosci.* 16, 4240–4249.

Taulu, S., Kajola, M., and Simola, J. (2004). Suppression of interference and artifacts by the Signal Space Separation Method. *Brain Topogr.* 16, 269–275. doi: 10.1023/B:BRAT.0000032864.93890.f9

Taulu, S., and Simola, J. (2006). Spatiotemporal signal space separation method for rejecting nearby interference in MEG measurements. *Phys. Med. Biol.* 51, 1759–1768. doi: 10.1088/0031-9155/51/7/008

Tommerdahl, M., Tannan, V., Cascio, C. J., Baranek, G. T., and Whitsel, B. L. (2007). Vibrotactile adaptation fails to enhance spatial localization in adults with autism. *Brain Res.* 1154, 116–123. doi: 10.1016/j.brainres.2007.04.032

Tyszka, J. M., Kennedy, D. P., Paul, L. K., and Adolphs, R. (2014). Largely typical patterns of resting-state functional connectivity in high-functioning adults with autism. *Cereb. Cortex* 24, 1894–1905. doi: 10.1093/cercor/bht040

Uutela, K., Taulu, S., and Hämäläinen, M. (2001). Detecting and correcting for head movements in neuromagnetic measurements. *Neuroimage* 14, 1424–1431. doi: 10.1006/nimg.2001.0915

Vissers, M. E., Cohen, M. X., and Geurts, H. M. (2012). Brain connectivity and high functioning autism: a promising path of research that needs refined models, methodological convergence, and stronger behavioral links. *Neurosci. Biobehav. Rev.* 36, 604–625. doi: 10.1016/j.neubiorev.2011.09.003

Wass, S. (2011). Distortions and disconnections: disrupted brain connectivity in autism. *Brain Cogn.* 75, 18–28. doi: 10.1016/j.bandc.2010.10.005

Wolff, J. J., Gu, H., Gerig, G., Elison, J. T., Styner, M., Gouttard, S., et al. (2012). Differences in white matter fiber tract development present From 6 to 24 months in infants with Autism. *Am. J. Psychiatry* 169, 589–600. doi: 10.1176/appi.ajp.2011.11091447

Zaidel, A., Spivak, A., Shpigelman, L., Bergman, H., and Israel, Z. (2009). Delimiting subterritories of the human subthalamic nucleus by means of microelectrode recordings and a Hidden Markov Model. *Movem. Disorders* 24, 1785–1793. doi: 10.1002/mds.22674

Conflict of Interest Statement: The authors declare that the research was conducted in the absence of any commercial or financial relationships that could be construed as a potential conflict of interest.

frontiers in Neuroscience

ORIGINAL RESEARCH
published: 09 June 2016
doi: 10.3389/fnins.2016.00258

Resting State Functional Connectivity MRI among Spectral MEG Current Sources in Children on the Autism Spectrum

Michael Datko[1,2]*, *Robert Gougelet*[1], *Ming-Xiong Huang*[3] and *Jaime A. Pineda*[1,2]

[1] Cognitive Science, University of California San Diego, La Jolla, CA, USA, [2] Neurosciences, University of California San Diego, La Jolla, CA, USA, [3] Department of Radiology, University of California San Diego, La Jolla, CA, USA

Social and communicative impairments are among the core symptoms of autism spectrum disorders (ASD), and a great deal of evidence supports the notion that these impairments are associated with aberrant functioning and connectivity of various cortical networks. The present study explored the links between sources of MEG amplitude in various frequency bands and functional connectivity MRI in the resting state. The goal of combining these modalities was to use sources of neural oscillatory activity, measured with MEG, as functionally relevant seed regions for a more traditional pairwise fMRI connectivity analysis. We performed a seed-based connectivity analysis on resting state fMRI data, using seed regions derived from frequency-specific amplitude sources in resting state MEG data in the same nine subjects with ASD (10–17 years of age). We then compared fMRI connectivity among these MEG-source-derived regions between participants with autism and typically developing, age-matched controls. We used a source modeling technique designed for MEG data to detect significant amplitude sources in six frequency bands: delta (2–4 Hz), theta (4–8 Hz), alpha (8–12 Hz), beta (12–30 Hz), low gamma (30–60 Hz), and high gamma (60–120 Hz). MEG-derived source maps for each participant were co-registered in standard MNI space, and group-level source maps were obtained for each frequency. For each frequency band, the 10 largest clusters resulting from these *t*-tests were used as regions of interest (ROIs) for the fMRI functional connectivity analysis. Pairwise BOLD signal correlations were obtained between each pair of these ROIs for each frequency band. Each pairwise correlation was compared between the ASD and TD groups using *t*-tests. We also constrained these pairwise correlations to known network structures, resulting in a follow-up set of correlation matrices specific to each network we considered. Frequency-specific MEG sources had distinct patterns of fMRI resting state functional connectivity in the ASD group, but perhaps the most significant was a finding of hypoconnectivity between many sources of low and high gamma activity. These novel findings suggest that in ASD there are differences in functionally defined networks as shown in previous fMRI studies, as well as between sets of regions defined by magnetoencephalographic neural oscillatory activity.

Keywords: autism, magnetoencephalography, fMRI, functional connectivity, multimodal

OPEN ACCESS

Edited by:
Roma Siugzdaite,
Ghent University, Belgium

Reviewed by:
Lutz Jäncke,
University of Zurich, Switzerland
Jesus M. Cortes,
Biocruces Health Research Institute, Spain

***Correspondence:**
Michael Datko
mdatko@ucsd.edu

Specialty section:
This article was submitted to Child and Adolescent Psychiatry, a section of the journal Frontiers in Neuroscience

Received: *08 February 2016*
Accepted: *23 May 2016*
Published: *09 June 2016*

Citation:
Datko M, Gougelet R, Huang M-X and Pineda JA (2016) Resting State Functional Connectivity MRI among Spectral MEG Current Sources in Children on the Autism Spectrum. Front. Neurosci. 10:258. doi: 10.3389/fnins.2016.00258

INTRODUCTION

Autism spectrum disorders (ASD) are characterized by social and communicative impairments, as well as repetitive and stereotyped behaviors (DSM-V, American Psychiatric Association (APA), 2013). It is well established that these impairments may result from aberrant anatomy and functional connectivity, defined as inter-regional correlations in the time-course of the fMRI BOLD signal (Biswal et al., 1995), within and between various cortical networks (Vissers et al., 2012). These atypical patterns of functional connectivity may underlie the disordered information integration characteristic of the ASD brain (Brock et al., 2002), therefore accounting for the myriad symptoms along the autism spectrum (Belmonte et al., 2004).

Unsurprisingly, functional connectivity in the ASD population is largely idiosyncratic across tasks (Vissers et al., 2012), methodologies (Müller et al., 2011), and behavioral symptoms (Hahamy et al., 2015). Findings include hypoconnectivity in some systems (Just et al., 2004, 2007; Kana et al., 2006, 2007), and hyperconnectivity in others (Welchew et al., 2005; Mizuno et al., 2006; Turner et al., 2006; Noonan et al., 2009; Shih et al., 2010). More recent studies have refined the characterization of functional connectivity in ASD, highlighting the contrast between within-network and out-of-network connectivity patterns, and argue for reduced within-network integration along with increased out-of-network connectivity, which ultimately results in reduced network segregation in ASD (Fair et al., 2009; Rudie et al., 2011, 2013; Shih et al., 2011; Fishman et al., 2014; Nebel et al., 2014). This characterization is supported by observations from Keown et al. (2013) and Supekar et al. (2013), who found functional hyperconnectivity in children with ASD across multiple networks, and from Pérez Velázquez and Galán (2013), who found an increase in information gain in the absence of external stimuli in ASD subjects, possibly as a consequence of hyperconnectivity and network cross-talk.

Current understanding about the neurophysiological etiology of ASD may shed light on the functional connectivity abnormalities observed during rest and task performance. It has been hypothesized that in ASD, cortical GABAergic interneurons may fail to preserve proper excitation/inhibition dynamics during development, causing irregularities in synaptic pruning and network maturation (Hensch, 2005; Coghlan et al., 2012; Rosenberg et al., 2015). In a recent study on adults with ASD, low GABA concentrations in visual cortex were shown to correlate with decreased performance on a binocular rivalry task (Robertson et al., 2016). In addition to these GABAergic interneuron dysfunctions, abnormalities in cortical minicolumns in the frontal cortex (Casanova et al., 2002), as well as enlarged frontal gray and white matter (Carper and Courchesne, 2005; Courchesne and Pierce, 2005), may also contribute to the functional connectivity issues in ASD. Whatever the sources of the abnormalities seen in ASD are, functional connectivity remains an important metric in elucidating the neurophysiological substrates of the disorder.

Non-invasive electrophysiological measures like EEG and MEG have been crucial in providing converging evidence for functional connectivity abnormalities in ASD (Vissers et al., 2012). These biophysical signals are often examined in spectral bands prescribed in the literature: delta (0–4 Hz), theta (4–8 Hz), alpha (8–12 Hz), beta (12–30 Hz), low gamma (30–60 Hz), and high gamma (60+ Hz), many of which exhibit abnormal patterns in ASD compared to typically developing controls. Subjects on the spectrum show reduced interhemispheric coherence in the gamma band (Peiker et al., 2015), a finding that provides support for the weak central coherence hypothesis of autism. Barttfeld et al. (2011), on the other hand, found distinct EEG connectivity patterns within the delta range during rest in an ASD population. These subjects lacked long-range connections, with most prominent deficits in fronto-occipital networks, and increased short-range connections in lateral-frontal networks. But while electrophysiological approaches provide important results like these on their own, the complementary use of MEG and fMRI can provide both millisecond and millimeter precision capable of spanning the multiple orders of temporal and spatial magnitudes involved in neocortical processing (Dale et al., 2000; Dale and Halgren, 2001; Liu et al., 2006; Salmelin and Baillet, 2009).

Research on these modalities suggests that the cortical neuronal activity that generates measurable electromagnetic fields imposes metabolic demands that are discernable by fMRI BOLD (Dale et al., 2000; Dale and Halgren, 2001; Logothetis et al., 2001; Arthurs and Boniface, 2002; Logothetis, 2002, 2003, 2008; Logothetis and Wandell, 2004). In particular, power in the mid-gamma band (60–120 Hz) has been shown to positively correlate with BOLD signals, whereas beta (13–30 Hz) power shows a negative correlation with BOLD (Conner et al., 2011). The higher co-localization of gamma band synchronous activity with fMRI BOLD becomes relevant in the discussion of ASD when considering that GABAergic interneurons are responsible for generating the gamma cortical oscillation (Cardin et al., 2009), and there may be dysfunction among GABAergic interneurons in ASD (Coghlan et al., 2012). Indeed, the combined use of MEG and fMRI to investigate functional connectivity could provide important new insights into the functional properties of gamma activity in ASD. Yet despite the complementarity of these two methods, there is a lack of cross-modal investigations that link measures of MEG and fMRI connectivity in autism.

The present study explored the links between MEG current source amplitudes in various frequency bands and functional connectivity MRI (fcMRI) in a resting state. More specifically, we performed a seed-based connectivity analysis on fMRI data, with seed regions based on amplitude sources from MEG data within a subgroup of subjects. We then compared connectivity among these regions between participants diagnosed with ASD and typically developing controls. First, we predicted that MEG amplitude sources for each frequency band would be located in areas previously associated with those frequencies for both ASD and typically developing controls. For instance, we predicted that alpha sources would be concentrated in visual areas, while areas associated with the mu rhythm centered more on somatosensory and premotor cortex (Pfurtscheller et al., 2006; Bernier et al., 2007). Furthermore, beta sources were expected near the central gyrus but also to extend to more frontal areas (Jensen et al., 2005). We predicted theta sources would be located in midline

frontal and prefrontal areas (Iramina et al., 1996), while gamma sources were expected to show a sparse and widely distributed pattern (Cardin et al., 2009). We further predicted that ASD would show abnormal resting state fMRI connectivity patterns among regions corresponding to MEG current sources in the various frequency bands. Based on previous observations of reduced within-network integration (Rudie et al., 2011, 2013), we predicted that MEG current sources falling within the same networks would show hypoconnectivity in ASD.

METHODS

Participants

Nine participants with high-functioning autism (mean age = 13.1 ± 2.59, range = 10–17; 1 female; mean WASI IQ = 96.1 ± 15.6, range = 72–121; mean ADOS Communication and Social Interaction score = 13.7 ± 3.14, range = 12–20) were scanned with both MEG and fMRI. A clinical psychologist collaborator verified autism diagnoses through the administration of the ADOS test (Rutter et al., 2012). Nine age-matched, typically developing (TD) participants (Mean age = 10.6 ± 2.75, range = 8–16; 3 female; mean WASI IQ = 118.33 ± 13.1, range = 103–138) completed both resting state fMRI and anatomical MRI scans, but not MEG scans. TD participants had no major diagnoses and did not have ASD siblings or parents. Groups did not differ significantly for age ($p = 0.14$), but were not matched for WASI IQ ($p = 0.005$). All participants gave informed consent or assent, and read forms describing the nature of the experiment and their rights as participants. There were two different age-appropriate forms, one for children ages 7–12 and the other for ages 13–17.

MEG Data Collection and Preprocessing

Participants in the ASD group completed two back-to-back, 4-min resting state MEG scans, during which they were instructed to keep their eyes open with their gaze directed at a fixation point, and let their mind wander. MEG data were collected for ASD participants using the Elekta/Neuromag Vectorview whole-head MEG system. Data were sampled at 1000 Hz and were bandpass filtered between 0.1 and 330 Hz. Eye blinks and eye movements as measured via electrooculography (EOG), and heart activity as measured by electrocardiogram (ECG) were collected MEG sensor data were filtered for movement-related artifacts using the program MaxFilter (Taulu et al., 2005). Feeding continuous magnetic sinusoidal signals to five head position indicator coils allowed for subjects' head positions to be continuously collected. These signals are used to continuously adjust the coordinate transformation from the device to the head frame of reference, necessary for applying MaxFilter. These signals were removed from the data *post-hoc*, in addition to interference from other magnetic sources (e.g., 60 Hz line frequency and its harmonics). The spatiotemporal signal space separation (tSSS) method was used in this case to remove noise and artifacts originating from outside the brain (Taulu et al., 2004b, 2005). By continuously tracking the subjects' head positions, we minimized the influence of movement artifacts on our analyses, a common consideration when working with the pediatric ASD population.

Precautions were taken to ensure head stability: foam wedges were inserted between the subject's head and the inside of the unit. During collection, the head positions were measured to ensure that head movement across different sessions was <5 mm (usually 2–3 mm). The ECG artifacts in the MEG data were also removed when the MEG data were passed through MaxFilter. This feature of MaxFilter has been described previously (Taulu et al., 2004a,b; Song et al., 2008).

Sensor data were co-registered with subjects' anatomical MRI scans for accurate source localization. To co-register the MEG with MRI coordinate systems, three anatomical landmarks (i.e., left and right preauricular points, and nasion) were measured for each subject using the Probe Position Identification system (Polhemus, USA). By identifying the same three points on the subject's MR images using MRILAB software developed by Elekta/Neuromag, a transformation matrix involving both rotation and translation between the MEG and MRI coordinate systems was generated. To increase the reliability of the MEG-MRI co-registration, ∼300 points on the scalp were digitized with the Polhemus system, in addition to the three landmarks, and those points were co-registered onto the scalp surface of the MR images.

MEG Analysis

We used a source modeling technique (Fast-VESTAL) designed for MEG data, which consists of two steps (Huang et al., 2014). First, L1-minimum-norm MEG source images were obtained for the dominant spatial (i.e., eigen-) modes of the sensor-waveform covariance matrix. Next, accurate source time-courses were obtained using an inverse operator constructed from the spatial source images of Step 1. This approach has been successfully used to obtain comprehensive MEG source-magnitude images covering the entire brain for different frequency bands of resting-state brain rhythms (Huang et al., 2014). The six different frequency bands of interest in the present study were: delta (2–4 Hz), theta (4–8 Hz), alpha (8–12 Hz), beta (12–30 Hz), low gamma (30–60 Hz), and high gamma (60–120 Hz).

In the present study, each of the artifact-free, 8-min long, resting-state MEG sensor-space scans were bandpass filtered for each frequency band of interest. The sensor-waveform covariance matrix was calculated and used to obtain MEG frequency band source magnitude images that cover the whole brain for each subject following the fast-VESTAL procedure (Huang et al., 2014). An Objective Prewhitening Method was applied to remove correlated environmental noise and to select the dominant eigen-modes of the sensor-waveform covariance matrix (Huang et al., 2014).

For each frequency band, a three-dimensional image volume showing the locations and intensities of each amplitude source was obtained for each participant. These individual subject volumes were then aligned to standard Montreal Neurological Institute (MNI) space. Using the neuroimaging software suite Analysis of Functional Neuroimages (AFNI; Cox, 1996), we then performed a one-sample *t*-test with a whole-brain field-of-view to determine the most significant amplitude sources at the group level. The resulting images met an uncorrected voxel wise statistical threshold of $p < 0.02$, and were cluster corrected for

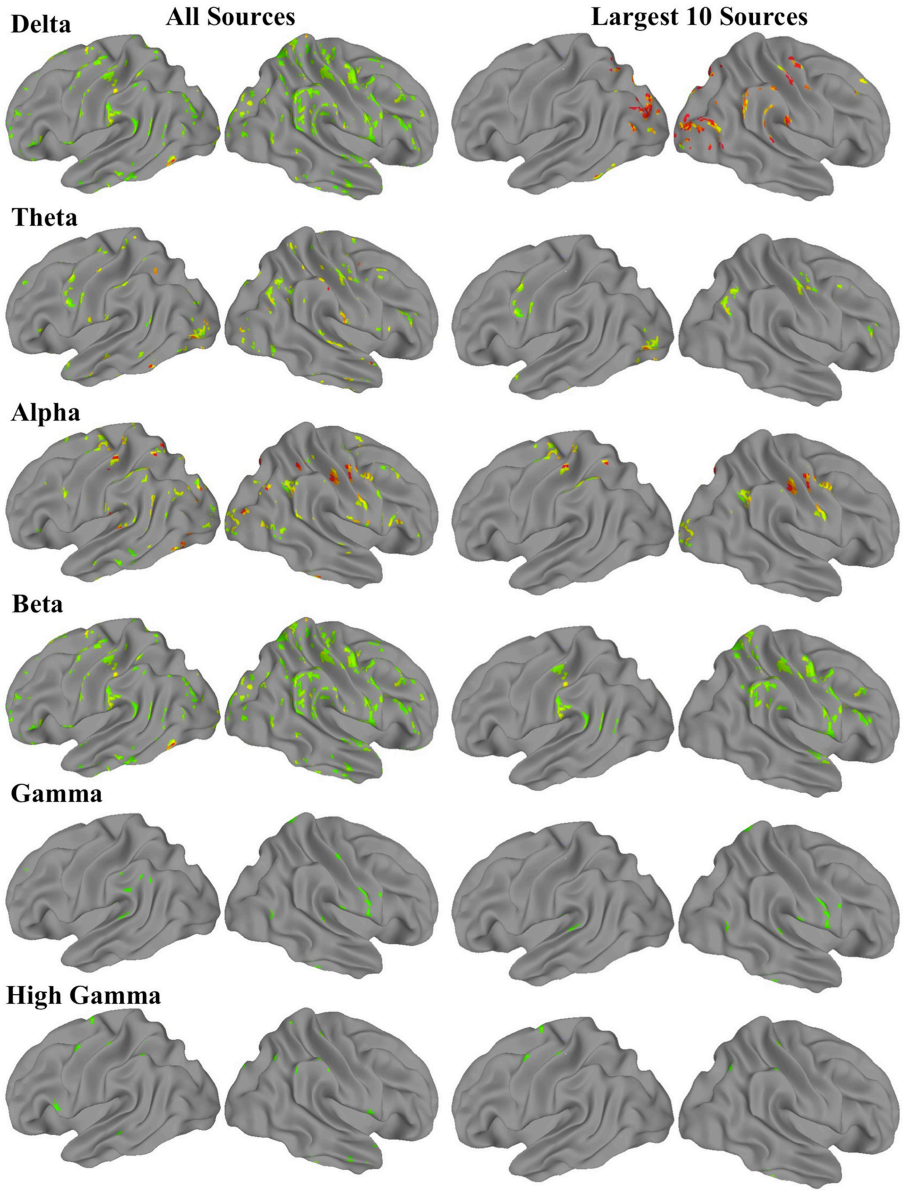

FIGURE 1 | Group-level MEG-derived source maps for each frequency band. The first column shows all sources that were significant at corrected $p < 0.01$, while the second column shows the 10 sources with the most voxels.

multiple comparisons at $p < 0.01$. For each frequency band, the 10 clusters with the largest volumes resulting from these *t*-tests were saved as regions of interest (ROIs) for the fMRI functional connectivity analysis (**Figure 1**).

fMRI Data Collection and Preprocessing

For ASD subjects, resting state and anatomical imaging data were acquired on a GE 1.5T Excite MRI scanner. The anatomical scan was acquired as a standard high-resolution anatomical volume with a resolution of $0.94 \times 0.94 \times 1.2\,mm^3$ using a T1-weighted 3D-IR-FSPGR pulse sequence. Functional T2*-weighted images were acquired with a single-shot gradient-recalled, echo-planar pulse sequence, as a single 7:48-min scan with 156 whole-brain volumes (TR = 3000 ms, TE = 40 ms, flip angle = 90°, FOV = 240 mm, 40 axial slices, $4 \times 4 \times 4\,mm^3$ resolution).

For TD subjects, resting state and anatomical imaging data were acquired on a GE 3T MR750 scanner with an eight-channel head coil. High-resolution anatomical images were obtained using a standard T1-weighted inversion recovery spoiled gradient echo sequence (TR = 8.108 ms, TE = 3.172 ms, flip angle 8°, 172 slices, $1\,mm^3$ resolution). Functional T2*-weighted images were acquired using a single-shot gradient-recalled, echo-planar pulse sequence, in one 6:10-min resting state scan consisting of 185 whole brain volumes (TR = 2000 ms, TE = 30 ms, flip angle 90°, FOV = 220 mm, 64×64 matrix, $3.4 \times 3.4 \times 3.4\,mm^3$ resolution, 42 axial slices).

The instructions to participants during resting state fMRI scans were identical to those received by ASD participants in the resting state MEG scans: they were told to keep their gaze on a fixation point, and remain awake. While ASD and TD groups were scanned on different magnets, all other scanning procedures and instructions to participants were identical, and subjects were scanned by the same researcher (MD).

Anatomical MRI scans for each subject were reconstructed using AFNI (Cox, 1996), and were warped to standard MNI space using FSL's nonlinear registration program *fnirt* (Andersson et al., 2007; Jenkinson et al., 2012). Standard preprocessing procedures were performed for the anatomical and resting state fMRI data, including image reconstruction, registration to MNI standard space, motion correction, spatial blurring to 6 mm full width at half maximum, spectral bandpass filtering from 0.008 to 0.08 Hz, and regression of nuisance signals derived from motion parameters, white matter, and ventricles. Time points with motion exceeding 1.5 mm from the previous time point were censored from the final analysis to reduce erroneously high correlations resulting from head motion (Power et al., 2012).

fMRI Analysis

Using the ROIs derived from the MEG source amplitude images, pairwise correlations were obtained between the BOLD time series of each possible pair of regions. These pairwise correlations were performed separately for each of the six sets of ROIs, corresponding to each of the six frequency bands for which we modeled amplitude sources. Each pairwise correlation was also compared between the ASD and TD groups using *t*-tests, to determine which nodes of each frequency-source-based network showed abnormal connectivity in ASD. Prior to these between-group tests, Pearson product moment correlation values were converted into Z-scores using the Fisher transformation.

We also sought to determine the extent to which the VESTAL-derived MEG amplitude sources overlapped with various functionally defined cortical networks. To define cortical network structure, we used a set of ROIs derived from a cortical parcellation created by Gordon et al. (2014). In that parcellation, which is shared publicly by the authors (http://www.nil.wustl.edu/labs/petersen/Resources.html), the cortex is divided into 333 separate ROIs. The authors of that paper then organized the parcels into 13 communities, which corresponded to various resting state and task-related networks and were derived from the Infomap community detection method developed by Rosvall and Bergstrom (2008). We focused on seven of the parcel communities they describe: default mode network (DMN), somatomotor (combining their separate somatomotor hand and mouth communities into one), visual, cingulo-operculum, frontoparietal, dorsal attention, and ventral attention. To adapt those regions for the present study, the parcels from each of the seven communities were combined into seven different community masks. Since the original parcels were created from a very thin layer of cortex, we then dilated our community masks by 1 voxel in all directions, using the AFNI command 3dmask_tool. The resulting community masks used for the present study are shown in **Figure 2**.

We conducted two follow-up correlation analyses with network-based constraints. Notably, unlike the first analysis, all between-group tests were bonferroni-corrected for multiple comparisons to a corrected $p < 0.05$. First, we looked at the pairwise correlations specifically within MEG amplitude sources that overlapped strongly with one of the seven previously discussed networks. We defined "strong" overlap as an ROI with >50% of its voxels falling within the bounds of one of our dilated network masks. For this analysis, MEG-source-based ROIs were included regardless of the frequency band from which they were derived, as it is argued that multiple frequency oscillations could emanate from the same region (Mantini et al., 2007). For instance, 1 beta source ROI, 1 gamma source ROI, and 2 high gamma source ROIs overlapped with the cingulo-opercular network, and these were examined together within one correlation matrix. ROIs included in these network-constrained correlation matrices are listed in **Table 7**.

Second, we focused on ROIs that were derived from the *same* MEG frequency band and *also* overlapped (>50% of voxels in each ROI) with the same network. Therefore, this analysis was limited to networks for which we found at least two MEG sources in the same band. Pairwise correlations were obtained for a total of nine of these sets of correlations (listed in **Table 8**). Between-group *t*-tests were performed for each pairwise correlation, and these were bonferroni-corrected for the number of multiple comparisons in each set, to a corrected $p < 0.05$.

RESULTS

MEG Fast-VESTAL Spectral Current Sources

We performed one-sample *t*-tests across all ASD subjects for the fast-VESTAL output for each frequency band. We applied a threshold to these group-level source maps in a voxel wise fashion at $p < 0.02$, and were then corrected for multiple comparisons at the cluster level to $p < 0.01$. Here we only report detailed results from the largest 10 clusters for each frequency band, although this level of correction resulted in the following number of clusters for each band: delta: 129, theta: 91, alpha: 84, beta: 128, low gamma: 19, and high gamma: 22. Anatomical labels, volumes, and MNI coordinates for the largest 10 clusters for each frequency band are listed in **Tables 1–6**.

FMRI Functional Connectivity among Regions Derived from MEG Amplitude Sources

Our first analysis compared the pairwise correlations of the BOLD signal among MEG-based ROIs in each frequency band of interest. For each of the six frequency bands, there were 10 ROIs, resulting in a 10 × 10 pairwise correlation matrix and a total of 45 between-group comparisons for each band. In this analysis, there were no significant between-group differences after strict bonferroni correction for multiple comparisons in each matrix (45), so we report results that passed an uncorrected $p < 0.05$. See **Tables 1–6** for reference of the anatomical locations of the numbered ROIs to which we refer in each frequency

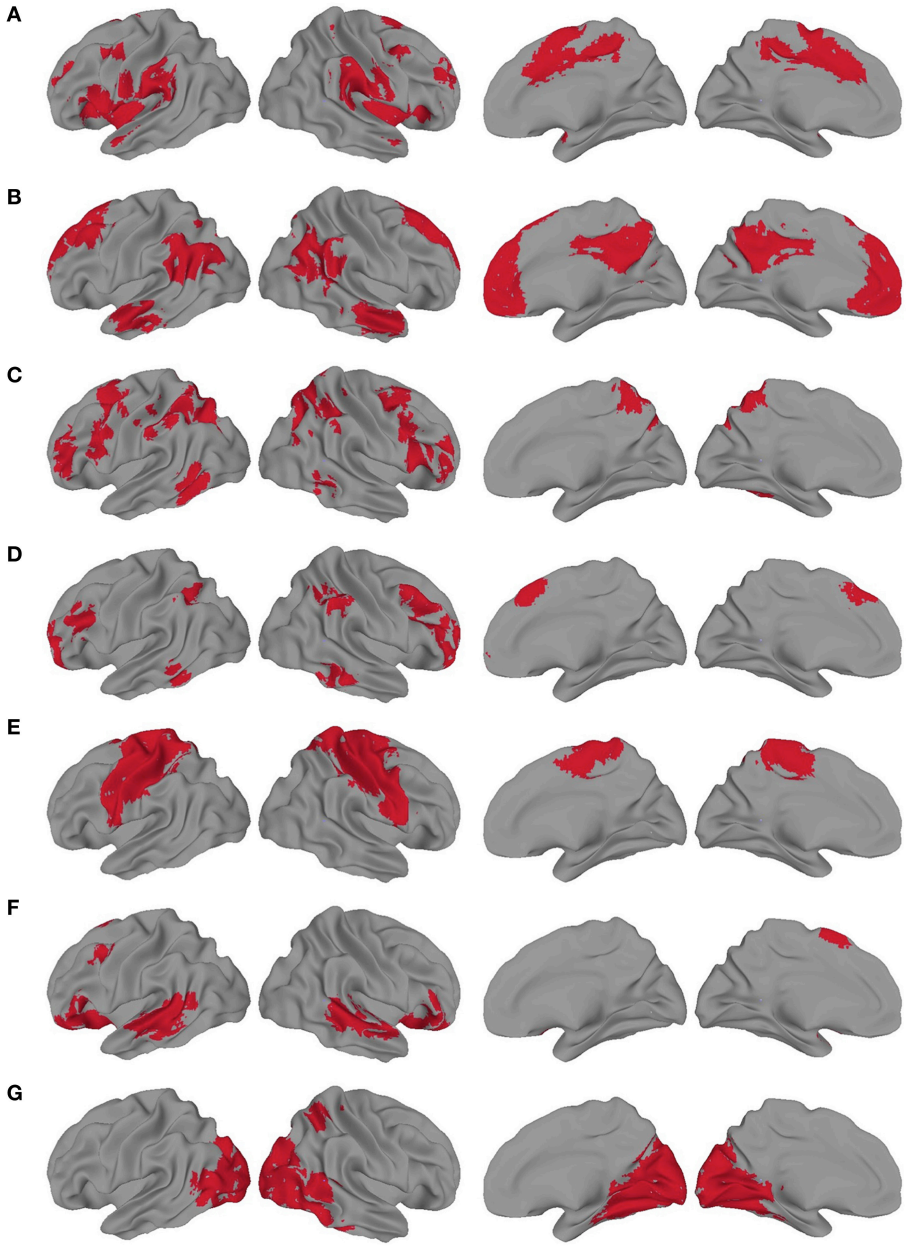

FIGURE 2 | Dilated network masks derived from the cortical parcellation from Gordon et al. (A) Cingulo-opercular, (B) Default mode network (DMN), (C) Dorsal Attention, (D) Frontoparietal, (E) Somatomotor, (F) Ventral attention, (G) Visual.

band. In the delta band, ASD showed hyperconnectivity between ROIs 1–4, 1–10, 6–10, and 7–10. Also in delta, ASD showed hypoconnectivity between ROIs 2–8, 2–9, 3–10, and 8–10. In theta, ASD showed hyperconnectivity between ROIs 1–7, 1–9, and 2–9, and hypoconnectivity between ROIs 4–6. In alpha, ASD showed hyperconnectivity between ROIs 1–2, 1–8, 1–10, 2–10, 3–10, and 8–10, and hypoconnectivity between ROIs 5–6, 5–9, and 5–10. In beta, ASD showed hyperconnectivity between ROIs 2–6, 4–10, and 6–8. In gamma, ASD showed hyperconnectivity between ROIs 2–3, 2–5, 4–7, 6–10, 7–10, and 9–10, and hypoconnectivity between ROIs 4–5. In high gamma, ASD showed hyperconnectivity between ROIs 1–4, and hypoconnectivity between ROIs 2–4, 2–9, 4–7, 7–8, and 8–10. See **Tables 1–6** and **Figure 3** for detailed summaries of these results.

The VESTAL-derived MEG amplitude sources overlapped with several of our dilated adaptations of the Gordon parcel communities. Details about the extent of these overlaps can be found in **Tables 1–6**. The 10 largest delta source clusters, totaling 842 voxels, overlapped with the following networks (each listed with number of overlapping voxels): DMN: 106, somatomotor: 80, visual: 280, frontoparietal: 18,

TABLE 1 | Delta band ROIs: Labels, Brodmann areas (BA), peak coordinates, size (voxels), and overlaps with networks.

ROI label	No. of voxels	Region	BA	x	y	z	DMN	SM	Vis	FP	Vent. attn.	Dor. attn.	C-O
1	134	L occipital	19	34	90	19	7 (5.2%)	0	120 (90%)	0	0	0	0
2	117	R precuneus	7	−18	78	52	0	0	51 (44%)	0	0	11 (9.4%)	0
3	106	R IPL	40	−66	39	28	44 (42%)	0	0	3 (2.8%)	0	2 (1.9%)	42 (40%)
4	83	L fusiform	37	49	69	−21	0	0	13 (16%)	5 (6%)	0	0	0
5	75	L SPL	7	28	69	61	21 (28%)	0	11 (15%)	0	0	5 (6.7%)	0
6	74	R IPL	40	−57	39	55	0	56 (76%)	0	0	0	10 (14%)	7 (9.5%)
7	73	R occipital	18	−24	99	1	0	0	61 (84%)	0	0	0	0
8	63	L cerebellum	7a	49	51	−48	0	0	0	0	0	0	0
9	60	R occipital	19	−42	84	22	13 (22%)	0	24 (40%)	0	0	0	0
10	57	L middle Frontal	9	−36	−37	46	21 (37%)	0	0	10 (18%)	0	2 (3.5%)	0

TABLE 2 | Theta band ROIs: Labels, Brodmann areas (BA), peak coordinates, size (voxels), and overlaps with networks.

ROI label	No. of voxels	Region	BA	x	y	z	DMN	SM	Vis	FP	Vent. attn.	Dor. attn.	C-O
1	58	L occ (V4)	18	43	84	−3	0	0	51 (88%)	0	0	0	0
2	46	L orbitofrontal	11	4	−37	−27	5 (11%)	0	0	0	0	0	0
3	44	L precentral	6	58	3	37	0	44 (100%)	0	0	0	6 (14%)	12 (27%)
4	43	R angular gyrus	39	−51	69	34	30 (70%)	0	0	0	0	0	0
5	36	R postcentral	2	−57	27	52	0	33 (92%)	0	0	0	1 (2.8%)	0
6	27	L V1	17	13	96	−18	0	0	7 (26%)	0	0	0	0
7	27	R IFG	46	−57	−31	19	0	0	0	7 (26%)	12 (44%)	2 (7.4%)	0
8	26	L ITG	20	58	36	−24	0	0	12 (46%)	8 (31%)	0	0	0
9	26	R middle frontal	6	−36	−1	43	11 (42%)	0	0	0	14 (54%)	12 (46%)	8 (31%)
10	24	L temporal pole	38	55	−10	−15	13 (54%)	0	0	0	0	0	7 (29%)

TABLE 3 | Alpha band ROIs: Labels, Brodmann areas (BA), peak coordinates, size (voxels), and overlaps with networks.

ROI Label	No. of voxels	Region	BA	x	y	z	DMN	SM	Vis	FP	Vent. attn.	Dor. attn.	C-O
1	88	L precentral	4	31	30	73	0	88 (100%)	0	0	0	8 (9.1%)	0
2	74	R Precentral	4	−42	15	52	0	72 (97%)	0	0	0	29 (39%)	6 (8.1%)
3	50	R occipital	18	−27	99	7	0	0	49 (98%)	0	0	0	0
4	42	L postcentral	2	49	33	58	0	13 (31%)	0	22 (52%)	0	0	22 (52%)
5	39	R cerebellum	8a	−12	69	−54	0	0	0	0	0	0	0
6	35	R angular gyrus	39	−54	60	34	32 (91%)	0	0	1 (2.9%)	0	1 (2.9%)	0
7	35	R precentral	6	−63	12	40	0	31 (89%)	0	0	0	0	6 (17%)
8	33	R precuneus	7	−21	78	49	0	0	19 (58%)	0	0	7 (21%)	0
9	31	L IPL	40	40	57	58	1 (3.2%)	0	4 (13%)	1 (3.2%)	0	4 (13%)	0
10	29	R precuneus	7	−3	54	67	0	5 (17%)	0	0	0	19 (66%)	0

ventral attention: 0, dorsal attention: 30, cingulo-operculum: 49. The 10 largest theta source clusters, totaling 357 voxels, overlapped with the following networks (each listed with number of overlapping voxels): DMN: 59, somatomotor: 93, visual: 70, frontoparietal: 15, ventral attention: 26, dorsal attention: 21, cingulo-operculum: 27. The largest alpha source clusters, totaling 456 voxels, overlapped with the following networks (each listed with number of overlapping voxels): DMN (33), somatomotor (224), visual (72), frontoparietal (24), dorsal attention (68), and cingulo-operculum (34). The 10 largest beta source clusters, totaling 734 voxels, overlapped with the following networks (each listed with number of overlapping voxels): DMN: 85, somatomotor: 331, visual: 46, frontoparietal: 35, ventral attention: 21, dorsal attention: 132, cingulo-operculum: 133. The 10 largest gamma source clusters, totaling 130 voxels, overlapped with the following networks (each listed with number of overlapping voxels): DMN: 9, somatomotor: 38, visual: 2, frontoparietal: 2, ventral attention: 0, dorsal attention: 20, cingulo-operculum: 16. The 10 largest high gamma source clusters, totaling 98 voxels, overlapped with the following networks (each listed with number of overlapping voxels): DMN: 10, somatomotor: 32, visual: 0, frontoparietal: 2, ventral attention: 0, dorsal attention: 7, cingulo-operculum: 15.

TABLE 4 | Beta band ROIs: Labels, Brodmann areas (BA), peak coordinates, size (voxels), and overlaps with networks.

ROI label	No. of voxels	Region	BA	x	y	z	DMN	SM	Vis	FP	Vent. attn.	Dor. attn.	C-O
1	121	R IPL	40	−45	45	46	1 (0.83%)	82 (68%)	0	0	0	68 (56%)	4 (3.3%)
2	98	R precentral	3	−45	18	55	1 (1%)	82 (84%)	0	0	1 (1%)	1 (1%)	13 (13%)
3	91	R STG	22	−60	−1	−6	13 (14%)	43 (47%)	0	0	3 (3.3%)	9 (9.9%)	29 (32%)
4	80	R IPL	40	−51	45	31	51 (64%)	1 (1.2%)	0	0	0	4 (5%)	30 (38%)
5	79	R mid frontal	9	−39	−22	34	1 (1.3%)	0	0	27 (34%)	15 (19%)	7 (8.9%)	4 (5.1%)
6	68	R SPL	7	−21	51	70	0	48 (71%)	0	0	0	39 (57%)	0
7	58	R/L cuneus	19	−6	90	28	0	0	43 (74%)	0	0	0	0
8	48	L IPL	2	43	30	43	0	46 (96%)	0	8 (17%)	0	4 (8.3%)	4 (8.3%)
9	46	L IPL	40	64	30	25	0	2 (4.3%)	0	0	0	0	46 (100%)
10	45	L pSTS	40	58	54	22	18 (40%)	0	3 (6.7%)	0	2 (4.4%)	0	3 (6.7%)

TABLE 5 | Gamma band ROIs: Labels, Brodmann areas (BA), peak coordinates, size (voxels), and overlaps with networks.

ROI label	No. of voxels	Region	BA	x	y	z	DMN	SM	Vis	FP	Vent. attn.	Dor. attn.	C-O
1	21	R precentral	6	−63	−1	31	0	20 (95%)	0	0	0	1 (4.8%)	1 (4.8%)
2	19	L postcentral	7	4	57	67	0	0	0	0	0	8 (42%)	0
3	15	R sup temporal	42	−66	30	16	0	0	0	0	0	0	4 (27%)
4	12	R cerebellum	7a	−48	45	−33	0	0	0	0	0	0	0
5	12	L mPFC	11	13	−61	−18	9 (75%)	0	0	2 (17%)	0	0	0
6	11	R ITG	20	−63	42	−24	0	0	0	0	0	0	0
7	11	R postcentral	7	−12	54	73	0	10 (91%)	0	0	0	9 (82%)	0
8	10	L pMTG	39	−57	69	13	0	0	2 (20%)	0	0	2 (20%)	0
9	10	L STG	22	64	36	16	0	0	0	0	0	0	6 (60%)
10	9	R postcentral	43	−66	9	19	0	8 (89%)	0	0	0	0	5 (56%)

TABLE 6 | High Gamma band ROIs: Labels, Brodmann areas (BA), peak coordinates, size (voxels), and overlaps with networks.

ROI label	No. of voxels	Region	BA	x	y	z	DMN	SM	Vis	FP	Vent. attn.	Dor. attn.	C-O
1	12	R med orbitofrontal	11	−12	−52	−24	2 (17%)	0	0	0	0	0	0
2	11	R cerebellum	8a	−33	45	−54	0	0	0	0	0	0	0
3	11	L precentral	6	25	12	73	0	9 (82%)	0	0	0	0	1 (9.1%)
4	10	L precuneus	7	4	69	64	0	0	0	0	0	1 (10%)	0
5	9	R inferior temporal	20	−63	39	−24	0	0	0	0	0	0	0
6	9	R SPL	7	−42	69	52	8 (89%)	0	0	0	0	0	0
7	9	R IPL	40	−54	39	58	0	0	0	0	0	3 (33%)	5 (56%)
8	9	L precentral	6	43	−1	58	0	5 (56%)	0	2 (22%)	0	3 (33%)	9 (100%)
9	9	L postcentral	1	49	27	61	0	9 (100%)	0	0	0	0	0
10	9	R postcentral	2	−42	36	67	0	9 (100%)	0	0	0	0	0

The first follow-up analysis included correlation matrices containing all ROIs overlapping with a specific network regardless of the MEG frequency band on which they were based. Overall, four networks overlapped with at least two ROIs each. Among the six ROIs that overlapped with the DMN (2 theta, 1 alpha, 1 beta, 1 gamma, 1 high gamma), there were no significant differences in connectivity between ASD and TD groups. Among the 16 ROIs that overlapped with the Somatomotor network (1 delta, 2 theta, 3 alpha, 4 beta, 3 gamma, 3 high gamma), there were three ROI pairs in which ASD showed *hypoconnectivity*: a delta to a high gamma ROI, theta to high gamma, and alpha to high gamma. Among the six ROIs that overlapped with the Visual network (2 delta, 1 theta, 2 alpha, 1 beta), there were no significant differences in connectivity between ASD and TD groups. Among the four ROIs that overlapped with the cingulo-operculum network (1 beta, 1 gamma, 2 high gamma), the ASD group showed *hypoconnectivity* between the gamma and a high gamma ROI. These results are further summarized in **Table 7** and **Figure 4**.

The second follow-up analysis looked only at correlations between sources that (a) were derived from the same MEG frequency band and (b) overlapped with the same network.

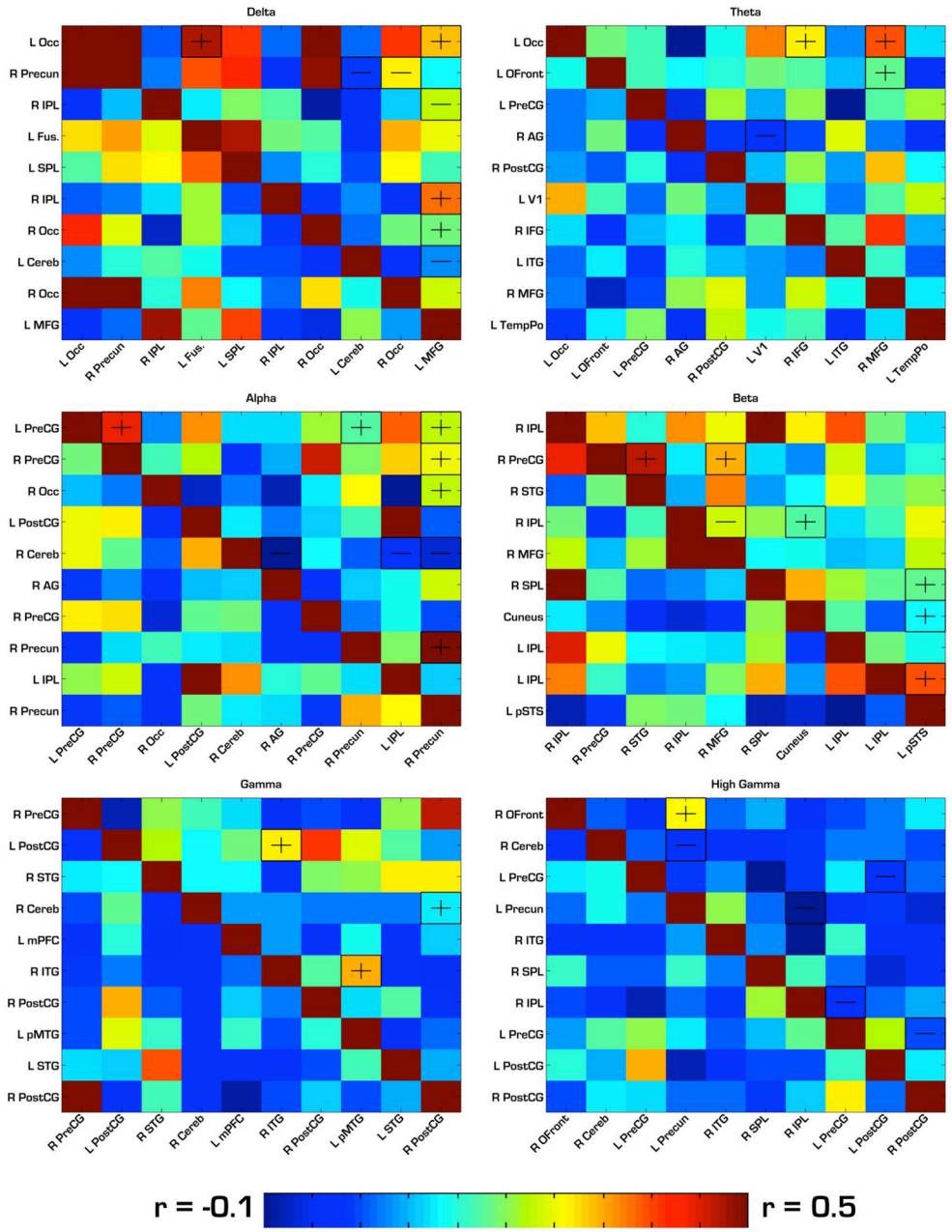

FIGURE 3 | Correlation matrices for ROIs derived from each frequency band. ASD correlations are in the top right triangle of each matrix, while TD correlations are in the bottom left. "−" and "+" indicates ROI pairs for which ASD trended toward hypo- or hyperconnectivity, respectively. In this first analysis, none of the group differences were significant after strict Bonferroni correction. Therefore, the group differences shown here had an uncorrected $p < 0.05$. Occ, Occipital; IPL, Inferior Parietal Lobule; SPL, Superior Parietal Lobule; PreCG, Precentral Gyrus; PostCG, Postcentral Gyrus; MFG, Middle Frontal Gyrus; Cereb, Cerebellum; Precun, Precuneus; STG, Superior Temporal Gyrus; MTG, Middle Temporal Gyrus; ITG, Inferior Temporal Gyrus; AG, Angular Gyrus; Ofront, Orbito Frontal Cortex; TempPo, Temporal Pole.

Overall, nine separate sets of correlations were performed based on this criteria. Three significant effects emerged from this analysis, all surviving bonferroni-correction for multiple comparisons at $p < 0.05$. In the ASD group, two alpha ROIs were *hyperconnected* to each other within the somatomotor network, two high gamma ROIs were *hypoconnected* to each other within the somatomotor network, and two high gamma ROIs were *hypoconnected* to each other within the cingulo-operculum network. See **Table 8** for a more detailed summary of results from this analysis.

TABLE 7 | ROIs used in network-constrained correlation matrices.

Network	Derived from MEG band	ROI label	Location	Percent overlap of ROI with network (%)
DMN	Theta	4	R angular gyrus	70
	Theta	10	L temporal pole	54
	Alpha	6	R angular gyrus	91
	Beta	4	R IPL	64
	Gamma	5	L mPFC	75
	High gamma	6	R SPL	89
Somatomotor	Delta	6	R IPL	76
	Theta	3	L precentral	100
	Theta	5	R postcentral	92
	Alpha	1	L precentral	100
	Alpha	2	R Precentral	97
	Alpha	7	R precentral	89
	Beta	1	R IPL	68
	Beta	2	R precentral	84
	Beta	6	R SPL	71
	Beta	8	L IPL	96
	Gamma	1	R precentral	95
	Gamma	7	R postcentral	91
	Gamma	10	R postcentral	89
	High gamma	3	L precentral	82
	High gamma	9	L postcentral	100
	High gamma	10	R postcentral	100
Visual	Delta	1	L occipital	90
	Delta	7	R occipital	84
	Theta	1	L occ (V4)	88
	Alpha	3	R occipital	98
	Alpha	8	R precuneus	58
	Beta	7	R/L cuneus	74
Cingulo-opercular	Beta	9	L IPL	100
	Gamma	9	L STG	60
	High gamma	7	R IPL	56
	High gamma	8	L precentral	100

DISCUSSION

The present study used a multimodal approach to investigate brain network dynamics in children with ASD, and provides new evidence for abnormal functional connectivity in cortical networks. The integration of both MEG and fMRI data collected during a resting state enabled groupwise comparisons of functional connectivity between MEG current sources for delta, theta, alpha, beta, and gamma bands. Our primary connectivity analysis was performed on fMRI data, while the ROIs derived from MEG amplitude-sources provided a novel framework within which to test that fMRI data. One advantage of this method is that MEG allowed us to localize important hubs of fast neuronal oscillations not normally detected with fMRI. Most studies define ROIs for connectivity analyses using data from task activation studies, anatomical atlases, meta-analyses, and data driven approaches such as independent component analyses. However, no study has explored the possibility of detecting novel differences between ASD and TD samples among regions that function as neuronal oscillatory generators. Another advantage is that the use of fMRI connectivity as an outcome measure allows us to compare our results to a large body of previous evidence. Unlike MEG, the literature on fcMRI in ASD is quite extensive.

Using a spectral MEG current source-modeling algorithm (fast-VESTAL) in resting state MEG scans, we found that the spatial distribution of spectral current sources in a group of ASD participants followed general patterns reported in a previous investigation of VESTAL-derived MEG sources in healthy adults (Huang et al., 2014). Alpha sources were highly concentrated in visual and somatosensory areas, in line with previous findings on both the mu rhythm and occipital alpha (Pfurtscheller et al., 2006; Bernier et al., 2007). Beta sources overlapped with some somatosensory alpha sources, but were concentrated in more anterior and fewer posterior regions compared to alpha. Low and high gamma sources showed a wider spatial distribution, including regions such as medial prefrontal cortex, precuneus, and inferior temporal gyrus.

To determine how the distribution of spectral MEG current sources compared to previously described resting state network structure, we looked at the number of voxels from each ROI that overlapped with an existing map of cortical parcel communities from Gordon et al. (2014). Delta ROIs overlapped largely with DMN and visual areas; theta ROIs overlapped somewhat evenly with DMN, visual, and somatomotor areas; alpha ROIs overlapped largely with somatomotor and visual areas; beta ROIs overlapped mostly with somatomotor areas, but also had considerable overlap with DMN, dorsal attention, and cingulo-opercular networks; gamma ROIs overlapped mostly with somatomotor, dorsal attention, and cingulo-opercular networks; and high gamma ROIs overlapped with somatomotor and cingulo-opercular networks. The pattern of activity that emerged was one where current sources of lower frequency bands (delta, theta) were found in areas associated with resting state activity, in line with electrophysiological findings on the DMN (Mantini et al., 2007). As expected, lower frequency sources were also found in primary sensory (visual and somatomotor) cortices (Pfurtscheller et al., 2006; Bernier et al., 2007). In contrast, higher frequency bands (beta, gamma, and high gamma) were associated with areas involved in higher-order sensory integration and attention regulation such as dorsal attention and cingulo-opercular networks. Notably, these sources were derived exclusively from an ASD group, yet they displayed a general distribution consistent with previous findings in healthy adults (Huang et al., 2014). This leaves open the possibility that, while MEG current sources have a typical distribution in ASD, there exist abnormalities in their functional, coordinated activity.

The results of our first analysis of functional connectivity in resting state fMRI data using seed ROIs based on MEG amplitude sources found pairs of regions showing trends toward differences between ASD and TD groups, although none proved statistically significant after correction for multiple comparisons. There was

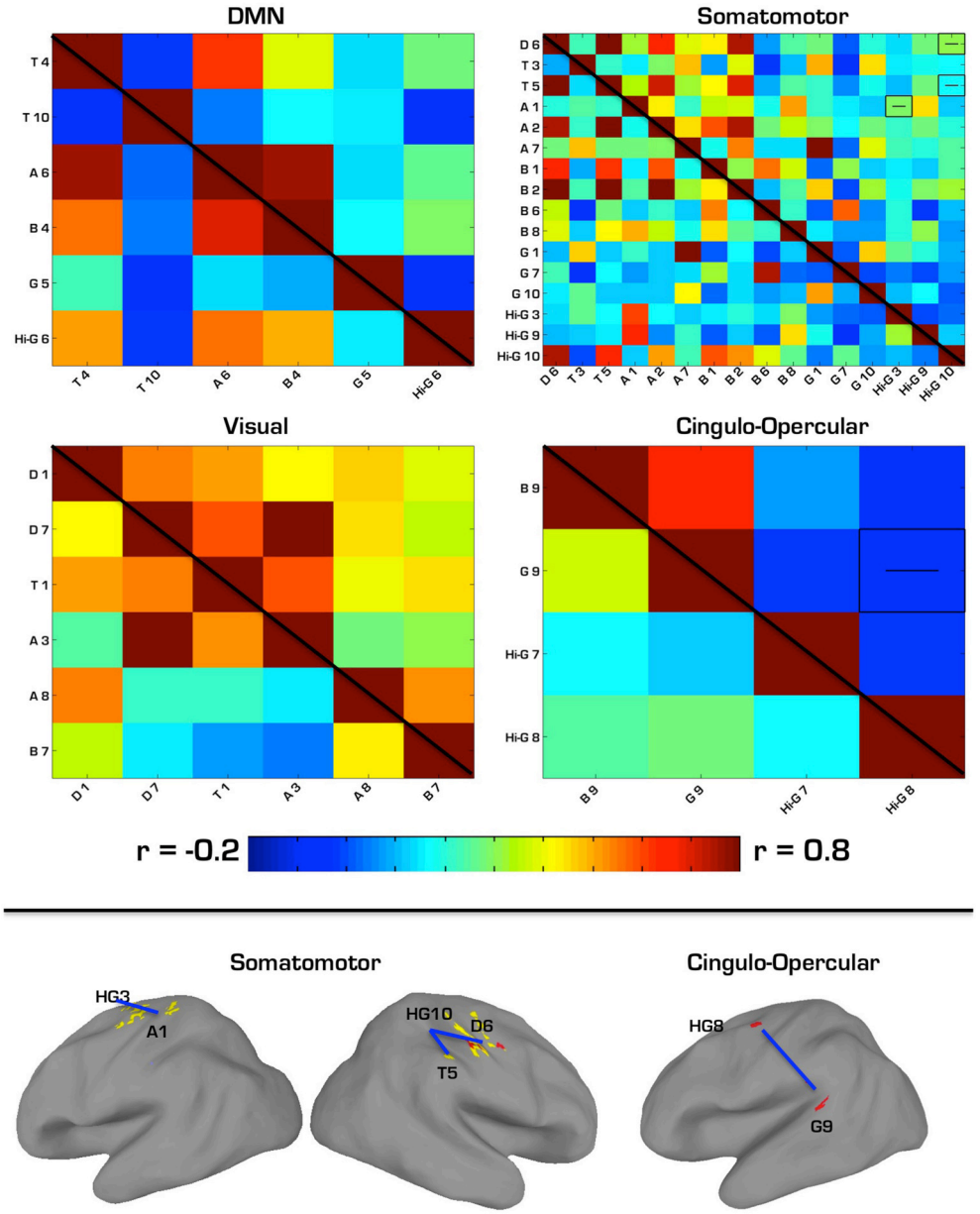

FIGURE 4 | (Top) Correlation matrices for network-constrained MEG source ROIs. ASD correlations are in the top right triangle of each matrix, while TD correlations are in the bottom left. Pairwise correlations with significant group differences ($p < 0.05$, Bonferroni corrected) are depicted by a "−" or "+" to indicate ASD hypo- or hyperconnectivity. Labels for each ROI correspond to the first letter of each ROI's frequency band, and the number it is associated with in **Tables 1–6**. **(Bottom)** Regions showing significant hypoconnectivity in ASD. Regions connected by blue lines correspond to those shown in the above correlation matrices as being hyperconnected.

a trend toward hyperconnectivity among alpha sources located in sensorimotor cortex, while an alpha source in the cerebellum showed a trend of hypoconnectivity to multiple regions in the parietal and temporal lobes. While not statistically significant in the present study, this trend is consistent with recent findings of cerebellum hypoconnectivity to supramodal cortical regions, including parietal and temporal regions (Khan et al., 2015).

We then performed two sets of follow-up correlation analyses based on the overlaps of our VESTAL-derived ROIs with previously described network structure. First, we looked at pairwise correlations between MEG-derived sources that overlapped with one of seven networks, based on the parcel communities described by Gordon et al. (2014). Unlike the first analysis, we used ROIs across any of the six frequency bands, as long as they overlapped with a network. This was done to highlight possible group differences in neural information encoding across multiple frequencies, in light of previous findings of abnormal coupling between different frequency

TABLE 8 | ROIs used in correlation matrices constrained by both network membership and frequency band of origin.

Network	Band	ROI label	Location	Percent overlap of ROI with network (%)	ASD vs. TD *P*-values for pairwise *r*
Visual	Delta	1	L occipital	90	0.14
		7	R occipital	84	
	Alpha	3	R occipital	98	0.4
		8	R precuneus	58	
DMN	Theta	4	R angular gyrus	70	0.82
		10	L temporal pole	54	
Somatomotor	Theta	3	L precentral	100	0.52
		5	R postcentral	92	
	Alpha	1	L precentral	100	0.01 (ROIs 1 and 2)
		2	R precentral	97	0.55 (ROIs 1 and 7)
		7	R precentral	89	0.10 (ROIs 2 and 7)
	Beta	1	R IPL	68	0.02 (1 and 2), 0.83 (1 and 6), 0.47 (1 and 8)
		2	R precentral	84	0.53 (2 and 6), 0.99 (2 and 8)
		6	R SPL	71	0.97 (6 and 8)
		8	L IPL	96	
	Gamma	1	R precentral	95	0.91 (1 and 7), 0.61 (1 and 10)
		7	R postcentral	91	0.25 (7 and 10)
		10	R postcentral	89	
	High gamma	3	L precentral	82	0.001 (3 and 9)
		9	L postcentral	100	0.43 (3 and 10)
		10	R postcentral	100	0.52 (9 and 10)
Cingulo-opercular	High gamma	7	R IPL	56	0.013
		8	L precentral	100	

bands in various disease states Voytek and Knight (2015). Hyperconnectivity of the BOLD signal between the MEG sources we identified could indicate problematic overcoupling between neuronal oscillations of different frequencies. Also unlike the first analysis, we found several between-group results that survived bonferroni correction for the number of pairwise correlations in each network's matrix. Within the somatomotor network, the ASD group showed *hypoconnectivity* in three ROIs based on high gamma MEG sources, including between a high gamma source in left postcentral gyrus to a delta source in right postcentral gyrus and to a theta source in right postcentral gyrus. Additionally, ASD was *hypoconnected* from a high gamma source in left precentral gyrus to an alpha source located more ventrally in left precentral gyrus. Within the cingulo-opercular network, the ASD group showed *hypoconnectivity* between a gamma ROI in right lateral visual cortex (V5) and a high gamma ROI in left precentral gyrus (Brodmann Area 6). In another follow-up fMRI correlation analysis, we further narrowed our focus to include only ROIs that overlapped with the same network and which were derived from the same MEG frequency band. ASD showed significant hypoconnectivity between two ROIs based on high-gamma sources within the somatomotor network. That group also showed hypoconnectivity between two other gamma ROIs (one low gamma and the other high gamma), which were instead located in the cingulo-operculum network. Thus, across both secondary analyses, there was a clear pattern of hypoconnectivity among many sources of gamma activity that overlapped with several networks. This pattern could represent the increased neural noise that is a consequence of dysfunctional inhibitory processing of GABAergic interneurons (Brock et al., 2002; Casanova et al., 2002; Brown et al., 2005; Wilson et al., 2007; Sun et al., 2012; Peiker et al., 2015). These stronger findings of within-network connectivity abnormalities support the notion of reduced within-network integration (Fair et al., 2009; Rudie et al., 2011, 2013; Fishman et al., 2014; Nebel et al., 2014), and recapitulate MEG and EEG findings on abnormal gamma connectivity, in ASD.

There were no significant differences between groups in any pairwise correlations among ROIs overlapping with the DMN, suggesting that electrophysiological activity may be relatively normal in ASD in this network. This is in contrast to some previous studies that have shown abnormal functional connectivity in DMN (Cherkassky et al., 2006; Monk et al., 2009; Lynch et al., 2013), but it could be the case that our VESTAL-derived MEG sources were located in unaffected sub regions of this network.

There are several limitations that call for caution in the interpretation of our results. First, we only collected MEG data from ASD subjects. It is possible that we would see a qualitatively different distribution of MEG amplitude sources if the VESTAL

algorithms were performed on TD participants alone, or on a combination of ASD and TD participants. However, many other studies, including the initial report of the VESTAL source localization technique (Huang et al., 2014), have found source distribution patterns in neurotypical individuals were similar to those displayed by our ASD sample. Thus, while the exact locations of some current sources may differ between groups, their overall similarity to previously observed typical patterns justifies the use of these sources as the basis for the rest of our analyses. Another caveat to these results is that the TD and ASD groups were scanned on magnets of differing strength: 3T and 1.5T, respectively. Although the acquisition parameters differed between these scanners, the larger voxel size, longer TR, longer total scan length for the 1.5T scans ensured that the signal-to-noise ratio was comparable between both groups. Finally, groups were not matched for IQ, with ASD showing a lower full score on the WASI. In a follow-up analysis, we used participant IQ as a covariate in the between-group *t*-tests of pairwise functional connectivity between sources. Of the eight source pairs showing significant group differences before accounting for IQ, two pairs still showed significant differences after doing so. These included an alpha to a high gamma source within the somatomotor network ($p = 0.019$, hypoconnected in ASD), and a theta to a beta source within the visual network ($p = 0.005$, hyperconnected in ASD). The persistence of these effects after controlling for IQ is evidence that, despite a low sample size and suboptimal group matching, this novel approach to integrating resting state MEG and fMRI data was still able to detect group differences in brain connectivity between ASD and TD individuals. Thus, this approach could inform future studies with larger, well-matched samples.

The present study demonstrates a novel approach to a multimodal investigation of brain connectivity in ASD. By using an MEG-amplitude source modeling technique as the basis for fcMRI analyses, we found further evidence supporting the notion of aberrant functional connectivity in ASD. This is also is the first study to report ASD hypoconnectivity of the BOLD signal specifically between sources of MEG gamma oscillations, providing supporting evidence that dysfunctional inhibitory processing mediated by gamma oscillations may play an important role in the neuroetiology of ASD.

AUTHOR CONTRIBUTIONS

MD collected fMRI and MEG data, preprocessed and analyzed data, and wrote much of the manuscript. RG collected MEG data, preprocessed MEG data, and contributed to the manuscript. MH contributed the VESTAL algorithm that was used to analyze MEG data, and trained other authors in the use of VESTAL. JP collected MEG data, advised during data preprocessing and analysis steps, and contributed to the manuscript.

ACKNOWLEDGMENTS

The authors would like to thank the following individuals for their assistance with participant recruitment, data collection and analysis for this study: Anne Marie Angeles, Nicolette Castro, Thomas Donoghue, Matthew Goodman, Mike Metke, Megan Kirchgessner, Nicole Mlynaryk, Ashley Swan, and Michael Widdowson. The authors would like to thank the UC San Diego Academic Senate for funding this work (RN038B-Pineda).

REFERENCES

American Psychiatric Association (APA) (2013). *Diagnostic and Statistical Manual of Mental Disorders, 5th Edn*. Arlington, VA: American Psychiatric Association.

Andersson, J. L. R., Jenkinson, M., and Smith, S. (2007). *Non-Linear Registration, Aka Spatial Normalisation FMRIB Technical Report TR07JA2*. FMRIB Analysis Group of the University of Oxford.

Arthurs, O., and Boniface, S. (2002). How well do we understand the neural origins of the fMRI BOLD signal? *Trends Neurosci.* 25, 27–31. doi: 10.1016/S0166-2236(00)01995-0

Barttfeld, P., Wicker, B., Cukier, S., Navarta, S., Lew, S., and Sigman, M. (2011). A big-world network in ASD: dynamical connectivity analysis reflects a deficit in long-range connections and an excess of short-range connections. *Neuropsychologia* 49, 254–263. doi: 10.1016/j.neuropsychologia.2010.11.024

Belmonte, M. K., Allen, G., Beckel-Mitchener, A., Boulanger, L. M., Carper, R. A., and Webb, S. J. (2004). Autism and abnormal development of brain connectivity. *J. Neurosci.* 24, 9228–9231. doi: 10.1523/JNEUROSCI.3340-04.2004

Bernier, R., Dawson, G., Webb, S., and Murias, M. (2007). EEG mu rhythm and imitation impairments in individuals with autism spectrum disorder. *Brain Cogn.* 64, 228–237. doi: 10.1016/j.bandc.2007.03.004

Biswal, B., Yetkin, F. Z., Haughton, V. M., and Hyde, J. S. (1995). Functional connectivity in the motor cortex of resting human brain using echo-planar MRI. *Magn. Reson. Med.* 34, 537–541.

Brock, J., Brown, C. C., Boucher, J., and Rippon, G. (2002). The temporal binding deficit hypothesis of autism. *Dev. Psychopathol.* 14, 209–224. doi: 10.1017/S0954579402002018

Brown, C., Gruber, T., Boucher, J., Rippon, G., and Brock, J. (2005). Gamma abnormalities during perception of illusory figures in autism. *Cortex* 41, 364–376. doi: 10.1016/S0010-9452(08)70273-9

Cardin, J. A., Carlén, M., Meletis, K., Knoblich, U., Zhang, F., Deisseroth, K., et al. (2009). Driving fast-spiking cells induces gamma rhythm and controls sensory responses. *Nature* 459, 663–667. doi: 10.1038/nature08002

Carper, R. A., and Courchesne, E. (2005). Localized enlargement of the frontal cortex in early autism. *Biol. Psychiatry* 57, 126–133. doi: 10.1016/j.biopsych.2004.11.005

Casanova, M. F., Buxhoeveden, D. P., Switala, A. E., and Roy, E. (2002). Minicolumnar pathology in autism. *Neurology* 58, 428–432. doi: 10.1212/WNL.58.3.428

Cherkassky, V. L., Kana, R. K., Keller, T. A., and Just, M. A. (2006). Functional connectivity in a baseline resting-state network in autism. *Neuroreport* 17, 1687–1690. doi: 10.1097/01.wnr.0000239956.45448.4c

Coghlan, S., Horder, J., Inkster, B., Mendez, M. A., Murphy, D. G., and Nutt, D. J. (2012). GABA system dysfunction in autism and related disorders: from synapse to symptoms. *Neurosci. Biobehav. Rev.* 36, 2044–2055. doi: 10.1016/j.neubiorev.2012.07.005

Conner, C. R., Ellmore, T. M., Pieters, T. A., Disano, M. A., and Tandon, N. (2011). Variability of the relationship between electrophysiology and BOLD-fMRI across cortical regions in humans. *J. Neurosci.* 31, 12855–12865. doi: 10.1523/JNEUROSCI.1457-11.2011

Courchesne, E., and Pierce, K. (2005). Why the frontal cortex in autism might be talking only to itself: local over-connectivity but long-distance disconnection. *Curr. Opin. Neurobiol.* 15, 225–230. doi: 10.1016/j.conb.2005.03.001

Cox, R. W. (1996). AFNI: software for analysis and visualization of functional magnetic resonance neuroimages. *Comput. Biomed. Res.* 29, 162–173.

Dale, A. M., and Halgren, E. (2001). Spatiotemporal mapping of brain activity by integration of multiple imaging modalities. *Curr. Opin. Neurobiol.* 11, 202–208. doi: 10.1016/S0959-4388(00)00197-5

Dale, A. M., Liu, A. K., Fischl, B. R., Buckner, R. L., Belliveau, J. W., Lewine, J. D., et al. (2000). Dynamic statistical parametric mapping: combining fMRI and MEG for high-resolution imaging of cortical activity. *Neuron* 26, 55–67. doi: 10.1016/S0896-6273(00)81138-1

Fair, D. A., Cohen, A. L., Power, J. D., Dosenbach, N. U., Church, J. A., Miezin, F. M., et al. (2009). Functional brain networks develop from a "local to distributed" organization. *PLoS Comput. Biol.* 5:e1000381. doi: 10.1371/journal.pcbi.1000381

Fishman, I., Keown, C. L., Lincoln, A. J., Pineda, J. A., and Müller, R. A. (2014). Atypical cross talk between mentalizing and mirror neuron networks in autism spectrum disorder. *JAMA Psychiatry* 71, 751–760. doi: 10.1001/jamapsychiatry.2014.83

Gordon, E. M., Laumann, T. O., Adeyemo, B., Huckins, J. F., Kelley, W. M., and Petersen, S. E. (2014). Generation and evaluation of a cortical area parcellation from resting-state correlations. *Cereb. Cortex* 26, 288–303. doi: 10.1093/cercor/bhu239

Hahamy, A., Behrmann, M., and Malach, R. (2015). The idiosyncratic brain: distortion of spontaneous connectivity patterns in autism spectrum disorder. *Nat. Neurosci.* 18, 302–309. doi: 10.1038/nn.3919

Hensch, T. K. (2005). Critical period plasticity in local cortical circuits. *Nat. Rev. Neurosci.* 6, 877–888. doi: 10.1038/nrn1787

Huang, M. X., Huang, C. W., Robb, A., Angeles, A., Nichols, S. L., Baker, D. G., et al. (2014). MEG source imaging method using fast L1 minimum-norm and its applications to signals with brain noise and human resting-state source amplitude images. *Neuroimage* 84, 585–604. doi: 10.1016/j.neuroimage.2013.09.022

Iramina, K., Ueno, S., and Matsuoka, S. (1996). MEG and EEG topography of frontal midline theta rhythm and source localization. *Brain Topogr.* 8, 329–331. doi: 10.1007/BF01184793

Jenkinson, M., Beckmann, C. F., Behrens, T. E., Woolrich, M. W., and Smith, S. M. (2012). FSL. *Neuroimage* 62, 782–790. doi: 10.1016/j.neuroimage.2011.09.015

Jensen, O., Goel, P., Kopell, N., Pohja, M., Hari, R., and Ermentrout, B. (2005). On the human sensorimotor-cortex beta rhythm: sources and modeling. *Neuroimage* 26, 347–355. doi: 10.1016/j.neuroimage.2005.02.008

Just, M. A., Cherkassky, V. L., Keller, T. A., Kana, R. K., and Minshew, N. J. (2007). Functional and anatomical cortical underconnectivity in autism: evidence from an FMRI study of an executive function task and corpus callosum morphometry. *Cereb. Cortex* 17, 951–961. doi: 10.1093/cercor/bhl006

Just, M. A., Cherkassky, V. L., Keller, T. A., and Minshew, N. J. (2004). Cortical activation and synchronization during sentence comprehension in high-functioning autism: evidence of underconnectivity. *Brain* 127, 1811–1821. doi: 10.1093/brain/awh199

Kana, R. K., Keller, T. A., Cherkassky, V. L., Minshew, N. J., and Just, M. A. (2006). Sentence comprehension in autism: thinking in pictures with decreased functional connectivity. *Brain* 129, 2484–2493. doi: 10.1093/brain/awl164

Kana, R. K., Keller, T. A., Minshew, N. J., and Just, M. A. (2007). Inhibitory control in high-functioning autism: decreased activation and underconnectivity in inhibition networks. *Biol. Psychiatry* 62, 198–206. doi: 10.1016/j.biopsych.2006.08.004

Keown, C. L., Shih, P., Nair, A., Peterson, N., Mulvey, M. E., and Müller, R. A. (2013). Local functional overconnectivity in posterior brain regions is associated with symptom severity in autism spectrum disorders. *Cell Rep.* 5, 567–572. doi: 10.1016/j.celrep.2013.10.003

Khan, A. J., Nair, A., Keown, C. L., Datko, M. C., Lincoln, A. J., and Müller, R. A. (2015). Cerebro-cerebellar resting-state functional connectivity in children and adolescents with autism spectrum disorder. *Biol. Psychiatry* 78, 625–634. doi: 10.1016/j.biopsych.2015.03.024

Liu, Z., Ding, L., and He, B. (2006). Integration of EEG/MEG with MRI and fMRI. *IEEE Eng. Med. Biol. Mag.* 25, 46–53. doi: 10.1109/MEMB.2006.1657787

Logothetis, N. K. (2002). The neural basis of the blood–oxygen–level–dependent functional magnetic resonance imaging signal. *Philos. Trans. R. Soc. Lond. B Biol. Sci.* 357, 1003–1037. doi: 10.1098/rstb.2002.1114

Logothetis, N. K. (2003). MR imaging in the non-human primate: studies of function and of dynamic connectivity. *Curr. Opin. Neurobiol.* 13, 630–642. doi: 10.1016/j.conb.2003.09.017

Logothetis, N. K. (2008). What we can do and what we cannot do with fMRI. *Nature* 453, 869–878. doi: 10.1038/nature06976

Logothetis, N. K., Pauls, J., Augath, M., Trinath, T., and Oeltermann, A. (2001). Neurophysiological investigation of the basis of the fMRI signal. *Nature* 412, 150–157. doi: 10.1038/35084005

Logothetis, N. K., and Wandell, B. A. (2004). Interpreting the BOLD signal. *Annu. Rev. Physiol.* 66, 735–769. doi: 10.1146/annurev.physiol.66.082602.092845

Lynch, C. J., Uddin, L. Q., Supekar, K., Khouzam, A., Phillips, J., and Menon, V. (2013). Default mode network in childhood autism: posteromedial cortex heterogeneity and relationship with social deficits. *Biol. Psychiatry* 74, 212–219. doi: 10.1016/j.biopsych.2012.12.013

Mantini, D., Perrucci, M. G., Del Gratta, C., Romani, G. L., and Corbetta, M. (2007). Electrophysiological signatures of resting state networks in the human brain. *Proc. Natl. Acad. Sci. U.S.A.* 104, 13170–13175. doi: 10.1073/pnas.0700668104

Mizuno, A., Villalobos, M. E., Davies, M. M., Dahl, B. C., and Müller, R. A. (2006). Partially enhanced thalamocortical functional connectivity in autism. *Brain Res.* 1104, 160–174. doi: 10.1016/j.brainres.2006.05.064

Monk, C. S., Peltier, S. J., Wiggins, J. L., Weng, S. J., Carrasco, M., Risi, S., et al. (2009). Abnormalities of intrinsic functional connectivity in autism spectrum disorders. *Neuroimage* 47, 764–772. doi: 10.1016/j.neuroimage.2009.04.069

Müller, R. A., Shih, P., Keehn, B., Deyoe, J. R., Leyden, K. M., and Shukla, D. K. (2011). Underconnected, but how? A survey of functional connectivity MRI studies in autism spectrum disorders. *Cereb. Cortex* 21, 2233–2243. doi: 10.1093/cercor/bhq296

Nebel, M. B., Joel, S. E., Muschelli, J., Barber, A. D., Caffo, B. S., Pekar, J. J., et al. (2014). Disruption of functional organization within the primary motor cortex in children with autism. *Hum. Brain Mapp.* 35, 567–580. doi: 10.1002/hbm.22188

Noonan, S. K., Haist, F., and Müller, R. A. (2009). Aberrant functional connectivity in autism: evidence from low-frequency BOLD signal fluctuations. *Brain Res.* 1262, 48–63. doi: 10.1016/j.brainres.2008.12.076

Peiker, I., David, N., Schneider, T. R., Nolte, G., Schöttle, D., and Engel, A. K. (2015). Perceptual integration deficits in autism spectrum disorders are associated with reduced interhemispheric gamma-band coherence. *J. Neurosci.* 35, 16352–16361. doi: 10.1523/JNEUROSCI.1442-15.2015

Pérez Velázquez, J. L., and Galán, R. F. (2013). Information gain in the brain's resting state: a new perspective on autism. *Front. Neuroinform.* 7:37. doi: 10.3389/fninf.2013.00037

Pfurtscheller, G., Brunner, C., Schlögl, A., and Da Silva, F. L. (2006). Mu rhythm (de) synchronization and EEG single-trial classification of different motor imagery tasks. *Neuroimage* 31, 153–159. doi: 10.1016/j.neuroimage.2005.12.003

Power, J. D., Barnes, K. A., Snyder, A. Z., Schlaggar, B. L., and Petersen, S. E. (2012). Spurious but systematic correlations in functional connectivity MRI networks arise from subject motion. *Neuroimage* 59, 2142–2154. doi: 10.1016/j.neuroimage.2011.10.018

Robertson, C. E., Ratai, E. M., and Kanwisher, N. (2016). Reduced GABAergic action in the autistic brain. *Curr. Biol.* 26, 80–85. doi: 10.1016/j.cub.2015.11.019

Rosenberg, A., Patterson, J. S., and Angelaki, D. E. (2015). A computational perspective on autism. *Proc. Natl. Acad. Sci. U.S.A.* 112, 9158–9165. doi: 10.1073/pnas.1510583112

Rosvall, M., and Bergstrom, C. T. (2008). Maps of random walks on complex networks reveal community structure. *Proc. Natl. Acad. Sci. U.S.A* 105, 1118–1123. doi: 10.1073/pnas.0706851105

Rudie, J. D., Brown, J. A., Beck-Pancer, D., Hernandez, L. M., Dennis, E. L., Thompson, P. M., et al. (2013). Altered functional and structural brain network organization in autism. *Neuroimage Clin.* 2, 79–94. doi: 10.1016/j.nicl.2012.11.006

Rudie, J. D., Shehzad, Z., Hernandez, L. M., Colich, N. L., Bookheimer, S. Y., Iacoboni, M., et al. (2011). Reduced functional integration and segregation of distributed neural systems underlying social and emotional information processing in autism spectrum disorders. *Cereb. Cortex* 22, 1025–1037. doi: 10.1093/cercor/bhr171

Rutter, M., DiLavore, P. C., Risi, S., Gotham, K., and Bishop, S. (2012). *Autism Diagnostic Observation Schedule: ADOS-2*. Los Angeles, CA: Western Psychological Services.

Salmelin, R., and Baillet, S. (2009). Electromagnetic brain imaging. *Hum. Brain Mapp.* 30, 1753–1757. doi: 10.1002/hbm.20795

Shih, P., Keehn, B., Oram, J. K., Leyden, K. M., Keown, C. L., and Müller, R. A. (2011). Functional differentiation of posterior superior temporal sulcus in autism: a functional connectivity magnetic resonance imaging study. *Biol. Psychiatry* 70, 270–277. doi: 10.1016/j.biopsych.2011.03.040

Shih, P., Shen, M., Öttl, B., Keehn, B., Gaffrey, M. S., and Müller, R. A. (2010). Atypical network connectivity for imitation in autism spectrum disorder. *Neuropsychologia* 48, 2931–2939. doi: 10.1016/j.neuropsychologia.2010.05.035

Song, T., Gaa, K., Cui, L., Feffer, L., Lee, R. R., and Huang, M. (2008). Evaluation of signal space separation via simulation. *Med. Biol. Eng. Comput.* 46, 923–932. doi: 10.1007/s11517-007-0290-y

Sun, L., Grützner, C., Bölte, S., Wibral, M., Tozman, T., Schlitt, S., et al. (2012). Impaired gamma-band activity during perceptual organization in adults with autism spectrum disorders: evidence for dysfunctional network activity in frontal-posterior cortices. *J. Neurosci.* 32, 9563–9573. doi: 10.1523/JNEUROSCI.1073-12.2012

Supekar, K., Uddin, L. Q., Khouzam, A., Phillips, J., Gaillard, W. D., Kenworthy, L. E., et al. (2013). Brain hyperconnectivity in children with autism and its links to social deficits. *Cell Rep.* 5, 738–747. doi: 10.1016/j.celrep.2013.10.001

Taulu, S., Kajola, M., and Simola, J. (2004b). Suppression of interference and artifacts by the signal space separation method. *Brain Topogr.* 16, 269–275. doi: 10.1023/B:BRAT.0000032864.93890.f9

Taulu, S., Simola, J., and Kajola, M. (2004a). MEG recordings of DC fields using the signal space separation method (SSS). *Neurol. Clin. Neurophysiol.* 2004:35.

Taulu, S., Simola, J., and Kajola, M. (2005). Applications of the signal space separation method. *IEEE Trans. Signal Process.* 53, 3359–3372. doi: 10.1109/TSP.2005.853302

Turner, K. C., Frost, L., Linsenbardt, D., McIlroy, J. R., and Müller, R. A. (2006). Atypically diffuse functional connectivity between caudate nuclei and cerebral cortex in autism. *Behav. Brain Funct.* 2, 1. doi: 10.1186/1744-9081-2-34

Vissers, M. E., Cohen, M. X., and Geurts, H. M. (2012). Brain connectivity and high functioning autism: a promising path of research that needs refined models, methodological convergence, and stronger behavioral links. *Neurosci. Biobehav. Rev.* 36, 604–625. doi: 10.1016/j.neubiorev.2011.09.003

Voytek, B., and Knight, R. T. (2015). Dynamic network communication as a unifying neural basis for cognition, development, aging, and disease. *Biol. Psychiatry* 77, 1089–1097. doi: 10.1016/j.biopsych.2015.04.016

Welchew, D. E., Ashwin, C., Berkouk, K., Salvador, R., Suckling, J., Baron-Cohen, S., et al. (2005). Functional disconnectivity of the medial temporal lobe in Asperger's syndrome. *Biol. Psychiatry* 57, 991–998. doi: 10.1016/j.biopsych.2005.01.028

Wilson, T. W., Rojas, D. C., Reite, M. L., Teale, P. D., and Rogers, S. J. (2007). Children and adolescents with autism exhibit reduced MEG steady-state gamma responses. *Biol. Psychiatry* 62, 192–197. doi: 10.1016/j.biopsych.2006.07.002

Conflict of Interest Statement: The authors declare that the research was conducted in the absence of any commercial or financial relationships that could be construed as a potential conflict of interest.

frontiers in Neuroscience

ORIGINAL RESEARCH
published: 29 June 2016
doi: 10.3389/fnins.2016.00306

One-Class Support Vector Machines Identify the Language and Default Mode Regions As Common Patterns of Structural Alterations in Young Children with Autism Spectrum Disorders

Alessandra Retico[1]*, *Ilaria Gori*[1,2], *Alessia Giuliano*[1,3], *Filippo Muratori*[4,5] and *Sara Calderoni*[4]

[1] Pisa Division, National Institute for Nuclear Physics, Pisa, Italy, [2] Department of Chemistry and Pharmacy, University of Sassari, Sassari, Italy, [3] Department of Physics, University of Pisa, Pisa, Italy, [4] Department of Developmental Neuroscience, IRCCS Stella Maris Foundation, Pisa, Italy, [5] Department of Clinical and Experimental Medicine, University of Pisa, Pisa, Italy

OPEN ACCESS

Edited by:
Roma Siugzdaite, Ghent University, Belgium

Reviewed by:
Luca Faes, University of Trento, Italy
Suhash Chakraborty, Hindustan Aeronautics Limited Hospital, India
Corrado Corradi-Dell'Acqua, University of Geneva, Switzerland

***Correspondence:**
Alessandra Retico
alessandra.retico@pi.infn.it

Specialty section:
This article was submitted to Child and Adolescent Psychiatry, a section of the journal Frontiers in Neuroscience

Received: *01 February 2016*
Accepted: *16 June 2016*
Published: *29 June 2016*

Citation:
Retico A, Gori I, Giuliano A, Muratori F and Calderoni S (2016) One-Class Support Vector Machines Identify the Language and Default Mode Regions As Common Patterns of Structural Alterations in Young Children with Autism Spectrum Disorders. Front. Neurosci. 10:306. doi: 10.3389/fnins.2016.00306

The identification of reliable brain endophenotypes of autism spectrum disorders (ASD) has been hampered to date by the heterogeneity in the neuroanatomical abnormalities detected in this condition. To handle the complexity of neuroimaging data and to convert brain images in informative biomarkers of pathology, multivariate analysis techniques based on Support Vector Machines (SVM) have been widely used in several disease conditions. They are usually trained to distinguish patients from healthy control subjects by making a binary classification. Here, we propose the use of the One-Class Classification (OCC) or Data Description method that, in contrast to two-class classification, is based on a description of one class of objects only. This approach, by defining a multivariate normative rule on one class of subjects, allows recognizing examples from a different category as outliers. We applied the OCC to 314 regional features extracted from brain structural Magnetic Resonance Imaging (MRI) scans of young children with ASD (21 males and 20 females) and control subjects (20 males and 20 females), matched on age [range: 22–72 months of age; mean = 49 months] and non-verbal intelligence quotient (NVIQ) [range: 31–123; mean = 73]. We demonstrated that a common pattern of features characterize the ASD population. The OCC SVM trained on the group of ASD subjects showed the following performances in the ASD vs. controls separation: the area under the receiver operating characteristic curve (AUC) was 0.74 for the male and 0.68 for the female population, respectively. Notably, the ASD vs. controls discrimination results were maximized when evaluated on the subsamples of subjects with NVIQ $\geq$ 70, leading to AUC = 0.81 for the male and AUC = 0.72 for the female populations, respectively. Language regions and regions from the default mode network—posterior cingulate cortex, pars opercularis and pars triangularis of the inferior frontal gyrus, and transverse temporal gyrus—contributed most to distinguishing

individuals with ASD from controls, arguing for the crucial role of these areas in the ASD pathophysiology. The observed brain patterns associate preschoolers with ASD independently of their age, gender and NVIQ and therefore they are expected to constitute part of the ASD brain endophenotype.

Keywords: features classification, One-class support vector machine, Brain Magnetic Resonance Imaging (MRI), autism spectrum disorders, preschool children

INTRODUCTION

Different approaches have been proposed to date to explore the clinical (Grzadzinski et al., 2013), genetic (De Rubeis and Buxbaum, 2015), and neurobiological (Hernandez et al., 2015) heterogeneity of Autism Spectrum Disorders (ASD), which are complex neurodevelopmental conditions affecting 1 in 68 children in USA (Centers for Disease Control Prevention, 2014), and are characterized by impairment in socio-communicative abilities, as well as restricted and stereotyped behaviors (American Psychiatric Association, 2013). The non-invasive and non-harmful Magnetic Resonance Imaging (MRI) is a promising tool to study and characterize ASD, as it allows the *in vivo* observation of the brain involvement in the disorder. Several post-processing methods to analyze brain MRI data were developed and a wide range of studies aimed to explore the predictive power of MRI by comparing the brain characteristics of patients with ASD and controls with the final aim of identifying reliable markers of ASD diagnosis (Ecker et al., 2010a,b; Jiao et al., 2010; Ingalhalikar et al., 2011; Calderoni et al., 2012; Wee et al., 2014; Zhou et al., 2014; Gori et al., 2015; Retico et al., 2016).

Machine-learning techniques, e.g., those based on support vector machines (SVMs; Vapnik, 1995), have been shown to be valuable tools to make predictive diagnoses in single subjects in a large variety of psychiatric and neurodevelopmental disorders (Wolfers et al., 2015), including ASD (Retico et al., 2014). They can be implemented for diagnosis prediction, for assessment of the disease progression and to evaluate the treatment effectiveness (Orrù et al., 2012). Machine learning refers to all procedures where the learning by example paradigm is implemented. In most cases conventional binary (also called two-class) classification algorithms are applied to image features to classify an unknown object into one of two pre-defined categories. The classification is particularly challenging when dealing with psychiatric disorders, as the reported neuroanatomical alterations are often very small and quite un-replicated among different studies. Subtle signs of pathology are difficult to catch especially in extremely heterogeneous conditions such as ASD.

In the present study, we propose the use of the One-Class Classification (OCC) or Data Description method (Moya et al., 1993), which, in contrast to two-class classification, makes a description of a single class of objects only (referred to as the positive class or target class) and detects which (new) objects resemble this target class, thus distinguishing them from examples considered outliers. Using OCC instead of two-class classification methods in standard binary classification problems, where objects from both the classes are at disposal, could result in worse recognition accuracy, as the complete knowledge encoded in the available training set is not fully exploited. However, OCC could provide more robustness in case of difficulties embedded in the nature of data, since they seek to describe properties of the target class instead of minimizing the classification error. Therefore, in case of difficult datasets (e.g., when the positive class is well-characterized, whereas the negative class is not sufficiently representative of the negative population) it could be useful to transform the binary classification problem into an OCC task.

The usefulness of OCC in the biomedical domain was already proved in a number of applications, e.g., the automatic recognition of the hypertension type (Krawczyk and Woźniak, 2015) or breast cancer biopsy and 3D optical coherence tomography (OCT) retinal image classification (Zhang et al., 2014) and on brain MRI data. In the latter domain OCC were implemented to learn multivariate normative rules on a group of healthy individuals, thus allowing the interpretation of the distance to the OCC boundary as an abnormality score (Mourão-Miranda et al., 2011; Sato et al., 2012a,b). Working on both voxel- and region-based features, Mourão-Miranda et al. (2011) investigated whether patterns of fMRI response to sad facial expressions in depressed patients would be classified as outliers in relation to patterns of healthy control subjects. They interestingly found out that most patients classified as non-outliers responded to treatments and most patients classified as outliers did not respond to treatments. Sato et al. (2012b) obtained an OCC-based abnormality index analyzing functional connectivity patterns of adults and children with Attention Deficit and Hyperactivity Disorder (ADHD), and found out that the ADHD patients differ significantly from the age-matched control group, showing instead stronger similarity to the group of younger control subjects.

We analyzed with OCC the features extracted from brain structural MRI data in order to measure the OCC performance in the discrimination of patients with ASD with respect to controls in the preschool age. Moreover, we used the OCC to define multivariate normative rules, i.e., we investigated the distribution of patterns of brain structures in control subjects to test the homogeneity of the latter sample and its potential to enable the definition of a robust boundary in relation to which the patients with ASD would be classified as outliers. To carry out a symmetry test, we investigated also whether a consistent neuroanatomical pattern among the ASD patients allows the definition of a robust boundary in relation to which the controls are classified as outliers.

Finally, the relative contribution of the anatomical brain features to the decision function was studied to localize the

regions more involved in the one-class classifier boundary definition. To this purpose we extended to the case of OCC the previous literature referring to the generation of a *preimage* when non-linear kernel SVM are used to localize the relevant brain features (Schölkopf et al., 1999). Moreover, the permutation testing usually implemented in two-class classification problems (Mourão-Miranda et al., 2005; Wanh et al., 2007; Gaonkar and Davatzikos, 2013; Gori et al., 2015) was extended to the OCC formulation to allow assigning a statistical significance both to the classification performances and to the brain features contributing most to the OCC boundary definition.

MATERIALS AND METHODS

Participants and MRI Data Acquisition

A group of 21 male and 20 female preschoolers with ASD [mean age ± standard deviation (*SD*) = 49 ± 12 months; age range = 28–70 months] and a group of 40 control subjects matched by gender, age, non-verbal IQ (NVIQ), and socioeconomic status were selected for this case-control study (see **Table 1**).

Participants in the ASD group were recruited at the ASD Unit of IRCCS Stella Maris Foundation (Pisa), a tertiary hospital and research university in Italy. They were rigorously diagnosed with ASD according to the DSM-IV-TR criteria (American Psychiatric Association, 2000) by a multidisciplinary team including a senior child psychiatrist, an experienced clinical child psychologist and a speech–language pathologist during 3–5 days of extensive evaluation, and confirmed by the ADOS-G (Lord et al., 2000) administrated by clinical psychologists who met standard requirements for research reliability. ASD patients were included if their age was between 2 and 6 years and their NVIQ ≥ 30. Exclusion criteria were: (a) anomalies detected by MRI (b) neurological syndromes or focal neurological signs; (c) significant sensory impairment (e.g., blindness, deafness); (d) anamnesis of birth asphyxia, premature birth, or epilepsy; (e) use of any psychotropic medication; (f) absence of major dysmorphic features including microcephaly or macrocephaly; and (g) potential secondary causes of ASD determined by high-resolution karyotyping, DNA analysis of Fragile-X, or screening tests for inborn errors of metabolism (plasma and urine aminoacid analysis, urine organic acid measurement, urine mucopolysaccarides quantitation, plasma and urine creatine, and guanidinoacetate analysis). The control group was composed of 20 preschoolers with idiopathic developmental delay (DD), i.e., with NVIQ score < 70, and 20 preschoolers without developmental delay (noDD), i.e., with NVIQ score ≥ 70, recruited at the same hospital. Subjects with DD were included within the control group in order to obtain a match for NVIQ between patients and controls, as well as to increase the size of the data sample under investigation. The diagnosis of idiopathic DD was made after a negative thorough assessment for underlying causes, including audiometry, thyroid hormone disorders, high-resolution karyotyping, DNA analysis of Fragile-X and screening tests for inborn errors of metabolism. The control group was selected so as to meet the same exclusionary criteria as the ASD patients—except the criterion (g) specified above—with the further requirements of exclusion of ASD diagnosis (performed

TABLE 1 | Dataset composition and sample characteristics.

Variable	Subject group, mean ± std [range]							
	ASD (*n* = 41)				Controls (*n* = 40)			
Age (months)	49 ± 12 [28–70]				49± 14 [22–72]			
NVIQ	73 ± 22 [34–113]				73 ± 23 [31–123]			
	Males (*n* = 21)		Females (*n* = 20)		Males (*n* = 20)		Females (*n* = 20)	
Age (months)	50 ± 10 [34–70]		48 ± 13 [28 – 69]		48 ± 13 [24–70]		50 ± 16 [22–72]	
NVIQ	75 ± 22 [40–113]		70 ± 23 [34–113]		73 ± 23 [32–123]		72 ± 24 [31–106]	
	DD (*n* = 9)	no-DD (*n* = 12)	DD (*n* = 10)	no-DD (*n* = 10)	DD (*n* = 10)	no-DD (*n* = 10)	DD (*n* = 10)	no-DD (*n* = 10)
Age (months)	52 ± 11 [37–70]	48 ± 9 [34–66]	43 ± 14 [28–69]	54 ± 10 [36–69]	52 ± 13 [24–70]	45 ± 13 [30–65]	51 ± 14 [30–66]	50 ± 18 [22–72]
NVIQ	54 ± 8 [40–66]	91 ± 14 [70–113]	51 ± 10 [34–65]	89 ± 14 [73–113]	54 ± 11 [32–68]	92 ± 15 [74–123]	52 ± 13 [31–68]	93 ± 10 [73–106]

ASD, autism spectrum disorders; NVIQ, non-verbal intelligence quotient; std, standard deviation; DD, developmental delay (NVIQ < 70); no-DD, without developmental delay (NVIQ ≥ 70).

by a senior child psychiatrist and based on the DSM-IV-TR criteria), and no family history of ASD. ASD and DD patients underwent the brain MRI examination as a completion of the assessment pathway with the aim of excluding brain alteration, whereas noDD subjects performed brain MRI because of various reasons (including headache, seizures with fever, strabismus, cataract, paroxysmal vertigo, diplopia).

MRI data were acquired using a GE 1.5 T Signa Neuro-optimized System (General Electric Medical Systems) at IRCCS Stella Maris Foundation, fitted with 40 mT/m high-speed gradients. Within the MRI protocol for children a whole-brain fast spoiled gradient recalled acquisition in the steady-state T1-weighted series (FSPGR) was collected in the axial plane with repetition time 12.4 ms, echo time 2.4 ms, inversion time 700 ms, flip angle of 10°, yielding to contiguous axial slices with voxel size of $1.1 \times 1.1 \times 1.1$ mm^3. All children were sedated with a general anesthesia with a halogenated agent while spontaneously breathing. For all MRIs performed between September 2006 and February 2013 the same sequence of acquisition was used and the written informed consent from a parent or guardian of children was obtained. The research protocol was approved by the Institutional Review Board of the Clinical Research Institute for Child and Adolescent Neurology and Psychiatry.

Data Preprocessing and Feature Extraction

The preprocessing of the entire data set of structural MRI included the volumetric segmentation and cortical reconstruction by the Freesurfer image analysis suite version 5.1.0, documented and freely available online (http://freesurfer.net/; Fischl et al., 1999, 2004; Klein and Tourville, 2012). In the cortical parcellation step, Freesurfer assigns a neuroanatomical label to each location on the cortical surface according to a previously prepared atlas file. We used the Desikan-Killiany-Tourville (DKT) cortical atlas which divides the cerebral cortex into 62 structures (31 structures per hemisphere) (Klein and Tourville, 2012): 14 in the temporal lobe, 20 in the frontal lobe, 10 in the parietal lobe, 8 in the occipital lobe, and 10 in the cingulate cortex.

The following five surface-based features for each of the 62 DTK structures are computed: *Area* (white surface area in mm^2); *Volume* (gray matter volume in mm^3); *Thickness* (average cortical thickness in mm); *ThicknessStd* (standard deviation of cortical thickness in mm); *Mean-Curv* (integrated rectified mean curvature in mm^{-1}). The *Volume* is computed according to a surface-based method, as the average of the white and pial surface areas, multiplied by the cortical thickness. In addition we considered the white surface total area (in mm^2) and the mean thickness (in mm) of the cerebral cortex in the two hemispheres, thus obtaining a vector of 314 characteristics for each subject.

Feature Classification

We analyzed the brain image features with both standard two-class classifiers and OCC based on SVMs. The SVM (Vapnik, 1995) are quite extensively applied as conventional binary classification algorithms. They are supervised binary classifiers that require a training set of labeled input examples to learn the differences between the two sample classes, and a labeled test set to quantify the classification performance.

In the context of classification of brain images, each input example is a vector $\boldsymbol{x}$ of features extracted from each input image. The label **y** associated to each input example indicates its membership, e.g., "1" for vectors belonging to the patients class, "−1" for controls. Detailed information about two-class SVM can be found in (Pontil and Verri, 1997; Ben-Hur and Weston, 2010). Basically, during the training phase an optimization problem is solved to identify the largest-margin hyperplane ($\mathbf{w}\cdot\boldsymbol{x} + \mathrm{b} = 0$ for linear kernel SVM) allowing for an optimal separation of the training examples of the two classes. The goal is to find a vector **w** and a scalar b, which maximize the margin, i.e., the distance between the two classes in the direction of **w**.

The SVM can then predict the classification of an unlabeled input vector by checking on which side of the separating hyperplane the example lies.

The SVM belong to the class of kernel methods (Schölkopf and Smola, 2002; Shawe-Taylor and Cristianini, 2004), i.e., they depend on data only through dot products. To achieve good separation results even in case of non-linearly separable classes, the dot product can be replaced by a kernel function, which computes a dot product in some (possibly) higher dimensional feature space. This allows carrying out a linear classification in the feature space, without explicitly mapping in it the original observations. The separating hyperplane found in the feature space corresponds to a non-linear boundary in the input space. This property is commonly known as kernel trick. Formally, a kernel function is defined as a function that, given two observations $\boldsymbol{x}$, $\boldsymbol{x}' \in X$, satisfies $k(\boldsymbol{x},\boldsymbol{x}') = \phi\ (\boldsymbol{x})\ \phi'(\boldsymbol{x}')$, where X is the input space or domain and ϕ is a function mapping from X to a feature space. In this case, the prediction of the class membership of an unlabeled input vector is performed by mapping it into the feature space, and checking on which side of the separating hyperplane the example lies.

Among the non-linear kernel functions the Radial Basis Function (RBF) kernel is the most popular. It depends on the Euclidean distance between the examples and it is defined as $k(\mathbf{x}, \mathbf{x}') = \exp(-\gamma\ ||\mathbf{x} - \mathbf{x}'||^2)$. The parameter γ determines the smoothness of the boundary (in the input space). Like the regularization parameter C in linear-kernel SVM, also the parameter γ is usually set using heuristics or tuned using cross-validation procedures.

Taking inspiration from the two-class SVM, Tax and Duin (2004) addressed the OCC problem by proposing a method to obtain a spherically shaped boundary around the target set. The method is called Support Vector Data Description (SVDD). During the training phase, an optimization problem is solved to minimize the volume of the sphere by minimizing the square of its radius, while demanding that the sphere contains most of the training objects. Similarly to what happens in two-class SVM, a regularization parameter C has to be set to control the trade-off between the sphere volume and the errors allowed in the target set.

Schölkopf et al. (2000) in presented a new formulation of two-class SVM, where the C parameter was removed and replaced with a new parameter ν with a more natural interpretation: it is

an upper bound to the fraction of misclassifications and margin errors and a lower bound on the fraction of support vectors (SV). The authors showed that for certain parameter settings, the results of this new algorithm coincide with the conventional one. Moreover, desirable properties of previous SV algorithms are retained.

In 2001, Schölkopf and colleagues modified the previous approach (Schölkopf et al., 2000) to address the OCC problem and called the new algorithm single-class SVM. During the training phase of a single-class SVM, a hyperplane is placed such that it separates the target set from the origin with maximal margin. Similarly to the standard two-class SVM, when a more flexible data description is required, an implicit mapping of the data into another (possibly high dimensional) feature space is defined, such that the dot product in this feature space can be computed by evaluating a simple kernel function. An ideal kernel function would map the target examples onto a bounded, spherically shaped area in the feature space and outlier objects outside this area.

The constrained optimization problem to be solved is formulated as follows:

$$\text{Minimize}_{(\mathbf{w},\boldsymbol{\xi},\boldsymbol{\rho})} \ldots\ldots\ldots \tfrac{1}{2}||\mathbf{w}||^2 + \frac{1}{\boldsymbol{\nu}\mathbf{N}} \sum\nolimits_{\mathrm{i}=1}^{\mathrm{N}} \xi_\mathrm{i} - \rho \quad (1)$$

subject to

$$\mathbf{w}\,\boldsymbol{\phi}(\mathbf{x}_\mathrm{i}) \geq \rho - \xi_\mathrm{i};\ \mathrm{i} = 1, ..., \mathbf{N};\ \xi_\mathrm{i} \geq 0. \quad (2)$$

where $\boldsymbol{x}_i$ are the target examples. The single-class SVM attributes a new point $\mathbf{x}$ to the target or the outlier class by evaluating which side of the hyperplane it falls on in the feature space.

As in two-class algorithm, the regularization parameter $\nu \in (0, 1]$ has to be set. Similarly to what happens in the two-class case, it can be interpreted as an upper bound on the fraction of training points outside the estimated region, and a lower bound on the fraction of support vectors. It is usually set based on its meaning or tuned using cross-validation procedures.

Although the method by Schölkopf et al. (2001) does not find a closed boundary around the data, it gives comparable solutions to Tax and Duin approach when the data is preprocessed to have unit norm (Tax and Duin, 2004). In particular, this happens when a RBF kernel is used. More in details, the solutions of the two approaches are identical when the same RBF kernel with γ and $C = 1/(\nu N)$, where N is the number of objects in the target set, are used, as reported by Sato et al. (2012a). In their practical implementation the two approaches operate comparably. Both perform best when the RBF kernel is used. Like in the two-class situation, the parameter γ can be set using heuristics or tuned using cross-validation procedures.

In this work, we first applied two-class SVM to the vector of 314 characteristics extracted for each subject of our datasets to obtain reference classification performances, and then we analyzed the same data with single-class SVM with RBF kernel. We performed the classification on the male subset and on the female subset separately, and then on the entire dataset. As pictorially shown in **Figure 1**, in contrast to the standard two-class classification approach to distinguish two well-characterized groups of subjects (**Figure 1A**), the OCC based on SVM can be implemented to make a multivariate description of the normative data, and thus to define a homogeneous baseline in comparison to which subjects with different diseases cluster out of the boundary enclosing the control group (**Figure 1B**). However, the latter approach relies on the hypothesis that the control group consists of typical individuals sharing a core of common distinctive features at neuroanatomical of functional levels, whereas non-typical individuals present alterations in many different ways, especially when highly heterogeneous condition are investigated, such as the ASD. Thus, in case the control class is not extremely homogeneous and it is matched to the patient class for many known aspects (e.g., age, gender, NVIQ) except for the presence of the disease condition, it may happen that OCC based on SVM capture common features according to which the patients can be described (**Figure 1C**). In the latter case, a boundary enclosing most patients can be identified, according to which most controls lie outside.

Pre-Image for RBF Kernel

In the linear kernel classifiers, the entries of the vector $\mathbf{w}$ can be directly considered as the relative weights of each characteristic for the decision function (Gori et al., 2015). Conversely, in the non-linear case (e.g., the RBF kernel), the interpretation of the vector $\mathbf{w}$ is non-intuitive and complex, since the separating hyperplane is found in the feature space. Since the map Φ is non-linear, we cannot generally assert that each vector $\mathbf{w}$ in the feature space will have a *preimage* under Φ, i.e., a point $\boldsymbol{z}$ in the input space such that $\Phi(\boldsymbol{z}) = \mathbf{w}$. In the present work we used for the single-class SVM with RBF kernel the approach proposed in by Schölkopf et al. (1999) to generate *preimages* by approximating the inverse mapping from the feature space to the input space.

Additionally, to understand which features and which neuroanatomical regions drive the SVM boundary definition, we tailored the permutation testing method (Mourão-Miranda et al., 2005; Wanh et al., 2007; Gaonkar and Davatzikos, 2013; Gori et al., 2015) to the case of single-class classifiers.

RESULTS

Classification Performance

The Freesurfer pipeline was applied to preprocess the MRI of each subject according to the Freesurfer guidelines.

Patients with ASD and controls were matched on age and NVIQ, thus resulting in 20 matched case-control pairs in the female subset and in 19 matched case-control pairs and one group constituted by two patients and one control in the male subset, because of its dimensionality. We used these M ($M = 20$ for male and female subsets considered separately, $M = 40$ for the entire dataset) matched groups as subsets in a cross-validation procedure to evaluate the performance of the SVM classifiers: for each subset S_j, $j = 1,...,\mathrm{M}$, we trained the SVM using the remaining subsets S_i, $i \neq j$, while retaining S_j as testing subset. Then we repeated the training and testing process for each subset, thus obtaining an estimate of the classifier performance on the entire dataset. Given the nature of the subsets, we refer

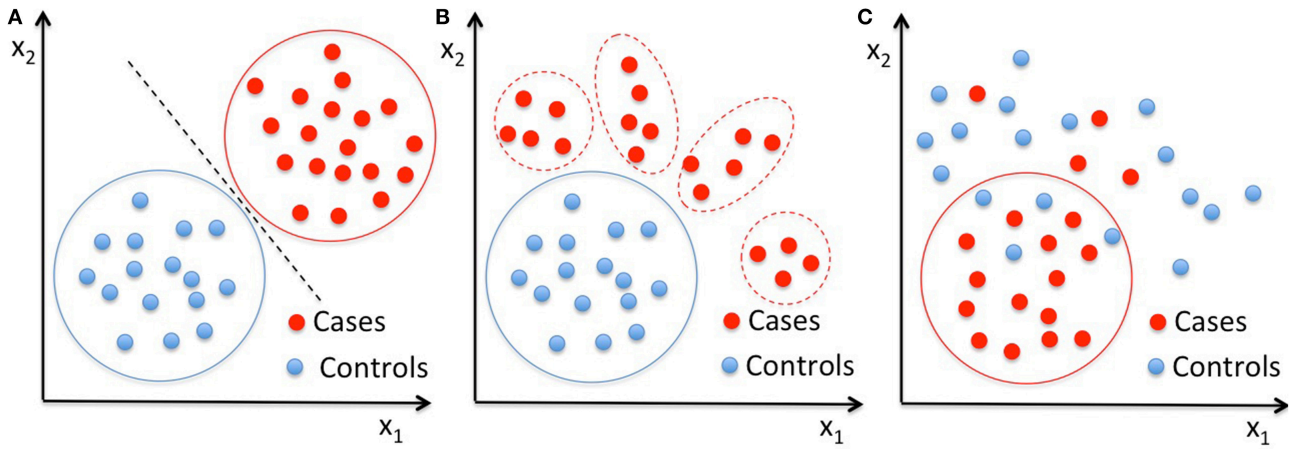

FIGURE 1 | Pictorial data representation in a two-dimensional space. (A) Classical application of a binary classifier to distinguish two well-characterized groups of subjects; **(B)** OCC approach based on the hypothesis that the control group is the homogeneous baseline in comparison to which, subjects with different diseases cluster out of the boundary enclosing the controls; **(C)** schematization of the OCC result in the case where common features associate the patients, thus the OCC boundary encloses most patients leaving outside most control cases. Solid lines are drawn around the groups entering the training of the classifiers, i.e., both case and control subjects are needed in training a binary classifier **(A)**, whereas only on control cases in **(B)** and only the patients' group in **(C)** are necessary to train a OCC, respectively.

to the cross-validation procedure we applied as leave-pair-out cross-validation (LPO-CV).

The performance of the SVM classifiers is evaluated in terms of the sensitivity (percentage of subjects with disease correctly identified, i.e., true positive rate) and the specificity (percentage of control subjects correctly identified, i.e., true negative rate). By varying the classifier decisional threshold, the trade-off between the sensitivity and the rate of false-positive detection can be represented in a curve known as Receiver Operating Characteristic (ROC) curve (Metz, 2006). The area under the ROC curve (AUC) is a global index to compare the ROC curves of different classifiers (Hanley and McNeil, 1982).

The LPO-CV scheme was implemented in the performance evaluation of both the two-class and the OCC SVM. A difference in the case of OCC SVM occurs only in the training step: to apply LPO-CV in the context of single-class classification we simply trained the single-class classifiers only on one class (target class) inside the cross validation, but tested it on both classes for the subset that was left out for testing.

To train and test two-class and single-class classifiers we used RapidMiner (http://rapidminer.com/) advanced analytics platform version 5.3, which includes both two-class and single-class SVM as a part of the LibSVM operator.

Two-Class Classification Performance

A standard two-class SVM classification with linear and RBF kernels was carried out to discriminate subjects with ASD from controls, including the optimization of the SVM free parameters during the training. We reported the results in **Table 2**. The best performances we obtained were: AUC = 0.74 by using the linear kernel for the male subset and AUC = 0.65 by using the RBF kernel for the female subset. The reported two-class SVM performance already take into account the regularization and kernel parameter optimization, carried out through the nested LPO-CV procedure. We obtained the best results with linear kernel for males and with RBF kernel for females. These results represent a reference classification performance to compare with the new OCC SVM approach we propose.

One-Class Classification Performance

We first performed single-class classification by setting $\nu = 0.1$ and γ using heuristics (i.e., as the inverse of the number of features). Then, following the procedure adopted in Mourão-Miranda et al. (2011), we carried out the optimization of the parameters ν and γ, within nested LPO-CV loops, as follows: at each iteration j of the outer LPO-CV scheme we had at disposal a subset $\boldsymbol{A_j} = \{\boldsymbol{S}_i\}_{i=1,\ldots,N, i\neq j}$ for training. Before training, we performed an optimization procedure based on an internal LPO-CV twice. In the first run, we kept the parameter ν fixed at an initial value (0.1) and we performed a LPO-CV for several values of γ in order to find its optimal estimate (i.e., the one that maximizes the AUC). To cover a wide range of possible γ-values, we let this parameter vary first on a coarse grid (19 steps from 2^{-15} to 2^3 by power of 2); then, we refined the search in the interesting regions we identified. In the second run, we kept γ fixed at the optimal value and we performed a second optimization procedure to choose the optimal ν, using a coarse optimization with 10 linearly spaced values in the [0.01–0.5] range, then a fine search in [0.01–0.3] range using 20 linearly spaced values. A single-class SVM was finally trained on $\boldsymbol{A}_j$ using the optimal values of γ and ν and tested on the subset $\boldsymbol{S}_j$ left out in the outer LPO-CV scheme. This procedure was repeated for each j, each time leaving a different subset outside as test subset.

The intuitive approach for transforming a binary discrimination problem into a single-class task in the context of highly heterogeneous conditions like ASD is to use the control

TABLE 2 | The performances obtained in the ASD vs. CTRL classification with the two-class SVM, the OCC-SVM trained on the CTRL class, and the OCC-SVM trained on the ASD class are reported.

Two-class SVM				**Male sample**	**Female sample**
Training set	**Test set**	**Training specification**		**AUC**	**AUC**
ASD and CTRL	ASD and CTRL	linear-kernel SVM for males/RBF for females	optimized C/optimized ν, γ	0.74	0.65
	ASD and CTRL with NVIQ $<$ 70			0.73	0.63
	ASD and CTRL with NVIQ $\geq$ 70			0.8	0.63
One-class SVM				**Male sample**	**Female sample**
Training set	**Test set**	**Training specification**		**AUC**	**AUC**
CTRL	ASD and CTRL	RBF	optimized ν, γ	0.50	0.50

One-class SVM				**Male sample**		**Female sample**	
Training set	**Test set**	**Training specification**		**AUC**	***p*-value**	**AUC**	***p*-value**
ASD	ASD and CTRL	RBF	optimized ν, γ	0.74	0.012	0.68	0.016
	ASD and CTRL with NVIQ $<$ 70			0.64	0.19	0.65	0.05
	ASD and CTRL with NVIQ $\geq$ 70			0.81	0.016	0.72	0.05

One-class SVM				**Male and female sample**
Training set	**Test set**	**Training specification**		**AUC**
ASD male and females	ASD and CTRL males and females	RBF	optimized ν, γ	0.64
	ASD and CTRL males and females with NVIQ $<$ 70			0.63
	ASD and CTRL males and females with NVIQ $\geq$ 70			0.65

All classification performances are obtained in a leave-pair-out cross validation scheme, where the classifier training parameters are optimized within nested loops. The performances of the classifiers were separately evaluated in most cases on the subsets of ASD and CTRL subjects with low and high NVIQ values. The permutation test was also performed to assign a statistical significance p-value to the AUC in the case of OCC classification of male and female samples. ASD, Subjects with Autism Spectrum Disorders; CL, chance level; CTRL, control sample; NVIQ, non-verbal intelligence quotient; RBF, Radial Basis Function; SVM, Support Vector Machine.

class as target class, figuring that it could enable the definition of a robust boundary, in relation to which the ASD patients would be classified as outliers. Consequently, we first trained a single-class SVM by considering only control examples to form the decision boundary, thus discarding information about the ASD class during the training phase.

This would be the optimal approach if the control class had characteristics of homogeneity, since the single-class SVM could capture the control class structure, by adjusting itself to its properties. This would allow recognizing ASD examples as outliers, even if the available ASD samples were not representative of the real ASD population, due to the extreme ASD heterogeneity.

However, the results obtained in this case in terms of AUC were not above the chance level, despite the optimization on of the parameters ν and γ.

Therefore, we repeated the same procedure using the ASD patient group as the target class to investigate whether there was a consistent neuroanatomical pattern among the ASD patients in relation to which the controls can be classified as outliers.

The results obtained in terms of AUC were: AUC = 0.73 for the male subset and AUC = 0.66 for the female subset by setting $\nu = 0.1$ and γ using heuristics; by optimizing the parameters ν and γ, AUC = 0.74 for the male subset and AUC = 0.68 for the female subset. We summarized in **Table 2** the classification results we obtained in the different classification experiments we conducted.

These results show that the control class does not have characteristics of homogeneity allowing recognizing ASD examples as outliers. Conversely, there is a common structure among the ASD patients that the OCC–SVM could capture. The OCC–SVM assigns to a test case a continuous output providing the confidence for it to belong to the target class or to be an outlier. To investigate whether the AUC performance obtained in the case-control discrimination were significantly above the chance level we implemented the permutation test. To obtain the null distribution of the AUC, we carried out a permutation test procedure in the training phase, tailoring it to the single-class classifiers. In a standard two-class classification the permutation test is performed by randomly exchanging several times the class labels (i.e., by randomly assigning positive and negative labels either to the ASD and the control cases) and repeating the classification procedure. In the OCC case, the training is performed on the target class only, e.g., the ASD class in our analysis. To find the null distribution for AUC, we permuted the group labels 10000 times, creating "artificial" training datasets where randomly chosen ASD cases were exchanged with their matched controls. Each "artificial" ASD dataset was then used to train one single-class SVM, i.e., to generate a decision function. We counted the number of times the AUC exceeded the value obtained with the real class labels. Dividing this value by the number of permutations provided a statistical significance for the AUC. The permutation testing procedure was applied separately for the male and the female subsets. We used the Matlab (The MathWorks, Inc.) interface to the LIBSVM package (http://www.csie.ntu.edu.tw/∼cjlin/libsvm/) to train the single-class classifiers in the permutation test procedure, implementing the RBF parameter optimization as nested LPO-CV loops. The AUC values and the significance values of the permutation test are reported in **Table 2**.

Finally, to investigate the impact of some known heterogeneity factors present in the ASD sample, we estimated the OCC performance on the entire dataset, by using the group of both male and female subjects with ASD as the target class. We achieved AUC = 0.64 in the case-control discrimination. This slight performance decrease is not surprising and we ascribed it to the introduction of the gender as additional heterogeneity factor.

Another relevant heterogeneity factor in our data is the NVIQ of subjects, which is in the [31–123] range. If the performance of OCC trained on male subjects with ASD (leading to AUC = 0.74 on the male population) is evaluated separately on the subsamples of subjects with NVIQ $\geq$ 70 and NVIQ $<$ 70, the values of AUC = 0.81 and AUC = 0.64 were obtained, respectively. A similar trend holds for the OCC trained on the female subjects with ASD (leading on AUC = 0.68 on the female population). In this case AUC = 0.72 and AUC = 0.65 were obtained on the subsamples of subjects with NVIQ $\geq$ 70 and NVIQ $<$ 70, respectively.

Maps of Discriminant Brain Regions

To understand which of the 314 characteristics (i.e., which brain regions and which of the five computed features) are the most relevant to the single-class SVM boundary definition, we trained a single-class SVM with RBF kernel using all the ASD patient group as the target class (with $\nu = 0.1$ and heuristic γ) and we applied the algorithm proposed in Schölkopf et al. (1999) to generate the *preimage* vector $\boldsymbol{z}$. We used the Statistical Pattern Recognition Toolbox for Matlab (STPRTool) (http://cmp.felk.cvut.cz/cmp/software/stprtool/index.html) to generate the *preimage*.

To obtain the null distribution of the preimage $\boldsymbol{z}$, we carried out a permutation test in the training phase by permuting the group labels 10000 times, as described above. Each "artificial" ASD dataset generated a decision function and a corresponding preimage vector $\boldsymbol{z}$. Since each component of $\boldsymbol{z}$ corresponds to one of the 314 characteristics, we obtained a null distribution associated with every characteristic. We counted the number of times the so-generated components of $\boldsymbol{z}$ exceeded (comparing the absolute values) the corresponding values in the $\boldsymbol{z}$ map obtained for the real ASD cases; dividing this value by the number of permutations provided a statistical significance map. Then, we retained only the characteristics with $p < 0.05$. The relevant characteristics (features and regions) resulting from the permutation test applied to male and female data groups are shown in **Tables 3, 4**. As stated before, in case of linear-kernel SVM, the separating hyperplane $\mathbf{w}$ can be represented as an image showing which brain regional features are more relevant for the classification problem. Additionally, the sign of each element of $\mathbf{w}$ directly identifies whether the corresponding feature is greater either in the case or in the control group. This information is inaccessible when using RBF, as the linear problem is solved in the space defined by the non-linear transformation $\mathbf{w} = \Phi(\boldsymbol{z})$, thus the signs of the elements of the z vector (i.e., the *preimage*)

do not indicate whether a relevant feature in the classification problem is greater in the case or in the control group. To foresee this information, which is important to compare the result we obtain with those presented in other studies, we simply analyzed the distributions of each feature and reported the trend of the sign of the case-control difference. We indicate in **Tables 3, 4** with arrows pointing up/down the features significantly contributing to the OCC boundary definition whose individual trend is toward increased/decreased values in the group of male subjects with ASD with respect to matched controls.

We show in **Figures 2**, **3** the brain regions contributing most to the definition of the OCC boundary, as reported in **Tables 3, 4** for male and female subsets, respectively. For the male population the main regions are: left (L) and right (R) medial orbito frontal cortices, L pars triangularis and R pars opercularis of the inferior frontal gyrus, middle temporal cortex and R insula. For the female population the main regions are: L and R caudate anterior cingulate, pars opercularis, posterior cingulated, cuneus; R pars triangularis postcentral gyrus, superior temporal cortex and superior parietal cortex. They are mostly among the network of structural brain alterations widely reported in the population with ASD, including frontal and temporal areas. Thus, despite the phenotypical heterogeneity in ASD, a common neuroanatomical profile of core features could be detected with the OCC SVM approach.

DISCUSSION

We analyzed the brain structural MRI features of patients with ASD with OCC SVM, starting with the estimation of the OCC performance in the ASD vs. controls discrimination task. Then, we investigated whether the distribution of patterns of brain structures in control subjects is homogeneous enough to enable the definition of a robust boundary, in relation to which the patients with ASD would be classified as outliers. This approach is consistent with previously proposed methods where OCC were implemented on fMRI features to build multivariate normative rules on the healthy control population, which would allow recognizing abnormal cases as outliers (Mourão-Miranda et al., 2011; Sato et al., 2012a,b). In the specific case of the population of young children with ASD we analyzed, we found out that an OCC boundary enclosing the controls, built upon structural MRI brain features, will allow most ASD cases to fall within the boundary. By contrast, a consistent pattern among the patients with ASD could be identified by the OCC approach, which provided a boundary in relation to which most controls were classified as outliers. In other words, we found out evidence that the control group is the more heterogeneous one and therefore the hypersphere or decision boundary enclosing most of the controls contains data in the ASD range. Vice versa, the ASD group showed a common structure that the SVM OCC could capture. This apparently counterintuitive result might be understood in the light of the following considerations. First, we performed a priori heterogeneity reduction of the ASD sample by excluding subjects with ASD secondary to known causes and/or with dysmorphic features (see Exclusion criteria in Section Participants and MRI Data Acquisition). Conversely, the control group was highly heterogeneous, since it comprises children who span the full range of cognitive ability (NVIQ score range: 31–123). This selection is motivated by the our primary choice of including within the cases all ASD children who performed MRI, since focusing just on those who are high-functioning would be non-representative of ASD population comprising about 55% of subjects in the intellectual disability range (Charman et al., 2011). As a necessary consequence, subjects with idiopathic developmental delay (DD) were included within the control group in order to obtain a match on NVIQ and thus a reliable MRI data interpretation (Crone et al., 2010). Therefore, the heterogeneity of MRI structural features within the control sample could be ascribed not only to the normal inter-individual brain variability that occurs among individuals with typical development (Wilke and Holland, 2003; Kanai and Rees, 2011), but also to the heterogeneous subsample of individuals with DD. In fact, by definition, idiopathic DD appears to be a highly heterogeneous disorder in terms of etiopathogenesis and clinical features: it is therefore plausible that also its neuroanatomical substrate is heterogeneous and hence contributes to amplify the cerebral differences detected in our control population. Moreover, we restricted our analysis to an early and relatively narrow age-range (2–6 years), a time-period in which structural MRI findings of ASD patients are more consistent and less heterogeneous across studies (Wolff and Piven, 2013). Specifically, a overgrowth of WM and GM before 2 years of age followed by a growth rate reduction that lead to brain volumes similar to typical children by approximately the school-age period was frequently reported (Lenroot and Yeung, 2013). In addition, by focusing on preschoolers only, we captured the pattern of brain alterations taking place near the clinical onset of the disorder and therefore we minimized the influence of different post-natal variables (e.g., environmental factors, psychiatric comorbidities, rehabilitative intervention) on brain structure. In other words, it is possible that a common altered brain presentation is more frequent in the early stage of the ASD disorder and that inter-subject variability in ASD populations progressively increases with age.

The present work is a proof of concept that the OCC framework can be applied to neuroimaging data to investigate if consistent patterns of alterations do exist even in heterogeneous populations such as ASD. Despite the results we found need to be confirmed against a larger population, the approach we present here is a preliminary step aiming to set up a strategy to identify common altered features in specific disorders.

Analogously, a common brain endophenotype in ASD individuals was detected with different methods of data acquisition, including electroencephalogram (EEG) spectral coherence (Duffy and Als, 2012), voxel based morphometry (Uddin et al., 2011), functional MRI (White et al., 2014), functional connectivity (Murdaugh et al., 2012), and diffusion tensor imaging (Ingalhalikar et al., 2011). These findings did not support the extreme variability of cerebral structure and function in ASD patients, as suggested by other investigations (Alexander et al., 2007; Nordahl et al., 2012; Hahamy et al., 2015).

TABLE 3 | Relevant brain regions and features for the male group ($p < 0.05$).

Male subset		Feature				
Hemisphere	**Region**	**Area**	**Mean curvature**	**Thickness**	**Thickness standard deviation**	**Volume**
lh	Medial orbitofrontal cortex		↑			
	Middle temporal gyrus	↑				
	Pars triangularis	↑	↓			
	Posterior cingulate cortex	↑				↑
	Transverse temporal gyrus	↑				
rh	Insula	↑	↑			
	Medial orbitofrontal cortex		↑			
	Pars opercularis	↑				↑

Arrows pointing up/down indicate the features significantly contributing to the OCC boundary definition, whose individual trend is toward increased/decreased values in the group of male subjects with ASD with respect to matched controls.

TABLE 4 | Relevant brain regions and features for the female group ($p < 0.05$).

Female subset		Feature				
Hemisphere	**Region**	**Area**	**Mean curvature**	**Thickness**	**Thickness standard deviation**	**Volume**
lh	Caudal anterior cingulate cortex			↑		↑
	Cuneus	↓				↑
	Enthorinal cortex				↑	
	Inferior temporal lobe	↓				
	Lateral orbitofrontal cortex				↑	
	Pars opercularis			↓		
	Posterior cingulate				↑	
	Precuneus	↑				↑
	Rostral anterior cingulate cortex		↓			
	Transverse temporal gyrus					↑
rh	Caudal middle frontal gyrus	↑				
	Cuneus				↓	
	Enthorinal cortex				↑	
	Pars opercularis		↓			↑
	Pars triangularis			↓	↓	
	Postcentral gyrus	↑				↑
	Precuneus	↓				
	Rostral anterior cingulate cortex		↑			↑
	Superior parietal cortex		↓			
	Superior temporal gyrus		↓			

Arrows pointing up/down indicate the features significantly contributing to the OCC boundary definition, whose individual trend is toward increased/decreased values in the group of female subjects with ASD with respect to matched controls.

Since we found the rather limited maximum AUC value of 0.74 for the male subset, it is important to highlight that among control subjects we included patients with DD that from a clinical point of view can frequently be considered in the ASD differential diagnosis. Therefore, it is possible that not only at the behavioral level, but also at the neuroanatomical level individuals with ASD and individuals with DD share some features that make the brain-based distinction between each other more difficult. This interpretation of our results is further supported by the fact that the AUC values reported on the subgroups of subjects with high NVIQ values are systematically higher than those obtained on the subgroups with low NVIQ values (see **Table 2**), whereas the performances obtained on the entire samples are positioned in between, as expected. It happens in the analysis of the male and the female subsamples and of the entire data sample. According to this view, the capability to differentiate participants into patient and control groups improved when we restricted the analysis to ASD patients with NVIQ $\geq$ 70 and therefore we

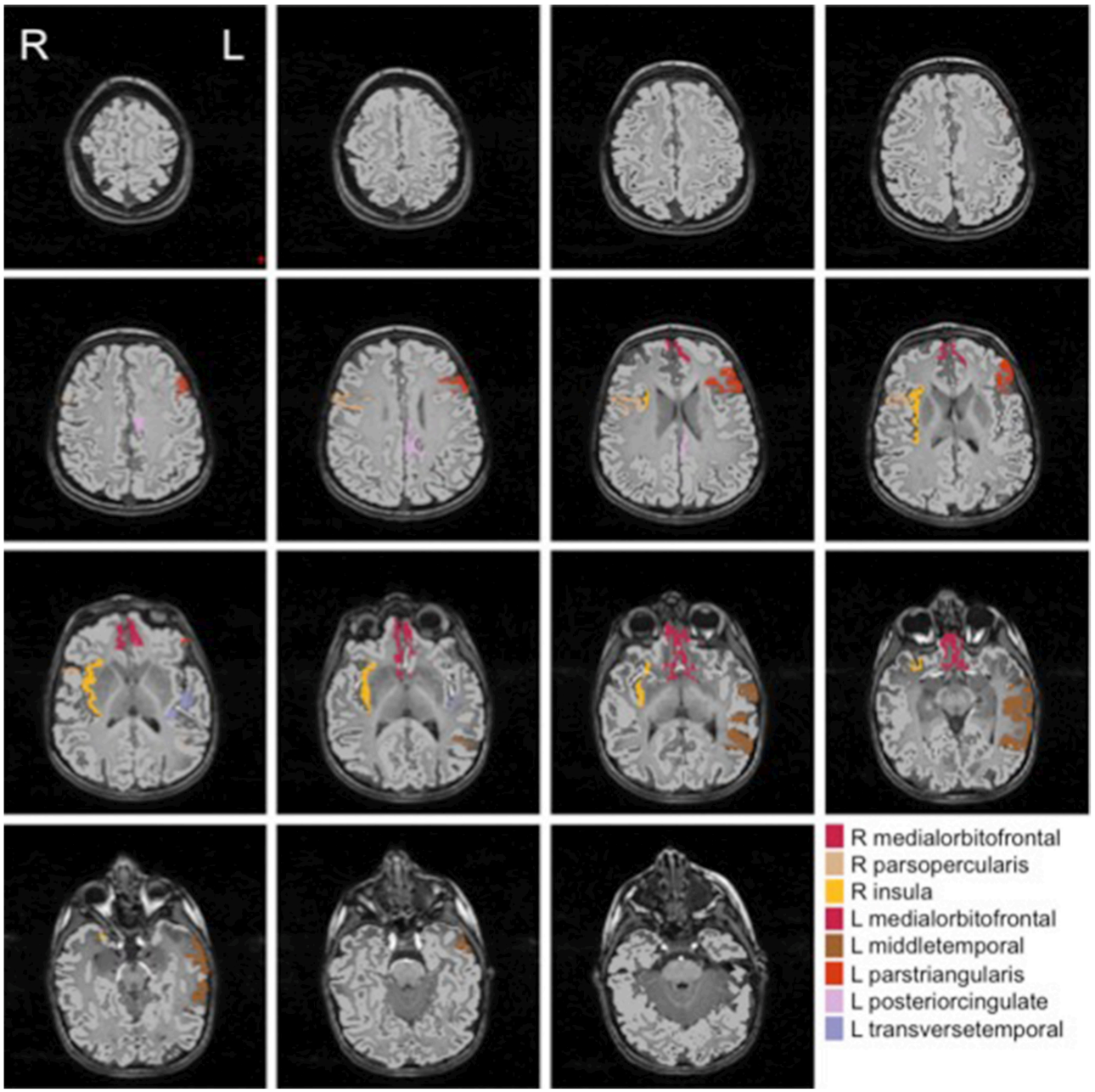

FIGURE 2 | Brain regions most contributing to the definition of the OCC boundary for the male group.

included among control subjects only individuals without DD (AUC = 0.81 and AUC = 0.72 for female and male subsamples, respectively).

The features which had the highest discriminative ability between the cases (both males and females) and the controls belong to four cerebral regions -posterior cingulate cortex (PCC), pars opercularis, and pars triangularis of inferior frontal gyrus, transverse temporal gyrus- all of which would represent a neuroanatomical signature of pre-schoolers with ASD. Specifically, we detected increased left PCC volume in ASD patients. Notably, this region has been included in the default mode network as one of the highest baseline energy consuming regions (Raichle et al., 2001) and has been implicated in arousal and awareness (Vogt and Laureys, 2005), autobiographical memory retrieval (Maddock et al., 2001), as well as in cognitive flexibility and in the ability to regulate the breadth of attention (Leech and Sharp, 2014), functions frequently impaired in patients with ASD (Bruck et al., 2007; Leung and Zakzanis, 2014; Orekhova and Stroganova, 2014).

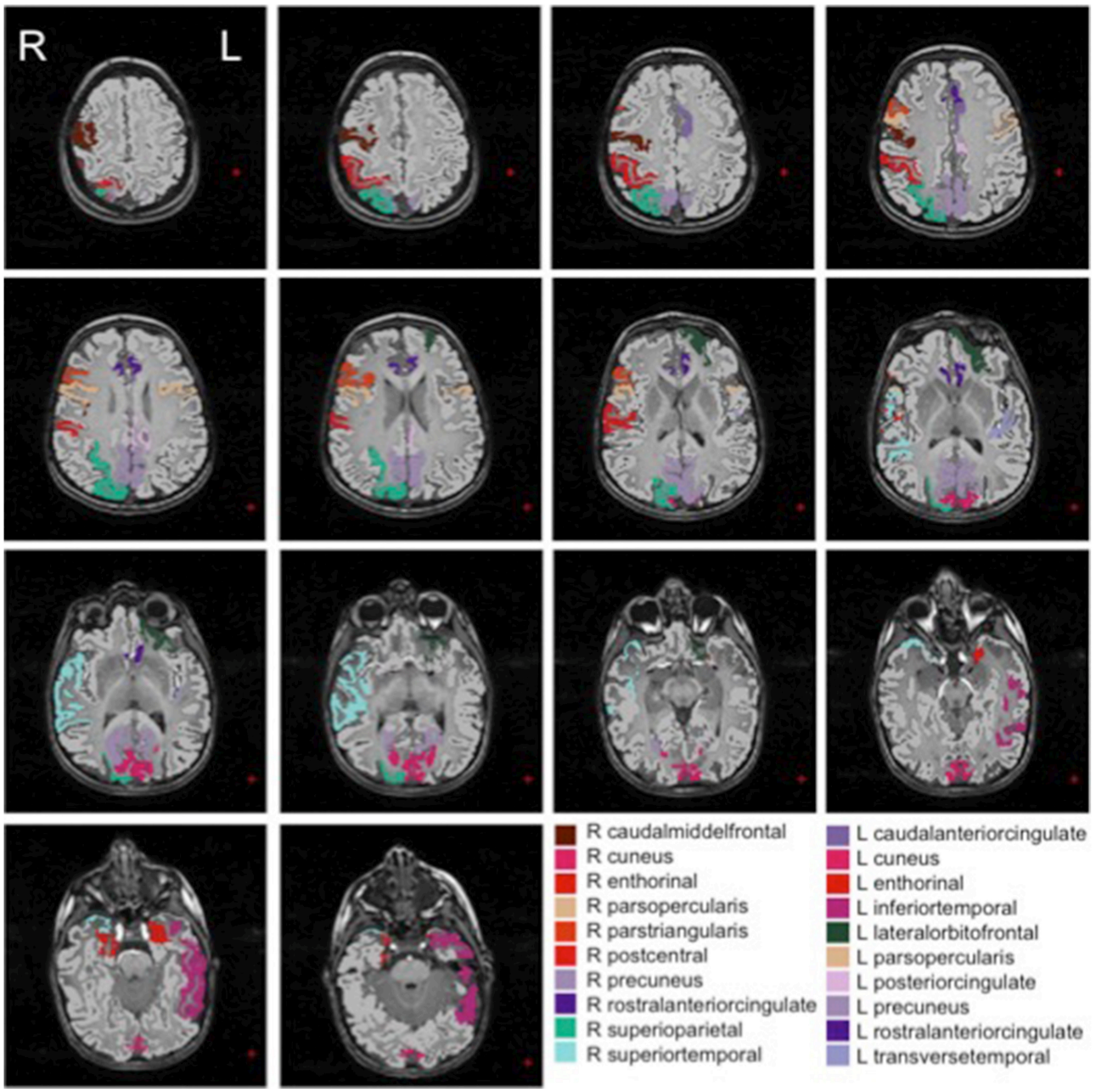

FIGURE 3 | Brain regions most contributing to the definition of the OCC boundary for the female group.

In addition, we identified a significant alteration of pars opercularis and pars triangularis in patients with ASD. These inferior frontal regions together comprise Broca's area, which is primarily involved in higher-order abilities such as expressive language, action imitation, attribution of mental states, and empathy (Iacoboni and Dapretto, 2006). Disruption of this area may therefore lead to core ASD symptoms (Dapretto et al., 2006). In particular, our finding of reduced cortical thickness (CT) in the pars opercularis is in line with results of Zielinski et al. (2014) in children and adolescents with ASD and of Hadjikhani et al. (2006), who reported a local decreases of CT in the pars opercularis of 14 high-functioning adults with ASD compared with matched control subjects. Also, decreased CT in the pars triangularis is in concordance with a previous study demonstrating focal patterns of cortical dysmaturation in children with ASD (Jiao et al., 2010). At the volumetric level, an increase in pars opercularis and pars triangularis was identified in children with ASD compared to controls (Knaus et al., 2009) while an opposite finding characterized adults with high-functioning ASD (Yamasaki et al., 2010), supporting an

altered trajectory of neurodevelopment in the autistic disorder. Interestingly, a highly localized structural alteration consisting in a significant reduction of the sulcus maximum depth was recently detected in the Broca's area of young children with ASD (Brun et al., 2016), suggesting its possible role in facilitating early ASD identification.

Our individuals with ASD showed increased volumes (females) and area (males) of the left transverse temporal (Heschl's) gyrus relative to controls. The transverse gyrus of Heschl includes the primary auditory cortex and is critically implicated in early auditory processing (Galaburda and Sanides, 1980). Several ASD symptoms, including altered auditory responsiveness (O'Connor, 2012), language perception and acquisition, are strictly related to this cerebral region. Previous cross-sectional investigations on older patients with ASD failed to observe any volumetric alteration in Heschl's gyrus (Gage et al., 2009; Knaus et al., 2009): it is possible that neuroanatomical differences in this area are age-related, and therefore detectable in our sample of ASD preschoolers, but not more during childhood and adolescence.

Crucially, a longitudinal investigation reported a reduced growth of Heschl's gyrus white matter in the left hemisphere as well as in the right Heschl's gyrus gray matter of children with ASD (Prigge et al., 2013), supporting an abnormality in the trajectory of cerebral development in the ASD group.

It is worth mentioning that the most discriminative brain features that characterize young children with ASD in the current investigation are largely overlapping with those identified in a resting-state connectivity analysis of brain lateralization in 447 high-functioning individuals with ASD (Nielsen et al., 2014). Therefore, a consistent finding was detected in these two studies, despite they do present substantial differences not only as to the numerosity, IQ sample and imaging modalities, but also as to the age of participants (preschoolers in our study vs. individuals across a wide range of ages starting from 6 years in the paper by Nielsen and colleagues), and sites of MRI acquisition (single site in our study vs. multiple sites in Nielsen's report). Hence, this replicated result would open the door to speculation that, irrespective of demographic and clinical features, selective alteration in language and default mode areas is a universal cerebral endophenotype of ASD.

In conclusion, results from the present study suggest that a distinctive neuroanatomical profile could be identified in preschoolers with ASD, independently of their gender, age, and NVIQ. In fact, beside the well-known heterogeneity of the ASD condition, patients seem to share common neuroanatomical substrates that appear to comprise language and default mode regions and could represent the core brain alterations of the disorder in the preschool age.

Several limitations of the current work and directions for future studies should be highlighted. First, the classification performances obtained are quite modest and, in some specific cases, the performances of the OCC classifiers are not significantly different from the chance level, as it happens for example on the sub group of male subjects with low NVIQ values (see **Table 2**). More populated data samples would be necessary to understand whether with improved statistical sensitivity the two overlapping classes can be effectively disentangled. Second, the relatively limited sample size prevented us from reliably subgrouping ASD patients on the basis of gender and NVIQ for investigating possible brain correlates of phenotypic differences. Third, we did not implement in our classification model any feature selection technique. Due to the large number of features (314) with respect to the data sample size we are working with a high risk of overfitting the models. As we are interested most in the discrimination maps generated by the OCC than in the classification performance by itself, the overfitting problem does not seem a major issue. However, to investigate in depth the separability of the ASD and control samples, and to understand whether the modest AUC values we obtained on cross validation are due to the lack of generalization abilities due to model overfitting, a feature selection technique should be implemented. Finally, since patients with ASD were recruited from an ASD Unit in a large tertiary hospital and research university that evaluates patients under 18 years of age from all over Italy, we may not have been fully able to capture children at the less severe end of the spectrum.

Future investigations will involve: (i) analyzing whether a distinct clinical symptoms or behavior profile characterized the outliers within the ASD cohort; (ii) evaluating whether the brain ASD endophenotype detected in the first years of life remains stable over time, or vice-versa developmental changes in ASD symptom profiles impact also on brain structure; (iii) including analysis of patients with other neurodevelopmental disorders which display overlapping clinical features with ASD [e.g., language disorder, social (pragmatic) communication disorder, attention-deficit/hyperactivity disorder, stereotypic movement disorder] in order to verify the specificity of the discriminative brain pattern here identified in ASD patients.

AUTHOR CONTRIBUTIONS

AR and SC designed the study; IG, AG, and AR carried out data processing and analysis; SC and FM interpreted the results; AR, IG, and SC drafted the manuscript; AG edited the manuscript; FM critically revised the manuscript for important intellectual content.

ACKNOWLEDGMENTS

This work has been partially founded by the Italian Ministry of Health and the Tuscany Government (GR2317873, PI: SC), by Sviluppo Toscana (Bando FAS Salute, ARIANNA Project), and by the National Institute of Nuclear Physics (nextMR project).

REFERENCES

Alexander, A. L., Lee, J. E., Lazar, M., Boudos, R., DuBray, M. B., Oakes, T. R., et al. (2007). Diffusion tensor imaging of the corpus callosum in Autism. *Neuroimage* 34, 61–73. doi: 10.1016/j.neuroimage.2006.08.032

American Psychiatric Association (2000). *DSM-IV-TR, Diagnostic and Statistical Manual of Mental Disorders, 4th Edn, Text Revision.* Washington, DC: American Psychiatric Association.

American Psychiatric Association (2013). *Diagnostic and Statistical Manual of Mental Disorders (DSM-5), 5th Edn.* Washington, DC: American Psychiatric Publishing.

Ben-Hur, A., and Weston, J. (2010). User's guide to support vector machines. *Methods Mol. Biol.* 609, 223–239. doi: 10.1007/978-1-60327-241-4_13

Bruck, M., London, K., Landa, R., and Goodman, J. (2007). Autobiographical memory and suggestibility in children with autism spectrum disorder. *Dev. Psychopathol.* 19, 73–95. doi: 10.1017/S0954579407070058

Brun, L., Auzias, G., Viellard, M., Villeneuve, N., Girard, N., Poinso, F., et al. (2016). Localized misfolding within Broca's area as a distinctive feature of autistic disorder. *Biol. Psychiatry Cogn. Neurosci. Neuroimaging* 1, 160–168. doi: 10.1016/j.bpsc.2015.11.003

Calderoni, S., Retico, A., Biagi, L., Tancredi, R., Muratori, F., and Tosetti, M. (2012). Female children with autism spectrum disorder: an insight from mass-univariate and pattern classification analyses. *Neuroimage* 59, 1013–1022. doi: 10.1016/j.neuroimage.2011.08.070

Centers for Disease Control and Prevention (2014). *Prevalence of ASD. MMWR* 63, 1–22.

Charman, T., Pickles, A., Simonoff, E., Chandler, S., Loucas, T., and Baird, G. (2011). IQ in children with autism spectrum disorders: data from the Special Needs and Autism Project (SNAP). *Psychol. Med.* 41, 619–627. doi: 10.1017/S0033291710000991

Crone, E. A., Poldrack, R. A., and Durston, S. (2010). Challenges and methods in developmental neuroimaging. *Hum. Brain Mapp.* 31, 835–837. doi: 10.1002/hbm.21053

Dapretto, M., Davies, M. S., Pfeifer, J. H., Scott, A. A., Sigman, M., Bookheimer, S. Y., et al. (2006). Understanding emotions in others: mirror neuron dysfunction in children with autism spectrum disorders. *Nat. Neurosci.* 9, 28–30. doi: 10.1038/nn1611

De Rubeis, S., and Buxbaum, J. D. (2015). Genetics and genomics of autism spectrum disorder: embracing complexity. *Hum. Mol. Genet.* 24, R24–R31. doi: 10.1093/hmg/ddv273

Duffy, F. H., and Als, H. (2012). A stable pattern of EEG spectral coherence distinguishes children with autism from neuro-typical controls - a large case control study. *BMC Med.* 10:64. doi: 10.1186/1741-7015-10-64

Ecker, C., Marquand, A., Mourão-Miranda, J., Johnston, P., Daly, E. M., Brammer, M. J., et al. (2010a). Describing the brain in autism in five dimensions-magnetic resonance imaging-assisted diagnosis of autism spectrum disorder using a multiparameter classification approach. *J. Neurosci.* 30, 10612–10623. doi: 10.1523/JNEUROSCI.5413-09.2010

Ecker, C., Rocha-Rego, V., Johnston, P., Mourao-Miranda, J., Marquand, A., Daly, E. M., et al. (2010b). Investigating the predictive value of whole-brain structural MR scans in autism: a pattern classification approach. *Neuroimage* 49, 44–56. doi: 10.1016/j.neuroimage.2009.08.024

Fischl, B., Sereno, M. I., and Dale, A. (1999). Cortical surface-based analysis. II: inflation, flattening, and a surface-based coordinate system. *Neuroimage* 9, 195–207. doi: 10.1006/nimg.1998.0396

Fischl, B., van der Kouwe, A., Destrieux, C., Halgren, E., Ségonne, F., Salat, D. H., et al. (2004). Automatically parcellating the human cerebral cortex. *Cereb. Cortex* 14, 11–22. doi: 10.1093/cercor/bhg087

Gage, N. M., Juranek, J., Filipek, P. A., Osann, K., Flodman, P., Isenberg, A. L., et al. (2009). Rightward hemispheric asymmetries in auditory language cortex in children with autistic disorder: an MRI investigation. *J. Neurodev. Disord.* 1, 205–214. doi: 10.1007/s11689-009-9010-2

Galaburda, A., and Sanides, F. (1980). Cytoarchitectonic organization of the human auditory cortex. *J. Comp. Neurol.* 190, 597–610. doi: 10.1002/cne.901900312

Gaonkar, B., and Davatzikos, C. (2013). Analytic estimation of statistical significance maps for support vector machine based multi-variate image analysis and classification. *Neuroimage* 78, 270–283. doi: 10.1016/j.neuroimage.2013.03.066

Gori, I., Giuliano, A., Muratori, F., Saviozzi, I., Oliva, P., Tancredi, R., et al. (2015). Gray matter alterations in young children with autism spectrum disorders: comparing morphometry at the voxel and regional level. *J. Neuroimaging* 25, 866–874. doi: 10.1111/jon.12280

Grzadzinski, R., Huerta, M., and Lord, C. (2013). DSM-5 and autism spectrum disorders (ASDs): an opportunity for identifying ASD subtypes. *Mol. Autism.* 4:12. doi: 10.1186/2040-2392-4-12

Hadjikhani, N., Joseph, R. M., Snyder, J., and Tager-Flusberg, H. (2006). Anatomical differences in the mirror neuron system and social cognition network in autism. *Cereb. Cortex* 16, 1276–1282. doi: 10.1093/cercor/bhj069

Hahamy, A., Behrmann, M., and Malach, R. (2015). The idiosyncratic brain: distortion of spontaneous connectivity patterns in autism spectrum disorder. *Nat. Neurosci.* 18, 302–309. doi: 10.1038/nn.3919

Hanley, J. A., and McNeil, B. J. (1982). The meaning and use of the area under a receiver operating charactertic (ROC) curve. *Radiology* 143, 29–36. doi: 10.1148/radiology.143.1.7063747

Hernandez, L. M., Rudie, J. D., Green, S. A., Bookheimer, S., and Dapretto, M. (2015). Neural signatures of autism spectrum disorders: insights into brain network dynamics. *Neuropsychopharmacology* 40, 171–189. doi: 10.1038/npp.2014.172

Iacoboni, M., and Dapretto, M. (2006). The mirror neuron system and the consequences of its dysfunction. *Nat. Rev. Neurosci.* 7, 942–951. doi: 10.1038/nrn2024

Ingalhalikar, M., Parker, D., Bloy, L., Roberts, T. P., and Verma, R. (2011). Diffusion based abnormality markers of pathology: toward learned diagnostic prediction of ASD. *Neuroimage* 57, 918–927. doi: 10.1016/j.neuroimage.2011.05.023

Jiao, Y., Chen, R., Ke, X., Chu, K., Lu, Z., and Herskovits, E. H. (2010). Predictive models of autism spectrum disorder based on brain regional cortical thickness. *Neuroimage* 50, 89–599. doi: 10.1016/j.neuroimage.2009.12.047

Kanai, R., and Rees, G. (2011). The structural basis of inter-individual differences in human behaviour and cognition. *Nat. Rev. Neurosci.* 12, 231–242. doi: 10.1038/nrn3000

Klein, A., and Tourville, J. (2012). 101 labeled brain images and a consistent human cortical labeling protocol. *Front. Neurosci.* 6:171. doi: 10.3389/fnins.2012.00171

Knaus, T. A., Silver, A. M., Dominick, K. C., Schuring, M. D., Shaffer, N., Lindgren, K. A., et al. (2009). Age-related changes in the anatomy of language regions in autism spectrum disorder. *Brain Imaging Behav.* 3, 51–63. doi: 10.1007/s11682-008-9048-x

Krawczyk, B., and Woźniak, M. (2015). Hypertension type classification using hierarchical ensemble of one-class classifiers for imbalanced data. *ICT Innov. Adv. Intell. Syst. Comput.* 311, 341–349. doi: 10.1007/978-3-319-09879-1_34

Leech, R., and Sharp, D. J. (2014). The role of the posterior cingulate cortex in cognition and disease. *Brain* 137(Pt 1), 12–32. doi: 10.1093/brain/awt162

Lenroot, R. K., and Yeung, P. K. (2013). Heterogeneity within autism spectrum disorders: what have we learned from neuroimaging studies? *Front. Hum. Neurosci.* 7:733. doi: 10.3389/fnhum.2013.00733

Leung, R. C., and Zakzanis, K. K. (2014). Brief report: cognitive flexibility in autism spectrum disorders: a quantitative review. *J. Autism Dev. Dis.* 44, 2628–2645. doi: 10.1007/s10803-014-2136-4

Lord, C., Risi, S., Lambrecht, L., Cook, E. H. Jr., Leventhal, B. L., DiLavore, P. C., et al. (2000). The autism diagnostic observation schedule–generic: a standard measure of social and communication deficits associated with the spectrum of autism. *J. Autism Dev. Disord.* 30, 205–223. doi: 10.1023/A:1005592401947

Maddock, R. J., Garrett, A. S., and Buonocore, M. H. (2001). Remembering familiar people: the posterior cingulate cortex and autobiographical memory retrieval. *Neuroscience* 104, 667–676. doi: 10.1016/S0306-4522(01)00108-7

Metz, C. E. (2006). Receiver operating characteristics analysis: a tool for the quantitative evaluation of observer performance and imaging systems. *J. Am. Coll. Radiol.* 3, 413–422. doi: 10.1016/j.jacr.2006.02.021

Mourão-Miranda, J., Bokde, A. L., Born, C., Hampel, H., and Stetter, M. (2005). Classifying brain states and determining the discriminating activation patterns: support vector machine on functional MRI data. *Neuroimage* 28, 980–995. doi: 10.1016/j.neuroimage.2005.06.070

Mourão-Miranda, J., Hardoon, D. R., Hahn, T., Marquand, A. F., Williams, S. C. R., Shawe-Taylor, J., et al. (2011). Patient classification as an outlier detection

problem: an application of the one-class support vector machine. *Neuroimage* 58, 793–804. doi: 10.1016/j.neuroimage.2011.06.042

Moya, M. M., Koch, M. W., and Hostetler, L. D. (1993). *One-Class Classifier Networks for Target Recognition Applications*. NASA STI/Recon Technical Report N, Vol. 93, 24043. Available online at: http://adsabs.harvard.edu/abs/1993STIN...9324043M

Murdaugh, D. L., Shinkareva, S. V., Deshpande, H. R., Wang, J., Pennick, M. R., and Kana, R. K. (2012). Differential deactivation during mentalizing and classification of autism based on default mode connectivity. *PLoS ONE* 7:e50064. doi: 10.1371/journal.pone.0050064

Nielsen, J. A., Zielinski, B. A., Fletcher, P. T., Alexander, A. L., Lange, N., Bigler, E. D., et al. (2014). Abnormal lateralization of functional connectivity between language and default mode regions in autism. *Mol. Autism* 5, 8. doi: 10.1186/2040-2392-5-8

Nordahl, C. W., Scholz, R., Yang, X., Buonocore, M. H., Simon, T., Rogers, S., et al. (2012). Increased rate of amygdala growth in children aged 2 to 4 years with autism spectrum disorders: a longitudinal study. *Arch. Gen. Psychiatry* 69, 53–61. doi: 10.1001/archgenpsychiatry.2011.145

O'Connor, K. (2012). Auditory processing in autism spectrum disorder: a review. *Neurosci. Biobehav. Rev.* 36, 836–854. doi: 10.1016/j.neubiorev.2011.11.008

Orekhova, E. V., and Stroganova, T. A. (2014). Arousal and Attention re-orienting in autism spectrum disorders: evidence from auditory event-related potentials. *Front. Hum. Neurosci.* 8:34. doi: 10.3389/fnhum.2014.00034

Orrù, G., Pettersson-Yeo, W., Marquand, A. F., Sartori, G., and Mechelli, A. (2012). Using support vector machine to identify imaging biomarkers of neurological and psychiatric disease: a critical review. *Neurosci. Biobehav. Rev.* 36, 1140–1152. doi: 10.1016/j.neubiorev.2012.01.004

Pontil, M., and Verri, A. (1997). *Properties of Support Vector Machines*. Available online at: ftp://publications.ai.mit.edu/ai-publications/pdf/AIM-1612.pdf

Prigge, M. D., Bigler, E. D., Fletcher, P. T., Zielinski, B. A., Ravichandran, C., Anderson, J., et al. (2013). Longitudinal Heschl's gyrus growth during childhood and adolescence in typical development and autism. *Autism Res.* 6, 78–90. doi: 10.1002/aur.1265

Raichle, M. E., MacLeod, A. M., Snyder, A. Z., Powers, W. J., Gusnard, D. A., and Shulman, G. L. (2001). A default mode of brain function. *Proc. Natl. Acad. Sci. U.S.A.* 98, 676–682. doi: 10.1073/pnas.98.2.676

Retico, A., Giuliano, A., Tancredi, R., Cosenza, A., Apicella, F., Narzisi, A., et al. (2016). The effect of gender on the neuroanatomy of children with autism spectrum disorders: a support vector machine case-control study. *Mol. Autism* 7, 5. doi: 10.1186/s13229-015-0067-3

Retico, A., Tosetti, M., Muratori, F., and Calderoni, S. (2014). Neuroimaging-based methods for autism identification: a possible translational application? *Funct. Neurol.* 29, 231–239. doi: 10.11138/fneur/2014.29.4.231

Sato, J. R., Hoexter, M. Q., Castellanos, X. F., and Rohde, L. A. (2012b). Abnormal brain connectivity patterns in adults with ADHD: a coherence study. *PLoS ONE* 7:e45671. doi: 10.1371/journal.pone.0045671

Sato, J. R., Rondina, J. M., and Mourão-Miranda, J. (2012a). Measuring abnormal brains: building normative rules in neuroimaging using one-class support vector machines. *Front. Neurosci.* 6:178. doi: 10.3389/fnins.2012.00178

Schölkopf, B., Mika, S., Burges, C. C., Knirsch, P., Müller, K. R., Rätsch, G., et al. (1999). Input space versus feature space in kernel-based methods. *IEEE Trans. Neural Netw.* 10, 1000–1017. doi: 10.1109/72.788641

Schölkopf, B., Platt, J. C., Shawe-Taylor, J., Smola, A. J., and Williamson, R. C. (2001). Estimating the support of a high-dimensional distribution. *Neural Comput.* 13, 1443–1471. doi: 10.1162/089976601750264965

Schölkopf, B., and Smola, A. (2002). *Learning with Kernels*. Cambridge, MA: MIT Press.

Schölkopf, B., Smola, A., J., Williamson, R., and Bartlett, P. L. (2000). New Support vector algorithms. *Neural Comput.* 12, 1207–1245. doi: 10.1162/089976600300015565

Shawe-Taylor, J., and Cristianini, N. (2004). *Kernel Methods for Pattern Analysis*. Cambridge, MA: Cambridge University Press.

Tax, D. M. J., and Duin, R. P. W. (2004). Support vector data description. *Mach. Learn.* 54, 45–66. doi: 10.1023/B:MACH.0000008084.60811.49

Uddin, L., Vinod, M., Young, C. B., Ryali, S., Chen, T., Khouzam, A., et al. (2011). Multivariate searchlight classification of structural magnetic resonance imaging in children and adolescents with autism. *Biol. Psychiatry* 70, 833–841. doi: 10.1016/j.biopsych.2011.07.014

Vapnik, V. (1995). *The Nature of Statistical Learning Theory*. Boston, MA: Kluwer Academic Publishers.

Vogt, B. A., and Laureys, S. (2005). Posterior cingulate, precuneal and retrosplenial cortices: cytology and components of the neural network correlates of consciousness. *Prog. Brain Res.* 150, 205–217. doi: 10.1016/S0079-6123(05)50015-3

Wanh, Z., Childress, A. R., Wang, J., and Detre, J. A. (2007). Support vector machine learning-based fMRI data group analysis. *Neuroimage* 36, 1139–1151. doi: 10.1016/j.neuroimage.2007.03.072

Wee, C. Y., Wang, L., Shi, F., Yap, P. T., and Shen, D. (2014). Diagnosis of autism spectrum disorders using regional and interregional morphological features. *Hum. Brain Mapp.* 35, 3414–3430. doi: 10.1002/hbm.22411

White, S. J., Frith, U., Rellecke, J., Al-Noor, Z., and Gilbert, S. J. (2014). Autistic adolescents show atypical activation of the brain's mentalizing system even without a prior history of mentalizing problems. *Neuropsychologia* 56, 17–25. doi: 10.1016/j.neuropsychologia.2013.12.013

Wilke, M., and Holland, S. K. (2003). Variability of gray and white matter during normal development: a voxel-based MRI analysis. *Neuroreport.* 14, 1887–1890. doi: 10.1097/00001756-200310270-00001

Wolfers, T., Buitelar, J. K., Beckmann, C. F., Franke, B., and Marquand, A. F. (2015). From estimating activation locality to predicting disorder: a review of pattern recognition for neuroimaging-based psychiatric diagnostics. *Neurosci. Biobehav. Rev.* 57, 328–349. doi: 10.1016/j.neubiorev.2015.08.001

Wolff, J. J., and Piven, J. (2013). On the emergence of autism: neuroimaging findings from birth to preschool. *Neuropsychiatry* 3, 209–222. doi: 10.2217/npy.13.11

Yamasaki, S., Yamasue, H., Abe, O., Suga, M., Yamada, H., Inoue, H., et al. (2010). Reduced gray matter volume of pars opercularis is associated with impaired social communication in high-functioning autism spectrum disorders. *Biol. Psychiatry* 68, 1141–1147. doi: 10.1016/j.biopsych.2010.07.012

Zhang, Y., Zhang, B., Coenen, F., Xiao, J., and Lu, W. (2014). One-class kernel subspace ensemble for medical image classification. *EURASIP J. Adv. Signal Process.* 2014, 1–13. doi: 10.1186/1687-6180-2014-17

Zhou, Y., Yu, F., and Duong, T. (2014). Multiparametric MRI characterization and prediction in autism spectrum disorder using graph theory and machine learning. *PLoS ONE* 9:e90405. doi: 10.1371/journal.pone.0090405

Zielinski, B. A., Prigge, M. B., Nielsen, J. A., Froehlich, A. L., Abildskov, T. J., Anderson, J. S., et al. (2014). Longitudinal changes in cortical thickness in autism and typical development. Brain 137(Pt 6), 1799–1812. doi: 10.1093/brain/awu083

Conflict of Interest Statement: The authors declare that the research was conducted in the absence of any commercial or financial relationships that could be construed as a potential conflict of interest.

frontiers in Neuroscience

ORIGINAL RESEARCH
published: 18 January 2017
doi: 10.3389/fnins.2016.00610

Restriction Spectrum Imaging As a Potential Measure of Cortical Neurite Density in Autism

Ruth A. Carper[1], Jeffrey M. Treiber[2], Nathan S. White[3], Jiwandeep S. Kohli[1] and Ralph-Axel Müller[1]*

[1] Brain Development Imaging Laboratory, Department of Psychology, San Diego State University, San Diego, CA, USA, [2] School of Medicine, University of California San Diego, La Jolla, CA, USA, [3] Multimodal Imaging Laboratory, Department of Radiology, University of California San Diego, La Jolla, CA, USA

Autism postmortem studies have shown various cytoarchitectural anomalies in cortical and limbic areas including increased cell packing density, laminar disorganization, and narrowed minicolumns. However, there is little evidence on dendritic and axonal organization in ASD. Recent imaging techniques have the potential for non-invasive, *in vivo* studies of small-scale structure in the human brain, including gray matter. Here, Restriction Spectrum Imaging (RSI), a multi-shell diffusion-weighted imaging technique, was used to examine gray matter microstructure in 24 children with ASD (5 female) and 20 matched typically developing (TD) participants (2 female), ages 7–17 years. RSI extends the spherical deconvolution model to multiple length scales to characterize neurite density (ND) and organization. Measures were examined in 48 cortical regions of interest per hemisphere. To our knowledge, this is the first time that a multi-compartmental diffusion model has been applied to cortical gray matter in ASD. The ND measure detected robust age effects showing a significant positive relationship to age in all lobes except left temporal when groups were combined. Results were also suggestive of group differences (ASD<TD) in anterior cingulate, right superior temporal lobe and much of the parietal lobes, but these fell short of statistical significance. For MD, significant group differences (ASD>TD) in bilateral parietal regions as well as widespread age effects were detected. Our findings support the value of multi-shell diffusion imaging for assays of cortical gray matter. This approach has the potential to add to postmortem literature, examining intracortical organization, intracortical axonal content, myelination, or caliber. Robust age effects further support the validity of the ND metric for *in vivo* examination of gray matter microstructure in ASD and across development. While diffusion MRI does not approach the precision of histological studies, *in vivo* imaging measures of microstructure can complement postmortem studies, by allowing access to large sample sizes, a whole-brain field of view, longitudinal designs, and combination with behavioral and functional assays. This makes multi-shell diffusion imaging a promising technique for understanding the underlying cytoarchitecture of the disorder.

Keywords: autism, diffusion, MRI, cerebral cortex, neurite, DTI, gray matter, connectivity

OPEN ACCESS

Edited by:
Roma Siugzdaite, Ghent University, Belgium

Reviewed by:
Pew-Thian Yap, University of North Carolina at Chapel Hill, USA
Ben Jeurissen, University of Antwerp, Belgium

****Correspondence:***
Ruth A. Carper
rcarper@mail.sdsu.edu

Specialty section:
This article was submitted to Child and Adolescent Psychiatry, a section of the journal Frontiers in Neuroscience

Received: *01 February 2016*
Accepted: *26 December 2016*
Published: *18 January 2017*

Citation:
Carper RA, Treiber JM, White NS, Kohli JS and Müller R-A (2017) Restriction Spectrum Imaging As a Potential Measure of Cortical Neurite Density in Autism. Front. Neurosci. 10:610. doi: 10.3389/fnins.2016.00610

INTRODUCTION

By general consensus, autism spectrum disorder (ASD) is a neurobiological disorder, likely of complex genetic, epigenetic, and possibly environmental origin, with brain development deviating from the typical path beginning in the prenatal period (Bailey et al., 1998; Palmen et al., 2004; Bauman and Kemper, 2005; Hutsler and and Casanova, 2016). Post-mortem studies are indispensible to our understanding of the underlying cellular anomalies. A reduction in the number of cerebellar Purkinje cells was among the earliest histologic reports (Bauman and Kemper, 1985), and a report of patchy neocortical thickening and laminar disorganization followed (Bailey et al., 1998). Increased cell packing density has been found in anterior cingulate, hippocampus and amygdala (Kemper and Bauman, 1998; Schumann and Amaral, 2006), and in prefrontal cortex by some (Bailey et al., 1998; Courchesne et al., 2011), but not all (Bauman and Kemper, 2005) research groups, while decreased density was found in fusiform gyrus (van Kooten et al., 2008). Increases in cortical cell packing density may relate to narrowed mini-columns in dorsolateral prefrontal cortex and superior temporal gyrus (Casanova et al., 2002, 2006; Buxhoeveden et al., 2006), suggesting a reduction in the amount of neuropil space surrounding neurons, which may reflect a decrease in inhibitory neurites in the affected regions. Ectopias (Bailey et al., 1998; Wegiel et al., 2010) and increased dendritic spine densities (Hutsler and Zhang, 2010) have also been reported. These neurostructural findings suggest altered rates of neurogenesis, delayed or reduced apoptosis or pruning or local failures of migration.

The postmortem literature is also quite variable, however, due to limitations which may be addressed through MRI and other *in vivo* imaging techniques. Some postmortem neuropathology is described as "patchy" at the individual case level (Bailey et al., 1998; Hutsler et al., 2007), and some findings are inconsistent across research groups or methods (Bailey et al., 1998; Bauman and Kemper, 2005; Hutsler et al., 2007). Furthermore, it is quite likely that histological differences that can be detected vary with the age of the case, particularly over the course of childhood, as indicated by *in vivo* MRI studies (Courchesne et al., 2001; Carper et al., 2002; Schumann et al., 2010; Hazlett et al., 2011). Such variability is difficult to overcome in postmortem studies, which are usually limited to small samples (averaging about 5 cases per study; Schumann and Nordahl, 2011) across wide age spans, with most cases in the adolescent or adult range. In addition, since histologic studies are extremely time consuming, studies are often limited to samples of only a few anatomical regions rather than whole-brain surveys. Longitudinal studies are furthermore impossible, limiting any developmental interpretations of post-mortem findings. *In vivo* imaging techniques may overcome many of these issues, allowing large sample sizes, whole-brain assessment, and longitudinal studies. However, examination of sub-voxel features such as dendritic or axonal organization and cortical cytoarchitecture has remained beyond the reach of *in vivo* imaging studies on ASD published to date.

The ability to describe cytoarchitecture and neuronal connectivity at the sub-millimeter level in living subjects would be a tremendous boon to research of neurodevelopmental and other neurologic disorders. Continuing improvements in system hardware and advances in acquisition techniques and sequence programming continue to push back the limits on spatial resolution. At the same time, new models for analysis of diffusion MRI allow examination of separate compartments within a single voxel. The combination of multi-shell diffusion acquisitions and multi-compartmental analysis approaches permits estimates of neurite (both axon and dendrite) content and organization within clinically manageable acquisition times (Jensen et al., 2005; Lu et al., 2006; Zhang et al., 2012; White et al., 2013). *Multi-shell* diffusion imaging (i.e., acquisition at multiple *b*-values and multiple diffusion directions), allows classification of diffusion at multiple length scales, disambiguating restricted (slow) diffusion from hindered (fast) diffusion. Inclusion of high *b*-values allows insight into micro-scale structures such as the organization and density of dendritic and axonal processes (neurites; Barazany et al., 2009; Raffelt et al., 2012; Assaf et al., 2013; Dell'Acqua et al., 2013). Here we used Restriction Spectrum Imaging (RSI, White et al., 2013), one such analysis approach, for *in vivo* examination of neurite organization within cerebral cortex in an ASD population.

RSI extends the spherical deconvolution model (Tournier et al., 2004) across these multiple length scales to characterize neurite density and organization at each imaged voxel. Analogous models have been used to examine white matter in one study of young adults with ASD (Lazar et al., 2014) but, to our knowledge, this is the first time that a multi-compartmental model has been applied to cortical gray matter in this population and the first time this age group has been addressed. We examined 48 cortical regions of interest per hemisphere in a population of 24 ASD and 20 TD children and adolescents.

MATERIALS AND METHODS

Participants

Participants ranged between 7 and 17 years of age and included both males and females. All potential ASD participants were administered the Autism Diagnostic Observation Schedule (ADOS, Lord et al., 2001), and their parents completed the Autism Diagnostic Interview-Revised (ADI-R, Rutter et al., 1995). Final diagnosis of Autism Spectrum Disorder was determined by a trained clinical psychologist according to DSM-V criteria (American Psychiatric Association, 2013) and with reference to ADOS and ADI-R scores. Children with known history of neurological disorders other than ASD (e.g., Fragile X syndrome, epilepsy) were excluded. Typically developing (TD) participants were recruited from the community, excluding anyone with a personal or family history of autism or a personal history of other neurologic or psychiatric conditions. Participants were also administered the Wechsler Abbreviated Scale of Intelligence (WASI, Wechsler, 1999), the Social Responsiveness Scale (SRS, Constantino and Gruber, 2005), and the Edinburgh Handedness Inventory (Oldfield, 1971). The study was approved by the University of California, San Diego, and San Diego State University Institutional Review Boards, with written

informed consent and assent provided by all participants and caregivers.

MRI Data Acquisition and Preprocessing

MRI data were collected on a GE Discovery MR 750 3.0T system using an 8-channel head coil. Diffusion was measured with a multi-shell EPI sequence encoded for 45 non-collinear diffusion directions, (15 unique directions at each of 3 *b*-values: 500, 1500, and 4000 s/mm^2) and 2 at b = 0 s/mm^2 (in-plane resolution=1.875 × 1.875 mm, thickness = 2.5 mm, TR = 7 s, TE = 87.4 ms, flip = 90°). An anatomical T1-weighted fast spoiled gradient echo (FSPGR) scan (1 mm^3, TR = 8.108 s, TE = 3.172 ms, flip = 8°) was also acquired. Preprocessing of diffusion data was performed using in-house software and included eddy current correction (Zhuang et al., 2006), rigid body correction for motion with corresponding adjustments to the vector matrix, correction of susceptibility-induced field distortions (Holland et al., 2010), and correction for gradient non-linearities (Jovicich et al., 2006).

Quality Assessment and Motion Quantification

Multi-shell diffusion images were initially collected from 33 ASD and 24 TD children and adolescents. Average translation and rotation between acquisitions was calculated for each participant and considered for group matching. All image data, including each diffusion direction and *b*-value, were also visually inspected for motion-related signal dropout and other artifacts. The high *b*-value shell is particularly sensitive to motion-related dropout leading to a high exclusion rate. Seven subjects were excluded for excessive dropout (5 ASD, 2 TD) and an additional six for translation >1 mm or rotation >.01 radians (0.6 degrees, 4 ASD, 2 TD). Participants who were excluded did not differ significantly from those who were included with regard to age, IQ, or symptom severity (ADOS, ADI, SRS), for either subject group.

Restriction Spectrum Imaging

The RSI model is based on the compartmentalization of water in brain tissue. Diffusion of water molecules within brain tissue is constrained by cell membranes and other structures and thus ranges from *restricted diffusion,* as in intra-cellular spaces where water is (on time scales examined here) unable to diffuse beyond the cellular or axonal membrane, to *free diffusion,* found in fluid spaces where diffusion is unencumbered by barriers such as membranes or large proteins (Le Bihan, 2012). Between these extremes, diffusion is *hindered*, e.g., in extracellular spaces where water must follow a tortuous path to pass around cell membranes or other obstacles, but is not enclosed by such barriers (Assaf and Basser, 2005). RSI applies a mathematical model (White et al., 2013, 2014) to determine the proportion of a voxel (*volume fraction*) and signal (*signal fraction*) stemming from hindered, restricted, or free water compartments and the geometry of diffusion within each of these compartments (isotropic or anisotropic). The algorithm is described in detail in the original validation study (White et al., 2013) and represents an extension of the linear spherical deconvolution model (Tournier et al., 2004; Dell'Acqua et al., 2007; Jian and Vemuri, 2007; Kaden et al., 2007) to multiple diffusion length scales. In the current application we used five diffusion length scales. The volume fraction of anisotropic restricted diffusion (the shortest length scale examined) is believed to reflect the relative density of neuronal processes (neurite density, ND; White et al., 2013). ND was calculated for each voxel, as were the fractional anisotropy (FA) and mean diffusivity (MD) derived from the diffusion tensor. The ND volume fraction was standardized to a 1–1000 range; FA ranged 0–1.

Analysis of Anatomical Images and Extraction of ROIs

Preprocessing of anatomical T1 scans included correction for gradient non-linearities (Jovicich et al., 2006) and brain extraction (Smith, 2002). A gray matter mask was derived for each subject (Avants et al., 2011b) and affine registration was used to align each participant's T1 to the corresponding RSI image and to a sample-specific template in MNI space which had been derived using Advanced Normalization Tools (ANTS, Avants et al., 2010, 2011a). This allowed backward transformation of the Harvard-Oxford cortical atlas (http://fsl.fmrib.ox.ac.uk/fsl/fslwiki/Atlases) from MNI space to each individual's native diffusion space, providing 48 gyral-level ROIs for each hemisphere. Average ND, FA, and MD within gray matter were calculated for each of these ROIs and for the overall cerebral lobes (see Supplementary Table 1 for ROIs and their lobar designations).

RESULTS

The final sample included 24 ASD participants (5 female) aged 7–17 years, and 20 TD participants (2 female) aged 8–17 years. Groups were well matched for age, non-verbal IQ, and motion measures with all $p > 0.5$ (**Table 1**). The ASD group had lower verbal IQ as is frequently found in this socio-communicative disorder.

Linear regressions were performed on ND, FA, and MD measures separately for each lobe and hemisphere with age, group, group-by-age interaction, and a constant included in each model. The false discovery rate (FDR, Benjamini and Hochberg, 1995) was used to correct for multiple comparisons. All regressions performed on a single dependent variable (ND, FA, or MD) were included within a statistical family with the significance of each overall *F*-test included in that correction. Coefficients were corrected in a similar fashion.

Lobar Effects

Regressions were significant for ND in all lobes in the right hemisphere and for frontal, parietal, and occipital lobes in the left hemisphere (**Table 2**). The effects of age were significant and positive (increasing with age) in all of these. Rates ranged from 1.38 per year (left occipital lobe) to 4.11 per year (right frontal lobe) with the volume fraction standardized to a 1–1000 scale (**Figures 1A,B**). Group differences showed reduced ND in left parietal and left occipital lobes in ASD compared to TD participants (**Figure 2**) with moderate effect sizes ranging

TABLE 1 | Demographics.

	ASD ($n = 24$) mean ± *SD* [range]	TD ($n = 20$) mean ± *SD* [range]	*p*-value
Age (years)	13.41 ± 3.30 [7.43–17.98]	13.72 ± 2.91 [8.19–17.69]	0.693
WASI_VIQ	91.83 ± 17.25 [56–118]	104.45 ± 10.28 [73–126]	0.005
WASI_NVIQ	98.54 ± 19.33 [53–140]	101.65 ± 15.06 [62–123]	0.552
Avg. Translation	0.61 ± 0.11 [0.41–0.86]	0.62 ± 0.12 [0.33–0.85]	0.791
Avg. Rotation	0.003 ± 0.0021 [0.0012–0.0081]	0.0029 ± 0.0025 [0.0011–0.0098]	0.893
SRS Total	84.13 ± 8.53 [62–100]	43.15 ± 5.61 [35–52]	<0.001
ADOS-2 SA	12.26 ± 3.86 [6–20]		
ADOS-2 RRB	3.44 ± 2.33 [1–12]		
ADOS-2 Severity	8.32 ± 1.70 [4–10]		
ADI Soc	18.50 ± 4.08 [13–28]		
ADI Comm	13.25 ± 4.40 [6–24]		
ADI Rep	5.96 ± 2.48 [1–12]		
Female	$n = 5$	$n = 2$	
Left Handed	$n = 5$	$n = 2$	

ASD, Autism Spectrum Disorder; TD, Typically Developing; WASI, Wechsler Abbreviated Scales of Intelligence; VIQ, Verbal IQ; NVIQ, Non-verbal IQ; SRS, Social Responsiveness Scale; ADOS-2, Autism Diagnostic Observation Schedule-2nd edition; SA, Social Affect; RRB, Restricted and Repetitive Behavior; ADI-R, Autism Diagnostic Interview, Revised; Soc, Social interaction subscale; Comm, Communication subscale; Rep, Restricted and Repetitive Behaviors subscale.

TABLE 2 | Linear regression results (*p*-values) for neurite density, fractional anisotropy, and mean diffusivity by lobe.

	Lobe		Group	Age	Age X Group	Overall *F*-test
ND	Left	Frontal	0.290	0.003*	0.425	0.011*
		Parietal	0.018	0.002*	0.471	0.001*
		Temporal	0.215	0.197	0.622	0.270
		Occipital	0.043	<0.001*	0.657	<0.001*
	Right	Frontal	0.237	<0.001*	0.281	<0.001*
		Parietal	0.051	0.015*	0.397	0.011*
		Temporal	0.106	0.005*	0.995	0.013*
		Occipital	0.121	0.003*	0.269	0.004*
FA	Left	Frontal	0.678	0.807	0.275	0.709
		Parietal	0.751	0.418	0.045	0.147
		Temporal	0.393	0.748	0.159	0.470
		Occipital	0.312	0.659	0.663	0.726
	Right	Frontal	0.984	0.090	0.417	0.284
		Parietal	0.640	0.083	0.035	0.037
		Temporal	0.656	0.147	0.698	0.438
		Occipital	0.368	0.561	0.453	0.664
MD	Left	Frontal	0.091	0.001*	0.788	0.002*
		Parietal	0.011	<0.001*	0.760	<0.001*
		Temporal	0.115	0.091	0.665	0.137
		Occipital	0.027	<0.001*	0.840	<0.001*
	Right	Frontal	0.080	<0.001*	0.547	<0.001*
		Parietal	0.020	<0.001*	0.864	<0.001*
		Temporal	0.088	0.025*	0.509	0.044
		Occipital	0.041	<0.001*	0.601	<0.001*

*Uncorrected p-values of each coefficient shown. *Significant following FDR correction for multiple comparisons. Tests of each coefficient and dependent variable (ND, FA, MD) treated as a statistical family for FDR.*

from 0.37 to 0.75, but these did not survive correction for multiple comparisons. Interactions between group and age were not significant.

On the MD measure, regressions were significant bilaterally in frontal, parietal and occipital lobes, but not temporal lobes. All of these showed significant negative effects of age (decreasing with age) with rates ranging from -2.445×10^{-6} mm^2/s per year (left frontal lobe) to -3.875×10^{-6} mm^2/s per year (left parietal lobe). MD was higher in ASD in the parietal and occipital lobes bilaterally (**Figure 2**) again with medium effect sizes (0.49 to 0.67). However, these did not survive correction for multiple comparisons. There were no significant interactions. By contrast, similar linear regression analyses for FA values did not reach significance after correction for multiple comparisons.

Localized Effects

Individual ROIs were also examined for a more localized understanding of effects in MD and ND (see Supplementary Table 1 for list of ROIs examined), using similar linear regression models. For each dependent variable, all regions were included bilaterally to correct each coefficient for multiple comparisons (48 regions x 2 hemispheres).

Regressions on ND were significant for all regions on the dorsolateral aspect of the right frontal lobe as well as the right anterior cingulate, paracingulate, operculum and insula (Supplementary Table 2, **Figures 1C,D**). Left frontal effects were restricted to anterior cingulate, paracingulate, central operculum, and posterior portions of the dorsal surface. Regressions were also significant for all subregions of parietal lobes (except bilateral superior parietal lobule, right precuneus, and right postcentral),

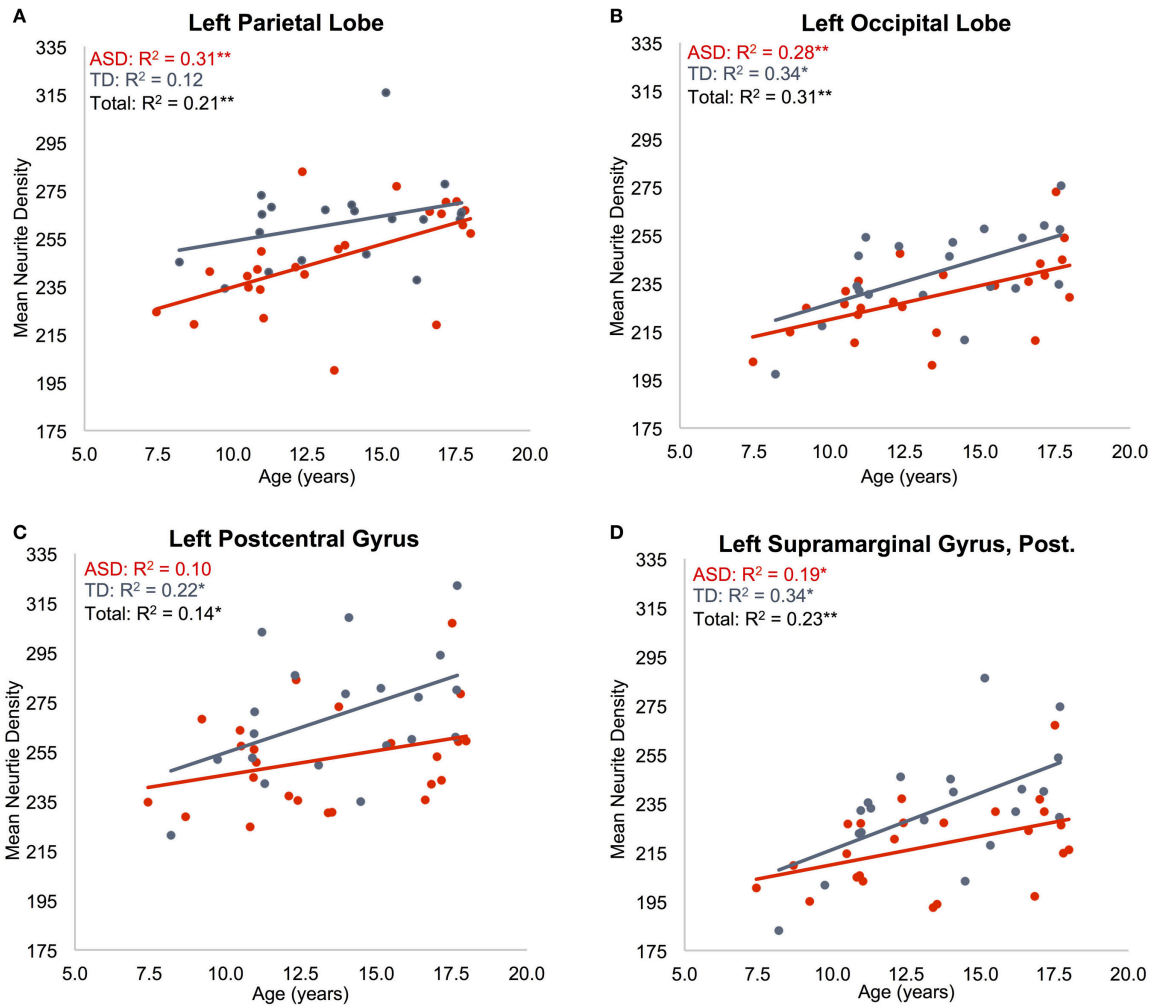

FIGURE 1 | Effects of age on neurite density. Mean ND is shown as a function of subject age for: **(A)** left parietal lobe, **(B)** left occipital lobe, **(C)** left postcentral gyrus, **(D)** posterior division of left supramarginal gyrus. ASD indicated in red, TD indicated in blue. Neurite density standardized to a 0–1000 range. *$p < 0.05$, **$p < 0.005$.

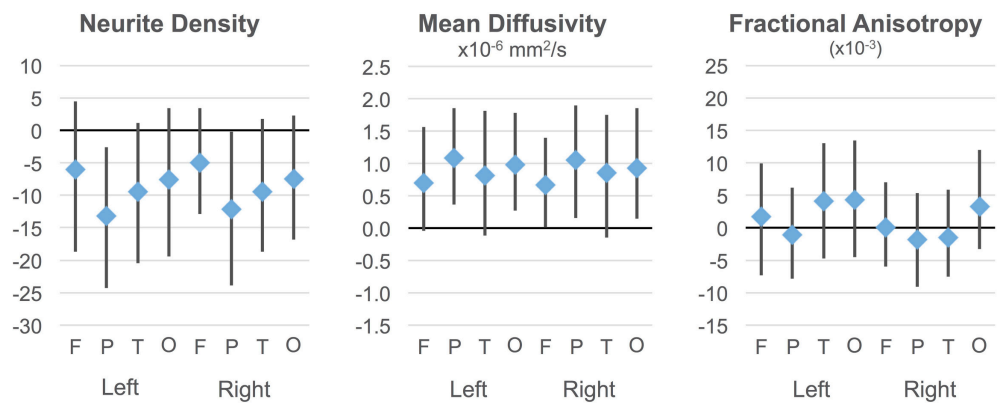

FIGURE 2 | Group differences in ND, MD, and FA. Group differences and 95% confidence intervals are shown for each cortical lobe. Positive values indicate ASD >TD. Neurite density standardized to a 0–1000 range.

a few bilateral temporal regions including posterolateral regions, planum temporale, Heschl's gyrus, and right temporal occipital fusiform gyrus, and portions of occipital lobe including bilateral posterior cingulate. All of these except left Heschl's gyrus exhibited significantly greater ND with increasing age.

Group effects (see Supplementary Figure 1 for group differences and confidence intervals) suggested that ND was reduced in ASD in a number of regions (e.g., anterior cingulate, precentral and supramarginal gyri bilaterally, parts of superior temporal gyrus, fusiform, and planum temporale on the right), but only left temporal occipital fusiform cortex survived correction for multiple comparisons (and overall regression was not significant). The only significant group-by-age interaction was in right anterior cingulate with ND increasing more rapidly with age in ASD.

With only one exception (right temporal occipital fusiform), all regions that showed significant positive age effects on ND also showed significant negative effects on the MD measure (Supplementary Figure 2, Supplementary Table 3). In addition, left superior parietal lobule was affected, and more of left frontal lobes (left middle frontal, subcallosal gyri), and occipital lobes (bilateral intracalcarine cortex and pole, right lateral occipital gyrus, left supracalcarine, cuneal, and lingual regions) showed age effects.

Group differences on MD did not survive correction, but the tendency was toward higher MD in ASD than TD particularly in parietal regions and in several frontal and occipital regions (see Supplementary Figure 2 for group differences and confidence intervals). Interactions were not significant.

DISCUSSION

The present study is—to our knowledge—the first to apply a multi-compartmental diffusion model using multishell MRI to the study of *cortical gray matter* microstructure in ASD. We found robust age effects for both ND (increasing) and MD (decreasing), but not FA, a measure more suited to tissues with well-aligned microstructure such as in the deep white matter. Trends toward decreased ND and increased MD in ASD did not survive correction for multiple comparisons when examined at the lobar level. More localized examination again showed robust age effects in the ND and MD measures, and a significant group difference was found on ND (ASD<TD) in the left temporal occipital fusiform gyrus. While other ND differences did not survive correction for multiple comparisons, examination of confidence intervals (Supplementary Figures 1, 2) suggests that larger sample sizes or improvements in signal-to-noise and motion control (see Limitations) may support such differences.

Our findings indicate that multi-shell, multi-compartmental approaches may provide a valuable addition to our ability to examine gray matter microstructure in ASD and other disorders. While the RSI derived ND measure may not be as sensitive as the tensor-derived MD measure, it offers greater interpretability and specificity as discussed below.

Neurite Density and Mean Diffusivity

The ND measure is likely driven primarily by axons, and particularly myelinated axons, rather than dendrites within cerebral cortex. At the diffusion time-scales examined here, unmyelinated neurites allow some amount of water exchange across the cellular membrane. Since the ND measure is derived from elements with cylindrical symmetry, wherein diffusion is restricted in the direction transverse to the cylinder, but relatively unencumbered along the long axis, unmyelinated elements will contribute less overall signal to the neurite water compartment due to greater water exchange. Hence, lower ND such as that seen in younger participants likely reflects: (1) lower density of myelinated axons, (2) thinner myelin (allowing greater average water exchange), or possibly (3) smaller average caliber of myelinated axons which would be associated with less water in the restricted cylindrical pool.

Cortical MD may be driven by the same factors (but in the opposite direction) since ND and MD measures will tend to correlate inversely with each other. MD is highest where diffusion is free and lowest where it is restricted (e.g., areas of high ND). However, MD is derived from a tensor model and does not distinguish intracellular from extracellular compartments as do RSI derived measures. Other possible causes of MD effects therefore cannot be excluded in regions where ND effects were not detected. Inflammatory responses also lead to increased MD due to increased tissue water (Alexander et al., 2007) but would not be expected to alter intracellular measures such as ND. Signs of inflammation have been reported in ASD (Vargas et al., 2005; Zimmerman et al., 2005; Morgan et al., 2010; Suzuki et al., 2013) so this potential contributor must be considered. Alternatively, MD may simply be a more robust measure than ND when examining gray matter. With only about 25% of the cortical diffusion volume fraction being restricted, ND signal-to-noise will be lower than in the composite MD measure. The relative simplicity of the tensor model may also make measures such as MD more robust than those derived from the more complex RSI model. However, since effect sizes for ND ranged from medium to large (0.37 to 0.75) the lack of more significant findings may have been due to limited sample size, accompanied by expected variability due to the known etiological heterogeneity in ASD (Geschwind and State, 2015).

Age Effects

The validity of the ND metric was supported by robust maturational effects detected in our study. ND increased significantly with age in all lobes except left temporal when groups were combined, showing clear sensitivity to developmental change. At first glance, the direction of change may appear unexpected: The number of cortical synapses, and presumably the complexity of dendritic branches, begins to decrease prior to age 8 years (Huttenlocher and Dabholkar, 1997), while cortical gray matter volume stabilizes (Courchesne et al., 2000), so that a measure of "neurite density" might be expected to decline during this period. However, as described above, the ND measure is probably particularly sensitive to the degree of axonal myelination, which continues well into adulthood. This is supported by multi-shell diffusion studies on neurotypical white matter development that also found age related increases in intraneurite compartments using compartmental diffusion models other than RSI. In a recent abstract, Chang et al. (2015) reported increasing intra-axonal

volume fractions across childhood and adolescence using neurite orientation dispersion and density imaging (NODDI). Significant age related increases were also reported by Jelescu et al. (2015) in infants and toddlers, and by Billiet et al. (2015) in adults, with both of these using both NODDI and diffusion kurtosis imaging. These latter studies concluded that the age effects must be at least partially reflective of ongoing myelination, rather than strictly of intra-axonal volume fractions. Indeed, the same NODDI measure was found to correlate with direct staining of myelin in a rat model (Jespersen et al., 2007).

Localization of Group Trends

While group differences on ND were only marginal,—surviving correction for multiple comparisons in only a single region—and therefore must be viewed with substantial caution, the localization of these results deserves some consideration in context of the postmortem literature. ND tended to be lower in ASD than TD in bilateral anterior cingulate gyri, for which increased cell packing density has been reported in several ASD post-mortem cases (Kemper and Bauman, 1998; Schumann and Amaral, 2006). This region also showed the only group-by-age interaction surviving correction, with the ASD group showing a greater increase in ND with age than TD. One of these postmortem studies also examined axons just beneath the cortex (Zikopoulos and Barbas, 2010). In that study, axons were sampled from white matter beneath four areas of frontal lobe in five adult ASD postmortem cases, finding a relative shift from larger to smaller caliber axons exiting the anterior cingulate cortex. As discussed above, smaller myelinated axons are one potential source of ND reductions, which would be consistent with our findings. Zikopoulos and Barbas (2010) also found decreased myelin thickness in axons exiting orbital frontal cortex compared to controls. But, while myelin thickness is another potential source of ND changes, we found little evidence of a group difference in orbital cortex. Other areas where shifts in cell packing density have been reported in ASD include the hippocampus and amygdala, which were not examined here, the prefrontal cortex (though not consistently), and potentially the superior temporal gyrus given findings of narrowed minicolumns. In our sample, ND did tend to be lower in the ASD group in the superior temporal gyrus and its superior aspect (Heschl's gyrus, planum temporale) primarily in the right hemisphere. We found no evidence of prefrontal differences. One group has reported *decreased* cell density in fusiform cortex, whereas we found lower ND that was limited to the posterior aspect of the gyrus.

LIMITATIONS

The absence of significant group differences in RSI may partly reflect the inter-case variability of cytoarchitectonic abnormalities in ASD, commonly found in the literature (Bailey et al., 1998; Hutsler et al., 2007; Wegiel et al., 2010). Additionally, some neuropathologies may not affect the same regions of cortex across all ASD cases, such as laminar differences that have been described as "patchy" (Hutsler et al., 2007). Group-wise analyses such as those used here would not be sensitive to such subject-specific anomalies. Notably, one recent study demonstrated the utility of a multi-compartment diffusion approach for identification of focal cortical dysplasias, not unlike those reported in ASD cases, on a case-wise basis (Winston et al., 2014). Intracellular volume fraction, their marker of neurite density, highlighted focal dysplasias more prominently than traditional diffusion or structural imaging. With a large normative sample, it might be possible to detect focal dysplasias *in vivo* on a case-wise basis in ASD and other disorders using RSI or other compartmental diffusion models.

As with all MRI methodologies, subject motion during scanning can be an issue, particularly when comparing groups that may differ in their likelihood of motion. We thoroughly screened all scans for subject motion resulting in well-matched subject groups. However, better protection of multi-shell diffusion sequences from motion may be possible. Our highest *b*-value shell ($b = 4000$ s/mm^2) was particularly susceptible to motion-related slice dropout, forcing us to exclude c. 27% of ASD participants. This could be improved either by reducing the maximum gradient strength while losing sensitivity to the shortest diffusion distances or, more simply, by repeating the acquisition of this highest shell to allow signal averaging.

Although RSI provides insight to subvoxel neural content in the form of separate intra and extracellular compartments, partial volume effects are still relevant. Voxel size was large (8.8 mm^3) leading to inclusion of both gray and white matter within voxels and averaging across lamina. Higher resolutions may be possible with accelerated imaging techniques, but are unlikely to reach sublaminar resolution in the near future.

RSI is not sensitive to all types of cytoarchitectonic anomalies reported in the ASD literature, such as dysmorphology of specific cell types, ectopias, and abnormal dendritic spine density.

The sample examined here spanned a broad and developmentally complex age range, from 7 to 17 years. After controlling for subject motion, sample sizes of 24 and 20 participants per group were somewhat limited for such a broad range. We were also limited to participants who were relatively high functioning in order to maximize subject cooperation during scanning. Results derived here may not, therefore, generalize to lower-functioning ASD populations or to populations outside of the examined age range.

CONCLUSION

DWI methods are typically restricted to examination of white matter. However, RSI shows substantial promise for microstructural examination of gray matter in ASD. The method is sensitive to effects of age, suggests that group differences may be detected with larger sample sizes, and offers greater interpretability than the traditional diffusion tensor measures FA and MD. The robust age effects that were found for ND support the validity and sensitivity of multi-shell, multi-compartment DWI for *in vivo* examination of gray matter in developmental populations. While RSI is not sensitive to all types

of cytoarchitectonic anomalies reported in the ASD literature, measures are likely to reflect intracortical axonal content, myelination, and caliber, which have received limited attention in postmortem studies and can thus complement these in important ways. In the context of fundamental advantages of *in vivo* studies, which can be combined with functional (functional imaging or behavioral) assays, provide a whole brain field of view, and can be administered in longitudinal designs, the first findings reported here suggest that multishell diffusion imaging may be a promising complement to postmortem neurohistology in ASD.

AUTHOR CONTRIBUTIONS

RC, NW, and RM contributed to the conception and design of the work; RC, JT, and JK contributed to the processing, analysis, and presentation of data; all authors contributed to the manuscript itself.

FUNDING

This study was supported by National Institutes of Health grants R01-MH081023 and K01-MH097972, and by National Science Foundation Grant No. 1430082.

ACKNOWLEDGMENTS

Our sincere thanks to our participants and their families for sharing their time with us. Additional thanks to Dr. Qidi Peng and Miss Afrooz Jahedi for statistical consultation.

SUPPLEMENTARY MATERIAL

The Supplementary Material for this article can be found online at: http://journal.frontiersin.org/article/10.3389/fnins.2016.00610/full#supplementary-material

REFERENCES

Alexander, A. L., Lee, J. E., Lazar, M., and Field, A. S. (2007). Diffusion tensor imaging of the brain. *Neurotherapeutics* 4, 316–329. doi: 10.1016/j.nurt.2007.05.011

Assaf, Y., Alexander, D. C., Jones, D. K., Bizzi, A., Behrens, T. E., Clark, C. A., et al. (2013). The CONNECT project: combining macro- and micro-structure. *Neuroimage* 80, 273–282. doi: 10.1016/j.neuroimage.2013.05.055

American Psychiatric Association (2013). *Diagnostic and Statistical Manual of Mental Disorders, 5th Edn*. Washington, DC: American Psychiatric Association.

Assaf, Y., and Basser, P. J. (2005). Composite hindered and restricted model of diffusion (CHARMED) MR imaging of the human brain. *Neuroimage* 27, 48–58. doi: 10.1016/j.neuroimage.2005.03.042

Avants, B. B., Tustison, N. J., Song, G., Cook, P. A., Klein, A., and Gee, J. C. (2011a). A reproducible evaluation of ANTs similarity metric performance in brain image registration. *Neuroimage* 54, 2033–2044. doi: 10.1016/j.neuroimage.2010.09.025

Avants, B. B., Tustison, N. J., Wu, J., Cook, P. A., and Gee, J., C. (2011b). An open source multivariate framework for n-tissue segmentation with evaluation on public data. *Neuroinformatics* 9, 381–400. doi: 10.1007/s12021-011-9109-y

Avants, B. B., Yushkevich, P., Pluta, J., Minkoff, D., Korczykowski, M., Detre, J., et al. (2010). The optimal template effect in hippocampus studies of diseased populations. *Neuroimage* 49, 2457–2466. doi: 10.1016/j.neuroimage.2009.09.062

Bailey, A., Luthert, P., Dean, A., Harding, B., Janota, I., Montgomery, M., et al. (1998). A clinicopathological study of autism. *Brain* 121 (Pt 5), 889–905.

Barazany, D., Basser, P. J., and Assaf, Y. (2009). *In vivo* measurement of axon diameter distribution in the corpus callosum of rat brain. *Brain* 132, 1210–1220. doi: 10.1093/brain/awp042

Bauman, M. L., and Kemper, T. L. (1985). Histoanatomic observations of the brain in early infantile autism. *Neurology* 35, 866–874.

Bauman, M. L., and Kemper, T. L. (2005). Neuroanatomic observations of the brain in autism: a review and future directions. *Int. J. Dev. Neurosci.* 23, 183–187. doi: 10.1016/j.ijdevneu.2004.09.006

Benjamini, Y., and Hochberg, Y. (1995). Controlling the false discovery rate - a practical and powerful approach to multiple testing. *J. R. Stat. Soc. Ser. B Methodol.* 57, 289–300.

Billiet, T., Vandenbulcke, M., Madler, B., Peeters, R., Dhollander, T., Zhang, H., et al. (2015). Age-related microstructural differences quantified using myelin water imaging and advanced diffusion MRI. *Neurobiol. Aging* 36, 2107–2121. doi: 10.1016/j.neurobiolaging.2015.02.029

Buxhoeveden, D. P., Semendeferi, K., Buckwalter, J., Schenker, N., Switzer, R., and Courchesne, E. (2006). Reduced minicolumns in the frontal cortex of patients with autism. *Neuropathol. Appl. Neurobiol.* 32, 483–491. doi: 10.1111/j.1365-2990.2006.00745.x

Carper, R. A., Moses, P., Tigue, Z. D., and Courchesne, E. (2002). Cerebral lobes in autism: early hyperplasia and abnormal age effects. *Neuroimage* 16, 1038–1051. doi: 10.1006/nimg.2002.1099

Casanova, M. F., Buxhoeveden, D. P., Switala, A. E., and Roy, E. (2002). Minicolumnar pathology in autism. *Neurology* 58, 428–432. doi: 10.1212/WNL.58.3.428

Casanova, M. F., van Kooten, I. A., Switala, A. E., van Engeland, H., Heinsen, H., Steinbusch, H. W., et al. (2006). Minicolumnar abnormalities in autism. *Acta Neuropathol.* 112, 287–303. doi: 10.1007/s00401-006-0085-5

Chang, Y.-S., Owen, J. P., Pojman, N. J., Thieu, T., Bukshpun, P., Wakahiro, M. L. J., et al. (2015). *White Matter Changes of Neurite Density and Orientation Dispersion during Human Brain Maturation (Abstract)*. Honolulu, HI: Organization for Human Brain Mapping.

Constantino, J. N., and Gruber, C. P. (2005). *Social Responsiveness Scale*. Los Angeles, CA: Western Psychological Services.

Courchesne, E., Chisum, H. J., Townsend, J., Cowles, A., Covington, J., Egaas, B., et al. (2000). Normal brain development and aging: quantitative analysis at *in vivo* MR imaging in healthy volunteers. *Radiology* 216, 672–682. doi: 10.1148/radiology.216.3.r00au37672

Courchesne, E., Karns, C. M., Davis, H. R., Ziccardi, R., Carper, R. A., Tigue, Z. D., et al. (2001). Unusual brain growth patterns in early life in patients with autistic disorder: an MRI study. *Neurology* 57, 245–254. doi: 10.1212/WNL.57.2.245

Courchesne, E., Mouton, P. R., Calhoun, M. E., Semendeferi, K., Ahrens-Barbeau, C., Hallet, M. J., et al. (2011). Neuron number and size in prefrontal cortex of children with autism. *JAMA* 306, 2001–2010. doi: 10.1001/jama.2011.1638

Dell'Acqua, F., Rizzo, G., Scifo, P., Clarke, R. A., Scotti, G., and Fazio, F. (2007). A model-based deconvolution approach to solve fiber crossing in diffusion-weighted MR imaging. *IEEE Trans. Biomed. Eng.* 54, 462–472. doi: 10.1109/TBME.2006.888830

Dell'Acqua, F., Simmons, A., Williams, S. C., and Catani, M. (2013). Can spherical deconvolution provide more information than fiber orientations? Hindrance modulated orientational anisotropy, a true-tract specific index to characterize white matter diffusion. *Hum. Brain Mapp.* 34, 2464–2483. doi: 10.1002/hbm.22080

Geschwind, D. H., and State, M. W. (2015). Gene hunting in autism spectrum disorder: on the path to precision medicine. *Lancet Neurol.* 14, 1109–1120. doi: 10.1016/S1474-4422(15)00044-7

Hazlett, H. C., Poe, M. D., Gerig, G., Styner, M., Chappell, C., Smith, R. G., et al. (2011). Early brain overgrowth in autism associated with an increase in cortical surface area before age 2 years. *Arch. Gen. Psychiatry* 68, 467–476. doi: 10.1001/archgenpsychiatry.2011.39

Holland, D., Kuperman, J. M., and Dale, A. M. (2010). Efficient correction of inhomogeneous static magnetic field-induced distortion in Echo Planar Imaging. *Neuroimage* 50, 175–183. doi: 10.1016/j.neuroimage.2009.11.044

Hutsler, J. J., and Casanova, M. F. (2016). Review: cortical construction in autism spectrum disorder: columns, connectivity and the subplate. *Neuropathol. Appl. Neurobiol.* 42, 115–134. doi: 10.1111/nan.12227

Hutsler, J. J., Love, T., and Zhang, H. (2007). Histological and magnetic resonance imaging assessment of cortical layering and thickness in autism spectrum disorders. *Biol. Psychiatry* 61, 449–457. doi: 10.1016/j.biopsych.2006.01.015

Hutsler, J. J., and Zhang, H. (2010). Increased dendritic spine densities on cortical projection neurons in autism spectrum disorders. *Brain Res.* 1309, 83–94. doi: 10.1016/j.brainres.2009.09.120

Huttenlocher, P. R., and Dabholkar, A. S. (1997). Regional differences in synaptogenesis in human cerebral cortex. *J. Comp. Neurol.* 387, 167–178.

Jelescu, I. O., Veraart, J., Adisetiyo, V., Milla, S. S., Novikov, D. S., and Fieremans, E. (2015). One diffusion acquisition and different white matter models: how does microstructure change in human early development based on WMTI and NODDI? *Neuroimage* 107, 242–256. doi: 10.1016/j.neuroimage.2014.12.009

Jensen, J. H., Helpern, J. A., Ramani, A., Lu, H., and Kaczynski, K. (2005). Diffusional kurtosis imaging: the quantification of non-gaussian water diffusion by means of magnetic resonance imaging. *Magn. Reson. Med.* 53, 1432–1440. doi: 10.1002/mrm.20508

Jespersen, S. N., Kroenke, C. D., Østergaard, L., Ackerman, J. J. H., and Yablonskiy, D. A (2007). Modeling dendrite density from magnetic resonance diffusion measurements. *Neuroimage* 34, 1473–1486. doi: 10.1016/j.neuroimage.2006.10.037

Jian, B., and Vemuri, B. C. (2007). A unified computational framework for deconvolution to reconstruct multiple fibers from diffusion weighted MRI. *IEEE Trans. Med. Imaging* 26, 1464–1471. doi: 10.1109/TMI.2007.907552

Jovicich, J., Czanner, S., Greve, D., Haley, E., van der Kouwe, A., Gollub, R., et al. (2006). Reliability in multi-site structural MRI studies: effects of gradient non-linearity correction on phantom and human data. *Neuroimage* 30, 436–443. doi: 10.1016/j.neuroimage.2005.09.046

Kaden, E., Knosche, T. R., and Anwander, A. (2007). Parametric spherical deconvolution: inferring anatomical connectivity using diffusion MR imaging. *Neuroimage* 37, 474–488. doi: 10.1016/j.neuroimage.2007.05.012

Kemper, T. L., and Bauman, M. (1998). Neuropathology of infantile autism. *J. Neuropathol. Exp. Neurol.* 57, 645–652.

Lazar, M., Miles, L. M., Babb, J. S., and Donaldson, J. B. (2014). Axonal deficits in young adults with High Functioning Autism and their impact on processing speed. *Neuroimage Clin.* 4, 417–425. doi: 10.1016/j.nicl.2014.01.014

Le Bihan, D. (2012). Diffusion, confusion and functional MRI. *Neuroimage* 62, 1131–1136. doi: 10.1016/j.neuroimage.2011.09.058

Lord, C., Rutter, M., DiLavore, P., and Risi, S. (2001). *Autism Diagnostic Observation Schedule.* Los Angeles, CA: Western Psychological Services.

Lu, H., Jensen, J. H., Ramani, A., and Helpern, J. A. (2006). Three-dimensional characterization of non-gaussian water diffusion in humans using diffusion kurtosis imaging. *NMR Biomed.* 19, 236–247. doi: 10.1002/nbm.1020

Morgan, J. T., Chana, G., Pardo, C. A., Achim, C., Semendeferi, K., Buckwalter, J., et al. (2010). Microglial activation and increased microglial density observed in the dorsolateral prefrontal cortex in autism. *Biol. Psychiatry* 68, 368–376. doi: 10.1016/j.biopsych.2010.05.024

Oldfield, R. C. (1971). The assessment and analysis of handedness: the Edinburgh inventory. *Neuropsychologia* 9, 97–113.

Palmen, S. J. M. C., van Engeland, H., Hof, P. R., and Schmitz, C. (2004). Neuropathological findings in autism. *Brain* 127, 2572–2583. doi: 10.1093/brain/awh287

Raffelt, D., Tournier, J. D., Rose, S., Ridgway, G. R., Henderson, R., Crozier, S., et al. (2012). Apparent Fibre Density: a novel measure for the analysis of diffusion-weighted magnetic resonance images. *Neuroimage* 59, 3976–3994. doi: 10.1016/j.neuroimage.2011.10.045

Rutter, M., Lord, C., and LeCouteur, A. (1995). *Autism Diagnostic Interview – R.* Chicago, IL: Department of Psychiatry, University of Chicago.

Schumann, C. M., and Amaral, D. G. (2006). Stereological analysis of amygdala neuron number in autism. *J. Neurosci.* 26, 7674–7679. doi: 10.1523/JNEUROSCI.1285-06.2006

Schumann, C. M., Bloss, C. S., Barnes, C. C., Wideman, G. M., Carper, R. A., Akshoomoff, N., et al. (2010). Longitudinal magnetic resonance imaging study of cortical development through early childhood in autism. *J. Neurosci.* 30, 4419–4427. doi: 10.1523/JNEUROSCI.5714-09.2010

Schumann, C. M., and Nordahl, C. W. (2011). Bridging the gap between MRI and postmortem research in autism. *Brain Res.* 1380, 175–186. doi: 10.1016/j.brainres.2010.09.061

Smith, S. M. (2002). Fast robust automated brain extraction. *Hum. Brain Mapp.* 17, 143–155. doi: 10.1002/hbm.10062

Suzuki, K., Sugihara, G., Ouchi, Y., Nakamura, K., Futatsubashi, M., Takebayashi, K., et al. (2013). Microglial activation in young adults with autism spectrum disorder. *JAMA Psychiatry* 70, 49–58. doi: 10.1001/jamapsychiatry.2013.272

Tournier, J. D., Calamante, F., Gadian, D. G., and Connelly, A. (2004). Direct estimation of the fiber orientation density function from diffusion-weighted MRI data using spherical deconvolution. *Neuroimage* 23, 1176–1185. doi: 10.1016/j.neuroimage.2004.07.037

van Kooten, I. A., Palmen, S. J., von Cappeln, P., Steinbusch, H. W., Korr, H., Heinsen, H., et al. (2008). Neurons in the fusiform gyrus are fewer and smaller in autism. *Brain* 131, 987–999. doi: 10.1093/brain/awn033

Vargas, D. L., Nascimbene, C., Krishnan, C., Zimmerman, A. W., and Pardo, C. A. (2005). Neuroglial activation and neuroinflammation in the brain of patients with autism. *Ann. Neurol.* 57, 67–81. doi: 10.1002/ana.20315

Wechsler, D. (1999). *Wechsler Abbreviated Scale of Intelligence.* San Antonio, TX: Psychological Corporation.

Wegiel, J., Kuchna, I., Nowicki, K., Imaki, H., Wegiel, J., Marchi, E., et al. (2010). The neuropathology of autism: defects of neurogenesis and neuronal migration, and dysplastic changes. *Acta Neuropathol.* 119, 755–770. doi: 10.1007/s00401-010-0655-4

White, N. S., Leergaard, T. B., D'Arceuil, H., Bjaalie, J. G., and Dale, A. M. (2013). Probing tissue microstructure with restriction spectrum imaging: Histological and theoretical validation. *Hum. Brain Mapp.* 34, 327–346.

White, N. S., Mcdonald, C. R., Farid, N., Kuperman, J., Karow, D., Schenker-Ahmed, N. M., et al. (2014). Diffusion-weighted imaging in cancer: physical foundations and applications of restriction spectrum imaging. *Cancer Res.* 74, 4638–4652. doi: 10.1158/0008-5472.CAN-13-3534

Winston, G. P., Micallef, C., Symms, M. R., Alexander, D. C., Duncan, J. S., and Zhang, H. (2014). Advanced diffusion imaging sequences could aid assessing patients with focal cortical dysplasia and epilepsy. *Epilepsy Res.* 108, 336–339. doi: 10.1016/j.eplepsyres.2013.11.004

Zhang, H., Schneider, T., Wheeler-Kingshott, C. A., and Alexander, D. C. (2012). NODDI: practical *in vivo* neurite orientation dispersion and density imaging of the human brain. *Neuroimage* 61, 1000–1016. doi: 10.1016/j.neuroimage.2012.03.072

Zhuang, J., Hrabe, J., Kangarlu, A., Xu, D., Bansal, R., Branch, C. A., et al. (2006). Correction of eddy-current distortions in diffusion tensor images using the known directions and strengths of diffusion gradients. *J. Magn. Reson. Imaging* 24, 1188–1193. doi: 10.1002/jmri.20727

Zikopoulos, B., and Barbas, H. (2010). Changes in prefrontal axons may disrupt the network in autism. *J. Neurosci.* 30, 14595–14609. doi: 10.1523/JNEUROSCI.2257-10.2010

Zimmerman, A. W., Jyonouchi, H., Comi, A. M., Connors, S. L., Milstien, S., Varsou, A., et al. (2005). Cerebrospinal fluid and serum markers of inflammation in autism. *Pediatr. Neurol.* 33, 195–201. doi: 10.1016/j.pediatrneurol.2005.03.014

Conflict of Interest Statement: The authors declare that the research was conducted in the absence of any commercial or financial relationships that could be construed as a potential conflict of interest.

frontiers in Neuroscience

GENERAL COMMENTARY
published: 03 August 2016
doi: 10.3389/fnins.2016.00353

Commentary: Semi-Metric Topology of the Human Connectome: Sensitivity and Specificity to Autism and Major Depressive Disorder

Tiago Simas[1]* *and John Suckling*[1, 2]

[1] Department of Psychiatry, University of Cambridge, Cambridge, UK, [2] Cambridge and Peterborough NHS Foundation Trust, Cambridge, UK

Keywords: neuroimaging, functional connectivity, transitivity, semi-metricity, connectome

A commentary on

Semi-Metric Topology of the Human Connectome: Sensitivity and Specificity to Autism and Major Depressive Disorder
by Simas, T., Chattopadhyay, S., Hagan, C., Kundu, P., Patel, A., Holt, R., et al. (2015). PLoS ONE 10:e0136388. doi: 10.1371/journal.pone.0136388

OPEN ACCESS

Edited by:
Roma Siugzdaite, Ghent University, Belgium

Reviewed by:
Sebastiano Stramaglia, University of Bari Aldo Moro, Italy
Maxime Taquet, Harvard Medical School, USA

***Correspondence:**
Tiago Simas
ts526@cam.ac.uk

Specialty section:
This article was submitted to Child and Adolescent Psychiatry, a section of the journal Frontiers in Neuroscience

Received: *31 March 2016*
Accepted: *12 July 2016*
Published: *03 August 2016*

Citation:
Simas T and Suckling J (2016) Commentary: Semi-Metric Topology of the Human Connectome: Sensitivity and Specificity to Autism and Major Depressive Disorder. Front. Neurosci. 10:353. doi: 10.3389/fnins.2016.00353

Functional Magnetic Resonance Imaging (fMRI) records the blood oxygenation level dependent (BOLD) endogenous contrast, a physiological surrogate for brain activity. Experimental and analytic procedures for fMRI remained largely unchanged in the decade following discovery of BOLD contrast, detecting localized magnitude changes in response to external stimuli. Observations of persistent patterns of activation present under a wide variety of cognitive conditions, now known as the default mode network (Raichle et al., 2001), led to significant changes in data acquisition and analysis; that is, fMRI data began to be acquired in task-absent states (so-called "rest") and the analysis proceeded by generation of the functional connectome (Bullmore and Sporns, 2009) that putatively supported the distributed exchange of information, and supplanted localized activity as the basic unit of interpretation.

The functional connectome is constructed from nodes (brain regions) connected by edges with associated strengths (edge weights) that represent functional proximity, often inter-regional synchronicity measured by Pearson's correlation of BOLD time-series. Other strengths can be estimated; for example, coherence, cross-correlation (Salvador et al., 2005) or spectral mutual information (Granger and Hatanaka, 1964; Granger and Lin, 1994; Simas et al., 2015) which may capture alternative properties of the connectome. With this approach, a large-scale functional organization of the brain has been proposed (Bota et al., 2015) and many common mental health disorders linked to the vulnerability of particular topological elements of the connectome (Crossley et al., 2014).

Through whatever means these graphical networks are generated, complex network analysis can be applied to characterize the topography and thus the presumed flow or exchange of information that the network represents (Watts and Strogatz, 1998; Barabási and Albert, 1999; Barrat et al., 2008). Examples are replete in natural and man-made systems: computer networks, transport infrastructure, social and ecological relationships, and microstructures of the central nervous system. Up to now, complex analysis of the functional connectome has been dominated by characterization with parameters derived from a graphical network that is sparse and frequently binary (Cao et al., 2014). These networks are mostly simply created by a threshold on the edge

weights, focusing then on the clique of edges with high values. Properties like small-worldness (Watts and Strogatz, 1998; Achard et al., 2006; Bassett and Bullmore, 2006; Simas, 2012; Suckling et al., 2015) can be estimated, implicitly assuming that information flows preferentially and most efficiently along paths with the fewest edges.

The role of "weak" edges has arguably been underrepresented in the complex analysis of the functional connectome (Suckling et al., 2015), although sociological theory has long recognized their central role in the distribution of information through friendship networks (Granovetter, 1973, 1983). Moreover, the complete transfer of information via shortest paths, i.e., the fewest edges between two nodes, is only possible if there is available a map of the connectome available to plan the most efficient routes, in the same way as a traveler has a map of the metro to efficiently navigate a city. It seems unlikely that the brain has to hand a representation of its own connectome, even more so given the connectome is time varying (Hutchison et al., 2013) (what is often measured by the functional connectome is a time average). More likely is that information is transferred across the entire, fully-connected network taking advantage of the proletariat of weak edges, with broadcast dynamics a potential strategy for dissemination. Nevertheless, the shortest path is a good starting point for a more expansive conceptualization.

Networks that are not transitive with edge weights representing proximities have homologs in the isomorphic distance space that are semi-metric (Klir and Bo, 1995; Simas and Rocha, 2015) (**Figure 1**). In other words, there are edges in the distance space that violate the triangle inequality when enforced by distance closure . Thus, it is possible to distinguish a metric edge from a semi-metric edge by determining whether the shortest path is the direct path between nodes, or if it is via

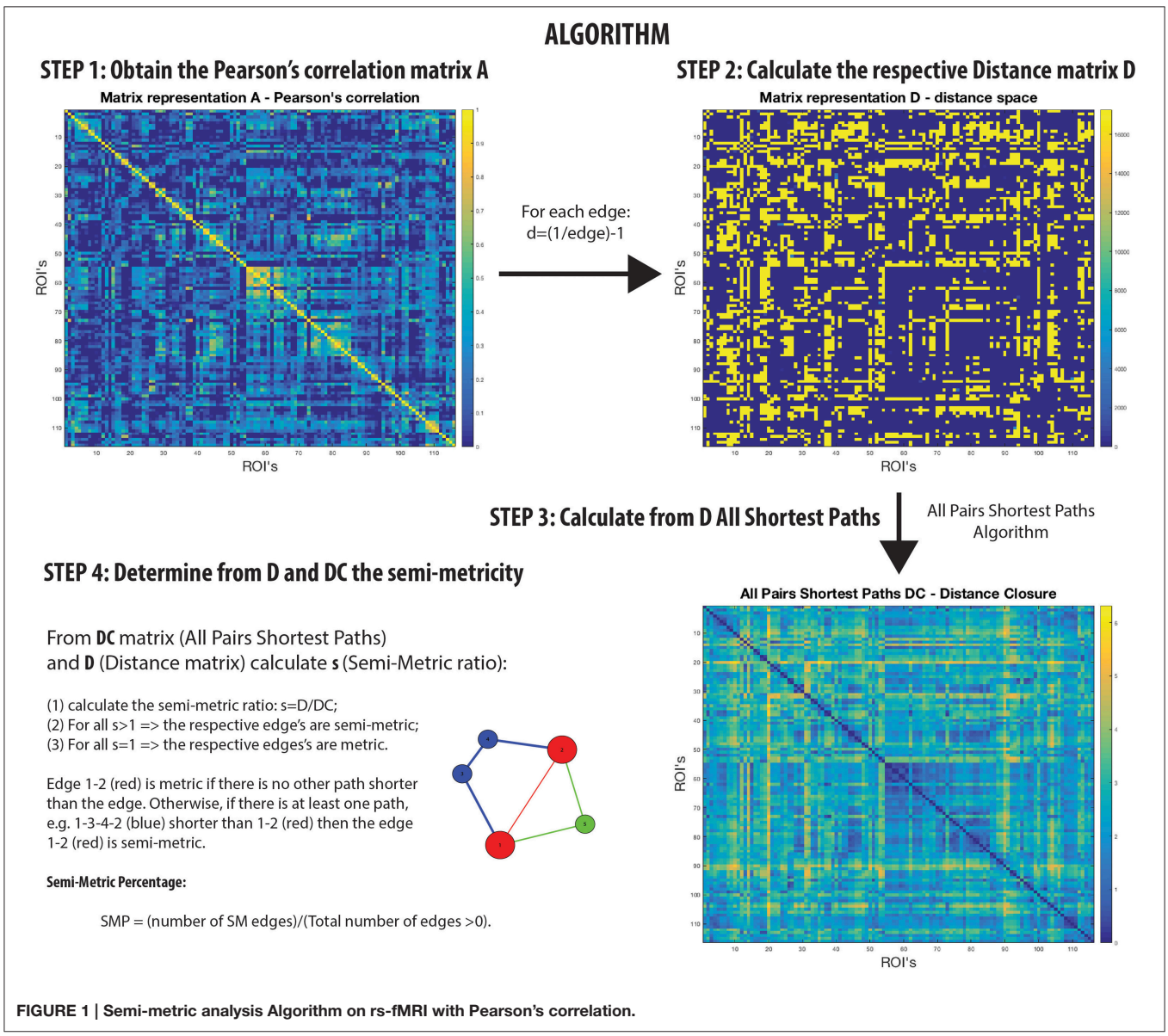

FIGURE 1 | Semi-metric analysis Algorithm on rs-fMRI with Pearson's correlation.

a circuitous route (and there may be more than one) involving additional nodes. This is a common phenomenon; for example, although it might be difficult to communicate directly with someone with whom you have no direct relationship, it is possible to transfer messages through intermediaries with whom you are mutually acquainted.

A semi-metric path in the functional connectome with edge weights estimated by Pearson's correlation between regional BOLD time-series, may be interpreted as the two regions synchronously co-activating along with all other regions involved the circuitous paths (Simas et al., 2015) (**Figure 1**). That is, there is a dispersion of communicability across the regions. Complementarily, metric connections do not have the significant involvement of other regions, and information exchange is constrained to the two regions. All non-trivially organized networks have some degree of semi-metricity, and in the healthy human functional connectome derived with Pearson's correlation they form around 80% of all the edges (Simas et al., 2015). There is also evidence that the degree of semi-metricity (i.e., transitivity) in anatomical networks predicts functional connectivity (Goñi et al., 2014).

Semi-metric analysis of the functional connectome (**Figure 1**) is sensitive and specific to psychopathologies (Peeters et al., 2015; Simas and Rocha, 2015; Simas et al., 2015; Suckling et al., 2015). Both positive and negative deviations in the global proportion of semi-metric edges, relative to neurotypical individuals, have been observed in Autism and Major Depressive Disorder respectively (Simas et al., 2015), occuring consistently across individuals in similar functional connections. Psychosis was also exclusively associated with only positive changes to semi-metricity, the severity of symptoms related to the magnitude of change (Peeters et al., 2015). However in Alzheimer's disease, both directions of effect were observed, with highly idiosyncratic patterns of change (Suckling et al., 2015). Together, these studies suggest that there exists an optimum value of semi-metricity both globally and locally that is associated with healthy brain function, and that disorders have their own particular pattern of change relative to control samples.

The human brain is the most complex system known. The evidence and analytic models to measure and predict its form and function have evolved toward an understanding of brain as a network of unceasing communication. Current tomographic technologies, like fMRI, limit the detectable time resolution and we are therefore only beginning to understand the topology of the connectome and how it might form the substrate for cognition and psychopathologies. Semi-metricity, and more generally the inclusion of all the brain's connections, is a next step toward a richer description of the functional topology and, subsequently, simulation and measurement of its complex dynamics and inter-regional information transmission.

AUTHOR CONTRIBUTIONS

Both authors made significant contributions to the drafting of the article.

FUNDING

This study was funded by the UK Medial Research Council (grant: G0802226), the National Institute for Health Research (NIHR) (grant: 06/05/01) and the Behavioural and Clinical Neuroscience Institute (BCNI), University of Cambridge. The BCNI is jointly funded by the Medical Research Council and the Wellcome Trust. Additional support was received from the NIHR Cambridge Biomedical Research Centre.

REFERENCES

Achard, S., Salvador, R., Whitcher, B., Suckling, J., and Bullmore, E. (2006). A resilient, low-frequency, small-world human brain functional network with highly connected association cortical hubs. *J. Neurosci.* 26, 63–72. doi: 10.1523/JNEUROSCI.3874-05.2006

Barabási, A.-L., and Albert, R. (1999). Emergence of scaling in random networks. *Science* 286, 509–512. doi: 10.1126/science.286.5439.509

Barrat, A., Barthelemy, M., and Vespignani, A. (2008). *Dynamical Processes on Complex Networks*. Cambridge: Cambridge University Press. doi: 10.1017/cbo9780511791383

Bassett, D. S., and Bullmore, E. (2006). Small-world brain networks. *Neuroscientist* 12, 512–523. doi: 10.1177/1073858406293182

Bota, M., Sporns, O., and Swanson, L. W. (2015). Architecture of the cerebral cortical association connectome underlying cognition. *Proc. Natl. Acad. Sci. U.S.A.* 112, E2093–E2101. doi: 10.1073/pnas.1504394112

Bullmore, E., and Sporns, O. (2009). Complex brain networks: graph theoretical analysis of structural and functional systems. *Nat. Rev. Neurosci.* 10, 312–312. doi: 10.1038/nrn2618

Cao, M., Wang, J.-H., Dai, Z.-J., Cao, X.-Y., Jiang, L.-L., Fan, F.-M., et al. (2014). Topological organization of the human brain functional connectome across the lifespan. *Dev. Cogn. Neurosci.* 7, 76–93. doi: 10.1038/nrn2618

Crossley, N. A., Mechelli, A., Scott, J., Carletti, F., Fox, P. T., McGuire, P., et al. (2014). The hubs of the human connectome are generally implicated in the anatomy of brain disorders. *Brain* 137, 2382–2395. doi: 10.1093/brain/awu132

Goñi, J., van den Heuvel, M. P., Avena-Koenigsberger, A., Velez de Mendizabal, N., Betzel, R. F., Griffa, A., et al. (2014). Resting-brain functional connectivity predicted by analytic measures of network communication. *Proc. Natl. Acad. Sci. U.S.A.* 111, 833–838. doi: 10.1073/pnas.1315529111

Granger, C., and Hatanaka, M. (1964). *Spectral Analysis of Economical Time Series*. Princeton, NJ: Princeton University Press.

Granger, C., and Lin, J.-L. (1994). Using the mutual information coefficient to identify lags in nonlinear models. *J. Time Ser. Anal.* 15, 371–384. doi: 10.1111/j.1467-9892.1994.tb00200.x

Granovetter, M. (1983). The strength of weak ties: a network theory revisited. *Sociol. Theory* 1, 201–233. doi: 10.2307/202051

Granovetter, M. S. (1973). The strength of weak ties. *Am. J. Sociol.* 78, 1360–1380. doi: 10.1086/225469

Hutchison, R. M., Womelsdorf, T., Allen, E. A., Bandettini, P. A., Calhoun, V. D., Corbetta, M., et al. (2013). Dynamic functional connectivity: promise, issues, and interpretations. *NeuroImage* 80, 360–378. doi: 10.1016/j.neuroimage.2013.05.079

Klir, G., and Bo, Y. (1995). *Fuzzy Sets and Fuzzy Logic: Theory and Applications*. New Jersey: Prentice Hall PTR.

Peeters, S., Simas, T., Suckling, J., Gronenschild, E., Patel, A., Habets, P., et al. (2015). Semi-metric analysis of the functional brain network: relationship with familial risk for psychotic disorder. *NeuroImage* 9, 607–616. doi: 10.1016/j.nicl.2015.10.003

Raichle, M. E., MacLeod, A. M., Snyder, A. Z., Powers, W. J., Gusnard, D. A., and Shulman, G. L. (2001). A default mode of brain function.

Proc. Natl. Acad. Sci. U.S.A. 98, 676–682. doi: 10.1073/pnas.98.2.676

Salvador, R., Suckling, J., Schwarzbauer, C., and Bullmore, E. (2005). Undirected graphs of frequency-dependent functional connectivity in whole brain networks. *Philos. Trans. R. Soc. B Biol. Sci.* 360, 937–946. doi: 10.1098/rstb.2005.1645

Simas, T. (2012). *Stochastic Models and Transitivity in Complex Networks*. PhD thesis, Indiana University.

Simas, T., Chattopadhyay, S., Hagan, C., Kundu, P., Patel, A., Holt, R., et al. (2015). Semi-metric topology of the human connectome: sensitivity and specificity to autism and major depressive disorder. *PLoS ONE* 10:e0136388. doi: 10.1371/journal.pone.0136388

Simas, T., and Rocha, L. M. (2015). Distance closures on complex networks. *Netw. Sci.* 3, 227–268. doi: 10.1017/nws.2015.11

Suckling, J., Simas, T., Chattopadhyay, S., Tait, R., Su, L., Williams, G., et al. (2015). A winding road: Alzheimer's disease increases circuitous functional connectivity pathways. *Front. Comput. Neurosci.* 9:140. doi: 10.3389/fncom.2015.00140

Watts, D. J., and Strogatz, S. H. (1998). Collective dynamics of 'small-world' networks. *Nature* 393, 440–442. doi: 10.1038/30918

Conflict of Interest Statement: The authors declare that the research was conducted in the absence of any commercial or financial relationships that could be construed as a potential conflict of interest.

frontiers in Neuroscience

REVIEW
published: 25 August 2016
doi: 10.3389/fnins.2016.00393

Aberrant Development of Speech Processing in Young Children with Autism: New Insights from Neuroimaging Biomarkers

Holger F. Sperdin[1]* *and Marie Schaer*[1,2]

[1] *Office Médico-Pédagogique, Department of Psychiatry, University of Geneva School of Medicine, Geneva, Switzerland,*
[2] *Stanford Cognitive & Systems Neuroscience Laboratory, Stanford University School of Medicine, Palo Alto, CA, USA*

From the time of birth, a newborn is continuously exposed and naturally attracted to human voices, and as he grows, he becomes increasingly responsive to these speech stimuli, which are strong drivers for his language development and knowledge acquisition about the world. In contrast, young children with autism spectrum disorder (ASD) are often insensitive to human voices, failing to orient and respond to them. Failure to attend to speech in turn results in altered development of language and social-communication skills. Here, we review the critical role of orienting to speech in ASD, as well as the neural substrates of human voice processing. Recent functional neuroimaging and electroencephalography studies demonstrate that aberrant voice processing could be a promising marker to identify ASD very early on. With the advent of refined brain imaging methods, coupled with the possibility of screening infants and toddlers, predictive brain function biomarkers are actively being examined and are starting to emerge. Their timely identification might not only help to differentiate between phenotypes, but also guide the clinicians in setting up appropriate therapies, and better predicting or quantifying long-term outcome.

Keywords: ASD, MRI, EEG, language development, voice, auditory processing, toddler, infant

OPEN ACCESS

Edited by:
Roma Siugzdaite,
Ghent University, Belgium

Reviewed by:
Nandini Chatterjee Singh,
National Brain Research Centre, India
Bart Boets,
KU Leuven, Belgium

***Correspondence:**
Holger F. Sperdin
holger.sperdin@unige.ch

Specialty section:
This article was submitted to Child and Adolescent Psychiatry, a section of the journal Frontiers in Neuroscience

Received: *04 April 2016*
Accepted: *10 August 2016*
Published: *25 August 2016*

Citation:
Sperdin HF and Schaer M (2016) Aberrant Development of Speech Processing in Young Children with Autism: New Insights from Neuroimaging Biomarkers. Front. Neurosci. 10:393. doi: 10.3389/fnins.2016.00393

INTRODUCTION

Autism, a term initially introduced by Kanner (1943) and almost at the same period by Asperger (1944), is a pervasive disorder of neurodevelopment with an early onset. According to the most recent census, autism affects up to 1 in 68 children (1.5%) in the United States (Baio, 2014). ASD is characterized by impairments in core areas of cognitive and adaptive function, social interactions, and communication (American Psychiatric Association and American Psychiatric Association. Dsm-5 Task Force, 2013). Individuals with ASD show a reduced interest in socially relevant stimuli (McPartland et al., 2011; Pelphrey et al., 2011; Chevallier et al., 2012; Kohls et al., 2012), tend to avoid eye-contact with their immediate surrounding (Senju and Johnson, 2009; Elsabbagh et al., 2012; Jones and Klin, 2013), and show repetitive behaviors and restricted interests (Turner, 1999; Watt et al., 2008; Arnott et al., 2010). Moreover, affected children often present language delay, with deficits in expressive and receptive language skills (Hudry et al., 2010; Eigsti et al., 2011; Mody et al., 2013; Simms and Jin, 2015). Multiple causes are implicated in autism

and recent accounts indicate the presence of abnormal development occurring at the cellular and molecular levels during prenatal life (Stoner et al., 2014; Baron-Cohen et al., 2015), with a clear impact of genetic, neurobiological, environmental factors, and combinations thereof (Geschwind and Levitt, 2007; Abrahams and Geschwind, 2010; Betancur, 2011; Zhubi et al., 2014; Robinson et al., 2015). One of the core domains that is particularly impaired and that constitutes a hallmark feature in autism is language. Behaviorally, children with autism do not orient naturally to vocal stimuli as typically developing (TD) children do (Dawson et al., 2004; Kuhl et al., 2005). They often show a reduced sensitivity to human voices, but are responsive to other non-vocal stimuli (Klin, 1991, 1992). This would suggest that the neural mechanisms underlying the orientation to voices and their processing might not develop in the same way as in TD individuals. Currently, the exact time when the developmental trajectory of the brain systems implicated in human voice processing starts to deviate from a normal path is unknown, but recent neuroimaging results that we discuss below suggest the presence of differences already from the age of 2 years (e.g., Lombardo et al., 2015).

Neuroimaging provides an excellent window to better understand the neural bases of speech and language abnormalities in young children with ASD. Differences in brain anatomy have been investigated using structural magnetic resonance imaging (MRI); patterns of changes to structural connectivity have been examined using diffusion tensor imaging (DTI); changes in cortical activity measured using functional MRI (fMRI); and altered spatio-temporal brain dynamics quantified using high-density electroencephalography (EEG). Despite the fact that all these techniques are non-invasive, their use in children involves numerous challenges (de Bie et al., 2010; Raschle et al., 2012). Perhaps the most noteworthy of these challenges is the requirement for the child to remain still for extended periods of time, otherwise creating difficulties for placing the electrode caps on a young child's head in EEG experiments, or leading to movement artifacts in MRI acquisitions. Nonetheless, recent years have seen practical and methodological advancements, which tremendously improved the feasibility of neuroimaging research studies in young children (in particular in the MRI field). For example, mock MRI scanning facilities are increasingly used to prepare preschoolers and school-aged children for a successful real MRI acquisition (Cantlon et al., 2006; Epstein et al., 2007; de Bie et al., 2010; Nordahl et al., 2016). Although initial studies of infants and toddlers used anesthesia or mild sedation (e.g., Boddaert et al., 2004a; Fransson et al., 2007), protocols for obtaining MRI acquisitions during natural sleep have been proposed for young children with ASD (e.g., Nordahl et al., 2008; Ortiz-Mantilla et al., 2010; Eyler et al., 2012; Shen et al., 2013; Lombardo et al., 2015). Scanning during natural sleep allows to study at the functional and structural levels how the brain systems implicated in human speech and language processing are developing in very young infants and toddlers and to detect early biomarkers for ASD. We will discuss how these recent neuroimaging studies performed in very young children with ASD or at risk have begun to reveal impairments at multiple levels in the brain systems implicated in speech and language processing.

In EEG, the experiments are generally performed during wakefulness (see **Figure 1**; e.g., Boersma et al., 2013; Kuhl et al., 2013; Seery et al., 2013, 2014). The EEG field has also seen recent methodological advancement. Modern electrical source estimations of high density EEG now reach an approximation in the whole brain of the 3-D distribution of the neuronal activity at each moment in time (Michel et al., 2004; Brunet et al., 2011; Michel and Murray, 2012; Custo et al., 2014) and have been shown to represent stable and reliable estimates when compared with intracranial recordings, lesions and animal studies and other neuroimaging methods (Pittau et al., 2014 for review). For this reason, EEG studies of infants at risk and toddlers with ASD should provide source estimations when possible as they may add valuable information regarding how they differ in their early brain development compared to their TD peers. Improving the precision of source localization by using individual MRI scans of infants/toddlers or age-appropriate template MRIs is also possible. Their estimation in normally and abnormally developing infants/toddlers (or those at risk) can subsequently be compared with results from available fMRI experiments. This is important as most fMRI experiments are currently being performed in a sleep state while EEG experiments are mostly being conducted in awake participants. Finally, compared to the EEG experiments using a traditional voltage waveform analysis approach and that will be reviewed here, electrical neuroimaging methods are reference-independent and take into account the additional information of multichannel electrodes recordings. As such, they avoid the traditional statistical pitfalls inherent to traditional voltage waveform analysis (see Murray et al., 2008 for discussion). So-called "microstate" analyses are also available, allowing to identify dominant state topographies in spontaneous EEG recordings acquired in young infants and toddlers with ASD (Koenig et al., 2002; Lehmann and Michel, 2011). These methods have been successfully applied on EEG

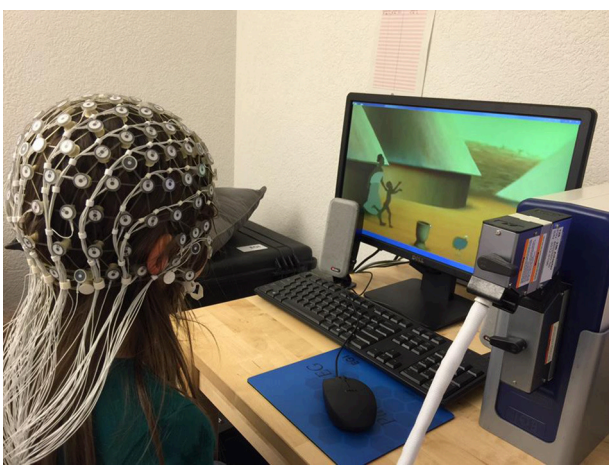

FIGURE 1 | Example of an EEG set-up with a young child. A video is displayed on a standard screen, and the child is wearing a 129 electrodes cap. Sounds are displayed via external speakers.

data acquired in clinical population of children and young adolescents (Rihs et al., 2013; Berchio et al., 2014; Tomescu et al., 2014) and could be used to examine the developmental trajectories of infants/toddlers with ASD and infants at risk for autism.

While other reviews of auditory and speech processing impairments have been published focusing on older children and adults (e.g., Haesen et al., 2011; Kujala et al., 2013), here, we provide an overview of some of the most recent neuroimaging experiments (primarily fMRI and EEG) of very young children (before 4 years of age) with ASD investigating impairments in the brain systems implicated in human vocalizations and henceforth speech and language processing (e.g., Kuhl et al., 2013; Lombardo et al., 2015) and in at-risk populations (before the age of 2) to identify early endophenotypes (Seery et al., 2013, 2014; Blasi et al., 2015). We will principally review recent experiments that have used voice related auditory stimuli (e.g., sentences, words, syllables). After a brief description of the language development in the typically developing individual during the first year, we will summarize part of the clinical body of evidence pointing to altered speech and language development in very young children with ASD and in infants at high-risk for ASD. Afterwards, we describe the neural systems within the superior temporal cortical regions implicated in human voice processing and their development in the TD brain and present functional evidence in adults and young adolescents indicating the presence of an aberrant form of voice processing. Next we focus on the cross-sectional studies using fMRI and EEG which were conducted at specific time points during infancy/toddlerhood. They address group differences in early speech and language-related processing within these voice areas within superior temporal cortical regions along other language related brain neural systems. The results thereof indicate the presence of structural, functional, and connectivity group differences being already present in infancy and/or toddlerhood. We finally highlight recent results from the few existing prospective fMRI and EEG studies which employed a longitudinal design and demonstrated by using voice related auditory stimuli that aberrant voice processing is not only a feature present in older children and adults with ASD but also a promising candidate to identify ASD very early on during the development.

LANGUAGE DEVELOPMENT IN TYPICALLY DEVELOPING INDIVIDUALS

The different steps involved in early speech perception and production have been extensively examined (see **Figure 2**; Kuhl, 2004, 2010 for reviews). TD newborns are rapidly attracted by human voices within the first days of life (Cheng et al., 2012). At 1 month of age, they are already responsive to speech sounds (Eimas et al., 1971). Language-related brain areas are activated in response to human speech sounds to some extent in 3 month old infants, well before the onset of speech production (Dehaene-Lambertz et al., 2002, 2006), while cerebral specialization for the human voice over other sounds emerges over the first 6 months of life (Minagawa-Kawai et al., 2011; Lloyd-Fox et al., 2012). By 4 months, infants know that speech conveys information that relate words to physical objects (Marno et al., 2015). Around 5 months, they can recognize the sound patterns of their own name, and between 6 and 9 months they are capable of correctly directing their gaze to named pictures suggesting the presence of some form of word comprehension (Mandel et al., 1995; Tincoff and Jusczyk, 1999, 2012; Bergelson and Swingley, 2012). With respect to pre-linguistic production skills, between 0 and 2 months, newborns first produce vegetative vocalizations (non-speech sounds such as burps, coughs, and cries). At 3 months, infants start to produce vowel-like sounds followed by the onset around 6 months of a babbling phase that becomes robust by 10 months of age. Canonical babbling is a precursor to the emergence of the first words production, which are generally produced by the end of the first year. During the first year of the infant's development and the following years into toddlerhood, the human voice is a natural driver for the infant's language skills development.

LANGUAGE DEVELOPMENT IN TODDLERS WITH ASD AND INFANTS AT RISK

In individuals with autism, the degree of impairment and delay in language greatly varies from one person to another, with a tremendous heterogeneity in early language development and later clinical outcomes (Mitchell et al., 2006; Geurts and Embrechts, 2008; Luyster et al., 2008; Tager-Flusberg et al., 2009; Lenroot and Yeung, 2013; Lord et al., 2015). Some toddlers present substantial delay or deficits while others have a typical early language development or mild delay and catch up. The former are children that often show the most severe and pertaining symptoms in the long term, compared to those with relatively preserved language abilities (Fein et al., 2013; Kasari et al., 2013; Tager-Flusberg and Kasari, 2013). Converging clinical estimates indicate that more than half of the children with ASD will have persisting language impairments throughout their lifespan (e.g., Anderson et al., 2007; Pickles et al., 2014). So far, the heterogeneity of early language development and the neurodevelopmental basis for this variability in clinical outcomes are not fully understood. In this review, we also discuss how neuroimaging studies examining the neural bases of early human speech and language impairments in autism have started to be used to predict outcome in affected children.

In toddlers with ASD, language difficulties are often present both when they are spoken to (i.e., receptive language) and when they express themselves (i.e., expressive language; Hudry et al., 2010; Simms and Jin, 2015). Indeed, parents of children diagnosed with ASD often sought medical advice because of strong concerns related to language development (Dahlgren and Gillberg, 1989; De Giacomo and Fombonne, 1998; Wetherby et al., 2004; Herlihy et al., 2015). Retrospective interviews with the families, analysis of retrospective video birthday tapes recorded at 12 months of age of children diagnosed with ASD, as well as prospective accounts of infants at risk often report an unresponsiveness to name and a general lack of

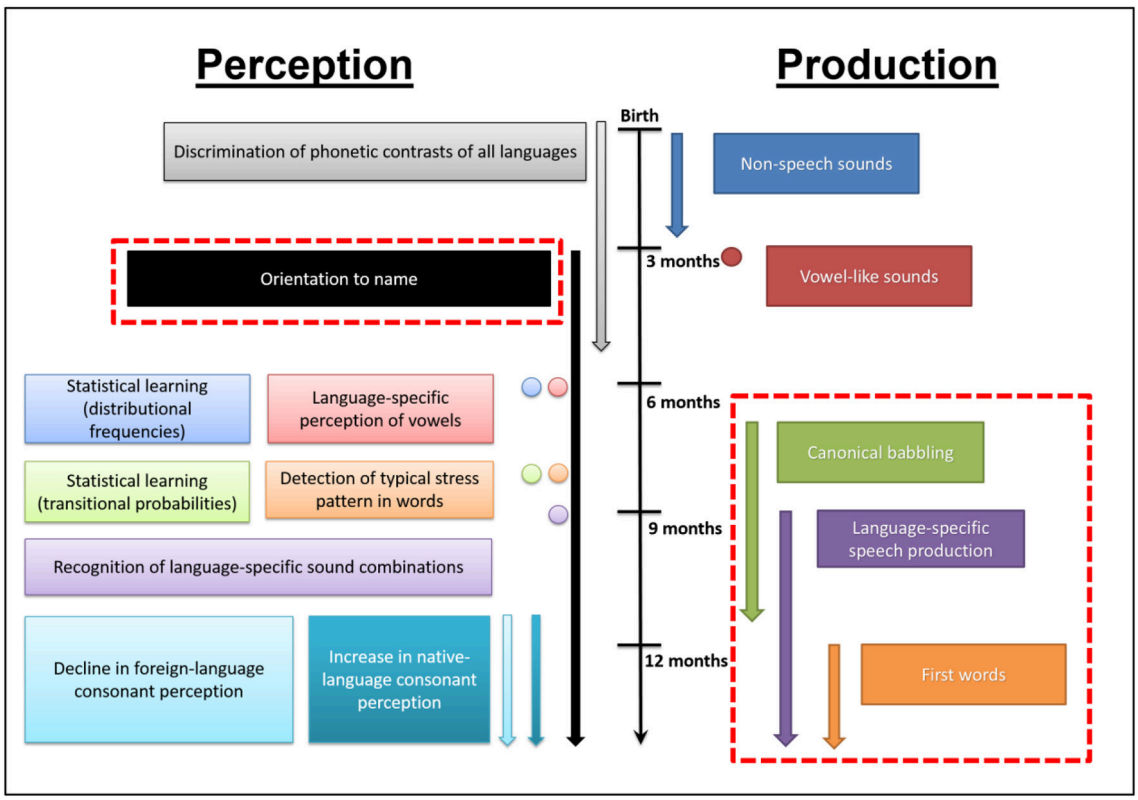

FIGURE 2 | Illustration of the changes occurring in speech perception and production in typically developing human infants during their first year of life (adapted from Kuhl, 2004). Red dashed rectangles indicate early expressive and receptive language delays/impairments (that is, unresponsiveness to name, delayed canonical babbling, increased non-speech productions, decreased speech-like vocalization, delayed occurrence of the first words) known to be sensitive indicators of an increased risk for later being diagnosed with ASD

orientation to human voices (Osterling and Dawson, 1994; Baranek, 1999; Yirmiya et al., 2006; Nadig et al., 2007; Oner et al., 2014; Stenberg et al., 2014). In sum, a large body of clinical studies to date point to expressive and receptive language deficits already in the first year of life for young children who will subsequently develop ASD during toddlerhood, suggesting that the neural systems responsible for orienting to and processing human vocalizations are altered very early on.

Infants at risk for autism are increasingly studied prospectively, to measure whether the abilities to understand language described above are already altered in infants who will develop autism later on. Siblings of a child with ASD have a very high risk to develop ASD, ~20 times higher compared to infants with no family history of ASD (Rogers, 2009; Ozonoff et al., 2011). In a context where early intensive non-pharmacological interventions are critical to improve the long term outcome of affected individuals (Dawson, 2008; Dawson et al., 2010; Klintwall et al., 2013), it is instrumental to detect ASD as early as possible, (see also Schaer et al., 2014 for a review). As such, studies of high-risk infants allow to map the early developmental trajectories of infants who will develop ASD, and to highlight endophenotypes of ASD (Viding and Blakemore, 2007). Numerous studies of high-risk infants focused on early language development as delays in communication and language development become apparent early in life, even before the first year or shortly thereafter. Differences in vocal production (such as consonant inventory, presence of canonical syllables, and non-speech vocalizations), between low-risk and high-risk infants between 9 and 12 months has been associated with later outcomes at 24 months (Paul et al., 2011; Jones et al., 2014 for review). Another prospective study of infants at risk tested at target ages 6, 14, and 24 months and who were followed up and diagnosed with ASD at 24 months indicates that language delays or deficits are already observable at around 14 months of age (Landa and Garrett-Mayer, 2006). A recent retrospective study of toddlers with ASD reported low rates of canonical babbling and vocalization frequency between 9 and 12 months and 15–18 month compared to age-matched TD peers, several months before a diagnosis of ASD was made (Patten et al., 2014). As a result, a delay or deficit in language development very early on has become integral part of the red flags indicating a greater susceptibility for developing autism (Barbaro and Dissanayake, 2009; Zwaigenbaum et al., 2013; see **Figure 2**, red dashed rectangles).

THE VOICE AS A UNIQUE AUDITORY STIMULUS IN THE TYPICALLY DEVELOPING BRAIN

The human voice is clearly one of the most salient and important auditory stimuli in our acoustic environment. It conveys both linguistic and extra-linguistic information. It delivers speech information permitting us as individuals to recognize the others and to attribute emotional states to them (Belin et al., 2000; Ethofer et al., 2009). While language is generally thought to be processed in specialized brain areas such as the inferior frontal gyrus (IFG; also known as Broca's area), the superior and middle temporal gyruses (STG, MTG, also termed Wernicke's area) and angular gyrus, voice selective areas have been located bilaterally in the upper bank of the middle superior temporal sulcus (STS) over the temporal poles (see **Figure 3A**). Their existence has particularly been highlighted by fMRI experiments in the adult brain by comparing the cortical activation patterns induced by vocal vs. non-vocal sounds (Belin et al., 2000, 2004; Kriegstein and Giraud, 2004; Belin, 2006, for review; Latinus and Belin, 2011; Deen et al., 2015; Pernet et al., 2015). When a voice is perceived, the brain begins by a low-level analysis of the acoustic features involving sub-cortical nuclei and primary auditory cortical regions. Subsequently, the voice is processed during a voice-specific stage where its structure is encoded. Three types of vocal information are then extracted and further processed in partially separable but functionally interacting pathways: the speech content, the affective content and the vocal identity (see **Figure 3B**). Early studies of very young infants have shown that voice sensitive cortices within the temporal areas develop as a voice selective brain system between 4 and 7 months of age in the typically developing brain and to become responsive to the quality of the voice during speech (emotional voice prosody) by the age of 7 months with a right hemispheric dominance (Belin and Grosbras, 2010; Grossmann et al., 2010; Blasi et al., 2011; Lloyd-Fox et al., 2012). A recent study of typically developing preschoolers (mean age = 5.8 years) compared voice-specific vs. speech-sound specific functional brain activity and demonstrated that the right STS already works as a specialized temporal voice system (Raschle et al., 2014), similarly to what has been reported in the adult brain (Belin et al., 2002; Belin and Zatorre, 2003; von Kriegstein et al., 2003).

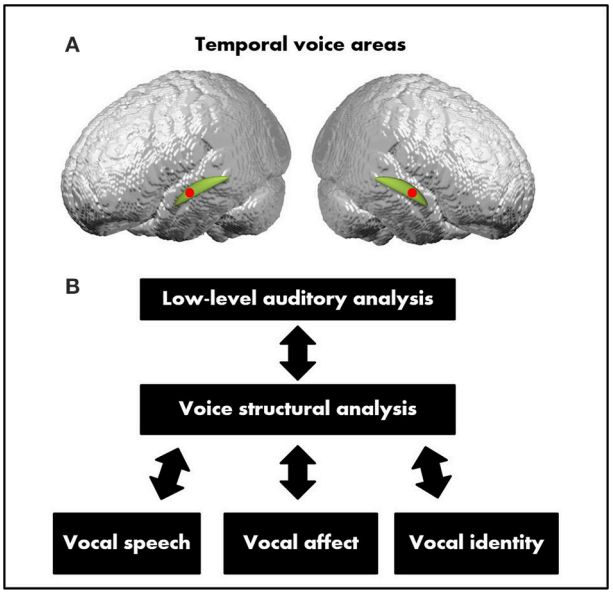

FIGURE 3 | (A) Temporal voice areas (TVA). The TVA (represented here by the red dots) are mostly located along the middle and anterior parts of the superior temporal sulcus (STS) bilaterally over the temporal plan (represented here in green). **(B)** A model of voice perception. After a stage of voice structural encoding constrained to vocal sounds, three partially dissociable functional pathways process the three main types of vocal information: speech, identity, and affect (adapted from Belin et al., 2004).

ABERRANT VOICE PROCESSING IN OLDER CHILDREN AND ADULTS WITH ASD

Difficulties to speak and to interact socially in an appropriate manner are central traits of autism and have been linked to abnormal processing of social information in both the visual and auditory modalities (e.g., Dawson et al., 1998, 2004; Klin et al., 2009; Chevallier et al., 2012 for review). Children and adults with ASD often tend to ignore human vocalizations in their surrounding but are responsive to other non-vocal stimuli indicating a detachment from their social environment (Klin, 1991, 1992; Kuhl et al., 2005). Early acquisition of language capacities is closely intertwined to social function in typically developing children and children on the spectrum (e.g., Goldstein et al., 2003; Kuhl et al., 2003; Norbury et al., 2010). Although, it is still not established why many individuals with ASD are often insensitive to human vocalizations, anomalies within voice selective areas have been highlighted in older children and adults with ASD. Using fMRI, Gervais and colleagues showed in a seminal study that adults on the spectrum (mean age = 25 years) failed to activate voice selective regions of the STS but showed similar activation patterns to the comparison group in response to non-vocal sounds (Gervais et al., 2004). This finding suggested an aberrant form of processing with respect to auditory information having a social content such as a voice does. This would suggest that a sound with a social content might not be adequately processed, most likely due to the abnormal development of cerebral regions implicated in the analysis of the social content of auditory stimuli (Gervais et al., 2004). Decreased gray matter volume in the bilateral voice specific STS have been observed in 10 year old children with ASD (Boddaert et al., 2004b). Abrams and colleagues hypothesized that this may be the consequence of individuals with ASD having impaired function of emotional and reward systems which in turn prevents them from engaging with acoustic information with a high social content such as speech stimuli (Abrams et al., 2013). In order to test their hypothesis, Abrams and colleagues scanned and compared 20 young children with

ASD to age- and intelligence quotient-matched TD controls (mean age = 9.8 years) using a resting-state fMRI protocol. By looking at the intrinsic functional connectivity in the voice-selective posterior STS (pSTS) bilaterally, they found the presence of underconnectivity between the left-hemisphere pSTS and the bilateral ventral tegmental areas in children with ASD. This was also the case for other regions such as the nucleus accumbens, left-hemisphere insula, orbitofrontal, and ventromedial prefrontal cortices. Moreover, diminished connectivity was evident between right-hemisphere pSTS and the orbitofrontal cortex and amygdala.

An important aspect of the study by Abrams and colleagues was that the degree of underconnectivity between voice-selective cortex and reward pathways predicted symptom severity for communication deficits in children with ASD, thus providing a connectivity biomarker for this specific group of patients. The study of the connectivity profile using a resting-state fMRI protocol during infancy and toddlerhood is now needed to further our understanding regarding how the functional connectivity between reward pathways and voice- and speech-related brain areas develops. Several neuroimaging studies performed in high-functioning older children and adults with ASD point to the presence of impairments in the neural basis of language processing in general (e.g., Gaffrey et al., 2007; Knaus et al., 2008; Herringshaw et al., 2016 for recent review). These experiments often including an overt task have revealed the existence of abnormal frontal and/or temporal responses during language processing tasks compared to TD individuals and reversed or reduced laterality within fronto-temporal language regions (e.g., Boddaert et al., 2003; Flagg et al., 2005; Kleinhans et al., 2008; Knaus et al., 2010; Lindell and Hudry, 2013; Herringshaw et al., 2016). In sum, experiments that used language tasks or rest scanning in the awake state indicate the presence of aberrant processing of human vocalizations in older children and adults with ASD.

In the following sections, we summarize the experiments investigating the neuronal underpinnings of human speech and language abnormalities during early periods of development: infancy and toddlerhood. These recent experiments have mostly used auditory speech stimuli which implicitly require analysis of the human voice. Importantly, several studies have included low-functioning toddlers with ASD or studied infants at high-risk for ASD. In contrast to experiments performed with older high-functioning children and adults with ASD and that include a task, scanning of very young infants is performed during natural sleep, at rest in the absence of an overt task or by passively presenting speech-stimuli (e.g., sentences, words, syllables). Overall, findings from these studies indicate that the brain systems implicated in human speech and language processing follow a different developmental pathway in individuals with ASD when compared to TD individuals very early on in the development already. We begin by a summary of the structural and functional differences that have been found in young toddlers with ASD and infants at risk.

STRUCTURAL DIFFERENCES IN TODDLERS WITH ASD AND INFANTS AT RISK

Several studies suggested brain overgrowth during the first year of life in toddlers with ASD (e.g., Courchesne et al., 2001, 2003, 2011; Redcay and Courchesne, 2005; Hazlett et al., 2011; Nordahl et al., 2011; Shen et al., 2013). For example, Sparks and colleagues measured an increased brain volume in toddlers with ASD (aged 3–4 years) compared to aged-matched TD controls and developmentally delayed (DD) children (Sparks et al., 2002). Longitudinal measurements indicate the presence of gray and white matter cerebral overgrowth in toddlers at 2 years (Hazlett et al., 2005). In a longitudinal study, Schumann and colleagues followed up toddlers and school aged children with ASD (1.5 years up to 5 years of age). They found both gray and white matter enlargements by 2.5 years of age in fronto-temporal regions along with cingulate cortices, regions related but not limited to language development (Schumann et al., 2010). A global increase in gray matter volumes in toddlers with ASD aged between 2 and 3 years compared to DD toddlers has recently been reported (Xiao et al., 2014). The locus of this difference manifested regionally in the right STG, a cortical region known to be involved in spoken language comprehension (Lattner et al., 2005). In older children with ASD, this locus has been shown to be enlarged to aged match controls (mean age = 13.5 years; Jou et al., 2010) and to exhibit a different pattern of activation during speech processing compared to TD adolescents (mean age = 12 years; Lai et al., 2011). Other studies indicate the presence of structural anomalies within language-related brain areas in older children and adults (e.g., Prigge et al., 2013; Itahashi et al., 2015; Lai et al., 2015). It is hypothesized that this early brain overgrowth during infancy and toddlerhood in ASD is followed by a period of decline in brain size from childhood to adulthood (Courchesne et al., 2011; Lange et al., 2015).

Diffusion imaging studies have also revealed the presence of widespread disruption of white matter integrity in long-range and short-range connections in toddlers, older children and adults with ASD (see Hoppenbrouwers et al., 2014; Conti et al., 2015 for reviews). For example, accelerated white matter maturation has been reported in a small sample of seven participants aged between 1.8 and 3.3 years (Ben Bashat et al., 2007). Altered white matter integrity has also been found in toddlers with ASD (mean age = 3.2 years; Weinstein et al., 2011). Xiao et al. (2014) showed altered structural brain connectivity in multiple regions that have been related but not limited to language functions such as the posterior cingulate cortex, subregions of the limbic lobes as well as the corpus callosum in toddlers with ASD aged between 2 and 3 years (Xiao et al., 2014). It even appears that white matter anomalies might develop before the first year in infants who are later diagnosed with ASD. Wolff and collegues observed abnormalities in white matter fiber tracts in infants at risk (at 6 months) and who were diagnosed at 24 months (Wolff et al., 2012). In a recent study of infants at high-risk for ASD and diagnosed at 24 months, white matter connectivity abnormalities were present specifically over Broca's

area in the frontal lobes, and more generally in the temporal, parietal, occipital lobes as compared to both low-and high-risk infants not classified as ASD (Lewis et al., 2014).

Anatomical data indicate a period of early brain overgrowth (between 1 and 5 years) followed by normalization during adolescence. Structural connectivity experiments also report a developmental shift from greater structural connectivity in very young children with ASD to lower connectivity in older children (see Hoppenbrouwers et al., 2014; Conti et al., 2015 for recent discussions). These alterations impinge on acquiring normal language functions and lead to other higher-order cognitive, social, and communicative functions deficits. However, it is still unclear how those differences relate and can yet reflect the early language development heterogeneity inherent to autism. The field is also currently hampered by the widespread methodology differences in terms of subject inclusion criteria (high vs. low functioning autism), control groups, size of cohorts, age range, neuroimaging methods and parameters. Future cross-sectional and longitudinal experiments spanning early childhood to adulthood are necessary including larger sample size. Only then it will be possible to get a clearer picture within this complex and increasingly expanding field of research.

FUNCTIONAL STUDIES IN TODDLERS WITH ASD USING VOICE-RELATED AUDITORY STIMULI

Brain abnormalities underlying human voice processing during toddlerhood have also been found. A seminal EEG experiment performed by Kuhl et al. (2005) indicated the presence of different event-related potential (ERP) response pattern to speech stimuli in toddlers with ASD compared to TD (mean age = 3.5 years). In this experiment, toddlers were passively presented with standard and deviant phonemes. In individuals with typical development, contrasting the brain responses that are produced by the deviant sound with the ones produced by the standard sound causes a mismatch negativity (MMN). The MMN is a robust index of automatic sound discrimination (MMN, Näätänen, 1995, 2003 for reviews). In toddlers with ASD, there was no evidence for an MMN, whereas in TD the MMN was present. Using an auditory preference test, the group of toddlers with ASD was subdivided between those who preferred human vocalization (i.e., motherese speech sounds) and those who preferred non-speech analogs. An MMN appeared in the group that preferred motherese sounds similarly to what was found in TD toddlers while toddlers with ASD who preferred the non-speech sounds still did not exhibit an MMN. These findings are important as they reveal a link between early social preferences and early language processing skills in toddlers with ASD.

A functional study by Redcay and Courchesne (2008) found that the brain systems of speech perception were responding differently to speech stimuli in toddlers with ASD compared to TD toddlers. In a cross-sectional experiment with a small sample size, the authors scanned toddlers aged between 2 and 3 years using a natural sleep fMRI experimental design. They recorded brain activity when toddlers were asleep and listened to normal speech of a human voice (forward and backward speech stimuli), and the ones from toddlers with ASD. Results indicated the recruitment of different regions and with a different laterality dominance. Specifically, toddlers with ASD exhibited hypoactivation of many regions traditionally recruited during early language acquisition in comparison to those with TD, suggesting that at that age toddlers with ASD are already on a deviant developmental trajectory characterized by a greater recruitment of right hemispheric regions during speech perception (Redcay and Courchesne, 2008). The same research group then performed an fMRI experiment where they increased their sample size and included even younger children (aged between 12 and 48 months; Eyler et al., 2012). Using a prospective, cross-sectional design this time, 80 toddlers listened to a bedtime story during their sleep (speech sound stimuli from a human voice). Toddlers were also followed up to get record of their evolution and to ensure confirmation of later ASD diagnosis. A different brain pattern of brain activation was found between toddlers who were at risk and who were later diagnosed with ASD and the toddlers who followed a normal development path. Specifically, toddlers with ASD had deficient left hemisphere responses to speech sounds with an abnormal right-lateralized temporal cortical response to language; this deficit worsened during growth to become most severe by the age of four. Contrarily, TD toddlers had a reversed pattern of brain activity and lateralization with the presence of more temporal cortical responses and a left lateralized pattern of brain activation that became stronger with development. Two important observations can be made. Firstly, lateralization in response to auditory speech sounds differs between groups. Abnormal lateralization in response to language has also been reported in experiments performed in older children and adults with ASD (e.g., Kleinhans et al., 2008; Minagawa-Kawai et al., 2009). Secondly, weaker brain responses to speech sounds over the temporal pole were present in the ASD group, suggesting the presence of an early specific and abnormal brain response pattern to speech sounds in toddlers with ASD (Eyler et al., 2012).

FUNCTIONAL STUDIES IN INFANTS AT RISK USING VOICE-RELATED AUDITORY STIMULI

In a recent study, Seery et al. (2013) suggested that this atypical lateralization is an ASD endophenotype already observable during the first year of life. Comparing infants at risk for ASD with low-risk infants aged between 6 and 12 months, the authors reported significant group differences in the development of lateralized ERP responses to speech (using consonant-vowel auditory stimuli). More specifically, the low-risk group displayed a lateralized response to the speech sounds whereas the high-risk group did not (Seery et al., 2013). In a subsequent study, the same research group found atypical ERPs to repeated speech sounds in 9 month old infants at risk (Seery et al., 2014). Atypical lateralization of the ERP to words at 2 years of age has also been observed in ASD toddlers with poor

social skills (Kuhl et al., 2013). In a very recent sleep fMRI study that also included behavioral assessment of parent-infant interactions, Blasi et al. (2015) compared cortical responses between emotional voices and environmental sound stimuli. They found that high-risk infants for ASD (aged between 4 and 7 months) did not show this early specialization suggesting the presence very early on of atypical neural responses to human voice with and without emotional valence in at-risk populations, at least (Blasi et al., 2015). Taken together, these results indicate that during early development, speech, and language-critical areas over the temporal poles do not show the same brain responses to voice related stimuli as observed in TD young individuals. An absence or atypical lateralization of brain responses and functional hypoactivation in response to speech related content were already reported in infants at risk and toddlers with ASD. Moreover, voice-selective cortices in populations show lesser degree of specialization already in infants at risk. In sum, similarly to the experiments performed in high-functioning older children and despite the use of different experimental conditions, abnormalities in lateralization and aberrant functional activation during voice processing are already found very early on, during infancy and toddlerhood.

DYSFUNCTIONAL CONNECTIVITY IN TODDLERS WITH ASD AND INFANTS AT RISK USING VOICE-RELATED AUDITORY STIMULI

Aside from the differences in functional activation described in the previous section, extant functional connectivity studies using fMRI or EEG with voice-related stimuli have shown altered connectivity between brain regions involved in language processing in young children with autism. Using fMRI, Dinstein and colleagues demonstrated reduced inter-hemispheric synchrony across language brain areas in young toddlers with ASD (Dinstein et al., 2011). They recorded spontaneous brain activity in three groups of toddlers during natural sleep (TD, ASD, and language delay). Seventy-two participants aged between 12 and 46 months (mean age = 29 months for the toddlers with ASD) were presented with auditory stimulation containing words, pseudo words, sentences, tones, or environmental sounds. The aim was to test for differences in synchronization between various brain regions between the three groups and explore a possible relation with the development of early autistic behavioral symptoms within the group of toddlers with ASD. Stimulus-evoked responses were regressed out so as to only keep spontaneous fMRI fluctuations in the data. In doing so, the authors controlled that any differences in synchronization between the groups were not due to differences in auditory-evoked responses between participants. Results indicated the presence of weaker interhemispheric synchronization between the IFG and the STG, two brain areas mediating speech and language processing in the ASD toddler group as compared to the two other groups. Moreover, analyses within the group of toddlers with ASD revealed that the synchronization strength was highest in those with overall good verbal capacities and was weakest in those with impaired verbal capacities. This indicates that, the functional connectivity between regions implicated in language processing has a different pattern compared to TD peers in toddlerhood already (Dinstein et al., 2011).

Using EEG, aberrant reduced functional connectivity has even been reported before the onset of any ASD symptoms, in infants at risk for ASD (Righi et al., 2014). They presented speech sounds (syllables) in the awake state, while EEG was concomitantly acquired in infants at high-risk and infants at low-risk for ASD. Acquisitions were performed at 6 and at 12 months of age. The participants were followed up at 36 months in order to identify which ones would develop ASD or not. By computing the intra-hemispheric linear coherence in the gamma frequency band, (that is, an estimation of synchronization across brain regions) between electrodes of interest located over the frontal and temporo-parietal regions in the left and right hemispheres, the authors found that at 6 months, linear coherence values were similar across groups. At 12 months however, infants at high-risk and later diagnosed with ASD showed reduced functional connectivity (that is, lower linear coherence, and thus less integration) compared to both infants at low-risk and those at high-risk who were not later diagnosed with ASD. In addition, significant differences in functional connectivity between the low-risk and high-risk infants who did not become autistic were found, with lower coherence values in the high-risk infant group. In contrast to what has been previously reported in fMRI with toddlers (Redcay and Courchesne, 2008; Eyler et al., 2012) or with EEG in infants at-risk for ASD (Seery et al., 2013), the study did not reveal any early group differences in hemispheric lateralization. However, as discussed by the authors, the estimation of the linear coherence is an approach less sensitive to stimulus-locked activity whereas fMRI and ERPs are. As such Righi's approach might not have captured existing hemispheric differences. Taken together, published functional connectivity studies examining the early development of language related brain areas demonstrate aberrant brain connectivity patterns in both toddlers with ASD (Dinstein et al., 2011), and in 12 month old infants at risk who later develop autism (Righi et al., 2014). This suggests that aberrant wiring of the cerebral regions responsible for language processing precede the onset of the typical autism phenotype, and might be responsible for the early signs clinically observed in infants who will develop ASD, such as unresponsiveness to name, lack of orientation to human voices and delay in the development of receptive and expressive language skills.

LANGUAGE HETEROGENEITY IN TODDLERS WITH ASD: INSIGHTS FROM EARLY BRAIN BIOMARKERS

Findings reviewed so far indicate early functional differences in speech-related processing within superior temporal cortical regions and other language-critical brain areas. The anatomical and connectivity differences reported above in toddlers with ASD and infants at risk for ASD mostly correspond to

group differences. While these results are informative, they do not permit to fully address the critical question of the heterogeneity of early language development in ASD and its relation to later outcome. To successfully tackle the question of heterogeneity, research groups have started using prospective and longitudinal designs with larger sample sizes to examine the hypothesis that different subgroups of individuals with ASD have different phenotypes and developmental pathways (Kuhl et al., 2013; Lombardo et al., 2015). These studies open avenues to better understand predictor of outcomes, as predictive brain biomarkers that can differentiate between these subtle phenotypes emerge (Bölte et al., 2013; Lenroot and Yeung, 2013; Ecker et al., 2015). For instance, in a recent developmental study, Lombardo et al. (2015) searched for early functional neuroimaging biomarkers that would reflect the heterogeneity observed in early language development in ASD. The authors measured early cortical responses to speech using a prospective sleep fMRI paradigm (participants aged between 12 and 48 months). The experiment included four different groups with TD infants, infants with a language/developmental delay (LD/DD), infants with ASD having a good language outcome at 4 years of age ("ASD good") or a bad language development outcome ("ASD Poor"; that is, they measured developmental trajectories of language growth over the first 4 years of life). Pre-diagnosis fMRI brain data in response to three types of speech stimuli (complex forward speech, simple forward speech, and backward speech) were acquired in each participants. The aim was to test whether early functional measures could have a predictive value when combined with clinical-behavioral information. First, they found that in response to speech stimuli, "ASD good" toddlers recruited language-sensitive superior temporal cortices in a very similar way to the control groups (that is, the non-ASD language/developmentally delayed individuals). However, in the "ASD poor" group, language-sensitive superior temporal cortices were found to be hypoactive in response to the same speech stimuli. The multivoxel activation pattern was different to the one observed in the three other control groups indicating a lack of functional differentiation to these speech stimuli in the ASD poor group. Another important finding by Lombardo et al. (2015) was that the brain response patterns to general auditory processing was preserved in the "ASD poor" group (that is, similar to the other control groups), whereas the brain activity specifically related to language and speech was weaker and less specific. For example no engagement of the left hemisphere was found as this was the case in the three other groups. This would suggest on the one hand a general preservation of the neural systems devoted to general auditory processing during infancy and on the other, the presence of a dysfunction of the neural systems at a higher level of processing and implicated in voice-related content leading to the aberrant processing of auditory stimuli containing speech and language related information. Interestingly, the connectivity between primary auditory cortex and the reward and affective brain circuitry seems to be preserved in high-functioning older children with ASD, whereas connectivity between the voice structural module (see **Figure 3B**) described in Belin's model above and the reward system is impaired, preventing the normal processing of speech related content but allowing low-level sensory processing to occur (Abrams et al., 2013).

The results provided by the study by Lombardo et al. are important for several reasons. First, they indicate the presence during toddlerhood already of brain related differences in the neural underpinnings implicated in the processing of early voice related auditory information and this between different subtypes of ASD (that is, differences between ASD poor and ASD good). Second, longitudinal measurements of pre-diagnostic clinical behavioral information and early fMRI language and speech-related brain responses and combination thereof was found to have a strong predictive value in terms of determining later ASD subgroup prognosis.

Other experiments also point to the presence of early brain biomarkers in EEG. Kuhl et al. (2013) found that the response pattern of ERPs to words at the age of 2 year was predictive of later receptive language capacities at ages 4 and 6 years (Kuhl et al., 2013). In comparison to the Lombardo et al. (2015) study where clinical groups were subdivided based on their language skills, Kuhl and colleagues compared the ERPs in response to words in 2 year old children that were subdivided as a function of social symptoms, into "ASD high" (sever social symptoms) and "ASD low" less social symptoms. Results showed only a left lateralized brain response similar to the TD group in the "ASD low" group. Only the single electrode where the time locked response manifested was different between those two groups (T3 for TD and P3 for "ASD low"). For the "ASD high" group on the other hand, the ERP was more diffuse and right lateralized. Then, in a second phase of the study, the authors looked at the predictive power of their P3 effect found in the first phase for all ASD toddlers on linguistic, cognitive, and adaptive functions at ages 4 and 6 years. For the ASD toddlers who had strong negativity in the ERP to known words at P3 measured at enrollment, a better outcome was observed at 6 years of age. In stark contrast, toddlers with ASD who did not show this ERP sensitivity at intake had worse outcomes (that is, they showed less improvement). Interestingly, the ERP measures to words furthermore exceeded the predictive value of cognitive measures performed at intake. Another important finding by this study was that the predictive aspect of the brain response to words at age 2 years of age did not modulate depending on the type of intensive treatments the toddlers received. Adding another control condition with no treatments may perhaps have added valuable information with respect to the effectiveness of the treatments as recent evidences indicate that early behavioral intervention is associated with normalized patterns of EEG brain activity in the visual modality at least (Dawson et al., 2012). Unfortunately and as mentioned by the authors, the source localization of those differences could not be performed. As already discussed, methods for estimating inverse solutions are now available and it will be important in further studies to include those when possible.

PERSPECTIVE AND FUTURE DIRECTIONS

Neuroimaging studies using exciting new approaches that combine early brain measurements with early behavioral data

are starting to highlight important differences in the functional and structural wiring of the young autistic brain compared to the TD one using auditory speech and language related stimuli. With time, the field will hopefully see the appearance of other experiments with larger sample sizes combined with longitudinal measurements to subtype ASD infants according to the core impaired dimension of early language development that was the main focus of the present review, and of social interaction and communication deficits that are both central hallmarks of autism. This will help to explore the efficiency of early intervention in correcting the developmental trajectories on the one hand, and to tackle the question of heterogeneity inherent to autism on the other. Ultimately this will lead to the possibility of improving, developing and modifying therapeutic interventions and adapting them depending to the infant's specific needs. Moreover, because autism cannot always be diagnosed with high certainty before the age of 2–3 years (Zwaigenbaum et al., 2009; Jones et al., 2014), additional prospective longitudinal studies of high-risk populations are necessary to provide understanding about how, when and where developmental trajectories that result in ASD deviate from the TD young brain. These later will in turn aid to understand the general heterogeneity observed in early language development in autism as well as allow early identification of toddlers who should receive intensive therapeutic intervention. The few experiments of infants at risk reported here indicate that brain differences in response to human voice and its speech and language related content are already present before the end of the first year in some cases suggesting that aberrant voice processing could be a promising marker to identify ASD very early on.

Achieving a better understanding regarding which neural systems implicated in speech and language-critical processing are impaired very early on is difficult to highlight and this for several reasons. First, scanning individuals aged between 6 months and 3 year implies using scanning conditions with passive presentation of stimuli most of the time. Implementing tasks that need an engagement of the participant at such a young age is difficult to achieve. For example asking what is voice specific vs. speech specific has only been addressed by one study so far, which used a behavioral task in preschool TD children aged around 6 years (Raschle et al., 2014). In the studies discussed in this review, based in infants and toddlers (i.e., before 4 years), the vast majority of experiments used contrast between speech stimuli and rest, reversed speech or other auditory stimuli (words, sentences, and syllables). Yet, contrasting speech stimuli vs. rest activation does not allow to determine what is specifically related to the voice and what is related to the speech content. The question remains open as to whether a voice specific impairment is present in the brain of young children with ASD. Thus, future experiments should include contrasts between voice specific vs. speech specific brain related activity. This would allow to test whether aberrant voice processing that has been reported in older children and young adults is indeed a hallmark in autism very early on leading to impairments in the social-communication language brain. Currently there is only one experiment to our knowledge where the brain responses to human vocalizations alone were contrasted with non-vocal sounds in infants at risk for autism (Blasi et al., 2015). However, the authors reported that their sample had not been assessed for ASD at the age of 3 years yet. Further work is thus needed to resolve this issue.

Some authors have also recently hypothesized that it is not human speech *per se* that is an issue in autism but rather the mode of communication of speech that might be challenging for individuals with ASD. For example, recent results suggest that the mode of presentation of human speech sounds might play a role in speech perception in older children and young adults with autism. In an fMRI experiments, Lai et al. (2012) passively presented familiar human speech stimuli (spoken sentences by parents) or song stimuli containing vocals to children with ASD (including low functioning ones) and aged matched controls. While brain activations were found to be different between the children with ASD and TD during the spoken condition, they turned out to be comparable when speech was delivered in a sung format (Lai et al., 2012). Another study found comparable brain activation patterns and preserved fronto-temporal connections between children with ASD and aged matched controls during perception of sung but not spoken words (Sharda et al., 2015). Most of the experiments reviewed here have shown abnormalities in lateralization and aberrant functional activation during speech processing during infancy and toddlerhood similarly to what has been reported in older children and adults. However, none of them varied the mode of presentation of the speech sounds that were always presented in a spoken format. Interestingly, one experiment found that toddlers with ASD (aged 2 years) who preferred motherese speech signals (that is, a pattern of speech characterized by high-pitch intonations) exhibit similar ERP responses compared to aged match TD controls in a passive syllable discrimination task (Kuhl et al., 2005). In this later, toddlers with ASD who didn't preferred an analog speech signal had different ERP responses compared to TD toddlers. It will be instrumental to detect how early the mode of communication impacts human speech processing in infants and toddlers with ASD and in at risk population as preliminary results now suggest that sung over spoken speech might effectively improve socio-communicative behaviors in toddlers with ASD at least (Paul et al., 2015).

Another final important aspect that has to be considered besides the various impairments in the development of speech processing highlighted by the relevant neuroimaging literature we reviewed here, is that functional and structural anomalies have also been reported at earlier stages of the auditory processing system in autism. Some studies highlight functional abnormalities within low level primary sensory auditory pathways in adults with ASD (Dinstein et al., 2012; Haigh et al., 2015). A recent experiment points toward the presence of maturational differences in the development of primary/secondary auditory areas in children with ASD aged between 6 and 14 years (Edgar et al., 2015). The presence of abnormal auditory brainstem response in newborns/infants (tested between 0 and 3 months) and toddlers (tested between 1.5 and 3.5 years) later diagnosed with ASD has also been demonstrated (Miron et al., 2015). Further work is thus required to understand how these impairments in the early stages of the

auditory processing system might impinge on the development of speech and language processing in autism.

AUTHOR CONTRIBUTIONS

HS and MS wrote the paper, read, and approved the final manuscript.

ACKNOWLEDGMENTS

This research review is supported by a grant from the National Center of Competence in Research (NCCR) "SYNAPSY—The Synaptic Bases of Mental Diseases" financed by the Swiss National Science Foundation (SNF, Grant number: 51AU40_125759). MS is further supported by an individual fellowship from the SNF (#158831).

REFERENCES

Abrahams, B. S., and Geschwind, D. H. (2010). Connecting genes to brain in the autism spectrum disorders. *Arch. Neurol.* 67, 395–399. doi: 10.1001/archneurol.2010.47

Abrams, D. A., Lynch, C. J., Cheng, K. M., Phillips, J., Supekar, K., Ryali, S., et al. (2013). Underconnectivity between voice-selective cortex and reward circuitry in children with autism. *Proc. Natl. Acad. Sci. U.S.A.* 110, 12060–12065. doi: 10.1073/pnas.1302982110

American Psychiatric Association and American Psychiatric Association. Dsm-5 Task Force (2013). *Diagnostic and Statistical Manual of Mental Disorders: DSM-5*. Washington, DC: American Psychiatric Association.

Anderson, D. K., Lord, C., Risi, S., Dilavore, P. S., Shulman, C., Thurm, A., et al. (2007). Patterns of growth in verbal abilities among children with autism spectrum disorder. *J. Consult. Clin. Psychol.* 75, 594–604. doi: 10.1037/0022-006X.75.4.594

Arnott, B., McConachie, H., Meins, E., Fernyhough, C., Couteur, A. L., Turner, M., et al. (2010). The frequency of restricted and repetitive behaviors in a community sample of 15-month-old infants. *J. Dev. Behav. Pediatr.* 31, 223–229. doi: 10.1097/DBP.0b013e3181d5a2ad

Asperger, H. (1944). The "autistic psychopathy" in childhood. *Arch. Psychiatrie Nervenkrankheiten* 117, 76–136. doi: 10.1007/BF01837709

Baio, J. (2014). Prevalence of autism spectrum disorder among children aged 8 years - autism and developmental disabilities monitoring network, 11 sites, United States, 2010. *MMWR. Surveill. Summ.* 63, 1–21.

Baranek, G. T. (1999). Autism during infancy: a retrospective video analysis of sensory-motor and social behaviors at 9-12 months of age. *J. Autism Dev. Disord.* 29, 213–224. doi: 10.1023/A:1023080005650

Barbaro, J., and Dissanayake, C. (2009). Autism spectrum disorders in infancy and toddlerhood: a review of the evidence on early signs, early identification tools, and early diagnosis. *J. Dev. Behav. Pediatr.* 30, 447–459. doi: 10.1097/DBP.0b013e3181ba0f9f

Baron-Cohen, S., Auyeung, B., Nørgaard-Pedersen, B., Hougaard, D. M., Abdallah, M. W., Melgaard, L., et al. (2015). Elevated fetal steroidogenic activity in autism. *Mol. Psychiatry* 20, 369–376. doi: 10.1038/mp.2014.48

Belin, P. (2006). Voice processing in human and non-human primates. *Philos. Trans. R. Soc. Lond. B Biol. Sci.* 361, 2091–2107. doi: 10.1098/rstb.2006.1933

Belin, P., Fecteau, S., and Bédard, C. (2004). Thinking the voice: neural correlates of voice perception. *Trends Cogn. Sci.* 8, 129–135. doi: 10.1016/j.tics.2004.01.008

Belin, P., and Grosbras, M. H. (2010). Before speech: cerebral voice processing in infants. *Neuron* 65, 733–735. doi: 10.1016/j.neuron.2010.03.018

Belin, P., and Zatorre, R. J. (2003). Adaptation to speaker's voice in right anterior temporal lobe. *Neuroreport* 14, 2105–2109. doi: 10.1097/00001756-200311140-00019

Belin, P., Zatorre, R. J., and Ahad, P. (2002). Human temporal-lobe response to vocal sounds. *Brain Res. Cogn. Brain Res.* 13, 17–26. doi: 10.1016/S0926-6410(01)00084-2

Belin, P., Zatorre, R. J., Lafaille, P., Ahad, P., and Pike, B. (2000). Voice-selective areas in human auditory cortex. *Nature* 403, 309–312. doi: 10.1038/35002078

Ben Bashat, D., Kronfeld-Duenias, V., Zachor, D. A., Ekstein, P. M., Hendler, T., Tarrasch, R., et al. (2007). Accelerated maturation of white matter in young children with autism: a high b value DWI study. *Neuroimage* 37, 40–47. doi: 10.1016/j.neuroimage.2007.04.060

Berchio, C., Rihs, T. A., Michel, C. M., Brunet, D., Apicella, F., Muratori, F., et al. (2014). Parieto-frontal circuits during observation of hidden and visible motor acts in children. A high-density EEG source imaging study. *Brain Topogr.* 27, 258–270. doi: 10.1007/s10548-013-0314-x

Bergelson, E., and Swingley, D. (2012). At 6-9 months, human infants know the meanings of many common nouns. *Proc. Natl. Acad. Sci. U.S.A.* 109, 3253–3258. doi: 10.1073/pnas.1113380109

Betancur, C. (2011). Etiological heterogeneity in autism spectrum disorders: more than 100 genetic and genomic disorders and still counting. *Brain Res.* 1380, 42–77. doi: 10.1016/j.brainres.2010.11.078

Blasi, A., Lloyd-Fox, S., Sethna, V., Brammer, M. J., Mercure, E., Murray, L., et al. (2015). Atypical processing of voice sounds in infants at risk for autism spectrum disorder. *Cortex* 71, 122–133. doi: 10.1016/j.cortex.2015.06.015

Blasi, A., Mercure, E., Lloyd-Fox, S., Thomson, A., Brammer, M., Sauter, D., et al. (2011). Early specialization for voice and emotion processing in the infant brain. *Curr. Biol.* 21, 1220–1224. doi: 10.1016/j.cub.2011.06.009

Boddaert, N., Belin, P., Chabane, N., Poline, J. B., Barthélémy, C., Mouren-Simeoni, M. C., et al. (2003). Perception of complex sounds: abnormal pattern of cortical activation in autism. *Am. J. Psychiatry* 160, 2057–2060. doi: 10.1176/appi.ajp.160.11.2057

Boddaert, N., Chabane, N., Belin, P., Bourgeois, M., Royer, V., Barthelemy, C., et al. (2004a). Perception of complex sounds in autism: abnormal auditory cortical processing in children. *Am. J. Psychiatry* 161, 2117–2120. doi: 10.1176/appi.ajp.161.11.2117

Boddaert, N., Chabane, N., Gervais, H., Good, C. D., Bourgeois, M., Plumet, M. H., et al. (2004b). Superior temporal sulcus anatomical abnormalities in childhood autism: a voxel-based morphometry MRI study. *Neuroimage* 23, 364–369. doi: 10.1016/j.neuroimage.2004.06.016

Boersma, M., Kemner, C., De Reus, M. A., Collin, G., Snijders, T. M., Hofman, D., et al. (2013). Disrupted functional brain networks in autistic toddlers. *Brain Connect.* 3, 41–49. doi: 10.1089/brain.2012.0127

Bölte, S., Marschik, P. B., Falck-Ytter, T., Charman, T., Roeyers, H., and Elsabbagh, M. (2013). Infants at risk for autism: a European perspective on current status, challenges and opportunities. *Eur. Child Adolesc. Psychiatry* 22, 341–348. doi: 10.1007/s00787-012-0368-4

Brunet, D., Murray, M. M., and Michel, C. M. (2011). Spatiotemporal analysis of multichannel EEG: CARTOOL. *Comput. Intell. Neurosci.* 2011:813870. doi: 10.1155/2011/813870

Cantlon, J. F., Brannon, E. M., Carter, E. J., and Pelphrey, K. A. (2006). Functional imaging of numerical processing in adults and 4-y-old children. *PLoS Biol.* 4:e125. doi: 10.1371/journal.pbio.0040125

Cheng, Y., Lee, S. Y., Chen, H. Y., Wang, P. Y., and Decety, J. (2012). Voice and emotion processing in the human neonatal brain. *J. Cogn. Neurosci.* 24, 1411–1419. doi: 10.1162/jocn_a_00214

Chevallier, C., Kohls, G., Troiani, V., Brodkin, E. S., and Schultz, R. T. (2012). The social motivation theory of autism. *Trends Cogn. Sci.* 16, 231–239. doi: 10.1016/j.tics.2012.02.007

Conti, E., Calderoni, S., Marchi, V., Muratori, F., Cioni, G., and Guzzetta, A. (2015). The first 1000 days of the autistic brain: a systematic review of diffusion imaging studies. *Front. Hum. Neurosci.* 9:159. doi: 10.3389/fnhum.2015.00159

Courchesne, E., Campbell, K., and Solso, S. (2011). Brain growth across the life span in autism: age-specific changes in anatomical pathology. *Brain Res.* 1380, 138–145. doi: 10.1016/j.brainres.2010.09.101

Courchesne, E., Carper, R., and Akshoomoff, N. (2003). Evidence of brain overgrowth in the first year of life in autism. *JAMA* 290, 337–344. doi: 10.1001/jama.290.3.337

Courchesne, E., Karns, C. M., Davis, H. R., Ziccardi, R., Carper, R. A., Tigue, Z. D., et al. (2001). Unusual brain growth patterns in early life in patients with autistic disorder: an MRI study. *Neurology* 57, 245–254. doi: 10.1212/WNL.57.2.245

Custo, A., Vulliemoz, S., Grouiller, F., Van De Ville, D., and Michel, C. (2014). EEG source imaging of brain states using spatiotemporal regression. *Neuroimage* 96, 106–116. doi: 10.1016/j.neuroimage.2014.04.002

Dahlgren, S. O., and Gillberg, C. (1989). Symptoms in the first two years of life. A preliminary population study of infantile autism. *Eur. Arch. Psychiatry Neurol. Sci.* 238, 169–174. doi: 10.1007/BF00451006

Dawson, G. (2008). Early behavioral intervention, brain plasticity, and the prevention of autism spectrum disorder. *Dev. Psychopathol.* 20, 775–803. doi: 10.1017/S0954579408000370

Dawson, G., Jones, E. J., Merkle, K., Venema, K., Lowy, R., Faja, S., et al. (2012). Early behavioral intervention is associated with normalized brain activity in young children with autism. *J. Am. Acad. Child Adolesc. Psychiatry* 51, 1150–1159. doi: 10.1016/j.jaac.2012.08.018

Dawson, G., Meltzoff, A. N., Osterling, J., Rinaldi, J., and Brown, E. (1998). Children with autism fail to orient to naturally occurring social stimuli. *J. Autism Dev. Disord.* 28, 479–485. doi: 10.1023/A:1026043926488

Dawson, G., Rogers, S., Munson, J., Smith, M., Winter, J., Greenson, J., et al. (2010). Randomized, controlled trial of an intervention for toddlers with autism: the Early Start Denver Model. *Pediatrics* 125, e17–23. doi: 10.1542/peds.2009-0958

Dawson, G., Toth, K., Abbott, R., Osterling, J., Munson, J., Estes, A., et al. (2004). Early social attention impairments in autism: social orienting, joint attention, and attention to distress. *Dev. Psychol.* 40, 271–283. doi: 10.1037/0012-1649.40.2.271

de Bie, H. M. A., Boersma, M., Wattjes, M. P., Adriaanse, S., Vermeulen, R. J., Oostrom, K. J., et al. (2010). Preparing children with a mock scanner training protocol results in high quality structural and functional MRI scans. *Eur. J. Pediatr.* 169, 1079–1085. doi: 10.1007/s00431-010-1181-z

Deen, B., Koldewyn, K., Kanwisher, N., and Saxe, R. (2015). Functional organization of social perception and cognition in the superior temporal sulcus. *Cereb. Cortex* 25, 4596–4609. doi: 10.1093/cercor/bhv111

De Giacomo, A., and Fombonne, E. (1998). Parental recognition of developmental abnormalities in autism. *Eur. Child Adolesc. Psychiatry* 7, 131–136. doi: 10.1007/s007870050058

Dehaene-Lambertz, G., Dehaene, S., and Hertz-Pannier, L. (2002). Functional neuroimaging of speech perception in infants. *Science* 298, 2013–2015. doi: 10.1126/science.1077066

Dehaene-Lambertz, G., Hertz-Pannier, L., Dubois, J., Mériaux, S., Roche, A., Sigman, M., et al. (2006). Functional organization of perisylvian activation during presentation of sentences in preverbal infants. *Proc. Natl. Acad. Sci. U.S.A.* 103, 14240–14245. doi: 10.1073/pnas.0606302103

Dinstein, I., Heeger, D. J., Lorenzi, L., Minshew, N. J., Malach, R., and Behrmann, M. (2012). Unreliable evoked responses in autism. *Neuron* 75, 981–991. doi: 10.1016/j.neuron.2012.07.026

Dinstein, I., Pierce, K., Eyler, L., Solso, S., Malach, R., Behrmann, M., et al. (2011). Disrupted neural synchronization in toddlers with autism. *Neuron* 70, 1218–1225. doi: 10.1016/j.neuron.2011.04.018

Ecker, C., Bookheimer, S. Y., and Murphy, D. G. (2015). Neuroimaging in autism spectrum disorder: brain structure and function across the lifespan. *Lancet Neurol.* 14, 1121–1134. doi: 10.1016/S1474-4422(15)00050-2

Edgar, J. C., Fisk Iv, C. L., Berman, J. I., Chudnovskaya, D., Liu, S., Pandey, J., et al. (2015). Auditory encoding abnormalities in children with autism spectrum disorder suggest delayed development of auditory cortex. *Mol. Autism* 6, 69. doi: 10.1186/s13229-015-0065-5

Eigsti, I. M., De Marchena, A. B., Schuh, J. M., and Kelley, E. (2011). Language acquisition in autism spectrum disorders: a developmental review. *Res. Autism Spectr. Disord.* 5, 681–691. doi: 10.1016/j.rasd.2010.09.001

Eimas, P. D., Siqueland, E. R., Jusczyk, P., and Vigorito, J. (1971). Speech perception in infants. *Science* 171, 303–306. doi: 10.1126/science.171.3968.303

Elsabbagh, M., Mercure, E., Hudry, K., Chandler, S., Pasco, G., Charman, T., et al. (2012). Infant neural sensitivity to dynamic eye gaze is associated with later emerging autism. *Curr. Biol.* 22, 338–342. doi: 10.1016/j.cub.2011.12.056

Epstein, J. N., Casey, B. J., Tonev, S. T., Davidson, M., Reiss, A. L., Garrett, A., et al. (2007). Assessment and prevention of head motion during imaging of patients with attention deficit hyperactivity disorder. *Psychiatry Res.* 155, 75–82. doi: 10.1016/j.pscychresns.2006.12.009

Ethofer, T., Van De Ville, D., Scherer, K., and Vuilleumier, P. (2009). Decoding of emotional information in voice-sensitive cortices. *Curr. Biol.* 19, 1028–1033. doi: 10.1016/j.cub.2009.04.054

Eyler, L. T., Pierce, K., and Courchesne, E. (2012). A failure of left temporal cortex to specialize for language is an early emerging and fundamental property of autism. *Brain* 135, 949–960. doi: 10.1093/brain/awr364

Fein, D., Barton, M., Eigsti, I. M., Kelley, E., Naigles, L., Schultz, R. T., et al. (2013). Optimal outcome in individuals with a history of autism. *J. Child Psychol. Psychiatry* 54, 195–205. doi: 10.1111/jcpp.12037

Flagg, E. J., Cardy, J. E., Roberts, W., and Roberts, T. P. (2005). Language lateralization development in children with autism: insights from the late field magnetoencephalogram. *Neurosci. Lett.* 386, 82–87. doi: 10.1016/j.neulet.2005.05.037

Fransson, P., Skiold, B., Horsch, S., Nordell, A., Blennow, M., Lagercrantz, H., et al. (2007). Resting-state networks in the infant brain. *Proc. Natl. Acad. Sci. U.S.A.* 104, 15531–15536. doi: 10.1073/pnas.0704380104

Gaffrey, M. S., Kleinhans, N. M., Haist, F., Akshoomoff, N., Campbell, A., Courchesne, E., et al. (2007). A typical participation of visual cortex during word processing in autism: an fMRI study of semantic decision. *Neuropsychologia* 45, 1672–1684. doi: 10.1016/j.neuropsychologia.2007.01.008

Gervais, H., Belin, P., Boddaert, N., Leboyer, M., Coez, A., Sfaello, I., et al. (2004). Abnormal cortical voice processing in autism. *Nat. Neurosci.* 7, 801–802. doi: 10.1038/nn1291

Geschwind, D. H., and Levitt, P. (2007). Autism spectrum disorders: developmental disconnection syndromes. *Curr. Opin. Neurobiol.* 17, 103–111. doi: 10.1016/j.conb.2007.01.009

Geurts, H. M., and Embrechts, M. (2008). Language profiles in ASD, SLI, and ADHD. *J. Autism Dev. Disord.* 38, 1931–1943. doi: 10.1007/s10803-008-0587-1

Goldstein, M. H., King, A. P., and West, M. J. (2003). Social interaction shapes babbling: testing parallels between birdsong and speech. *Proc. Natl. Acad. Sci. U.S.A.* 100, 8030–8035. doi: 10.1073/pnas.1332441100

Grossmann, T., Oberecker, R., Koch, S. P., and Friederici, A. D. (2010). The developmental origins of voice processing in the human brain. *Neuron* 65, 852–858. doi: 10.1016/j.neuron.2010.03.001

Haesen, B., Boets, B., and Wagemans, J. (2011). A review of behavioural and electrophysiological studies on auditory processing and speech perception in autism spectrum disorders. *Res. Autism Spectr. Disord.* 5, 701–714. doi: 10.1016/j.rasd.2010.11.006

Haigh, S. M., Heeger, D. J., Dinstein, I., Minshew, N., and Behrmann, M. (2015). Cortical variability in the sensory-evoked response in autism. *J. Autism Dev. Disord.* 45, 1176–1190. doi: 10.1007/s10803-014-2276-6

Hazlett, H. C., Poe, M., Gerig, G., Smith, R. G., Provenzale, J., Ross, A., et al. (2005). Magnetic resonance imaging and head circumference study of brain size in autism: birth through age 2 years. *Arch. Gen. Psychiatry* 62, 1366–1376. doi: 10.1001/archpsyc.62.12.1366

Hazlett, H. C., Poe, M. D., Gerig, G., Styner, M., Chappell, C., Smith, R. G., et al. (2011). Early brain overgrowth in autism associated with an increase in cortical surface area before age 2 years. *Arch. Gen. Psychiatry* 68, 467–476. doi: 10.1001/archgenpsychiatry.2011.39

Herlihy, L., Knoch, K., Vibert, B., and Fein, D. (2015). Parents' first concerns about toddlers with autism spectrum disorder: effect of sibling status. *Autism* 19, 20–28. doi: 10.1177/1362361313509731

Herringshaw, A. J., Ammons, C. J., Deramus, T. P., and Kana, R. K. (2016). Hemispheric differences in language processing in autism spectrum disorders: a meta-analysis of neuroimaging studies. *Autism Res.* doi: 10.1002/aur.1599. [Epub ahead of print].

Hoppenbrouwers, M., Vandermosten, M., and Boets, B. (2014). Autism as a disconnection syndrome: a qualitative and quantitative review of diffusion tensor imaging studies. *Res. Autism Spectr. Disord.* 8, 387–412. doi: 10.1016/j.rasd.2013.12.018

Hudry, K., Leadbitter, K., Temple, K., Slonims, V., McConachie, H., Aldred, C., et al. (2010). Preschoolers with autism show greater impairment in receptive compared with expressive language abilities. *Int. J. Lang. Commun. Disord.* 45, 681–690. doi: 10.3109/13682820903461493

Itahashi, T., Yamada, T., Nakamura, M., Watanabe, H., Yamagata, B., Jimbo, D., et al. (2015). Linked alterations in gray and white matter morphology in adults with high-functioning autism spectrum disorder: a multimodal brain imaging study. *Neuroimage Clin.* 7, 155–169. doi: 10.1016/j.nicl.2014.11.019

Jones, E. J., Gliga, T., Bedford, R., Charman, T., and Johnson, M. H. (2014). Developmental pathways to autism: a review of prospective studies of infants at risk. *Neurosci. Biobehav. Rev.* 39, 1–33. doi: 10.1016/j.neubiorev.2013.12.001

Jones, W., and Klin, A. (2013). Attention to eyes is present but in decline in 2-6-month-old infants later diagnosed with autism. *Nature* 504, 427–431. doi: 10.1038/nature12715

Jou, R. J., Minshew, N. J., Keshavan, M. S., Vitale, M. P., and Hardan, A. Y. (2010). Enlarged right superior temporal gyrus in children and adolescents with autism. *Brain Res.* 1360, 205–212. doi: 10.1016/j.brainres.2010.09.005

Kanner, L. (1943). Autistic disturbances of affective contact. *Nervous Child* 2, 217–250.

Kasari, C., Brady, N., Lord, C., and Tager-Flusberg, H. (2013). Assessing the minimally verbal school-aged child with autism spectrum disorder. *Autism Res.* 6, 479–493. doi: 10.1002/aur.1334

Kleinhans, N. M., Müller, R. A., Cohen, D. N., and Courchesne, E. (2008). Atypical functional lateralization of language in autism spectrum disorders. *Brain Res.* 1221, 115–125. doi: 10.1016/j.brainres.2008.04.080

Klin, A. (1991). Young autistic children's listening preferences in regard to speech: a possible characterization of the symptom of social withdrawal. *J. Autism Dev. Disord.* 21, 29–42. doi: 10.1007/BF02206995

Klin, A. (1992). Listening preferences in regard to speech in four children with developmental disabilities. *J. Child Psychol. Psychiatry* 33, 763–769. doi: 10.1111/j.1469-7610.1992.tb00911.x

Klin, A., Lin, D. J., Gorrindo, P., Ramsay, G., and Jones, W. (2009). Two-year-olds with autism orient to non-social contingencies rather than biological motion. *Nature* 459, 257–261. doi: 10.1038/nature07868

Klintwall, L., Eldevik, S., and Eikeseth, S. (2013). Narrowing the gap: effects of intervention on developmental trajectories in autism. *Autism.* 19, 53–63. doi: 10.1177/1362361313510067

Knaus, T. A., Silver, A. M., Kennedy, M., Lindgren, K. A., Dominick, K. C., Siegel, J., et al. (2010). Language laterality in autism spectrum disorder and typical controls: a functional, volumetric, and diffusion tensor MRI study. *Brain Lang.* 112, 113–120. doi: 10.1016/j.bandl.2009.11.005

Knaus, T. A., Silver, A. M., Lindgren, K. A., Hadjikhani, N., and Tager-Flusberg, H. (2008). fMRI activation during a language task in adolescents with ASD. *J. Int. Neuropsychol. Soc.* 14, 967–979. doi: 10.1017/S1355617708081216

Koenig, T., Prichep, L., Lehmann, D., Sosa, P. V., Braeker, E., Kleinlogel, H., et al. (2002). Millisecond by millisecond, year by year: normative EEG microstates and developmental stages. *Neuroimage* 16, 41–48. doi: 10.1006/nimg.2002.1070

Kohls, G., Chevallier, C., Troiani, V., and Schultz, R. T. (2012). Social 'wanting' dysfunction in autism: neurobiological underpinnings and treatment implications. *J. Neurodev. Disord.* 4:10. doi: 10.1186/1866-1955-4-10

Kriegstein, K. V., and Giraud, A. L. (2004). Distinct functional substrates along the right superior temporal sulcus for the processing of voices. *Neuroimage* 22, 948–955. doi: 10.1016/j.neuroimage.2004.02.020

Kuhl, P. K. (2004). Early language acquisition: cracking the speech code. *Nat. Rev. Neurosci.* 5, 831–843. doi: 10.1038/nrn1533

Kuhl, P. K. (2010). Brain mechanisms in early language acquisition. *Neuron* 67, 713–727. doi: 10.1016/j.neuron.2010.08.038

Kuhl, P. K., Coffey-Corina, S., Padden, D., and Dawson, G. (2005). Links between social and linguistic processing of speech in preschool children with autism: behavioral and electrophysiological measures. *Dev. Sci.* 8, F1–F12. doi: 10.1111/j.1467-7687.2004.00384.x

Kuhl, P. K., Coffey-Corina, S., Padden, D., Munson, J., Estes, A., and Dawson, G. (2013). Brain responses to words in 2-year-olds with autism predict developmental outcomes at age 6. *PLoS ONE* 8:e64967. doi: 10.1371/journal.pone.0064967

Kuhl, P. K., Tsao, F. M., and Liu, H. M. (2003). Foreign-language experience in infancy: effects of short-term exposure and social interaction on phonetic learning. *Proc. Natl. Acad. Sci. U.S.A.* 100, 9096–9101. doi: 10.1073/pnas.1532872100

Kujala, T., Lepistö, T., and Näätänen, R. (2013). The neural basis of aberrant speech and audition in autism spectrum disorders. *Neurosci. Biobehav. Rev.* 37, 697–704. doi: 10.1016/j.neubiorev.2013.01.006

Lai, G., Pantazatos, S. P., Schneider, H., and Hirsch, J. (2012). Neural systems for speech and song in autism. *Brain* 135, 961–975. doi: 10.1093/brain/awr335

Lai, G., Schneider, H. D., Schwarzenberger, J. C., and Hirsch, J. (2011). Speech stimulation during functional MR imaging as a potential indicator of autism. *Radiology* 260, 521–530. doi: 10.1148/radiol.11101576

Lai, M. C., Lombardo, M. V., Ecker, C., Chakrabarti, B., Suckling, J., Bullmore, E. T., et al. (2015). Neuroanatomy of individual differences in language in adult males with autism. *Cereb. Cortex* 25, 3613–3628. doi: 10.1093/cercor/bhu211

Landa, R., and Garrett-Mayer, E. (2006). Development in infants with autism spectrum disorders: a prospective study. *J. Child Psychol. Psychiatry* 47, 629–638. doi: 10.1111/j.1469-7610.2006.01531.x

Lange, N., Travers, B. G., Bigler, E. D., Prigge, M. B., Froehlich, A. L., Nielsen, J. A., et al. (2015). Longitudinal volumetric brain changes in autism spectrum disorder ages 6-35 years. *Autism Res.* 8, 82–93. doi: 10.1002/aur.1427

Latinus, M., and Belin, P. (2011). Human voice perception. *Curr. Biol.* 21, R143–R145. doi: 10.1016/j.cub.2010.12.033

Lattner, S., Meyer, M. E., and Friederici, A. D. (2005). Voice perception: sex, pitch, and the right hemisphere. *Hum. Brain Mapp.* 24, 11–20. doi: 10.1002/hbm.20065

Lehmann, D., and Michel, C. M. (2011). EEG-defined functional microstates as basic building blocks of mental processes. *Clin. Neurophysiol.* 122, 1073–1074. doi: 10.1016/j.clinph.2010.11.003

Lenroot, R. K., and Yeung, P. K. (2013). Heterogeneity within autism spectrum disorders: what have we learned from neuroimaging studies? *Front. Hum. Neurosci.* 7:733. doi: 10.3389/fnhum.2013.00733

Lewis, J. D., Evans, A. C., Pruett, J. R., Botteron, K., Zwaigenbaum, L., Estes, A., et al. (2014). Network inefficiencies in autism spectrum disorder at 24 months. *Transl. Psychiatry* 4:e388. doi: 10.1038/tp.2014.24

Lindell, A. K., and Hudry, K. (2013). Atypicalities in cortical structure, handedness, and functional lateralization for language in autism spectrum disorders. *Neuropsychol. Rev.* 23, 257–270. doi: 10.1007/s11065-013-9234-5

Lloyd-Fox, S., Blasi, A., Mercure, E., Elwell, C. E., and Johnson, M. H. (2012). The emergence of cerebral specialization for the human voice over the first months of life. *Soc. Neurosci.* 7, 317–330. doi: 10.1080/17470919.2011.614696

Lombardo, M. V., Pierce, K., Eyler, L. T., Carter Barnes, C., Ahrens-Barbeau, C., Solso, S., et al. (2015). Different functional neural substrates for good and poor language outcome in autism. *Neuron* 86, 567–577. doi: 10.1016/j.neuron.2015.03.023

Lord, C., Bishop, S., and Anderson, D. (2015). Developmental trajectories as autism phenotypes. *Am. J. Med. Genet. C Semin. Med. Genet.* 169, 198–208. doi: 10.1002/ajmg.c.31440

Luyster, R. J., Kadlec, M. B., Carter, A., and Tager-Flusberg, H. (2008). Language assessment and development in toddlers with autism spectrum disorders. *J. Autism Dev. Disord.* 38, 1426–1438. doi: 10.1007/s10803-007-0510-1

Mandel, D. R., Jusczyk, P. W., and Pisoni, D. B. (1995). Infants recognition of the sound patterns of their own names. *Psychol. Sci.* 6, 314–317. doi: 10.1111/j.1467-9280.1995.tb00517.x

Marno, H., Farroni, T., Vidal Dos Santos, Y., Ekramnia, M., Nespor, M., and Mehler, J. (2015). Can you see what I am talking about? Human speech triggers referential expectation in four-month-old infants. *Sci. Rep.* 5:13594. doi: 10.1038/srep13594

McPartland, J. C., Coffman, M., and Pelphrey, K. A. (2011). Recent advances in understanding the neural bases of autism spectrum disorder. *Curr. Opin. Pediatr.* 23, 628–632. doi: 10.1097/MOP.0b013e32834cb9c9

Michel, C. M., and Murray, M. M. (2012). Towards the utilization of EEG as a brain imaging tool. *Neuroimage* 61, 371–385. doi: 10.1016/j.neuroimage.2011.12.039

Michel, C. M., Murray, M. M., Lantz, G., Gonzalez, S., Spinelli, L., and Grave De Peralta, R. (2004). EEG source imaging. *Clin. Neurophysiol.* 115, 2195–2222. doi: 10.1016/j.clinph.2004.06.001

Minagawa-Kawai, Y., Naoi, N., Kikuchi, N., Yamamoto, J., Nakamura, K., and Kojima, S. (2009). Cerebral laterality for phonemic and prosodic cue decoding in children with autism. *Neuroreport* 20, 1219–1224. doi: 10.1097/WNR.0b013e32832fa65f

Minagawa-Kawai, Y., Van Der Lely, H., Ramus, F., Sato, Y., Mazuka, R., and Dupoux, E. (2011). Optical brain imaging reveals general auditory and language-specific processing in early infant development. *Cereb. Cortex* 21, 254–261. doi: 10.1093/cercor/bhq082

Miron, O., Ari-Even Roth, D., Gabis, L. V., Henkin, Y., Shefer, S., Dinstein, I., et al. (2015). Prolonged auditory brainstem responses in infants with autism. *Autism Res.* 9, 689–695. doi: 10.1002/aur.1561

Mitchell, S., Brian, J., Zwaigenbaum, L., Roberts, W., Szatmari, P., Smith, I., et al. (2006). Early language and communication development of infants later diagnosed with autism spectrum disorder. *J. Dev. Behav. Pediatr.* 27, S69–S78. doi: 10.1097/00004703-200604002-00004

Mody, M., Manoach, D. S., Guenther, F. H., Kenet, T., Bruno, K. A., McDougle, C. J., et al. (2013). Speech and language in autism spectrum disorder: a view through the lens of behavior and brain imaging. *Neuropsychiatry* 3, 223–232. doi: 10.2217/npy.13.19

Murray, M. M., Brunet, D., and Michel, C. M. (2008). Topographic ERP analyses: a step-by-step tutorial review. *Brain Topogr.* 20, 249–264. doi: 10.1007/s10548-008-0054-5

Näätänen, R. (1995). The mismatch negativity: a powerful tool for cognitive neuroscience. *Ear Hear.* 16, 6–18. doi: 10.1097/00003446-199502000-00002

Näätänen, R. (2003). Mismatch negativity: clinical research and possible applications. *Int. J. Psychophysiol.* 48, 179–188. doi: 10.1016/S0167-8760(03)00053-9

Nadig, A. S., Ozonoff, S., Young, G. S., Rozga, A., Sigman, M., and Rogers, S. J. (2007). A prospective study of response to name in infants at risk for autism. *Arch. Pediatr. Adolesc. Med.* 161, 378–383. doi: 10.1001/archpedi.161.4.378

Norbury, C. F., Griffiths, H., and Nation, K. (2010). Sound before meaning: word learning in autistic disorders. *Neuropsychologia* 48, 4012–4019. doi: 10.1016/j.neuropsychologia.2010.10.015

Nordahl, C. W., Lange, N., Li, D. D., Barnett, L. A., Lee, A., Buonocore, M. H., et al. (2011). Brain enlargement is associated with regression in preschool-age boys with autism spectrum disorders. *Proc. Natl. Acad. Sci. U.S.A.* 108, 20195–20200. doi: 10.1073/pnas.1107560108

Nordahl, C. W., Mello, M., Shen, A. M., Shen, M. D., Vismara, L. A., Li, D., et al. (2016). Methods for acquiring MRI data in children with autism spectrum disorder and intellectual impairment without the use of sedation. *J. Neurodev. Disord.* 8, 20. doi: 10.1186/s11689-016-9154-9

Nordahl, C. W., Simon, T. J., Zierhut, C., Solomon, M., Rogers, S. J., and Amaral, D. G. (2008). Brief report: methods for acquiring structural MRI data in very young children with autism without the use of sedation. *J. Autism Dev. Disord.* 38, 1581–1590. doi: 10.1007/s10803-007-0514-x

Oner, P., Oner, O., and Munir, K. (2014). Three-item Direct Observation Screen (TIDOS) for autism spectrum disorder. *Autism* 18, 733–742. doi: 10.1177/1362361313487028

Ortiz-Mantilla, S., Choe, M. S., Flax, J., Grant, P. E., and Benasich, A. A. (2010). Associations between the size of the amygdala in infancy and language abilities during the preschool years in normally developing children. *Neuroimage* 49, 2791–2799. doi: 10.1016/j.neuroimage.2009.10.029

Osterling, J., and Dawson, G. (1994). Early recognition of children with autism: a study of first birthday home videotapes. *J. Autism Dev. Disord.* 24, 247–257. doi: 10.1007/BF02172225

Ozonoff, S., Young, G. S., Carter, A., Messinger, D., Yirmiya, N., Zwaigenbaum, L., et al. (2011). Recurrence risk for autism spectrum disorders: a baby siblings research consortium study. *Pediatrics* 128, E488–E495. doi: 10.1542/peds.2010-2825

Patten, E., Belardi, K., Baranek, G. T., Watson, L. R., Labban, J. D., and Oller, D. K. (2014). Vocal patterns in infants with autism spectrum disorder: canonical babbling status and vocalization frequency. *J. Autism Dev. Disord.* 44, 2413–2428. doi: 10.1007/s10803-014-2047-4

Paul, A., Sharda, M., Menon, S., Arora, I., Kansal, N., Arora, K., et al. (2015). The effect of sung speech on socio-communicative responsiveness in children with autism spectrum disorders. *Front. Hum. Neurosci.* 9:555. doi: 10.3389/fnhum.2015.00555

Paul, R., Fuerst, Y., Ramsay, G., Chawarska, K., and Klin, A. (2011). Out of the mouths of babes: vocal production in infant siblings of children with ASD. *J. Child Psychol. Psychiatry* 52, 588–598. doi: 10.1111/j.1469-7610.2010.02332.x

Pelphrey, K. A., Shultz, S., Hudac, C. M., and Vander Wyk, B. C. (2011). Research review: constraining heterogeneity: the social brain and its development in autism spectrum disorder. *J. Child Psychol. Psychiatry* 52, 631–644. doi: 10.1111/j.1469-7610.2010.02349.x

Pernet, C. R., McAleer, P., Latinus, M., Gorgolewski, K. J., Charest, I., Bestelmeyer, P. E., et al. (2015). The human voice areas: spatial organization and inter-individual variability in temporal and extra-temporal cortices. *Neuroimage* 119, 164–174. doi: 10.1016/j.neuroimage.2015.06.050

Pickles, A., Anderson, D. K., and Lord, C. (2014). Heterogeneity and plasticity in the development of language: a 17-year follow-up of children referred early for possible autism. *J. Child Psychol. Psychiatry* 55, 1354–1362. doi: 10.1111/jcpp.12269

Pittau, F., Megevand, P., Sheybani, L., Abela, E., Grouiller, F., Spinelli, L., et al. (2014). Mapping epileptic activity: sources or networks for the clinicians? *Front. Neurol.* 5:218. doi: 10.3389/fneur.2014.00218

Prigge, M. D., Bigler, E. D., Fletcher, P. T., Zielinski, B. A., Ravichandran, C., Anderson, J., et al. (2013). Longitudinal Heschl's gyrus growth during childhood and adolescence in typical development and autism. *Autism Res.* 6, 78–90. doi: 10.1002/aur.1265

Raschle, N., Zuk, J., Ortiz-Mantilla, S., Sliva, D. D., Franceschi, A., Grant, P. E., et al. (2012). Pediatric neuroimaging in early childhood and infancy: challenges and practical guidelines. *Ann. N.Y. Acad. Sci.* 1252, 43–50. doi: 10.1111/j.1749-6632.2012.06457.x

Raschle, N. M., Smith, S. A., Zuk, J., Dauvermann, M. R., Figuccio, M. J., and Gaab, N. (2014). Investigating the neural correlates of voice versus speech-sound directed information in pre-school children. *PLoS ONE* 9:e115549. doi: 10.1371/journal.pone.0115549

Redcay, E., and Courchesne, E. (2005). When is the brain enlarged in autism? A meta-analysis of all brain size reports. *Biol. Psychiatry* 58, 1–9. doi: 10.1016/j.biopsych.2005.03.026

Redcay, E., and Courchesne, E. (2008). Deviant functional magnetic resonance imaging patterns of brain activity to speech in 2-3-year-old children with autism spectrum disorder. *Biol. Psychiatry* 64, 589–598. doi: 10.1016/j.biopsych.2008.05.020

Righi, G., Tierney, A. L., Tager-Flusberg, H., and Nelson, C. A. (2014). Functional connectivity in the first year of life in infants at risk for autism spectrum disorder: an EEG study. *PLoS ONE* 9:e105176. doi: 10.1371/journal.pone.0105176

Rihs, T. A., Tomescu, M. I., Britz, J., Rochas, V., Custo, A., Schneider, M., et al. (2013). Altered auditory processing in frontal and left temporal cortex in 22q11.2 deletion syndrome: a group at high genetic risk for schizophrenia. *Psychiatry Res.* 212, 141–149. doi: 10.1016/j.pscychresns.2012.09.002

Robinson, E. B., Neale, B. M., and Hyman, S. E. (2015). Genetic research in autism spectrum disorders. *Curr. Opin. Pediatr.* 27, 685–691. doi: 10.1097/MOP.0000000000000278

Rogers, S. J. (2009). What are infant siblings teaching us about autism in infancy? *Autism Res.* 2, 125–137. doi: 10.1002/aur.81

Schaer, M., Franchini, M., and Eliez, S. (2014). Latest findings in autism research. *Swiss Arch. Neurol. Psychiatry* 165, 277–289.

Schumann, C. M., Bloss, C. S., Barnes, C. C., Wideman, G. M., Carper, R. A., Akshoomoff, N., et al. (2010). Longitudinal magnetic resonance imaging study of cortical development through early childhood in autism. *J. Neurosci.* 30, 4419–4427. doi: 10.1523/JNEUROSCI.5714-09.2010

Seery, A., Tager-Flusberg, H., and Nelson, C. A. (2014). Event-related potentials to repeated speech in 9-month-old infants at risk for autism spectrum disorder. *J. Neurodev. Disord.* 6:43. doi: 10.1186/1866-1955-6-43

Seery, A. M., Vogel-Farley, V., Tager-Flusberg, H., and Nelson, C. A. (2013). Atypical lateralization of ERP response to native and non-native speech in infants at risk for autism spectrum disorder. *Dev. Cogn. Neurosci.* 5, 10–24. doi: 10.1016/j.dcn.2012.11.007

Senju, A., and Johnson, M. H. (2009). Atypical eye contact in autism: models, mechanisms and development. *Neurosci. Biobehav. Rev.* 33, 1204–1214. doi: 10.1016/j.neubiorev.2009.06.001

Sharda, M., Midha, R., Malik, S., Mukerji, S., and Singh, N. C. (2015). Fronto-temporal connectivity is preserved during sung but not spoken word listening, across the autism spectrum. *Autism Res.* 8, 174–186. doi: 10.1002/aur.1437

Shen, M. D., Nordahl, C. W., Young, G. S., Wootton-Gorges, S. L., Lee, A., Liston, S. E., et al. (2013). Early brain enlargement and elevated extra-axial fluid in infants who develop autism spectrum disorder. *Brain* 136, 2825–2835. doi: 10.1093/brain/awt166

Simms, M. D., and Jin, X. M. (2015). Autism, language disorder, and social (pragmatic) communication disorder: DSM-V and differential diagnoses. *Pediatr Rev.* 36, 355–362. doi: 10.1542/pir.36-8-355

Sparks, B. F., Friedman, S. D., Shaw, D. W., Aylward, E. H., Echelard, D., Artru, A. A., et al. (2002). Brain structural abnormalities in young children with autism spectrum disorder. *Neurology* 59, 184–192. doi: 10.1212/WNL.59.2.184

Stenberg, N., Bresnahan, M., Gunnes, N., Hirtz, D., Hornig, M., Lie, K. K., et al. (2014). Identifying children with autism spectrum disorder at 18 months in a general population sample. *Paediatr. Perinat. Epidemiol.* 28, 255–262. doi: 10.1111/ppe.12114

Stoner, R., Chow, M. L., Boyle, M. P., Sunkin, S. M., Mouton, P. R., Roy, S., et al. (2014). Patches of disorganization in the neocortex of children with autism. *N. Engl. J. Med.* 370, 1209–1219. doi: 10.1056/NEJMoa1307491

Tager-Flusberg, H., and Kasari, C. (2013). Minimally verbal school-aged children with autism spectrum disorder: the neglected end of the spectrum. *Autism Res.* 6, 468–478. doi: 10.1002/aur.1329

Tager-Flusberg, H., Rogers, S., Cooper, J., Landa, R., Lord, C., Paul, R., et al. (2009). Defining spoken language benchmarks and selecting measures of expressive language development for young children with autism spectrum disorders. *J. Speech Lang. Hear. Res.* 52, 643–652. doi: 10.1044/1092-4388(2009/08-0136)

Tincoff, R., and Jusczyk, P. W. (1999). Some beginnings of word comprehension in 6-month-olds. *Psychol. Sci.* 10, 172–175. doi: 10.1111/1467-9280.00127

Tincoff, R., and Jusczyk, P. W. (2012). Six-month-olds comprehend words that refer to parts of the body. *Infancy* 17, 432–444. doi: 10.1111/j.1532-7078.2011.00084.x

Tomescu, M. I., Rihs, T. A., Becker, R., Britz, J., Custo, A., Grouiller, F., et al. (2014). Deviant dynamics of EEG resting state pattern in 22q11.2 deletion syndrome adolescents: a vulnerability marker of schizophrenia? *Schizophr. Res.* 157, 175–181. doi: 10.1016/j.schres.2014.05.036

Turner, M. (1999). Annotation: repetitive behaviour in autism: a review of psychological research. *J. Child Psychol. Psychiatry* 40, 839–849. doi: 10.1111/1469-7610.00502

Viding, E., and Blakemore, S. J. (2007). Endophenotype approach to developmental psychopathology: implications for autism research. *Behav. Genet.* 37, 51–60. doi: 10.1007/s10519-006-9105-4

von Kriegstein, K., Eger, E., Kleinschmidt, A., and Giraud, A. L. (2003). Modulation of neural responses to speech by directing attention to voices or verbal content. *Brain Res. Cogn. Brain Res.* 17, 48–55. doi: 10.1016/S0926-6410(03)00079-X

Watt, N., Wetherby, A. M., Barber, A., and Morgan, L. (2008). Repetitive and stereotyped behaviors in children with autism spectrum disorders in the second year of life. *J. Autism Dev. Disord.* 38, 1518–1533. doi: 10.1007/s10803-007-0532-8

Weinstein, M., Ben-Sira, L., Levy, Y., Zachor, D. A., Ben Itzhak, E., Artzi, M., et al. (2011). Abnormal white matter integrity in young children with autism. *Hum. Brain Mapp.* 32, 534–543. doi: 10.1002/hbm.21042

Wetherby, A. M., Woods, J., Allen, L., Cleary, J., Dickinson, H., and Lord, C. (2004). Early indicators of autism spectrum disorders in the second year of life. *J. Autism Dev. Disord.* 34, 473–493. doi: 10.1007/s10803-004-2544-y

Wolff, J. J., Gu, H., Gerig, G., Elison, J. T., Styner, M., Gouttard, S., et al. (2012). Differences in white matter fiber tract development present from 6 to 24 months in infants with autism. *Am. J. Psychiatry* 169, 589–600. doi: 10.1176/appi.ajp.2011.11091447

Xiao, Z., Qiu, T., Ke, X., Xiao, X., Xiao, T., Liang, F., et al. (2014). Autism spectrum disorder as early neurodevelopmental disorder: evidence from the brain imaging abnormalities in 2-3 years old toddlers. *J. Autism Dev. Disord.* 44, 1633–1640. doi: 10.1007/s10803-014-2033-x

Yirmiya, N., Gamliel, I., Pilowsky, T., Feldman, R., Baron-Cohen, S., and Sigman, M. (2006). The development of siblings of children with autism at 4 and 14 months: social engagement, communication, and cognition. *J. Child Psychol. Psychiatry* 47, 511–523. doi: 10.1111/j.1469-7610.2005.01528.x

Zhubi, A., Cook, E. H., Guidotti, A., and Grayson, D. R. (2014). Epigenetic mechanisms in autism spectrum disorder. *Int. Rev. Neurobiol.* 115, 203–244. doi: 10.1016/B978-0-12-801311-3.00006-8

Zwaigenbaum, L., Bryson, S., and Garon, N. (2013). Early identification of autism spectrum disorders. *Behav. Brain Res.* 251, 133–146. doi: 10.1016/j.bbr.2013.04.004

Zwaigenbaum, L., Bryson, S., Lord, C., Rogers, S., Carter, A., Carver, L., et al. (2009). Clinical assessment and management of toddlers with suspected autism spectrum disorder: insights from studies of high-risk infants. *Pediatrics* 123, 1383–1391. doi: 10.1542/peds.2008-1606

Conflict of Interest Statement: The authors declare that the research was conducted in the absence of any commercial or financial relationships that could be construed as a potential conflict of interest.

frontiers in Neuroscience

PERSPECTIVE
published: 31 March 2016
doi: 10.3389/fnins.2016.00139

Rehabilitative Interventions and Brain Plasticity in Autism Spectrum Disorders: Focus on MRI-Based Studies

Sara Calderoni[1], Lucia Billeci[2], Antonio Narzisi[1], Paolo Brambilla[3,4], Alessandra Retico[5] and Filippo Muratori[1,2]*

[1] IRCCS Stella Maris Foundation, Pisa, Italy, [2] Department of Clinical and Experimental Medicine, University of Pisa, Pisa, Italy, [3] Department of Neurosciences and Mental Health, Fondazione IRCCS Ca' Granda Ospedale Maggiore Policlinico, University of Milan, Milan, Italy, [4] Department of Psychiatry and Behavioral Sciences, University of Texas Health Science Center at Houston, Houston, TX, USA, [5] Pisa Section of National Institute of Nuclear Physics, Pisa, Italy

Clinical and research evidence supports the efficacy of rehabilitative intervention for improving targeted skills or global outcomes in individuals with autism spectrum disorder (ASD). However, putative mechanisms of structural and functional brain changes are poorly understood. This review aims to investigate the research literature on the neural circuit modifications after non-pharmacological intervention. For this purpose, longitudinal studies that used magnetic resonance imaging (MRI)-based techniques at the start and at the end of the trial to evaluate the neural effects of rehabilitative treatment in subjects with ASD were identified. The six included studies involved a limited number of patients in the active group (from 2 to 16), and differed by acquisition method (task-related and resting-state functional MRI) as well as by functional MRI tasks. Overall, the results produced by the selected investigations demonstrated brain plasticity during the treatment interval that results in an activation/functional connectivity more similar to those of subjects with typical development (TD). Repeated MRI evaluation may represent a promising tool for the detection of neural changes in response to treatment in patients with ASD. However, large-scale randomized controlled trials after standardized rehabilitative intervention are required before translating these preliminary results into clinical use.

Keywords: autism spectrum disorder, brain plasticity, magnetic resonance imaging, treatment effects, outcome

OPEN ACCESS

Edited by:
Remo Job,
University of Trento, Italy

Reviewed by:
Rajshekhar Bipeta,
Gandhi Medical College and Hospital, India
Stephanie Ameis,
University of Toronto, Canada

****Correspondence:***
Sara Calderoni
sara.calderoni@fsm.unipi.it

Specialty section:
This article was submitted to Child and Adolescent Psychiatry, a section of the journal Frontiers in Neuroscience

Received: *25 November 2015*
Accepted: *18 March 2016*
Published: *31 March 2016*

Citation:
Calderoni S, Billeci L, Narzisi A, Brambilla P, Retico A and Muratori F (2016) Rehabilitative Interventions and Brain Plasticity in Autism Spectrum Disorders: Focus on MRI-Based Studies. Front. Neurosci. 10:139. doi: 10.3389/fnins.2016.00139

INTRODUCTION

Autism spectrum disorders (ASD) are a heterogeneous group of neurodevelopmental conditions characterized by persistent deficits in social communication and interaction across multiple contexts, in addition to restricted, repetitive patterns of behavior, interests, or activities, all of which significantly impact on adaptive functioning (American Psychiatric Association, 2013). Although the exact etiology of ASD remains elusive, a combination of genetic and environmental factors during critical periods of development has been implicated (Hallmayer et al., 2011), possibly leading to altered brain architecture beginning early in life (Wolff and Piven, 2013; Conti et al., 2015), or even in prenatal developmental stages (Stoner et al., 2014). Specifically, brain underpinnings revealed by magnetic resonance imaging (MRI) include an early altered developmental trajectory of global and regional brain structures (see Chen et al., 2011 and Bellani et al., 2013 for reviews

of structural MRI studies in ASD), with an atypical growing of white matter tracts (see Ameis and Catani, 2015 for a review of diffusion tensor imaging -DTI- studies in ASD), altered task-dependent cerebral response (see Dickstein et al., 2013 for a review of functional MRI -fMRI- studies in ASD), and abnormal neuronal activity in the absence of stimulation (see Uddin et al., 2013 for a review of resting-state fMRI -rs-fMRI- studies in ASD). Notably, abnormalities in brain correlates of ASD are likely to be influenced by study design characteristics and a wide range of clinical and demographic features (Lenroot and Yeung, 2013). In particular, an age-dependency of brain volume differences between ASD patients and controls with typical development (TD) has been repeatedly detected: in fact, while an increased total brain volume is noted in infants and toddlers with ASD compared to TD, an absence of group differences later in childhood is frequently reported (Courchesne et al., 2007; Amaral et al., 2008). The deviation from the normal brain growth trajectory described in young subjects with ASD can lead to atypical organization of structural and functional cerebral connectivity (Lewis and Elman, 2008).Indeed, an excess of short-distance with diminished long-range connectivity has been proposed (Just et al., 2007), producing a brain profile ineffective for processing and integrating "higher-order" information that ultimately leads to several of the most common ASD neuropsychological characteristics (Wass, 2011; Narzisi et al., 2013). In this framework, a rehabilitative intervention for patients with ASD is considered a treatment able to enhance neuroplasticity (Dawson, 2008), i.e., the capacity of cerebral neurons and neural circuits to structurally and functionally change in response to external stimuli, environmental modifications, or injuries (Pascual-Leone et al., 2005). However, neural substrates underlying observed clinical improvement after early interventions are not yet fully elucidate (Sullivan et al., 2014). In this view, the introduction of advanced MRI techniques, such as fMRI, rs-fMRI, and DTI, have been recently used to investigate brain plasticity by monitoring the effects of rehabilitative therapy in ASD patients. Specifically, longitudinal studies that include pre- and post-treatment MRI acquisition have provided new insights on the neural mechanisms targeted in rehabilitative therapy and, in addition, an objective measure of response to treatment.

Therefore, the goal of the current review is to summarize the existing MRI-based evidences of functional and structural plasticity induced by rehabilitation therapy in patients with ASD. To this aim, longitudinal studies that use MRI-based techniques pre- and post- rehabilitative intervention to explore the impact of treatment on neural substrates in ASD patients were analyzed. To our knowledge, no review article exists addressing the question of whether and how non-psychopharmacological interventions shape the brain of patients with ASD.

METHODS

Studies in which functional or structural MRI was used to evaluate rehabilitative treatment response in patients with ASD were eligible for inclusion. Relevant articles were identified from searches in two electronic databases (Pubmed and Scopus). Search terms included the following: "autis*," "neuroimaging," "MRI," "magnetic resonance," "fMRI," "rs-fMRI," "DTI," "diffusion tensor," "training," "treatment," and "rehabilitation" both in isolation and in combination. We further limited the results to "English" and "Humans." No article type limitations or time period restrictions were applied, and the latest search was undertaken in September 2015. We identified longitudinal studies that examined MRI-based differences in brain structure and function between pre- and post- rehabilitative treatment in individuals with ASD. This paper reports a selective narrative description of the identified investigations.

RESULTS

We found six studies published between 2006 and 2015 that investigated whether rehabilitation strategies enhance brain plasticity, as evaluated by either rs-fMRI ($n = 1$) (Murdaugh et al., 2015), or task-related fMRI ($n = 5$; Bölte et al., 2006, 2015; Voos et al., 2013; Ventola et al., 2015; Murdaugh et al., 2016). A list of these studies and their characteristics are detailed in **Table 1**.

The first attempt to demonstrate the presence of brain plasticity in ASD following a specific rehabilitation treatment was performed by Bölte et al. (2006) who selected (with randomization) 10 adult patients. Of them, five received a 5-weeks computer-based facial affect training program (2-h per week), while the remaining five ASD patients did not undergo any special training. The effects of training program have been demonstrated on both behavioral and neurobiological level.

However, an atypical pattern of increased activation in the right superior parietal lobule post-training in ASD subjects, rather than the activation of the fusiform face area usually found in participants with TD, was detected. Therefore, the authors concluded that the intervention group learned to recognize emotions by using compensatory mechanisms involving the recruitment of different brain regions.

More recently, a similar study was conducted by the same group (Bölte et al., 2015) to explore the neural effects of the same computer based training (1 h/week for 8 weeks) aimed at improving facial affect recognition. The investigation focused on 32 adolescent with high-functioning ASD: half of them received the specific training plus standard care, whereas the other half received standard care only. Each ASD group was scanned twice, pre and post-training, using task-related fMRI consisting of facial affect recognition. A control group of 25 subjects with TD was also enrolled to compare the behavioral assessment and the brain activations to that of patients with ASD at baseline. As expected, reduced ability to recognize facial expressions coupled with reduced social brain activity was found in individuals with ASD. After training was completed, a relevant improvement in facial recognition characterized the active group and was associated with an increased activity in the social brain areas.

To investigate the possibility that early rehabilitative treatment induces activation changes of brain regions involved in social perception in young children with ASD, Voos et al.

TABLE 1 | Summary of studies utilizing MRI pre- and post-rehabilitative treatment of ASD patients.

	Bölte et al., 2006	Voos et al., 2013	Ventola et al., 2015	Murdaugh et al., 2015	Bölte et al., 2015	Murdaugh et al., 2016
Study type	Randomized cross-over trial	Case series	Uncontrolled pre-post trial	Randomized cross-over trial	Non-randomized parallel group trial	Randomized cross-over trial
Center	Frankfurt University, Germany	Yale University, USA	Yale University, USA	University of Alabama at Birmingham, USA	Frankfurt University, Germany	University of Alabama at Birmingham, USA
Number of ASD patients in the active group	5 males	2 (1 male and 1 female)	10 (8 males)	16 (12 males)	16 males	13 (11 males)
Controls	5 ASD males	No	5 TD (2 males)	15 ASD (12 males) and 22 TD (16 males)	16 ASD (14 males) and 25 TD (21 males)	13 ASD (10 males) and 19 TD (14 males)
Mean age of ASD patients	29.4 years	∼5 years	∼5 years	10.3 years	19.3 years	10.9 years
ID in ASD patients	No	No	No	No	No	No
MRI technique	fMRI (facial affect recognition task)	fMRI (social perception task)	fMRI (social perception task)	rs-fMRI	fMRI (facial affect recognition task)	fMRI (sentence comprehension task) and rs-fMRI
Type of treatment	Computer-based facial affect recognition training	PRT	PRT	Reading intervention	Computer-based facial affect recognition training	Reading intervention
Duration of treatment	2 h per week for 5 weeks	8–10 h per week for 4 months	7 h per week for 16 weeks	20 h per week for 10 weeks	1 h per week for 8 weeks	20 h per week for 10 weeks
Clinical outcome(s) in the active group	Improvements in facial affect recognition	Improvement on ADOS, CELF-4, and Vineland-II scores	Improvement on SRS-2 and ADOS scores	Improvement in reading comprehension, as measured by the GORT-4 Comprehension subtest	Improvements in facial affect recognition	Improvement in reading comprehension, as measured by the GORT-4 Comprehension subtest
MRI outcome(s) in the active group	Increased activation in the R superior parietal lobule and maintained activation in the R medial occipital gyrus	Different increased activation in the two patients: L dorsolateral prefrontal cortex and L fusiform gyrus in one subject, R posterior superior temporal sulcus, L ventrolateral prefrontal cortex and bilateral fusiform gyri in the other patient	5 ASD patients showed significant increased activation in R posterior superior temporal sulcus, ventral striatum, and putamen; 5 ASD patients showed significant decreased activation in R posterior superior temporal sulcus, thalamus, amygdala, and hippocampus	Enhanced connectivity of Broca's area with R middle frontal gyrus, R superior temporal gyrus, L supramarginal gyrus, and R caudate; reduced connectivity of Broca's area with R middle occipital gyrus and R posterior cingulate cortex	Increased activation in amygdala, fusiform gyrus, and temporal pole bilaterally, medial prefrontal cortex, and L posterior superior temporal sulcus	Increased activation in brain regions underlying language and visuospatial processing, bilateral insula, R postcentral gyrus, and compensatory recruitment of R-hemisphere and subcortical regions
						Increased functional connectivity between L middle temporal gyrus and L frontal regions
					Enhanced connectivity of Wernicke's area with R anterior cingulate, L middle orbital gyrus, bilateral inferior frontal gyrus, R middle frontal gyrus, R middle cingulate, R precentral gyrus	
Follow-up period	No	No	No	No	No	No

ASD, Autism Spectrum Disorders; MRI, Magnetic Resonance Imaging; DTI, Diffusion Tensor Imaging; fMRI, functional Magnetic Resonance Imaging; rs-fMRI, resting-state functional Magnetic Resonance Imaging; ID, intellectual disability; TD, controls with typical developing; PRT, Pivotal Response Treatment; CELF-4, Clinical Evaluation of Language Fundamentals—Fourth Edition; ADOS, Autism Diagnostic Observation Schedule; SRS-2, Social Responsiveness Scale-Second Edition; GORT-4, Gray Oral Reading Tests-4th Edition; R, right; L, left.

(2013) included two ASD preschoolers to receive 8–10 h per week for 4 months of Pivotal Response Treatment (PRT), a well-known empirically validated behavioral treatment for children with ASD (Koegel et al., 1987). After rehabilitation, significant behavioral improvements in core ASD deficits, adaptive skills, and language were signaled and, at the neural level, a modification in the processing of biological motion. Interestingly, the effects of the same treatment on brain activation are different in the two children, in line with the heterogeneity of the response to therapy in the ASD condition (Kim et al., 2015).

The same group performed a subsequent work based on an enlarged sample size of 10 preschoolers with ASD (Ventola et al., 2015). Before treatment, two groups of ASD children could be distinguished based on their activation profiles–reduced or increased- in posterior superior temporal sulcus (pSTS) in comparison with TD controls. Following a 16-week PRT treatment (7-h per week) a significant improvement of clinical ASD manifestations emerged, coupled with an activation in pSTS more similar to that of TD children. Therefore, treatment modifications are reached through two different neural modalities: a decrease in activation following treatment for ASD subjects who exhibited hyper-activation in the pSTS at baseline and *vice-versa*.

A randomized clinical trial (Murdaugh et al., 2015) was designed to explore modifications in functional connectivity after the intensive reading intervention "Visualizing and Verbalizing for Language Comprehension and Thinking" (Lindamood and Bell, 1997) in children with ASD. A total of 31 ASD patients were randomized either to a 10-week reading intervention (active group) or to receive the same intervention after the two imaging sessions were completed (wait-list control group). An additional control group of TD children served as a baseline comparison for brain activation and did not participate in the intervention protocol. Rs-fMRI revealed that after the training the active group had an increased connectivity using Broca's and Wernicke's area as seeding points. In order to verify whether functional connectivity changes in the active group were specifically related to the targeted training, a comparison between post-intervention connectivity in active and control ASD participants was conducted. After rehabilitation, increased rs-fMRI within the reading network was found in the active group, as well as an additional recruitment of frontal regions (left superior frontal gyrus and middle frontal gyrus), interpreted as compensatory mechanisms for language comprehension.

Some subjects originally enrolled in this latter study also underwent fMRI (Murdaugh et al., 2016), in order to investigate changes in brain activation following the reading intervention (Lindamood and Bell, 1997). Pre- and post-training task-related fMRI (sentence comprehension) revealed increased activation in visual and posterior language regions, bilateral insula and right postcentral gyrus, with an additional recruitment of right-hemisphere and subcortical regions as possible compensatory mechanisms for language comprehension. Moreover, an increased functional connectivity between left middle temporal gyrus and left frontal regions has been found after training in the active group. Intriguingly, the intervention-induced brain modifications positively correlated with the improvements in individual reading comprehension. Compared to ASD wait-list control group at the second imaging session, patients in the active group showed an increased activation in some areas of frontal, parietal, and temporal cortices.

DISCUSSION

Designing studies able to measure neural change in response to therapy is thought to be an important goal for autism research (McPartland and Pelphrey, 2012). According to this view, the current review investigated studies that applied MRI-based neuroimaging techniques pre- and post-rehabilitative treatment in ASD. Results from the six included investigations (Bölte et al., 2006, 2015; Voos et al., 2013; Murdaugh et al., 2015, 2016; Ventola et al., 2015) suggested that training-induced behavioral changes were accompanied by significant modifications in neural activity and/or functional connectivity that varied as a function of the specific training intervention. Preliminary evidence suggests that early intervention can mitigate the severity of core and associated features of autism (Warren et al., 2011), improve the long-term outcome of treated patients (Estes et al., 2015), and even reverse some of the ASD symptoms (Rogers et al., 2014). These behavioral improvements are supposed to result from changes in brain structure and function that are particularly achievable in critical period plasticity in early life. At these specific time windows, environmental stimuli most potently shape cortical brain circuitries responsible for the acquisition of different types of skills and abilities (Bardin, 2012). However, results from the studies included in this review reflect that brain plasticity, also in ASD patients, is not limited to early developmental stage (Voos et al., 2013; Ventola et al., 2015), but includes also the school-age period (Murdaugh et al., 2015, 2016), and adulthood (Bölte et al., 2006, 2015).

Notably, the six included studies pertained to three research group, each of whom performed two investigations to evaluate the effects of a specific rehabilitative treatment. In this context, rehabilitation treatments received by patients with ASD are highly heterogeneous in terms of targeted impairments. In particular, the group coordinated by Ventola focused on the neural effects of a comprehensive intervention program specifically developed to target the core social and communication deficits of children with ASD (Voos et al., 2013; Ventola et al., 2015); Bölte and colleagues utilized a computer-based program to target specific impairment in facial affect recognition (Bölte et al., 2006, 2015), while Murdaugh et al. administered a protocol to improve reading comprehension, an ancillary deficit in ASD individuals (Murdaugh et al., 2015, 2016).

In spite of the encouraging results on behavioral and brain plasticity, the studies examined in this review suffer from several drawbacks. In fact, reports generally comprised of a limited number of subjects (ranging from 2 to 16 ASD individuals in the active group), and the relatively small sample size makes it difficult to homogeneously subgroup ASD patients based on their clinical profile (e.g., level of intelligence quotient and language, core ASD symptom severity, adaptive functioning,

psychiatric comorbidities). Therefore, it is difficult to identify baseline clinical characteristics that influence behavioral and brain outcome of examined patients. Moreover, the lack of MRI follow-up data after the second scan hampered testing for stability of brain modifications obtained following rehabilitative treatment. In fact, it remains to investigate whether such improvements in brain functions are sustained without further intervention or whether maintenance training is necessary.

In addition, the studies included in the current review had different design. Two investigations (Voos et al., 2013; Ventola et al., 2015) lacked of a non-active control group of ASD subjects, whereas the others included as control group subjects in the waitlist (Bölte et al., 2006; Murdaugh et al., 2015, 2016), or patients receiving standard care only (Bölte et al., 2015). The presence of a non-active control group of ASD individuals is essential to discern whether an hypothesized biomarker for the prediction of treatment response is really predictive of response to a specific intervention, or rather is predictive of prognosis, independent from the type of rehabilitative treatment or even in the absence of it. Four studies included TD controls who underwent one MRI session (Bölte et al., 2015; Murdaugh et al., 2015, 2016; Ventola et al., 2015) in order to compare brain profiles of ASD patients and controls at baseline. Unfortunately, no study included MRI measures of TD subjects after the treatment under investigation: the lack of these data do not allow to provide evidence that neural changes are ascribable to effects of treatment rather than to normal brain maturation.

Despite their heterogeneity, all the six included studies reported significant modifications in task-related brain activation or in functional connectivity following rehabilitative intervention: crucially, the absence of negative or inconclusive results suggests the risk of publication bias. Instead, it could be useful the clinical and neural characterization of "non-responders" to a specific rehabilitative treatment in order to redirect these patients toward different intervention strategies.

Of particular interest, participants in these studies are generally highly selected individuals (e.g., exclusion of younger patients, and/or subjects with intellectual disability), who differ from patients seen in the clinical practice. Even if this choice is surely motivated by the necessity of patient compliance with the MRI examination (capacity of lying still in a confined space for a long time, as well as of tolerating the acoustic noise and of understanding task instructions), it limited information about brain plasticity in the full range of the autistic spectrum. Future naturalistic studies in larger samples could contribute to identifying biomarkers sensitive to rehabilitative treatment in the conventional clinical population. In this context, the use of sleep MRI (Pierce, 2011), and of task-free MRI techniques (DTI, rs-fMRI) would aid inclusion of non-collaborative ASD patients.

Future Directions

Prognostic factors of effective rehabilitative intervention in ASD are to date poorly clarified and generally based on patient's clinical characteristics and family profile only (Vivanti et al., 2014). The inclusion of MRI-based measures pre- and post-treatment will be crucial for understanding the neural mechanisms underlying different patient outcome. In other words, specific brain regions/network as putative biomarkers for treatment response would be identified, contributing to the knowledge on "what works for whom and why," and thus paving the way for the individualization of treatment in ASD. In order to overcome this limitation, future randomized control trials should incorporate pre and post-treatment neuroimaging protocols and compare the effects of distinct therapeutic treatments on patient's baseline neural biomarker.

Future investigations would also benefit from machine learning classification techniques to predict response to rehabilitative treatment at an individual level. In these studies, subjects are split into responders and non-responders after treatment, and machine-learning techniques are used to allocate patients to either category based on their pretreatment brain profile. However, the accuracy of these methods is currently not sufficiently satisfactory to suggest their use in clinical practice (Retico et al., 2014; Wolfers et al., 2015).

Finally, it will be crucial the use of multimodal neuroimaging techniques for detecting brain change between baseline and post-training in ASD. In this perspective, some recent studies have investigated connectivity in ASD using simultaneous structural -DTI- and functional -fcMRI- methods (Kana et al., 2012; Delmonte et al., 2013; Deshpande et al., 2013; Mueller et al., 2013; Nair et al., 2013): the integration of these data with neurophysiological approaches (electroencephalography–EEG- and magnetoencephalography–MEG-) may significantly enhance their temporal resolution. Moreover, the combination of both structural (MRI/DTI) and functional (fMRI/EEG) neuroimaging techniques could provide new insights on the timecourse by which the neural changes occur after rehabilitation: preliminary results on healthy older adults suggest that functional change may precede structural and cognitive change (Lampit et al., 2015), but the temporal dynamics of training-induced neural modifications have not been investigated yet in ASD subjects. In this perspective, the detection of functional changes could suggest that the rehabilitative intervention is effective, even if clinical modifications are not yet perceptible in the ASD patient. Thus, it would be possible to prevent dropout from a potentially beneficial intervention and consequently to reduce waste of resources as well as of valuable time for improving ASD prognosis.

AUTHOR CONTRIBUTIONS

SC wrote the paper with contributions from LB, AN, PB, AR, and FM. All authors read and approved the final manuscript.

ACKNOWLEDGMENTS

This work was *partly* supported by grant from the IRCCS Stella Maris Foundation (Ricerca Corrente, and the "5 × 1000" voluntary contributions, Italian Ministry of Health to FM). SC and AR were partly supported by the Italian Ministry of Health and by Tuscany Region with the grant (GR-2010-2317873). PB was partly supported by the Italian Ministry of Health (GR-2010-2316745), and by the BIAL Foundation to Dr. Brambilla (Fellowship #262/12).

REFERENCES

Amaral, D. G., Schumann, C. M., and Nordahl, C. W. (2008). Neuroanatomy of autism. *Trends Neurosci.* 31, 137–145. doi: 10.1016/j.tins.2007.12.005

Ameis, S. H., and Catani, M. (2015). Altered white matter connectivity as a neural substrate for social impairment in Autism Spectrum Disorder. *Cortex* 62, 158–181. doi: 10.1016/j.cortex.2014.10.014

American Psychiatric Association (2013). *Diagnostic and Statistical Manual of Mental Disorders (DSM-5), 5th Edn.* Washington, DC: American Psychiatric Publishing.

Bardin, J. (2012). Neurodevelopment: unlocking the brain. *Nature* 487, 24–26. doi: 10.1038/487024a

Bellani, M., Calderoni, S., Muratori, F., and Brambilla, P. (2013). Brain anatomy of autism spectrum disorders II. Focus on amygdala. *Epidemiol. Psychiatr. Sci.* 22, 309–312. doi: 10.1017/S2045796013000346

Bölte, S., Ciaramidaro, A., Schlitt, S., Hainz, D., Kliemann, D., Beyer, A., et al. (2015). Training-induced plasticity of the social brain in autism spectrum disorder. *Br. J. Psychiatry* 207, 149–157. doi: 10.1192/bjp.bp.113.143784

Bölte, S., Hubl, D., Feineis-Matthews, S., Prvulovic, D., Dierks, T., and Poustka, F. (2006). Facial affect recognition training in autism: can we animate the fusiform gyrus? *Behav. Neurosci.* 120, 211–216. doi: 10.1037/0735-7044.120.1.211

Chen, R., Jiao, Y., and Herskovits, E. H. (2011). Structural MRI in autism spectrum disorder. *Pediatr. Res.* 69, 63R–68R. doi: 10.1203/PDR.0b013e318212c2b3

Conti, E., Calderoni, S., Marchi, V., Muratori, F., Cioni, G., and Guzzetta, A. (2015). The first 1000 days of the autistic brain: a systematic review of diffusion imaging studies. *Front. Hum. Neurosci.* 9:159. doi: 10.3389/fnhum.2015.00159

Courchesne, E., Pierce, K., Schumann, C. M., Redcay, E., Buckwalter, J. A., Kennedy, D. P., et al. (2007). Mapping early brain development in autism. *Neuron* 56, 399–413. doi: 10.1016/j.neuron.2007.10.016

Dawson, G. (2008). Early behavioral intervention, brain plasticity, and the prevention of autism. *Dev. Psychopathol.* 20, 775–803. doi: 10.1017/S0954579408000370

Delmonte, S., Gallagher, L., O'Hanlon, E., McGrath, J., and Balsters, J. H. (2013). Functional and structural connectivity of frontostriatal circuitry in Autism Spectrum Disorder. *Front. Hum. Neurosci.* 7:430. doi: 10.3389/fnhum.2013.00430

Deshpande, G., Libero, L. E., Sreenivasan, K. R., Deshpande, H. D., and Kana, R. K. (2013). Identification of neural connectivity signatures of autism using machine learning. *Front. Hum. Neurosci.* 7:670. doi: 10.3389/fnhum.2013.00670

Dickstein, D. P., Pescosolido, M. F., Reidy, B. L., Galvan, T., Kim, K. L., Seymour, K. E., et al. (2013). Developmental meta-analysis of the functional neural correlates of autism spectrum disorders. *J. Am. Acad. Child Adolesc. Psychiatry* 52, 279–289. doi: 10.1016/j.jaac.2012.12.012

Estes, A., Munson, J., Rogers, S. J., Greenson, J., Winter, J., and Dawson, G. (2015). Long-term outcomes of early intervention in 6-year-old children with autism spectrum disorder. *J. Am. Acad. Child Adolesc. Psychiatry* 54, 580–587. doi: 10.1016/j.jaac.2015.04.005

Hallmayer, J., Cleveland, S., Torres, A., Phillips, J., Cohen, B., Torigoe, T., et al. (2011). Genetic heritability and shared environmental factors among twin pairs with autism. *Arch. Gen. Psychiatry* 68, 1095–1102. doi: 10.1001/archgenpsychiatry.2011.76

Just, M. A., Cherkassky, V. L., Keller, T. A., Kana, R. K., and Minshew, N. J. (2007). Functional and anatomical cortical underconnectivity in autism: evidence from an fMRI study of an executive function task and corpus callosum morphometry. *Cereb. Cortex* 17, 951–961. doi: 10.1093/cercor/bhl006

Kana, R. K., Libero, L. E., Hu, C. P., Deshpande, H. D., and Colburn, J. S. (2012). Functional brain networks and white matter underlying theory-of-mind in autism. *Soc. Cogn. Affect. Neurosci.* 9, 98–105. doi: 10.1093/scan/nss106

Kim, S. H., Macari, S., Koller, J., and Chawarska, K. (2015). Examining the phenotypic heterogeneity of early Autism Spectrum Disorder: subtypes and short-term outcomes. *J Child Psychol Psychiatry.* doi: 10.1111/jcpp.12448. [Epub ahead of print].

Koegel, R. L., O'Dell, M. C., and Koegel, L. K. (1987). A natural language paradigm for nonverbal autistic children. *J. Autism Dev. Disord.* 17, 187–200.

Lampit, A., Hallock, H., Suo, C., Naismith, S. L., and Valenzuela, M. (2015). Cognitive training-induced short-term functional and long-term structural plastic change is related to gains in global cognition in healthy older adults: a pilot study. *Front. Aging Neurosci.* 7:14. doi: 10.3389/fnagi.2015.00014

Lenroot, R. K., and Yeung, P. K. (2013). Heterogeneity within Autism Spectrum Disorders: what have we learned from neuroimaging studies? *Front. Hum. Neurosci.* 7:733. doi: 10.3389/fnhum.2013.00733

Lewis, J. D., and Elman, J. L. (2008). Growth-related neural reorganization and the autism phenotype: a test of the hypothesis that altered brain growth leads to altered connectivity. *Dev. Sci.* 11, 135–155. doi: 10.1111/j.1467-7687.2007.00634.x

Lindamood, P., and Bell, N. (1997). Sensory-cognitive factors in the controversy over reading instruction. *J. Dev. Learn. Dis.* 1, 143–182.

McPartland, J. C., and Pelphrey, K. A. (2012). The implications of social neuroscience for social disability. *J. Autism Dev. Disord.* 42, 1256–1262. doi: 10.1007/s10803-012-1514-z

Mueller, S., Keeser, D., Samson, A. C., Kirsch, V., Blautzik, J., Grothe, M., et al. (2013). Convergent findings of altered functional and structural brain connectivity in individuals with high functioning autism: a multimodal MRI study. *PLoS ONE* 8:e67329. doi: 10.1371/journal.pone.0067329

Murdaugh, D. L., Deshpande, H. D., and Kana, R. K. (2016). The impact of reading intervention on brain responses underlying language in children with autism. *Autism Res.* 9, 141–154. doi: 10.1002/aur.1503

Murdaugh, D. L., Maximo, J. O., and Kana, R. K. (2015). Changes in intrinsic connectivity of the brain's reading network following intervention in children with autism. *Hum. Brain Mapp.* 36, 2965–2979. doi: 10.1002/hbm.22821

Nair, A., Treiber, J. M., Shukla, D. K., Shih, P., and Müller, R. A. (2013). Thalamocortical connectivity in autism spectrum disorder: a study of functional and anatomical connectivity. *Brain* 136, 1942–1955. doi: 10.1093/brain/awt079

Narzisi, A., Muratori, F., Calderoni, S., Fabbro, F., and Urgesi, C. (2013). Neuropsychological profile in high functioning autism spectrum disorders. *J. Autism Dev. Disord.* 43, 1895–1909. doi: 10.1007/s10803-012-1736-0

Pascual-Leone, A., Amedi, A., Fregni, F., and Merabet, L. B. (2005). The plastic human brain cortex. *Annu. Rev. Neurosci.* 28, 377–401. doi: 10.1146/annurev.neuro.27.070203.144216

Pierce, K. (2011). Early functional brain development in autism and the promise of sleep fMRI. *Brain Res.* 1380, 162–174. doi: 10.1016/j.brainres.2010.09.028

Retico, A., Tosetti, M., Muratori, F., and Calderoni, S. (2014). Neuroimaging-based methods for autism identification: a possible translational application? *Funct. Neurol.* 29, 231–239. doi: 10.11138/fneur/2014.29.4.231

Rogers, S. J., Vismara, L., Wagner, A. L., McCormick, C., Young, G., and Ozonoff, S. (2014). Autism treatment in the first year of life: a pilot study of infant start, a parent-implemented intervention for symptomatic infants. *J. Autism Dev. Disord.* 44, 2981–2995. doi: 10.1007/s10803-014-2202-y

Stoner, R., Chow, M. L., Boyle, M. P., Sunkin, S. M., Mouton, P. R., Roy, S., et al. (2014). Patches of disorganization in the neocortex of children with autism. *N. Engl. J. Med.* 370, 1209–1219. doi: 10.1056/NEJMoa1307491

Sullivan, K., Stone, W. L., and Dawson, G. (2014). Potential neural mechanisms underlying the effectiveness of early intervention for children with autism spectrum disorder. *Res. Dev. Disabil.* 35, 2921–2932. doi: 10.1016/j.ridd.2014.07.027

Uddin, L. Q., Supekar, K., and Menon, V. (2013). Reconceptualizing functional brain connectivity in autism from a developmental perspective. *Front. Hum. Neurosci.* 7:458. doi: 10.3389/fnhum.2013.00458

Ventola, P., Yang, D. Y., Friedman, H. E., Oosting, D., Wolf, J., Sukhodolsky, D. G., et al. (2015). Heterogeneity of neural mechanisms of response to pivotal response treatment. *Brain Imaging Behav.* 9, 74–88. doi: 10.1007/s11682-014-9331-y

Vivanti, G., Prior, M., Williams, K., and Dissanayake, C. (2014). Predictors of outcomes in autism early intervention: why don't we know more? *Front. Pediatr.* 2:58. doi: 10.3389/fped.2014.00058

Voos, A. C., Pelphrey, K. A., Tirrell, J., Bolling, D. Z., Vander Wyk, B., Kaiser, M. D., et al. (2013). Neural mechanisms of improvements in social motivation after pivotal response treatment: two case studies. *J. Autism Dev. Disord.* 43, 1–10. doi: 10.1007/s10803-012-1683-9

Warren, Z., McPheeters, M. L., Sathe, N., Foss-Feig, J. H., Glasser, A., and Veenstra-Vanderweele, J. (2011). A systematic review of early intensive intervention for autism spectrum disorders. *Pediatrics* 127, e1303–e1311. doi: 10.1542/peds.2011-0426

Wass, S. (2011). Distortions and disconnections: disrupted brain connectivity in autism. *Brain Cogn.* 75, 18–28. doi: 10.1016/j.bandc.2010.10.005

Wolfers, T., Buitelaar, J. K., Beckmann, C., Franke, B., and Marquand, A. F. (2015). From estimating activation locality to predicting disorder: a review of pattern recognition for neuroimaging-based psychiatric diagnostics. *Neurosci. Biobehav. Rev.* 57, 328–349. doi: 10.1016/j.neubiorev.2015.08.001

Wolff, J. J., and Piven, J. (2013). On the emergence of autism: neuroimaging findings from birth to preschool. *Neuropsychiatry* 3, 209–222. doi: 10.2217/npy.13.11

Conflict of Interest Statement: The authors declare that the research was conducted in the absence of any commercial or financial relationships that could be construed as a potential conflict of interest.

Advantages of publishing in Frontiers

OPEN ACCESS
Articles are free to read, for greatest visibility

COLLABORATIVE PEER-REVIEW
Designed to be rigorous – yet also collaborative, fair and constructive

FAST PUBLICATION
Average 85 days from submission to publication (across all journals)

COPYRIGHT TO AUTHORS
No limit to article distribution and re-use

TRANSPARENT
Editors and reviewers acknowledged by name on published articles

SUPPORT
By our Swiss-based editorial team

IMPACT METRICS
Advanced metrics track your article's impact

GLOBAL SPREAD
5'100'000+ monthly article views and downloads

LOOP RESEARCH NETWORK
Our network increases readership for your article

Frontiers
EPFL Innovation Park, Building I • 1015 Lausanne • Switzerland
Tel +41 21 510 17 00 • Fax +41 21 510 17 01 • info@frontiersin.org
www.frontiersin.org

Find us on